# Control of autonomous surface marine vessels for underwater vehicle localization using single range acoustic measurements

**Mandić, Filip**

**Doctoral thesis / Disertacija**

**2019**

*Degree Grantor / Ustanova koja je dodijelila akademski / stručni stupanj:* **University of Zagreb, Faculty of Electrical Engineering and Computing / Sveučilište u Zagrebu, Fakultet elektrotehnike i računarstva**

University of Zagreb

## FACULTY OF ELECTRICAL ENGINEERING AND COMPUTING

Filip Mandić

# Control of autonomous surface marine vessels for underwater vehicle localization using single range acoustic measurements

DOCTORAL THESIS

Zagreb, 2019

University of Zagreb

FACULTY OF ELECTRICAL ENGINEERING AND COMPUTING

Filip Mandić

# Control of autonomous surface marine vessels for underwater vehicle localization using single range acoustic measurements

DOCTORAL THESIS

Supervisor: Associate Professor Nikola Mišković, PhD

Zagreb, 2019

Sveučilište u Zagrebu

FAKULTET ELEKTROTEHNIKE I RAČUNARSTVA

Filip Mandić

# Upravljanje autonomnim površinskim plovilima u svrhu lokalizacije podvodnoga vozila korištenjem jednostrukih akustičkih mjerenja udaljenosti

DOKTORSKI RAD

Mentor: izv. prof. dr. sc. Nikola Mišković

Zagreb, 2019.

# About the Supervisor

**Nikola Mišković** was born in Zagreb on 17 March 1982. He received his diploma and Ph.D. degrees in electrical engineering from the University of Zagreb, Faculty of Electrical Engineering and Computing (FER), Zagreb, Croatia, in 2005 and 2010, respectively. From July 2005 he is working at the Department of control and computer engineering at FER. He was a visiting researcher at the Consiglio Nazionale delle Ricerche in Genoa, Italy (in 2008). In June 2016 he was promoted to Associate Professor. He participated in 14 European projects (H2020, FP7, DG-ECHO, INTERREG), 4 Office of Naval Research Global (ONR-G) projects, 2 NATO projects, and 7 national projects, out of which he coordinated 7: H2020 project "APAD - smaller, lighter, smarter autonomous marine surface vehicle", H2020 project "EXCELLABUST – Excelling LABUST in marine robotics", FP7 project "CADDY – Cognitive Autonomous Diving Buddy", ONR-G project "SPATEL - Spatial Auditory HMI for UxV Teleoperation", ONR-G project "DINARO - Diver navigation using range-only measurements from an autonomous surface vehicle", Croatian National Foundation project "CroMarX – Cooperative robotics in marine monitoring and exploration" and BICRO project "Autonomous surface platform for diver tracking and navigation". He published more than 70 papers in journals and conference proceedings in the area of navigation, guidance and control, as well as cooperative control in marine robotics. Assoc. Prof. Mišković is a member of IEEE (president of Chapter for Robotics and Automation of the Croatian Section from 2016 to 2017), IFAC (member of the Technical Committee on Marine Systems) and Centre for Underwater Systems and Technologies (vice-president since 2010). He participated in 8 conference international programs committees, he is member of 2 journal editorial boards and he serves as a technical reviewer for various international journals. In 2013 he received the young scientist award "Vera Johanides" of the Croatian Academy of Engineering (HATZ) for scientific achievements, and he received the annual State science award for 2015, awarded by the Croatian Parliament.

# O mentoru

**Nikola Mišković** rođen je u Zagrebu 17. ožujka 1982. godine. Diplomirao je, i doktorirao u polju elektrotehnike na Sveučilištu u Zagrebu Fakultetu elektrotehnike i računarstva (FER), 2005. odnosno 2010. godine. Od srpnja 2005. godine radi na Zavodu za automatiku i računalno inženjerstvo FER-a. Bio je gostujući istraživač na Consiglio Nazionale delle Ricerche u Genovi, Italija (u 2008. godini). U lipnju 2016. godine izabran je u zvanje izvanrednog profesora. Sudjelovao je na 14 europska projekta (H2020, FP7, DG-ECHO, INTERREG), 4 Office of Naval Research Global (ONR-G) projekta, 2 NATO projekta, te 7 nacionalnih projekata. Od toga je koordinirao 7 projekata: H2020 projekt „APAD - smaller, lighter, smarter autonomous marine surface vehicle", H2020 projekt „EXCELLABUST – Excelling LABUST in marine robotics", FP7 projekt „CADDY – Cognitive Autonomous Diving Buddy", ONR-G projekt „SPATEL - Spatial Auditory HMI for UxV Teleoperation", ONR-G projekt „DINARO - Diver navigation using range-only measurements from an autonomous surface vehicle", HRZZ projekt „CroMarX - Kooperativna robotika u nadzoru i istraživanju mora" i BICRO projekt „Autonomous surface platform for diver tracking and navigation". Objavio je više od 70 radova u časopisima i zbornicima konferencija u području navigacije, vođenje i upravljanja, te kooperativnog upravljanja u pomorskoj robotici. Izv. prof. Mišković član je stručnih udruga IEEE (predsjednik Odjela za robotiku i automatizaciju Hrvatske sekcije od 2016. do 2017.), IFAC (član Technical Committee on Marine Systems) i Centra za podvodne sustave i tehnologije (dopredsjednik društva od 2010.). Sudjeluje u 8 međunarodnih programskih odbora znanstvenih konferencija, član je dvaju uredničkih odbora znanstvenih časopisa te sudjeluje kao recenzent u većem broju inozemnih časopisa. Godine 2013. primio je nagradu Hrvatske akademije tehničkih znanosti „Vera Johanides" mladom znanstveniku za uspjehe u području istraživanja, te je nagrađen godišnjom Državnom nagradom za znanost za 2015. godinu.

...

# Acknowledgements

First, I would like to thank my advisor Associate Prof. Nikola Mišković for his support during my Ph.D study. In times when my motivation was low, his optimistic views on the research subject were invaluable.

Especially, I would like to thank to all the current and former colleagues form the Laboratory for Underwater Systems and Technologies (LABUST), not only for their technical and scientific support, but also for all the fun times we've had in the office, at coffee breaks, and during our sometimes long and exhaustive field trials.

Thanks to my Mom and Dad for all the love and care they gave me but also for letting me choose my own paths in life, my brother Mateo for all the discussions about music, movies, games (ME1 > ME2), and my grandma Marijana for allowing me to start breaking things apart around her house at the very young age which probably contributed to my love for engineering.

Many thanks to my love Kristina for genuinely sharing interest in topics we discuss, for understanding all my quirks, and for being supportive every single day we share.

Thanks to my best friends Nikola and William for sticking with me through both the good and bad times, and through my philosophical conversations.

Finally, I would like to thank to all the people that I didn't mention, but that contributed to this thesis in any way, from the beginning until the end, whether as a direct help in the execution of this thesis or as a moral support.

# Abstract

The interest in marine environment (underwater and surface) constantly increases, both for scientific and economic reasons. In order to accomplish many tasks in such environment, reliable localization of underwater objects is necessary. The cost of the conventional underwater localization systems can compromise a significant share of the total vehicle cost. The focus of this thesis are control algorithms for autonomous surface marine vehicles that are equipped with affordable acoustic sensors and whose goal is localizing or enhancing underwater localization of the objects of interest.

Mobile beacon vehicles are used as a navigational aid for autonomous underwater vehicles when performing navigation using single range measurements. They remove the constraints imposed on the underwater vehicle trajectory by executing trajectory that provides informative range measurements. In thesis, control algorithm for the beacon vehicle which ensures observability of the underwater vehicle's navigation filter is presented. It is characterized by a small communication overhead, low computational complexity and it is deployable on both fully actuated and underactuated vehicles. The algorithm was tested in real–life environment and the acquired experimental results were validated using a metric proposed in the thesis.

Control algorithm for an autonomous surface system carrying a two-sensor array consisting of two acoustic receivers, capable of measuring the time difference of arrival of a quasiperiodic underwater acoustic signal and utilizing this value in order to steer the system towards the acoustic source in the horizontal plane, is another major contribution of the thesis. Stability properties of the proposed algorithm are analysed using the Lie bracket approximation technique. Furthermore, simulation results are shown, where particular attention is given to the influence of a constant disturbance caused by sea currents and a relationship between the time difference of arrival measurement noise and the sensor baseline. Experimental results in which the algorithm was deployed on two autonomous surface vehicles, each equipped with a single acoustic receiver, are presented. The algorithm successfully steers the vehicle formation towards the acoustic source, despite the noisy and intermittent measurements, thus showing the feasibility of the proposed algorithm in real-life conditions.


**Keywords**: underwater localization, single range measurements, navigation, mobile beacon, source seeking, time difference of arrival, autonomous surface vehicles

# Upravljanje autonomnim površinskim plovilima u svrhu lokalizacije podvodnoga vozila korištenjem jednostrukih akustičkih mjerenja udaljenosti

Ljudi od davnina teže istraživanju različitih prostora koji ih okružuju. Od kopnenih površina, mora i morskih dubina do neba i svemirskih prostranstva. Istraživanje svakog od tih područja predstavljalo je, i dan danas predstavlja znatne izazove. Posebno se to odnosi na istraživanje morskih dubina. Naime, iako smo okruženi morima i oceanima uz dostupnu tehnologiju još uvijek vrlo malo znamo o najvećim morskim dubinama i tajnama koje skrivaju. Razlozi tomu su višestruki, od velikih hidrostatskih tlakova prisutnih na velikim dubinama, sigurnosti ljudski posada pod morem pa sve do problema koji se javljaju pri navigaciji u dubinama. U posljednje vrijeme sve je veći interes istraživača za korištenjem autonomnih podvodnih vozila koja bi samostalno mogla pokriti velika podmorska prostranstva i omogućiti nove spoznaje.

Veliku prepreku uspješnom istraživanju podmorja predstavlja upravo navigacija pod morem. Na kopnu su dostupni razni oblici lokalizacije vozila i tu se ponajprije misli na globalni pozicijski sustav, odnosno GPS. Korištenje GPS signala pod vodom, i općenito komunikaciju pod vodom onemogućavaju fizikalna svojstva vode, naime, pod vodom se elektromagnetski signali jako brzo prigušuju i nije moguće uspostaviti takav oblik komunikacije i lokalizacije. Stoga se autonomna podvodna vozila oslanjaju na koračnu navigaciju, korištenjem mjerenja dobivenih od senzora brzine i inercijalnih senzora, zbog koje imaju neograničnu lokalizacijsku pogrešku koja raste s vremenom, brzinom ovisnom o kvaliteti senzora i navigacijskog algoritma. Mnoga autonomna podvodna vozila zbog toga povremeno izranjaju na površinu kako bi dobili GPS mjerenje i time odredili vlastitu poziciju. Alternativna tehnika lokalizacije i komunikacije, i ona koja se najviše koristi kod podvodnih vozila, jest korištenje akustičkih uređaja za komunikaciju i lokalizaciju. Međutim, postojeća rješenja koja se temelje na akustičkoj navigaciji su nepraktična i često preskupa. Primjerice, postavljanje podvodnih LBL ( *engl. Long baseline*) sustava, kod kojih se u podmorje spušta veći broj predajnika i potom se iz mjerenja udaljenosti vozila u odnosu na njih i poznavanja njihovoga točnoga položaja može trilateracijom odrediti položaj vozila, vrlo je zahtjevno. Nedostatak USBL-a ( *engl. Ultra short baseline*), uređaja koji osim mjerenja udaljenosti, daje i mjerenja kuta između vozila i predajnika, predstavlja njegova vrlo visoka cijena.

Navedeni problemi u lokalizaciji jesu jedan od glavnih razloga zašto veliki interes pobuđuje istraživanje navigacije korištenjem jednostrukih mjerenja udaljenosti koje predstavlja jeftiniju alternativu danas dostupnim tehnikama podvodne navigacije. Doktorski

rad rezultat je istraživanja u području podvodne lokalizacije i upravljanje autonomnim plovilima korištenjem jednostrukih mjerenja udaljenosti. Istraživanje je usredotočeno na upravljačke algoritme za plovila koji potpomažu lokalizaciju podvodnih objekata kada su dostupna mjerenja udaljenosti. Temeljem upravljačkih algoritama i metodologija za validaciju algoritama razvijenih unutar doktorata izdvojena su tri znanstvena doprinosa:

- Algoritam upravljanja autonomnim površinskim plovilom s ciljem povećanja pokazatelja osmotrivosti navigacijskog sustava podvodnog vozila koje koristi jednostruka mjerenja udaljenosti od predajnika na površinskom plovilu

- Algoritam kooperativnog upravljanja dvama autonomnim površinskim plovilima koji koristi razliku vremena dolaska akustičkog signala s podvodnog izvora u svrhu njegove lokalizacije

- Postupak validacije kvalitete algoritama za podvodnu navigaciju i lokalizaciju korištenjem jednostrukih mjerenja udaljenosti, te njegova primjena u analizi rezultata terenskih eksperimenata.

Doktorski rad podijeljen je na uvodni dio, matematičko modeliranje plovila, navigaciju i upravljanje plovilima korištenjem jednostrukih mjerenja udaljenosti, upravljanje mobilnim predajnikom pri navigaciji jednostrukim mjerenjima udaljenosti, traženje izvora signala korištenjem razlike vremena dolaska signala te zaključni dio.

Prvo poglavlje („1. Introduction") daje kratak pregled tehnika podvodne lokalizacije i poteškoća prilikom iste. Potreba za jednostavnom i dostupnom podvodnom lokalizacijom u prisustvu više vozila opremljenih akustičkim senzorima naglašena je kao motivacija za disertaciju. Nadalje, razrađene su hipoteze i doprinosi doktorskog rada. Poglavlje završava pregledom ostalih poglavlja doktorskog rada i opisom autonomnih vozila i akustičkih senzora korištenih unutar disertacije.

Matematičko modeliranje podvodnih plovila obrađuje se u drugom poglavlju („2. Mathematical modelling of underwater vehicles"). Unutar poglavlja, proveden je teoretski pregled i prikazani su osnovni matematički modeli raspodjele potiska, dinamičkih i kinematičkih modela koji su korišteni tijekom istraživanja. Prikazani su isključivo pojednostavljeni modeli koji su korišteni prilikom sinteze sustava upravljanja i simulacijama predstavljenim u drugim poglavljima Također, prikazana je struktura navigacije, vođenja i upravljanja korištena na vozilima za potrebe simulacija i provođenja eksperimenata.

Treće poglavlje ("3. Navigation and Control of Marine Vehicles Using Single Range Measurements") započinje pregledom tehnika akvizicije akustičkih mjerenja udaljenosti. U podvodnom okolišu mjerenja udaljenosti uobičajeno se pribavljaju korištenjem akustičkih modema. Udaljenost se može odrediti korištenjem tehnike mjerenja jednostrukog puta ili dvostrukog puta signala. Kod tehnike jednostrukog puta udaljenost se određuje iz vremena putovanja akustičkog signala koji se propagira između modema na

strani predajnika te na strani vozila. Takvo mjerenje zahtijeva vrlo precizne satove kako bi se postigla sinkronizacija. Tehnika mjerenja dvostrukog puta signala najčešće je korištena tehnika mjerenja udaljenosti budući da ne zahtijeva preciznu sinkronizaciju satova, već zahtijeva interakciju između dva modema tako da modem na strani vozila akustički šalje zahtjev modemu na strani predajnika koji odgovara na zahtjev. Modem na strani vozila prima odgovor i na temelju ukupnog vremena propagacije signala estimira se udaljenost između uređaja. Korištenje mjerenja udaljenosti pribavljenih akustičkom komunikacijom predstavlja veliki izazov budući da takva mjerenja nisu dostupna u svakom trenutku. Također ona su pod utjecajem raznih čimbenika koji uvode pogrešku poput promjenjive brzine zvuka u vodi, refleksija od fizičkih prepreka, opadajućem omjeru snage signala i šuma kako se udaljenost između dva objekta povećava.

U nastavku poglavlja, prikazana je navigacija korištenjem jednostrukih mjerenja udaljenosti u odnosu na statični i mobilni predajnik. Obrađen je problem osmotrivosti pri navigaciji jednostrukim mjerenjima udaljenosti koji predstavlja jednu od glavnih prepreka prilikom navigacije jednostrukim mjerenjima udaljenosti jest pitanje osmotrivosti sustava budući da jedno mjerenje udaljenosti, zajedno s mjerenjem dubine vozila, ograničava moguću poziciju na skup rješenja opisanih kružnicom. Između pojedinih mjerenja udaljenosti relativno gibanje vozila estimira se koristeći mjerenja brzine i orijentacije vozila. Pokazano je da postoji velik broj radova koji se bave ostmotrivošću navigacije jednostrukim mjerenjima udaljenosti korištenjem različitih metodologija i generalni zaključak navedenih radova jest da kako bi se postigla osmotrivost sustava u slučaju nepoznatih struja, vozilo mora izvršavati trajektorije sa određenom zakrivljenošću, odnosno trajektorije koje dovoljno pobuđuju sustav.

Slučaj u kojemu predajnik miruje zanimljiv je za primjene poput pronalaženja neke početne točke ronilice, lociranja objekata poput 'crnih kutija' pri avionskim nesrećama. No kao što je već spomenuto, nedostatak leži u tome što kako bi vozilo estimiralo svoj položaj mora putovati dovoljno informativnom trajektorijom kako bi sustav bio osmotriv i pritom ne može obavljati neke druge zadatke koji zahtjevaju trajektorije koje nisu pogodne za estimaciju položaja. Stoga je zanimljiv pristup gdje je predajnik također vozilo, površinsko ili podvodno, koje se može gibati. U tom slučaju vozilo koje koristi navigaciju jednostrukim mjerenjima udaljenosti može odrađivati svoj zadatak bez obzira koliko je zadana trajektorija informativna, dok se predajnik giba kako bi mjerenja udaljenosti u odnosu na vozilo bila dovoljno informativna, a samim time i sustav navigacije osmotriv. Pri takvoj navigaciji bitno je da predajnik dobro zna svoj položaj što je u slučaju površinskoga predajnika lako ostvarivo korištenjem GPS mjerenja. U poglavlju su predstavljeni i pokazatelji kvalitete korišteni za validaciju trajektorija mobilnoga predajnika pri navigaciji korištenjem jednostrukih mjerenja udaljenosti koji u obzir uzimaju

osmotrivost ostvarenih trajektorija mobilnoga predajnika i ukupan ostvaren put za postiznje iste.

Osim teme navigacije, obrađena je i tema upravljanja koje koristi jednostruka mjerenja udaljenosti. Ponekad je cilj vozila postići isključivo ekstrem nekoga kriterija, primijerice minimizirati udaljenost vozila i nekoga objekta, i pritom apsolutna pozicija vozila nije bitna informacija. U literaturi koja se dotiče podvodnih vozila postoje pristupi kod kojih se unutar navigacijskog filtra, najčešće proširenog Kalmanovog filtra, estimira položaj izvora koristeći jednostruka mjerenja udaljenosti, a potom se konvencionalni upravljački algoritmi koriste kako bi se dosegnula željena točka. Također, korištenje tehnike traženja ekstrema (engl. Extremum seeking) za navigaciju autonomnih vozila prema nepoznatom izvoru u okolišu bez GPS signala koristeći mjerenja koja daju vrijednost nekoga polja u pojedinoj točki je čest istraživački problem. Tehnika traženja ekstrema uobičajeno se primjenjuje u slučaju kada je model sustava slabo poznat ili u potpunosti nepoznat. Njegova velika prednost leži u tome da konstantni poremećaji koji djeluju na vozilo poput gravitacije, plovnosti te struja se automatski kompenziraju unutar upravljačke petlje. U poglavlju je prikazan kratak pregled tehnike traženja ekstrema , i pokazano je kako se ista može koristiti kao sredstvo navigacije prema podvodnim objektima kad su dostupna isključivo mjerenja udaljenosti. Pokazatelji kvalitete za validaciju takvih algoritama, koji uzimaju u obzir ukupan put i ukupno vrijeme potrebno za pronalaženje signala, su uvedeni i primijenjeni na simulacijskim i eksperimentalnim rezultatima koji su pokazali primjenjivost algoritma u realnim uvjetima.

U četvrtom poglavlju ("4. Mobile Beacon Control in Single Range Navigation") prikazan je algoritam za upravljanje mobilnim predajnikom u svrhu smanjenja lokalizacijske pogreške prilikom navigacije podvodnoga vozila jednostrukim mjerenjima udaljenosti. Prikazani algoritam karakteriziraju vrlo niski računalni i komunikacijski zahtjevi što ga čini izrazito pogodnim za zadatke poput praćenja podvodnih objekata uz istovremeno pružanje dovoljno informativnih mjerenja udaljenosti za potrebe lokalizacije objekta.

Glavna ideja algoritma jest vođenje površinskoga mobilnoga predajnika uz trajektorije koje smanjuju lokalizacijsku pogrešku podvodnoga vozila. Površinski predajnik akustički šalje svoju apsolutnu poziciju navigacijskome filtru koji se izvodi na podvodnome vozilu. Informacija generirana u navigacijskome filtru se koristi kako bi se izračunao skalarni pokazatelj lokalizacijske pogreške podvodnoga vozila. Navedeni skalarni pokazatelj, se potom akustički šalje mobilnome predajniku, koji ga koristi u upravljačkoj shemi inspiriranoj upravljačkim shemama kakve se koriste pri tehnikama traženja ekstrema, kako bi vodio mobilni predajnik prema trajektorijama kojima se ostvaruje osmotrivost navigacijskog filtra na podvodnom vozilu. U upravljačkoj shemi referenca brzine zaošijanja ima konstantan iznos, dok je referenca unaprijedne brzine porporcionalna iznosu pokazatelja

lokalizacijske pogreške. Ponovnim slanjem pozicije predajnika prema podvodnom vozilu dobiva se mjerenje udaljenosti između mobilnoga predjanika i podvodnoga vozila te se time i zatvara upravljačka petlja.

Predstavljeni algoritam rezultira sprialnim trajektorijama kojima mobilni predajnik prilazi podvodnome vozilu, te u konačnici kružnim trajektorijama predajnika oko podvodnoga vozila za koje je pokazano da osiguravaju osmotrivost lokalizacijskoga sustava, što je potvrđeno simulacijskim rezultatima. Dan je i matematički uvid u stabilnost algoritma. Pokazuje se da prilikom spiralnoga gibanja, u trenucima kada su kut između vektora relativne udaljenosti i vektora relativne brzine približno ortogonalni, vrijednost pokazatelja lokalizacijske pogreške se smanjuje što uzrokuje da mobilni predajnik prilazi vozilu brže nego što se udaljava od njega, odnosno u prosjeku udaljenost između vozila i predajnika se smanjuje, sve dok se ne uspostavi kružna trajektorija predajnika oko podvodnoga vozila. Naposljetku, prikazani su opširni eksperimentalni rezultati, za podaktuirani i nadaktuirani mobilni predajnik te su primijenjeni odgovarajući pokazatelji kvalitete za usporedbu predstavljenoga algoritma s već postojećim.

U situacijama kada su mjerenja udaljenosti nedostupna, tehnika mjerenja razlike dolaska akustičkoga signala na fiksne prijemnike se može koristiti za lokalizaciju akustičkih izvora signala. Kako bi se to ostvarilo potrebna su minimalno tri fiksna prijemenika. U petom poglavlju ("5. Time Difference of Arrival Source Seeking"), predstavljen je algoritam namjenjen autonomnom površinskom sustavu opremeljenom s isključivo dva akustička senzora koji omogućuju mjerenja razlike vremena dolaska podvodnog akustičkog signala i korištenje tog signala kako bi se naveo sustav prema izvoru signala. Dva akustička prijemenika su postavljena tako da tvore osnovicu kojom je moguće upravljati u horizontalnoj ravnini. Upravljački algoritam sastoji se od sheme za traženje ekstrema zadužene za upravljanje orijentacijom sustava odnosno okretanje osnovice prema izvoru akustičkoga signala, te regulatora unaprijedne brzine koji je zadužen za gibanje osnovice prema izvoru signala. Stabilnost predloženoga algoritma analizirana je korištenjem aproksimacije Lievim zagradama, gdje je pokazano da sustav konvergira prema izvoru akustičkoga signala u horizontalnoj ravnini. U pratećim simulacijskim rezultatima, posebna pažnja je posvećena vezi između mjernoga šuma i udaljenosti između dva akustička senzora. Izazovi prisutni u praktičnoj implementaciji algoritma, vezani uz činjenicu da je pozicija izvora akustičkoga signala nepoznata, su istraženi. Konačno, prikazani su eksperentalni rezultati u kojima su korištena dva autonomna površinska plovila opremljena jednim akustičkim prijemnikom. Navedena konfiguracija omogućava promjenu duljine osnovice ovisno o mjernom šumu senzora. Rezultati pokazuju da je algoritam, usprkos mjernom šumu i isprekidanim mjerenjima, primjenjiv u stvarnim uvjetima.

Doktorski rad završava elaboracijom hipoteza i doprinosa prezentiranih u sadržaju doktorskoga rada.

**Ključne riječi**: podvodna lokalizacija, jednostruka mjerenja udaljenosti, navigacija, mobilni predajnik, traženje ekstrema, razlika vremena dolaska signala, autonomna plovila

# Contents

# Chapter 1

# Introduction

The research area of marine robotics is becoming more popular as the need to understand the marine environment (underwater and surface) increases both for scientific and economic reasons. Unmanned underwater vehicles (UUVs) are today used in a variety of applications, from oil and gas exploration to underwater archaeology missions or autonomous ship hull inspections. The commercial use of UUVs centers mainly on the gas and oil industry. With development of technology, UUVs are expanding into the mainstream with the ability to complete a wider variety of missions than their research-specific predecessors. Intervention tasks (turning valves, cleaning etc.) as well as persistent autonomy and cooperation among vehicles is in focus of research today. Cognitive robotics that is the hot topic in land and aerial robotics is slowly entering the marine robotics domain. In commercial use, high resolution seabed mapping and imaging for commercial mapping and oil/gas pipeline surveying in shallow and deep waters are major tasks done for the oil and gas industry. Inspection, maintenance and repair (IRM) are done in depths over 300m almost exclusively with remotely operated vehicles (ROVs) which are main type of vehicles for IRM tasks. Military use of UUVs focuses on surveillance, minesweeping and mine countermeasure work. Maritime security of ports and sailing routes are today in high priority. Autonomous Underwater Vehicle (AUV) and remotely operated vehicles are equally in use here, [1]. Today, Underwater Sensor Networks (USNs) are a promising solution for exploring underwater environment. Many applications such as environmental monitoring, seismic monitoring for oil extraction, pollution and water quality control, disaster prevention, military surveillance uses USNs that use acoustic signals for communication because radio waves get attenuated in underwater environment [2]. The AMussel robot swarm developed in the Horizon 2020 FET project subCULTron is an example of an underwater sensor network used for environmental monitoring [3].

Surface and underwater marine robots allow humans to explore the ocean in a new ways, lowering costs, improving efficiency and reducing the risks of marine operations.

And marine robotics is rapidly going toward its ultimate goal: full autonomy. An new generation of systems are now being developed inside academia with intention to operate independently and make online decisions with no direct human intervention. In order to acomplish such complex tasks, robots need to know their location and location of objects of interest, e.g. underwater pipeline inspection vehicle needs to know its position so that gathered data or pipeline damage can be related with exact location and reported back to operator. Localization involves question: *"Where is the vehicle now?"*, therefore localization means determining vehicle position and orientation in space. Its position does not have to be absolute position in space, it can also be relative to some landmark, usually the point of origin or the destination. Navigation can be defined as the activity or process of vehicle finding the way to get to a desired location. Localization and navigation are the two most important tasks for underwater vehicles as is for practically any type of vehicle. We want to know where we are, and we need to be able to make a plan for how to reach a goal destination. These two problems are interconnected. If a vehicle does not know its exact position at the start of a planned trajectory, it will encounter problems in reaching the destination, [4].

In an underwater environment, Global Navigation Satellite System (GNSS) signals, that are available and widely used for localization in numerous land and air applications, are absent due to the very weak propagation of electromagnetic waves through the water. An electromagnetic homing system, presented in [5], is an example of the alternative that can provide accurate measurement of the autonomous vehicle position and orientation to the dock during homing, but also with very limited range due to same propagation constraints. Therefore, in the underwater environment acoustic based localization techniques are predominantly used.

Underwater navigation systems can be categorized in three categories, [6]. First, inertial navigation navigation systems which use accelerometers and gyroscopes for increased accuracy to propagate the current vehicle state state, but all of the in three categories. Methods in this category have position error growth that is unbounded. Second, external acoustic systems are based on measuring the time–of–flight of signals from acoustic beacons or modems to perform navigation with bounded position error. The main focus of this thesis is in this category. Finally, geophysical navigation category contains techniques that use external environmental information as references for navigation. This is done with sensors and processing that are capable of detecting, identifying, and classifying some environmental features, e.g. cameras, sonars. Beside these three categories, when talking about localization we need to distinguish between two cases. In one case we want to determine vehicle position aboard the vehicle, while in second case, outside observer wants to determine vehicle position.

## 1.1 Brief Overview of Underwater Localization Techniques

Underwater acoustic channels are generally recognized as one of the most difficult communication media in use today. Large propagation delay, high bit error rate, low data rate and low bandwidth are characteristics of acoustic communication, [7]. Acoustic propagation is characterized by three major factors: attenuation that increases with signal frequency, time-varying multipath propagation, and low speed of sound (1500 m/s). The background noise, although often characterized as Gaussian, is not white, but has a decaying power spectral density. The channel capacity depends on the distance, and may be extremely limited. Multipath formation in the ocean is governed by two effects: sound reflection at the surface, bottom, and any objects, and sound refraction in the water, [8].

Underwater localization methods started with Radio Acoustic Ranging (RAR), a method for determining a ship's precise location at sea by detonating an explosive charge underwater near the ship, detecting the arrival of the underwater sound waves at remote locations, and radioing the time of arrival of the sound waves at the remote stations to the ship, allowing the ship's crew to use triangulation to determine the ship's position. Developed by the United States Coast and Geodetic Survey in 1923 and 1924 for use in accurately fixing the position of survey ships during hydrographic survey operations, it was the first navigation technique in human history other than dead reckoning that did not require visual observation of a landmark, marker, light, or celestial body, and the first non-visual means to provide precise positions. First employed operationally in 1924, radio acoustic ranging remained in use until 1944, when new radio navigation techniques developed during World War II rendered it obsolete, [9]. Today, piezoelectric transducers are used in order to generate acoustic soundwawes in the frequency ranges from a few kHz to hundreds of kHz with data rates typically under 1000 bps are used in different array configurations in order to localize underwater objects, [10].

Short review of the following underwater localization systems is given: long baseline, short baseline, ultra short baseline, GPS intelligent buoy, and time difference of arrival based systems.

**Ultra Short Base-Line systems**

An Ultra Short Base-Line (USBL) system comprises of two elements, a transceiver with an array of transducers that are usually less than 10 cm apart, thus forming the ultra short baseline, and a transponder. The transceiver sends an acoustic pulse and when the transponder that is mounted on the tracked object receives this pulse, it replies with its own acoustic pulse. The round-trip propagation time of this send–reply cycle is used to

compute the range between them. The direction of the transponder from the transceiver is measured on the transceiver with a phase-differencing within this transducer array to calculate the angle to the underwater transponder. The position of the undersea object is then obtained using the range, bearing and elevation of the transceiver with respect to the transponder. USBL is the most popular category of underwater positioning systems due to its easy deployment, at the cost of positioning accuracy. Transciever can also be mounted on the underwater vehicle resulting in so–called inverted USBL (iUSBL), [11]. In such configuration all the processing is done inside the vehicle to allow it to locate the transponder for applications such as automatic docking and target tracking or to localize itself in the operational area.

## Long Base-Line systems

Long Base-Line (LBL) systems are compound of several underwater transponders that are usually deployed on the seafloor along the edge of the operational area thus forming the baseline. The name derives from the fact that the distance between the baseline stations is long or similar to the distance between object and transponders. Baseline distance typically ranges from $50\,\text{m}$ to more than $2000\,\text{m}$. It operates in such way that first interrogating signal from the object is sent. Upon the reception, the transponder sends a reply. The signal propagation times are then used to compute the distances between the object and transponders. Then, together with depth data from pressure sensors, the position of the object can be computed using trilateration. This position is relative to the baseline transponders but it can be easily converted into geo-referenced coordinates if the geographic positions of the baseline transponders are known a priori. LBL systems are independent of water depth and provide high accuracy of more than $1\,\text{m}$, with the capability of achieving accuracies of a few centimetres. This exceeds the accuracies of USBL and Short Base-Line (SBL) systems, [12].

## Short Base-Line systems

SBL systems are mounted on floating platforms like boats or ships and are used for tracking underwater targets. Like LBL systems, they use round-trip signal propagation time of acoustic signals between transponders and target to compute the distance and then trilateration to determine the position [12]. They often have supplementary depth data from a pressure sensor. Since they are mounted on mobile objects, SBL systems are characterized by smaller inter-baseline transponder distance of 20 to $50\,\text{m}$ compared to LBL. The accuracy of SBL system improves as the distance between baseline transponders increases and can achieve similar performance levels as sea floor mounted LBL systems. On the other hand, the accuracy of the system deteriorates when mounted on the smaller

vessels due to reduced transponder distance.

**GNSS Intelligent Buoy systems**

Instead of deploying the baseline transponders on the seafloor, they can installed on GPS equipped sonobuoys that are either drifting or moored, resulting in a system called GNSS Intelligent Buoy (GIB), [13]. Such system, can be viewed as inverted LBL devices. In a typical deployment scenario, several GIBs are deployed over a given area of operation where the total number required is determined by the size of the operation area and the desired accuracy. Accuracies of centimeter to meter level can be achieved. The position of the tracked object is calculated in real time based on the acoustic signals transmitted by the underwater object. GIB uses one-way acoustic signal transmission from object (emitter) to buoys as compared to the round-trip transmission of LBL, SBL and USBL, making it less susceptible to reflections from surface or other undersea structures.

**Time Difference of Arrival based systems**

In general, Time Difference of Arrival (TDOA) is a method that calculates location from the differences of arrival times measured on transmission paths between the source and fixed receivers, [14]. TDOA–based localization schemes usually consist of two steps: the measurement acquisition step and the multilateration step. In the measurement acquisition step, the differences of acoustic signal arrival times on several receiver nodes are measured. Based on the property of hyperbola, the source will be located on a hyperbola whose difference between ranges to respective receivers is a constant. The difference in ranges is easily calculated from the measured difference in time of arrival and the known speed of the acoustic signal. With more than two receivers, we can compute more hyperbolic functions which ideally intersect in one unique point, thus determining source location, [15]. Traditional 3D underwater localization techniques require four non-coplanar receivers to localize the underwater signal source successfully, [16]. However, that need can be eliminated via the use of depth information acquired by a pressure sensor, and a projection-based technique that translates receiver nodes to the plane of the signal source, [17]. This makes localization using only three anchors possible, assuming the projection of the three non–colinear anchors is non–degenerative.

## 1.2   Thesis Contributions and Overview

The cost of the conventional underwater localization systems compromises significant share of the total vehicle cost. The goal of this thesis is to develop online algorithms for underwater localization and improving underwater localization of the objects of interest

in the case of multiple vehicles equipped with affordable and easy to deploy sensors. Hypotheses that were analysed inside thesis in order to check feasibility of the envisioned goal are stated as follows:

- *Autonomous marine surface vessel control in order to improve the observability index of the underwater vehicle navigation system that uses single range measurements with respect to the beacon on the autonomous marine surface vessel can be achieved without knowing vehicle trajectory in advance.*

- *Autonomous marine surface vessel control in order to improve the observability index of the underwater vehicle navigation system that uses single range measurements with respect to the beacon on the autonomous marine surface vessel can be deployed on both fully-actuated and underactuated vehicles.*

- *Cooperative control of two autonomous marine surface vessels that use signal time of arrival difference for localization of an underwater acoustic signal source can be achieved.*

- *Due to their robustness, proposed algorithms can be deployed in the presence of unknown currents.*

In the scope of the thesis, autonomous marine surface vessel control algorithm which improves the observability index of the underwater vehicle navigation system that uses single range measurements with respect to the beacon on the autonomous marine surface vessel was researched. Proposed algorithm was intended for both underactuated and fully–actuated vehicles, and communication constraints were taken into consideration. Control algorithm for time–difference of arrival source seeking of underwater acoustic signal that can be executed by two autonomous marine surface vessels that uses signal time of arrival difference for localization of an underwater acoustic signal source was investigated. Both algorithms were tested in real life conditions. Finally, methods for validating vehicle trajectories in single range navigation and source seeking scenarios based on appropriate performance indices were applied in the analysis of field experiment results.

Therefore, scientific contributions of this thesis are summarized as follows:

1. **Autonomous marine surface vessel control algorithm which improves the observability index of the underwater vehicle navigation system that uses single range measurements with respect to the beacon on the marine surface vessel.**

2. **Cooperative control algorithm for two autonomous marine surface vessels that uses time of arrival difference of an acoustic signal for localization of an underwater source.**

3. **Validation method for underwater single range navigation and localization algorithm quality, and its application in the analysis of field experi-**

**ment results.**

The thesis is organized as follows. In Section 1.3 overview of the vehicles and the sensors used in this thesis is shown. In Chapter 2 general mathematical models for marine vehicles are described, before navigation, guidance and control structure of the marine vehicles used is presented. Simplified models that were used for control and estimation are shown, while references to more complex models are given. Chapter 3 describes single range navigation and control approaches that use range measurements from a single beacon. In there, validation methods that are related to the third contribution are introduced. First contribution, mobile beacon control algorithm which ensures observability of the single range navigation system is presented in Chapter 4. In Chapter 5, the second contribution, a control algorithm for an autonomous surface system carrying a two-sensor array consisting of two acoustic receivers, capable of measuring the time difference of arrival of a quasiperiodic underwater acoustic signal and utilizing this value in order to steer the system towards the acoustic source in the horizontal plane. Both chapters with control algorithm contributions are complemented with simulation and experimental results. The thesis is concluded with Chapter 6 where a summary of the most important points from the dissertation is given.

## 1.3   Systems

Consideration of vehicle maneuvering capabilities is very important for selection of appropriate control and localization algorithms. Depending on the actuator types and allocation, autonomous underwater and surface vehicles can be categorized as: overactuated, fully–actuated, underactuated. Looking specifically at underwater vehicles, vehicle depth control is usually decoupled from horizontal motion and vertical movement is achieved using vertically positioned thrusters which enable hovering at certain depth. Exception are torpedo like AUVs, because they usually need to achieve certain forward velocity to generate enough lift with horizontal rudders in order to dive, thus they are unable to hover. As vehicles are used to execute desired motion, sensors are used for the perception of the required quantities. All the vehicles used were equipped with standard navigation sensors usually found in underwater and surface marine vehicles.

During this thesis, one of the goals was to experimentally validate algorithms developed inside simulation environments, e.g MATLAB, GAZEBO, which required vehicles with adequate meneuvering capabilites, equipped with sensors that enable navigation and localization of these vehicles. In Section 1.3.1 and Section 1.3.2 vehicles and the most critical sensors used in the experimental validation of the algorithms presented in this thesis are shown.

## 1.3.1 Available vehicles

### Pladypos Unmanned Surface Vehicle (USV)



(a)                                                    (b)

**Figure 1.1:** The autonomous surface vehicle Pladypos in both incarnations. First (a) and second (b) versions built in 2012 and 2016, respectively.

The autonomous surface vehicle Pladypos (named after its initial purpose as a dynamic positioning platform) is developed in the Laboratory for Underwater Systems and Technologies (LABUST) at the University of Zagreb, Faculty of Electrical Engineering and Computing. The vehicle is equipped with four thrusters in the "X" configuration allowing omnidirectional motion, i.e. free motion in the horizontal plane under any orientation. Such vessel configuration is convenient for research purposes due to easy deployment procedure, robustness in real environmental conditions, and low power consumption. Omnidirectional motion makes it agile and thus applicable in tracking underwater agents capable of quick change of direction such as human divers.

Pladypos vehicles, usually, have a single control computer (isolated from environmental disturbances within the platform hull) in charge of performing navigation, guidance and control (NGC) and other data processing. They are approximately 0.35 m high, 0.707 m wide and long, and weigh up to 25 kg depending on version, payload and battery type. Basic vehicle payload consists of

- u-blox 6PPP
- Advanced Navigation Spatial for orientation and inertial navigation
- ubiquity 2.4 GHz wireless communication
- 12 V VRLA battery
- SeaBotix BTD150

while more advanced payload, described in 1.3.2, is supported via external mounting.

## H2Omni–X USV

Pladypos has experienced two development iterations during the thesis. The first version (1.1a), developed in 2012, was used for initial diver tracking experiments and NGC system development, [18]. During 2016 the second version (1.1b) was developed that was used as the emulated diver tracking platform during final diver tracking experiments.

The H2Omni–X, also known as aPad is autonomous over–actuated marine surface platforms, developed in the LABUST and based on the Pladypos USV. The H2Omni–X retained all the maneuvering capabilities of its predecessor. Vehicle dimensions and weight have changed together with some hardware components. The vehicle is 0.385 m high, 0.756 m wide and long, and weighs approximately 25 kg.

- Emlid Reach RTK GPS
- MPU9250 MEMS Inertial Measurement Unit
- ubiquity 2.4 GHz wireless communication
- 12 V VRLA battery
- BlueRobotics T200 thrusters
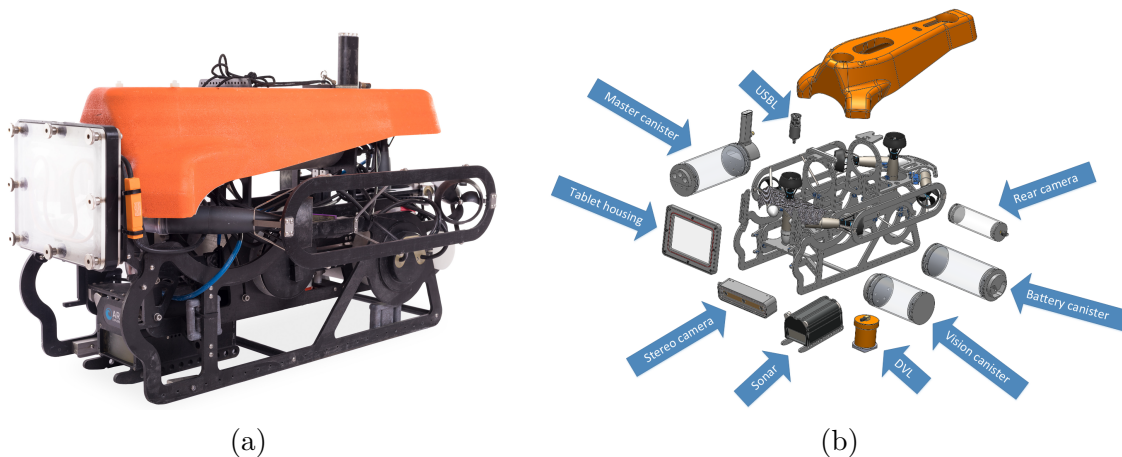
## Buddy AUV



**Figure 1.2:** The Buddy AUV with the pressure housing for the tablet in (a). The vehicle consists of many elements and sensors as seen in (b).

The AUV, conveniently named Buddy, was developed under the European project "CADDY - Cognitive Autonomous Diving Buddy". It acts as a diving partner and provides constant diver monitoring, guidance, notification, tool fetching and similar services. It is fully-actuated in the horizontal plane and can independently control heave and pitch degree of freedom (DoF). The vehicle, shown in Figure 1.2, is equipped with a wide range of sensors required to achieve envisioned functionalities related with diver-robot interaction in the underwater environment. Buddy is 1.27 m long, 0.7 m wide, 0.7 m high

and weighs about 70 kg. The basic payload is:

- U-blox Neo 5M GPS
- Microstrain GX3 Inertial Measurement Unit (IMU)
- LinkQuest Navquest 600M Doppler velocity logger (DVL)
- Ubiquity wireless communication
- 48 V lithium battery
- VideoRay Pro4 brushless thrusters

In addition the vehicle is equipped with acoustic, stereo and mono cameras. Visual interaction with the diver is achieved through an underwater tablet, mounted in front, capable of displaying and alerting the diver when necessary. Underwater experiments with the diver employed BUDDY to autonomously track and observe the diver.
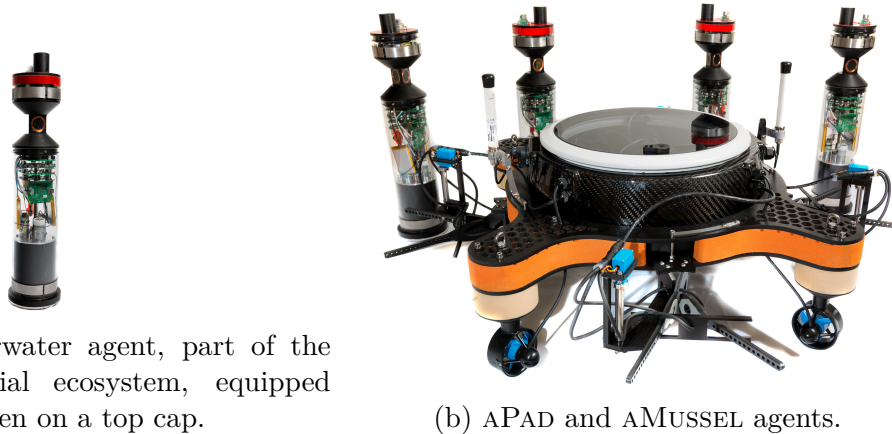


(a) aMUSSEL underwater agent, part of the subCULTron artificial ecosystem, equipped with Nanomodem seen on a top cap.

(b) aPAD and aMUSSEL agents.

**Figure 1.3:** Agents in the subCULTron artificial ecosystem.

### aMUSSEL

The aMUSSEL, shown in Figure 1.3a, represents the biggest part of the autonomous marine robot swarm developed in the H2020 subCULTron project. They are equipped with a wide variety of sensors, as their role is long-term data collection and observation, but they have no movement capabilities save for a buoyancy system that allows them to sit on the bottom of the sea or float to the water's surface [19]. In the scope of the thesis it was used as a source of the underwater acoustic signal since it was equipped with a simple acoustic Nanomodem device.

### SPARUS II AUV

Two additonal vehicles from the Underwater Robotics Laboratory of the University of Girona, Spain were available for experimentation. SPARUS II AUV, shown in Figure 1.4b, is hovering AUV for surveying and inspection applications developed at the Underwater
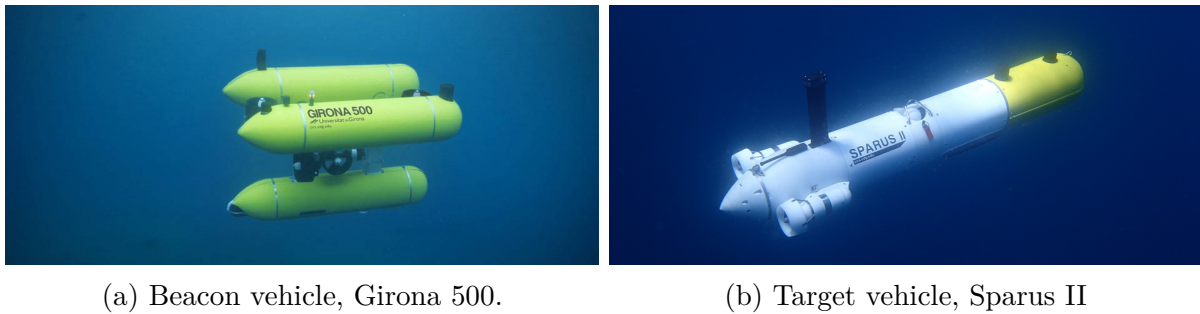
(a) Beacon vehicle, Girona 500.

(b) Target vehicle, Sparus II

**Figure 1.4:** Vehicles used in the experiment.

Robotics Laboratory of the University of Girona, Spain. It has a torpedo-like shape to be efficient when navigating at medium to high velocities with the maximum surge velocity of $2 \frac{m}{s}$. It is equipped with three thrusters, two horizontal for control of surge and yaw DoFs and one vertical that allows the control of the heave DoF, but also two fins behind the horizontal thrusters are used for controlling the pitch DOF and, thus, controlling the depth or altitude of the vehicle. Fins are used when the vehicle is in torpedo–based mode, while vertical thrusters are used for depth control when moving in hovering mode. The fins are also used for stabilization at low and high surge velocities where the differential movement of the fins is also used to stabilize the roll DoF, [20].

### GIRONA 500 AUV

GIRONA 500 AUV, shown in Figure 1.4a and also developed at the Underwater Robotics Laboratory of the University of Girona, Spain, has been designed as a modular research platform capable for use in wide range of different applications, from the classical sonar and video imaging surveys to the challenging autonomous intervention tasks. The standard GIRONA 500 configuration is the four thruster setup, two horizontal thrusters to actuate the surge and yaw DoF and two vertical to actuate the heave and pitch DoF. The vehicle, designed for a maximum operating depth of up to $500\,m$, is composed of an aluminum frame that supports three torpedo-shaped hulls of $0.3\,m$ in diameter and $1.5\,m$ in length as well as other elements like the thrusters. This design offers a good hydrodynamic performance and a large space for housing the equipment while maintaining a compact size that allows us to operate the vehicle from small boats. The overall dimensions of the vehicle are $1\,m$ in height, $1\,m$ in width, $1.5\,m$ in length, and a weight of less than $200\,kg$ [21]. During the the experiments, conducted in the scope of this thesis, the five–thruster configuration of GIRONA 500 was used. Two thrusters that actuate surge and yaw, and two that actuate the heave degree of freedom were used. An additional, lateral thruster was mounted and used in the presence of currents, or when the task at hand demanded the capacity of executing lateral movements.

## 1.3.2 Available sensors

**SeaTrac USBL**



(a) The SeaTrac USBL system.          (b) The Nanomodem acoustic device.

**Figure 1.5:** Acoustic communication and localization equipment.

The SeaTrac USBL system, shown in Figure 1.5a, was developed within the CADDY project by the Newcastle University in order to improve underwater localization and communication between vehicles and the diver. It consists of transceiver with transducer array and transponder which is mounted on tracked object. Flexible payload length selection allows optimized communication and localization to average of 2.5 s per node. This system was used in the scope of this thesis for acquiring range and ground truth measurements.

**Nanomodem**

Nanomodem is a low-cost acoustic modem capable of transmitting data and ranging. Signal proccessing algorithms and electronics were developed at Newcastle University [22], while the mechanical integration of the components was done by LABUST as shown in Figure 1.5b. Interesting feature of the nanomodems are acoustic receive flags RxS and RxM. When the start of any acoustic packet is detected by a nanomodem, the RxS flag is raised. The timing of this rising edge coincides precisely with the detection of the packet header waveform and so it may be used for time difference of arrival (TDOA) estimates where multiple nanomodems are placed in an array. When a nanomodem receives a unicast data message addressed to that unit, the RxM flag is raised for a short period corresponding to the transmissions of the received serial data. This signal may be used, for example, to wake up connected circuitry from a low power state. The RxS flag was used in experimental validation of the algorithm presented in Chapter 5.

# Chapter 2

# Navigation, Guidance and Control of Marine Vehicles

The navigation, guidance and control (NGC) system is responsible for directing the actuating forces and stabilizing the vehicle along the desired path. The NGC system has to define the trajectory in real time to reach the specified target and steer the vehicle along the desired path. The navigation system measures the instantaneous state of the vehicle, and using this information, the guidance system generates the trajectory to achieve the target and desired vehicle steering command to realize the trajectory in real time. The vehicle control system, receives the steering commands from the guidance system and steers the vehicle to follow the desired attitude in the presence of all disturbances [23].

Navigation, guidance and control of marine vehicles is a challenging task, mainly due to coupling between DoFs, hydrodynamic effects and highly unpredictable environmental influences. Sea operation and deployment cost for different types of autonomous marine vehicles is high, and risk of vehicle loss during untethered operation of AUVs is high. As a consequence, good mathematical models are needed to properly test and simulate NGC systems beforehand. Sensor and external disturbance modelling has to correctly approximate the harsh and stochastic nature of underwater environments [24]. Therefore, before NGC development, the vehicle, from high-level kinematics down to thruster mapping, is mathematically modelled providing basis for navigation and controller tuning.

In Section 2.1 vehicle dynamic and kinematic models, used throughout the thesis for theoretical analysis or for the experimental execution, are presented. The state estimation equations are given, and basic low–level and high–level controllers used for experimentation are presented. Most of the models and controllers presented herein can also be found in [25] where these controllers where thoroughly experimentally tested on the PLADYPOS USV.
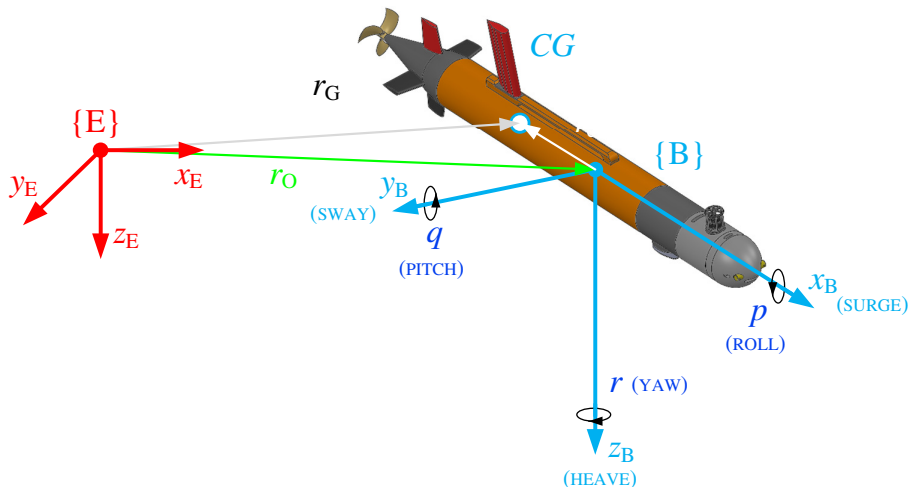
# 2.1   Mathematical Modelling



**Figure 2.1:** Representation of {**E**} and {**B**} frames.

**Table 2.1:** Rigid body degrees of freedom and their SNAME notation [26].

| Description | Symbol | Surge | Sway | Heave | Roll | Pitch | Yaw | Frame |
|---|---|---|---|---|---|---|---|---|
| velocity | $\boldsymbol{\nu}$ | $u$ | $v$ | $w$ | $p$ | $q$ | $r$ | {**B**} |
| position | $\boldsymbol{\eta}$ | $x$ | $y$ | $z$ | $\phi$ | $\theta$ | $\psi$ | {**E**} |
| force and torque | $\boldsymbol{\tau}$ | $X$ | $Y$ | $Z$ | $K$ | $M$ | $N$ | {**B**} |

In order to define the mathematical model of a general marine vehicle used throught this thesis, the terminology and definitions already established in vehicle modelling literature [26, 27, 28, 29] are used. Vectors and matrices are always shown in bold, e.g. **p**, **R**, with upper-case letters reserved for matrices. Scalars are written in italic, e.g. $n$, $e$. Symbol $\mathbb{N}$ denotes the set of positive integers, symbol $\mathbb{N}_0$ denotes the set of positive integers including zero, $\mathbb{Z}$ denotes set of integers, while $\mathbb{R}$ denotes set of real numbers. Expression $\boldsymbol{M} \in \mathbb{R}^{n \times m}$ denotes $n$-by-$m$ matrix $\boldsymbol{M}$ whose elements are real numbers.

The notation in this thesis is based on The Society of Naval Architects and Marine Engineers (SNAME) notation as given in [26]. Vehicle model vectors, from the nomenclature, are given in Table 2.1 where {**B**} represents body–fixed frame and {**E**} so called North-East-Down (NED) frame. The NED frame is also known as the Local Tangent Plane (LTP). Angular latitude and longitude define the NED frame origin on the reference ellipsoid used to approximate Earth's surface. The altitude information defines the height above the ellipsoid. The abscissa points toward true north and the ordinate points to east, and the NED vertical axis is perpendicular to the ellipsoid thus completing the

right-handed coordinate system. Generally speaking, the vertical axis does not point into the centre of the Earth [24]. The frame $\{\mathbf{E}\}$ is the common navigational frame for marine and aerial systems. Throughout the thesis coordinate frames are right-handed and angles with corresponding angular rates follow the same convention. Vectors are linked with the corresponding frame through a superscript symbol, while transforms additionally use subscript notation, e.g. $\mathbf{p}^e = \mathbf{R}_b^e \mathbf{p}^b$. The matrix $\mathbf{R}_b^e$ represents a rotation from $\{\mathbf{B}\}$ to $\{\mathbf{E}\}$ frame.

Surge, sway and heave are defined as translational motion in the x–, y– and z– direction of $\{\mathbf{B}\}$ coordinate system, respectively, while roll, pitch and yaw are defined as rotation about x–, y– and z–axis in $\{\mathbf{B}\}$ coordinate system, respectively, as shown in Figure 2.1. Vehicle's positions and orientations given in $\{\mathbf{E}\}$ are defined with:

$$\boldsymbol{\eta} = \begin{bmatrix} \boldsymbol{\eta}_1^T & \boldsymbol{\eta}_2^T \end{bmatrix}^T, \quad \boldsymbol{\eta}_1 = [x\ y\ z]^T, \quad \boldsymbol{\eta}_2 = [\phi\ \theta\ \psi]^T \tag{2.1}$$

Notice how vector $\boldsymbol{\eta}$ can be split into vectors $\boldsymbol{\eta}_1$ and $\boldsymbol{\eta}_2$ representing the vehicle's position and the vehicle rotation, respectively. Vehicle's translational and rotational velocities are defined with:

$$\boldsymbol{\nu} = \begin{bmatrix} \boldsymbol{\nu}_1^T & \boldsymbol{\nu}_2^T \end{bmatrix}^T, \quad \boldsymbol{\nu}_1 = [u\ v\ w]^T, \quad \boldsymbol{\nu}_2 = [p\ q\ r]^T \tag{2.2}$$

where vectors $\boldsymbol{\nu}_1$ and $\boldsymbol{\nu}_2$, defined in $\{\mathbf{B}\}$, represent the linear and the angular vehicle velocities, respectively. Finally, vector of external forces and moments $\boldsymbol{\tau}$ acting on the vehicle in $\{\mathbf{B}\}$ is defined as:

$$\boldsymbol{\tau} = \begin{bmatrix} \boldsymbol{\tau}_1^T & \boldsymbol{\tau}_2^T \end{bmatrix}, \quad \boldsymbol{\tau}_1 = [X\ Y\ Z]^T, \quad \boldsymbol{\tau}_2 = [K\ M\ N]^T. \tag{2.3}$$

In Figure 2.2 block diagram of marine vehicle model is given. It consists of four main
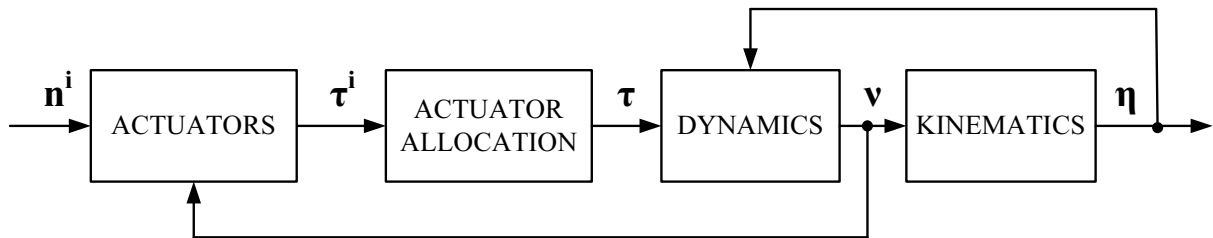


**Figure 2.2:** Block diagram of marine vehicle.

blocks: actuators, actuators allocation, dynamics, and kinematics. In the following sections these blocks will be described in more detail.

## 2.1.1 Actuators and Actuator allocation

Actuators in all technical systems are actuating devices that perform desired action on the system. The actuators used in underwater and surface marine vehicles can be roughly divided into thrusters (propulsors, propellers), control surfaces (rudders, fins, etc.) and mass. Thrusters that are most commonly used in marine vehicles are based on a rotating propeller motion and exist in many forms (bow thrusters, azimuth thrusters, etc.) Control surfaces are usually rudders and fins. Fins are mostly used for roll stabilization, but also for indirect control of the heave motion via pitch control, [30]. In the field of marine robotics, practically every vehicle is equipped with multiple thrusters, or with a combination of a single thruster and a rudder and/or fins.

If we denote commanded thrust for a single actuator as $\tau_i$ where $i = 1, ..., m$ is the number of actuators. These thrusts form a generalized vector $\boldsymbol{\tau_i}$ of size $m$. Let $n_i$ denote commanded input for the $i$–th actuator which can be rotation speed of the propeller, rudder deflection, etc. These inputs form a generalized vector $\boldsymbol{n}_i$ of size $m$. Then, *Actuator allocation* block in Figure 2.2 gives relations between forces exerted by actuators $\boldsymbol{\tau}_i$ and forces that act on the vessel $\boldsymbol{\tau}$, while *Actuators* block models the thrust exerted by actuators $\boldsymbol{\tau}_i$ with regard to commanded input $\boldsymbol{n}^i$ of each actuator. Notice that vehicle manual control is performed at this level, where desired control forces and moments are through inverse allocation distributed on the available thrusters .
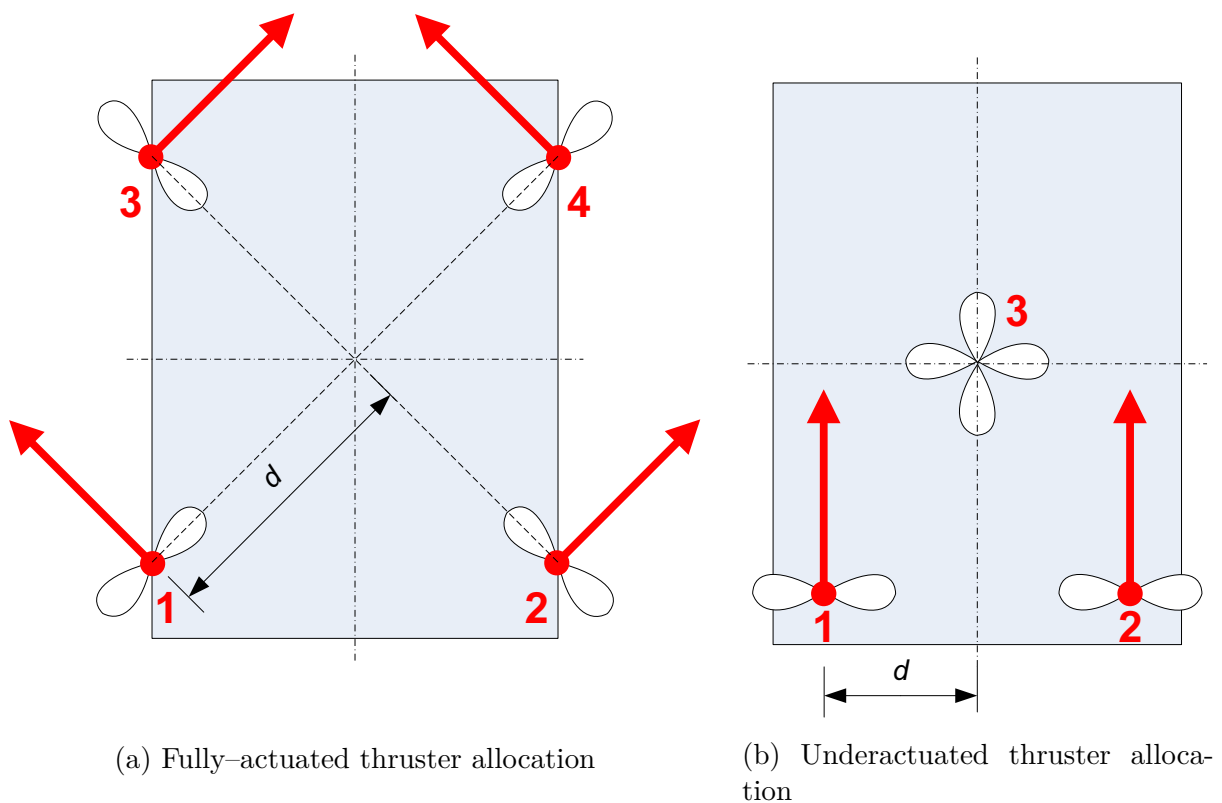


(a) Fully–actuated thruster allocation

(b) Underactuated thruster allocation

**Figure 2.3:** Thruster allocation.

The actuator allocation matrix $\mathbf{\Phi}$, defined with (2.4), gives relation between the forces exerted by thrusters $\boldsymbol{\tau_i} = \begin{bmatrix} \tau_1 & \tau_2 & \tau_3 & \tau_4 \end{bmatrix}^{\mathrm{T}}$ and the forces and moments $\boldsymbol{\tau}$ acting on the rigid body. Variable $d$ and $\gamma$ denote the thruster distance from the $\{\mathbf{B}\}$ origin and thruster rotation with respect to $\{\mathbf{B}\}$, respectively. Actuator configuration of the fully–actuated autonomous surface platform, such as aPad, with so–called "X" thruster configuration is given in Figure 2.3a where $\gamma = 45°$. Such thruster configuration is particularly suitable for dynamic positioning or diver tracking applications.

$$
\begin{bmatrix} X \\ Y \\ N \end{bmatrix} = \begin{bmatrix} \cos\gamma & \cos\gamma & -\cos\gamma & -\cos\gamma \\ \sin\gamma & -\sin\gamma & \sin\gamma & -\sin\gamma \\ d & -d & -d & d \end{bmatrix} \begin{bmatrix} \tau^1 \\ \tau^2 \\ \tau^3 \\ \tau^4 \end{bmatrix} \tag{2.4}
$$

Underactuated vehicle allocation matrix, of the thruster configuration shown in Figure 2.3b, is given with:

$$
\begin{bmatrix} X \\ Z \\ N \end{bmatrix} = \begin{bmatrix} 1 & 1 & 0 \\ 0 & 0 & 1 \\ d & -d & 0 \end{bmatrix} \begin{bmatrix} \tau^1 \\ \tau^2 \\ \tau^3 \end{bmatrix}. \tag{2.5}
$$

Allocation of underactuated vehicles like Girona 500 and Sparus II can be described with such matrix but it is important to note that these are basic allocation examples. In practice allocation is due to varying vehicle design and thruster placement often unique to the specific vehicle type. More about actuator allocation can be found in [24, 31].

## 2.1.2   Dynamic model

Dynamic model which gives relations between the forces that act on the vessel $\boldsymbol{\tau}$ and the speeds $\boldsymbol{\nu}$ exhibited by the vessel and it is denoted with *Dynamics* block in Figure 2.2. Throughout this paper, uncoupled dynamic model of the vehicle is used. For more details about marine vehicle modelling and parameter estimation check [32], [30]. While realistic simulations benefit from increased model complexity, most control and estimation designs are performed with a simplified, uncoupled model. It is further assumed that vehicle roll ($\phi$) and pitch ($\theta$) angles are zero. This simplification is justified, since the main focus of this thesis is vehicle localization in terms of vehicle position in $\{\mathbf{E}\}$ coordinate frame and not its orientation.

Therefore, 4-DoF model is used for underwater vehicles, while 3-DoF is used for surface vehicles. In order to have same notation of the presented vectors in the case of a 4-DoF or a 3-DoF vehicles, which were predominately used in this thesis, small inconsistency in the notation will be introduced. For example, in the case of a 3-DoF model, position and orientation vector, although lower dimension, still is denoted with $\boldsymbol{\eta} = \begin{bmatrix} x & y & \psi \end{bmatrix}^T$. Accordingly, following the notation given in this chapter, dynamic model of the underwater

vehicle with 4-DOF can be described using the velocity vector $\boldsymbol{\nu} = \begin{bmatrix} u & v & w & r \end{bmatrix}^{\mathrm{T}}$ where $u$, $v$, $w$ and $r$ are surge, sway, heave and yaw speed, respectively; and the vector of actuating forces and moments acting on the underwater vehicle $\boldsymbol{\tau} = \begin{bmatrix} X & Y & Z & N \end{bmatrix}^{\mathrm{T}}$ where $X$, $Y$, $Z$ are surge, sway and heave forces and $N$ is yaw moment. Both vectors are defined in the body–fixed (mobile) coordinate frame. The uncoupled dynamic model for a 4-DOF vehicle is given with:

$$\mathbf{M}\dot{\boldsymbol{\nu}} = -\mathbf{D}(\boldsymbol{\nu}) + \boldsymbol{\tau} + \boldsymbol{g}, \tag{2.6}$$

where $\boldsymbol{M}$ is a matrix with mass and added mass terms, and $\boldsymbol{D}(\boldsymbol{\nu})$ is a matrix consisting of nonlinear hydrodynamic damping terms. Since we observe uncoupled dynamics, the following forms of the two matrices are adopted: $\mathbf{M} = diag\left(\alpha_u, \ \alpha_v, \ \alpha_w, \ \alpha_r\right)$, $\mathbf{D}(\boldsymbol{\nu}) = diag\left(\beta_u(u), \ \beta_v(v), \ \beta_w(w), \ \beta_r(r)\right)$. Vector of restoring forces $\boldsymbol{g}$ consists of a gravitational force $\boldsymbol{W}$ and a buoyant force $\boldsymbol{B}$ which affect the vehicle. Gravitational force is induced by weight $\boldsymbol{W}$ of the vehicle and acts through the centre of gravity $\boldsymbol{r_G}$ of the vehicle. Buoyant force is induced by buoyancy $\boldsymbol{B}$ and elevates the vehicle to the surface. It acts through the centre of buoyancy $\boldsymbol{r_B}$ which need not necessarily be at the same place as the centre of gravity (CG). With small vhicles, which have been used in this thesis, it can be safely assumed that both $\boldsymbol{r_g}$ and $\boldsymbol{r_b}$ are in the origin of the body–fixed frame $\{\mathbf{E}\}$.

The uncoupled dynamic model for 4-DoF underwater vehicles is defined based on as:

$$\dot{u} = -\frac{\beta(u)}{\alpha_u}u + \frac{1}{\alpha_u}X + \zeta_u \tag{2.7}$$

$$\dot{v} = -\frac{\beta(v)}{\alpha_v}v + \frac{1}{\alpha_v}Y + \zeta_v \tag{2.8}$$

$$\dot{w} = -\frac{\beta(w)}{\alpha_w}w + \frac{1}{\alpha_w}(Z + W - B) + \zeta_w \tag{2.9}$$

$$\dot{r} = -\frac{\beta(r)}{\alpha_r}r + \frac{1}{\alpha_r}N + \zeta_r \tag{2.10}$$

## 2.1.3   Kinematic model

Kinematic model, denoted with *Kinematics* block in Figure 2.2, gives relations between positions and orientations $\boldsymbol{\eta}$ defined in $\{\mathbf{E}\}$ and speeds $\boldsymbol{\nu}$ defined in $\{\mathbf{B}\}$. For underwater vehicles, kinematic models are the most common model type for state estimation. These models contain only spatial equations and are considered deterministic. They include easily measurable parameters as opposed to dynamic models, and are commonly used in target tracking applications since knowledge about dynamic parameters is unavailable or reduced to generic assumptions. Two main kinematic models are encountered in the thesis: fully-actuated and underactuated model. The uncoupled fully-actuated model is

reserved for state estimation where, for some reason, the dynamic model is unavailable. The underactuated model is used for targets that lack omnidirectional motion.

Certain control algorithms, like dynamic positioning or line following, which were deployed on the vehicles during the some experiments conducted in the scope of this thesis required particular kinematic models which are omitted in this section and presented together with control algorithms in Section 2.2.2.

**Fully actuated model**

In Section 2.1.2 model simplifications for uncoupled dynamics assumed that roll and pitch kinetics is stable and angles are around zero. This is not true for torpedo shaped vehicles utilizing pitch actuation   but all vehicle types used in the thesis satisfy this assumption which greatly simplifies kinematics as only rotation in the horizontal plane is present. Applying the assumptions, the kinematic equations for the 4–DoF vehicle motion, where $x$, $y$ and $z$ are the position and $\psi$ is the orientation of the vehicle in the Earth–fixed coordinate frame $\{\mathbf{E}\}$, are defined with:

$$
\begin{bmatrix} \dot{x} \\ \dot{y} \\ \dot{z} \\ \dot{\psi} \end{bmatrix} = \begin{bmatrix} \cos\psi & -\sin\psi & 0 & 0 \\ \sin\psi & \cos\psi & 0 & 0 \\ 0 & 0 & 1 & 0 \\ 0 & 0 & 0 & 1 \end{bmatrix} \begin{bmatrix} u \\ v \\ w \\ r \end{bmatrix} + \begin{bmatrix} \xi_x \\ \xi_y \\ \xi_z \\ 0 \end{bmatrix}, \tag{2.11}
$$

where the terms $\xi_x$, $\xi_y$, $\xi_z$ embed slowly changing environmental disturbances, e.g. currents. Vehicle modelled in such way is overactuated, i.e. it can move in any direction in the horizontal plane by modifying the surge and sway speed, while attaining arbitrary orientation.

**Underactuated model**

When sway motion is ignored, such as in underactuated vehicles or modelling of human diver motion, the model is reduced to:

$$
\begin{bmatrix} \dot{x} \\ \dot{y} \\ \dot{z} \\ \dot{\psi} \end{bmatrix} = \begin{bmatrix} \cos\psi & 0 & 0 \\ \sin\psi & 0 & 0 \\ 0 & 1 & 0 \\ 0 & 0 & 1 \end{bmatrix} \begin{bmatrix} u \\ w \\ r \end{bmatrix} + \begin{bmatrix} \xi_x \\ \xi_y \\ \xi_z \\ 0 \end{bmatrix}. \tag{2.12}
$$

Such kinematic model is also known as unicycle–like model, [33]. Velocities could be used as inputs in these models, but uncertainties related to velocity measurement are neglected this way. Several alternative approaches exist to circumvent the unknown kinetic model. The common approach introduces velocities as additional states with a dummy, constant velocity, kinetic model $\dot{\boldsymbol{\nu}} = \boldsymbol{\zeta}_{\boldsymbol{\nu}}$, $\boldsymbol{\zeta}_{\boldsymbol{\nu}} \sim \mathcal{N}(0, \mathbf{Q})$. Alternative assumptions are

possible depending on a-priori knowledge about the target. For vehicles, extending the filter with acceleration allows filter propagation by an inertial system without need for assumptions [29]. However, this approach drastically increases the number of states and is not applicable for target tracking. Notice that, fully actuated vehicle can execute underatcuated vehicle motion, while the other way around is not true.

**Constant current model**

In real–life applications, external disturbances like sea currents, waves and, winds affect the vehicle motion. Kinematic model (2.11) and (2.12) states can be augmented with constant current estimation model as:

$$\begin{bmatrix} \dot{\boldsymbol{\eta}} \\ \dot{\boldsymbol{\xi}}_c \end{bmatrix} = \begin{bmatrix} \mathbf{R}_b^n & \boldsymbol{I} \\ \boldsymbol{0} & \boldsymbol{0} \end{bmatrix} \begin{bmatrix} \boldsymbol{\nu} \\ \boldsymbol{\xi}_c \end{bmatrix} + \begin{bmatrix} \boldsymbol{0} \\ \boldsymbol{\zeta} \end{bmatrix}, \tag{2.13}$$

where $\boldsymbol{\xi}_c$ represents current estimates modelled as constant velocity disturbance in the global coordinate frame $\{\mathbf{E}\}$ contributing to the vehicle movement and $\boldsymbol{\zeta} \sim \mathcal{N}(0, \mathbf{Q})$. It is assumed that there are no rotational currents influencing yaw DoF.

## 2.2 Navigation, Guidance and Control Structure

This chapter describes parts of the implemented multi–level control structure shown in Figure 2.4. After the implemented navigation filter is described, the control structure description is provided in a top–down approach. Implemented NGC structure was used as a basis for experimentation, and further algorithm development shown in this thesis. High–level and low–level control structure, which is a part of LABUST toolset, presented in [25] is shown herein, abeit expanded with depth and heave controllers.
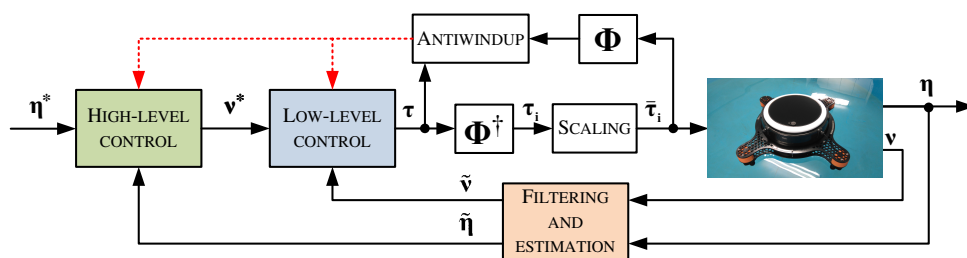


**Figure 2.4:** Closed–loop control scheme in a double loop structure (inner loop is low–level control and outer loop is high–level control) with filtering and estimation block providing state estimates based on available measurements. The description of the implemented antiwindup mechanism is omitted and the interested reader is referred to [34].

### 2.2.1 Navigation filter

In real–life conditions, measurements provided by sensors are not ideal. They are noisy, may contain outliers, they are often delayed or intermittent. Some of them cannot even be directly measured. Due to that, measurements are rarely used directly in control systems. Instead, they are first estimated using some of the many available filters. Also, mathematical models in practice are are mostly nonlinear. Several nonlinear estimation techniques exist, some of which are the particle filter, unscented and extended Kalman filter. Particle filtering is a brute-force statistical estimator offering superior performance to Kalman filters for highly nonlinear systems. Unscented Kalman filtering (UKF) applies unscented transformations providing more accuracy than linearisation, especially when propagating means and covariances. However, both the particle filter and UKF require more computation resources than the extended Kalman Filter, [35]. Nonlinear extensions of the Kalman filter use model linearisation around the operating point. The most famous and used extension, using a first order linearisation, is Extended Kalman Filter. Therefore, main equations are presented in this subsection for overview while complete Extended Kalman Filter (EKF) derivations can be found in [35, 36]. Let a discrete nonlinear system be described with the following set of equations

$$\mathbf{x}_k = \mathbf{f}_{k-1}\left(\mathbf{x}_{k-1}, \mathbf{u}_{k-1}, \mathbf{w}_{k-1}\right) \tag{2.14}$$

$$\mathbf{y}_k = \mathbf{h}_k\left(\mathbf{x}_k, \mathbf{v}_k\right) \tag{2.15}$$

$$\mathbf{w}_k \sim (0, \mathbf{Q}_k) \tag{2.16}$$

$$\mathbf{v}_k \sim (0, \mathbf{R}_k) \tag{2.17}$$

where $\mathbf{x}_k$ are system states, $\mathbf{y}_k$ outputs, and $\mathbf{u}_k$ inputs. Vectors $\mathbf{w}_k$ i $\mathbf{v}_k$ represent process and measurement noise described as Gaussian white noise with covariance matrices $\mathbf{Q}_k$ and $\mathbf{R}_k$, respectively. The main difference between a Kalman filter and its extended version is in the linearisation of nonlinear $\mathbf{f}$ and $\mathbf{h}$ functions around the current state estimate. The general EKF algorithm is then summarized as, [37]:

1. Initialize the filter with:

$$\hat{\mathbf{x}} = \mathbf{E}(\mathbf{x}_0) \tag{2.18}$$

$$\mathbf{P}_0^+ = \mathbf{E}\left(\left(\mathbf{x}_0 - \hat{\mathbf{x}}_0^+\right)\left(\mathbf{x}_0 - \hat{\mathbf{x}}_0^+\right)^{\mathsf{T}}\right) \tag{2.19}$$

where $\mathbf{E}(\cdot)$ is a expectation operator and $\mathbf{P}$ is the estimation error covariance matrix.

2. For each time-step $k$:

(a) Compute partial derivatives of the state equation:

$$\mathbf{F}_{k-1} = \left.\frac{\partial \mathbf{f}_{k-1}}{\partial \mathbf{x}}\right|_{\hat{\mathbf{x}}_{k-1}^+} \tag{2.20}$$

$$\mathbf{L}_{k-1} = \left.\frac{\partial \mathbf{f}_{k-1}}{\partial \mathbf{w}}\right|_{\hat{\mathbf{x}}_{k-1}^+} \tag{2.21}$$

(b) Update the state estimate and covariance (*prediction*):

$$\hat{\mathbf{x}}_k^- = \mathbf{f}_{k-1}(\hat{\mathbf{x}}_{k-1}^+, \mathbf{u}_{k-1}, 0) \tag{2.22}$$

$$\mathbf{P}_k^- = \mathbf{F}_{k-1}\mathbf{P}_{k-1}^+\mathbf{F}_{k-1}^T + \mathbf{L}_{k-1}\mathbf{Q}_{k-1}\mathbf{L}_{k-1}^T \tag{2.23}$$

(c) Compute partial derivatives of the output equation:

$$\mathbf{H}_k = \left.\frac{\partial \mathbf{h}_k}{\partial \mathbf{x}}\right|_{\hat{\mathbf{x}}_k^-} \tag{2.24}$$

$$\mathbf{M}_k = \left.\frac{\partial \mathbf{h}_k}{\partial \mathbf{v}}\right|_{\hat{\mathbf{x}}_k^-} \tag{2.25}$$

(d) Update the state estimate and covariance using the measurement innovation (*correction*):

$$\mathbf{K}_k = \mathbf{P}_k^-\mathbf{H}_k^T(\mathbf{H}_k\mathbf{P}_k^-\mathbf{H}_k^T + \mathbf{M}_k\mathbf{R}_k\mathbf{M}_k^T)^{-1} \tag{2.26}$$

$$\hat{\mathbf{x}}_k^+ = \hat{\mathbf{x}}_k^- + \mathbf{K}_k\left[\mathbf{y}_k - \mathbf{h}_k(\hat{\mathbf{x}}_k^-, 0)\right] \tag{2.27}$$

$$\mathbf{P}_k^+ = (\mathbf{I} - \mathbf{K}_k\mathbf{H}_k)\mathbf{P}_k^- \tag{2.28}$$

where $\mathbf{K_k}$ is known as the Kalman filter gain.

EKF is commonly used in practice since the systems we want to estimate are non-linear. Due to model linearisation around the operating point EKF, which introduces approximation error, is not an optimal estimator. If the initial state of the filter is chosen poorly, or the process model has large errors, filter can easily diverge. Despite that EKF gives satisfying performance, and presents de–facto standard in navigation systems.

Marine vehicles are equipped with different sensors which provide measurements at different update rates. Hence, the navigation filter has a task to fuse available measurements, and by using the mathematical models described in Section 2.1.2 and Section 2.1.3, provide state estimates at an update rate required by the control system. The implemented navigation filter takes available measurements as inputs and provides state estimates that are required for low–level and high–level control as it can be seen from Figure 2.4.

Estimators which use dynamic models have several benefits over kinematic models. First, velocities are modelled exactly and generalized assumptions are not required. Kinematic models update their velocity estimate with position measurements which are often slow and infrequent, but command inputs to the kinetic model ($X$, $Y$, $Z$, $N$) are continuously available for velocity updates. Therefore, use of dynamic models enables separate kinematic and kinetic controller design uniformly across a wide range of vehicles and sensor suites, [24]. When dynamic model parameters are available, the model can be used as velocity measurement input into the kinematic model. However, combining the dynamic and kinematic model is more compact. The combined model inputs are generalized forces and moments which propagate the estimator at the controller update rate.

**Incorporating delayed measurement**

Distributed systems often exhibit transmission delay or out-of-sequence packet arrival. When delays become noticeable, i.e. larger than the sampling time, they start affecting system performance. Directly incorporating delayed measurements in present time leads to suboptimal state estimation. Measurement delays smaller than the sampling time are incorporated by adjusting Kalman filter output equations [38]. These adjustments maintain the optimal solution of the state estimator. Larger delays require measurement updates to occur in the past and states forward propagated into present. This entails repeating multiple Kalman filter iteration within a single sampling time, leading to increased computation load. Alternatives for filter recalculation were reviewed in [39] and some are proposed in [40, 41, 42].

In this thesis filter recalculation was implemented and used for incorporating delayed measurements, mainly from the acoustic sensors which generally have a significant delay. Corrections are made in the past and the filter propagated into present. For nonlinear systems, linearisation introduces dependence between filter matrices and estimated states. Therefore, when this dependence is pronounced and unavoidable, recalculation is the only option. Measurements, states and covariances have to be saved in the memory aboard the vehicle for the desired time-window. Consider the problem for a separable nonlinear system defined as:

$$\mathbf{x}_k = \mathbf{A}_{k-1}\mathbf{x}_{k-1} + \mathbf{B}_{k-1}\mathbf{u}_{k-1} + \mathbf{w}_{k-1} \tag{2.29}$$

$$\mathbf{y}_k = \mathbf{H}_k\mathbf{x}_k + \mathbf{v}_k \tag{2.30}$$

where $\mathbf{w}_{k-1}$ and $\mathbf{v}_k$ are defined in Section 2.2.1. The current state $x_k^+$ is then corrected

with the measurement $y_s$ as

$$\hat{\mathbf{x}}_k^+ = \left(\prod_{i=0}^{N} \left(\mathbf{I} - \mathbf{K}_{k-i}\mathbf{H}_{k-i}\right) \mathbf{A}_{k-i-1}\right) \hat{\mathbf{x}}_{s-1}^+ + \tag{2.31}$$

$$\sum_{i=0}^{N} \left(\prod_{j=0}^{i-1} \left(\mathbf{I} - \mathbf{K}_{k-j}\mathbf{H}_{k-j}\right) \mathbf{A}_{k-j-1}\right) \left(\mathbf{I} - \mathbf{K}_{k-i}\mathbf{H}_{k-i}\right) \mathbf{B}_{k-i-1}\mathbf{u}_{k-i-1} + \tag{2.32}$$

$$\sum_{i=0}^{N} \left(\prod_{j=0}^{i-1} \left(\mathbf{I} - \mathbf{K}_{k-j}\mathbf{H}_{k-j}\right) \mathbf{A}_{k-j-1}\right) \mathbf{K}_{k-i}\mathbf{y}_{k-i} \tag{2.33}$$

where $y_s$ is taken at time instant $s = k - N$, with $N$ representing delay in number of samples. The Kalman gain and covariance matrix are calculated using the standard EKF equations. When no measurements are arriving between samples $s$ and $k$, (2.33) can be omitted. Since no corrections are performed, the matrix $(\mathbf{I} - \mathbf{KH})$ reduces to $\mathbf{I}$. Interestingly, for autonomous systems $(u = 0)$, the term (2.32) is zero and single-step recalculation is possible, assuming $\prod_{i=0}^{N} A_{k-i-1}$ can be calculated analytically. This is the case with the vehicle kinematic model [43].

**Outlier rejection**

In statistics, an outlier is an observation point that is distant from other observations. Outliers may arise from sensor noise (producing values that fall outside the valid range of values), from temporary sensor failures, or from unanticipated disturbances in the environment (e.g., a brief change of lighting conditions for a visual sensor). A typical approach of detecting outliers is to characterize what normal observations look like, and then to single out samples that deviate from these normal properties. There are many approaches in the literuture for oulier detection e.g. Mahalanobis distance, a measure of the distance between a point and some distribution, can be used as a way to determine outliers, [44].

In the implementation of the outlier rejection, two cases with respect to the measurement type were differentiated: direct measurement of the filter state, measurement that is linear or nonlinear combination of the filter states. If measurement is one of the filter states, the standard condition to detect outliers is defined with, [45]:

$$|x_{im} - \hat{x}_i| > a\sqrt{P_{ii}}, \tag{2.34}$$

where $x_{im}$ is $i$-th state measurement which is being tested, $\hat{x}_i$ is state estimate, $P_{ii}$ represents $i$-th state variance, and it can be extracted from cavarinace matrix $\mathbf{P}$. Parameter $a$ is a rejection treshold. Outlier classification based on a condition (2.34) can work quite well but tends to require the setting of threshold $a$ that defines whether a point is an

outlier or not. This threshold value typically needs to be tuned manually beforehand in order to determine its empirically optimal value for the system.

If a measurement model contains measurements that are some linear or even nonlinear combination of system states, e.g. range and bearing measurement provided by USBL unit, then covariance transformation must be performed in order to perform test given with (2.34). If a vector transformation from one coordinate system to another is written as $\boldsymbol{x_2} = \boldsymbol{f}(\boldsymbol{x_1})$ then the covariance transformation between the two coordinate systems is given with:

$$\mathbf{P_2} = \mathbf{J}\mathbf{P_1}\mathbf{J}^T, \tag{2.35}$$

where $\boldsymbol{J}$ is a Jacobian matrix defined with $\mathbf{J} = \frac{\partial \boldsymbol{f}(\boldsymbol{x_1})}{\partial \boldsymbol{x_1}}$.

In thesis, most common transformation was transformation of relative range and bearing measurements in polar coordinates to $\{\mathbf{E}\}$. This transformation was done in two steps, from polar coordinates to $\{\mathbf{B}\}$, and finally to $\{\mathbf{E}\}$, [46]. By definition, covariance matrix of vehicle and target relative position can be written as :

$$\boldsymbol{\Sigma} = \mathbf{E}\left[(\mathbf{p}_p - \mathbf{E}(\mathbf{p}_p))(\mathbf{p}_p - \mathbf{E}(\mathbf{p}_p))^T\right], \tag{2.36}$$

where $\mathbf{p}_p = \begin{bmatrix} \Delta x & \Delta y \end{bmatrix}^T$. Covariance transformation between relative position in Earth–fixed $\{\mathbf{E}\}$ and relative position in body–fixed frame $\{\mathbf{B}\}$ is given with (2.35) where $\boldsymbol{\Sigma}$ is $\{\mathbf{E}\}$ frame coordinate covariance matrix and $\mathbf{R}$ is the rotation matrix, [47].

$$\boldsymbol{\Sigma}_{rel} = \mathbf{R}_p \boldsymbol{\Sigma} \mathbf{R}_p^T \tag{2.37}$$

Relationship between relative Cartesian and polar coordinate system is given with nonlinear equation expression:

$$\begin{bmatrix} r \\ \Theta \end{bmatrix} = \begin{bmatrix} \sqrt{\Delta x_{rel}^2 + \Delta y_{rel}^2} \\ \arctan\left(\Delta y_{rel}, \Delta x_{rel}\right) \end{bmatrix}. \tag{2.38}$$

In order to transform the covariance matrix, Jacobian of Cartesian-to-polar covariance transformation is written as [48]:

$$\mathbf{J} = \begin{bmatrix} \frac{\partial r}{\partial \Delta x_{rel}} & \frac{\partial r}{\partial \Delta y_{rel}} \\ \frac{\partial \Theta}{\partial \Delta x_{rel}} & \frac{\partial \Theta}{\partial \Delta y_{rel}} \end{bmatrix} = \begin{bmatrix} \frac{\Delta x_{rel}}{r} & \frac{\Delta y_{rel}}{r} \\ -\frac{\Delta y_{rel}}{r^2} & \frac{\Delta x_{rel}}{r^2} \end{bmatrix} \tag{2.39}$$

Finally, covariance matrix in relative polar coordinates $\boldsymbol{\Sigma}_{pol}$ is calculated as:

$$\boldsymbol{\Sigma}_{pol} = \mathbf{J}\boldsymbol{\Sigma}_{rel}\mathbf{J}^T, \tag{2.40}$$

and such covariance matrix can be used to test if range or bearing measurement is considered an outlier, as shown in [46].

In some cases, measurements are used outside the filter and measurement model is not available. In such cases, approach from [49], where a Bayesian weighted regression algorithm that is able to automatically detect and eliminate outliers in real-time, without requiring any interference from the user, parameter tuning, sampling or model assumptions about the underlying data structure was used.

Since range measurements are integral for localization and navigation problems presented in this thesis, outlier rejection filter based on incremental version of the outlier rejection algorithm presented in [49] was implemented in Robot Operating System (ROS) and tested online on range measurements provided by SeaTrac USBL unit described in Section 1.3.2. Testing was conducted inside outdoor pool area. In such environment outliers in range measurements are quite common due to reflections from the side walls of the pool. Some results are shown in Figure 2.5. In the beginning all measurements are considered outliers because Bayesian weighted regression filter converges to the measurement value. Despite abrupt changes in the range measurement as at time instant $t = 100\,\text{s}$, outliers are successfully detected, with two false detections during the 400 seconds segment. In general, from conducted trials it was shown that sufficiently accurate range measurements can be acquired and therefore implementation and testing of underwater localization and navigation algorithms envisioned in this thesis in the real life conditions was deemed feasible at the early stages of the research conducted in the scope of this thesis.
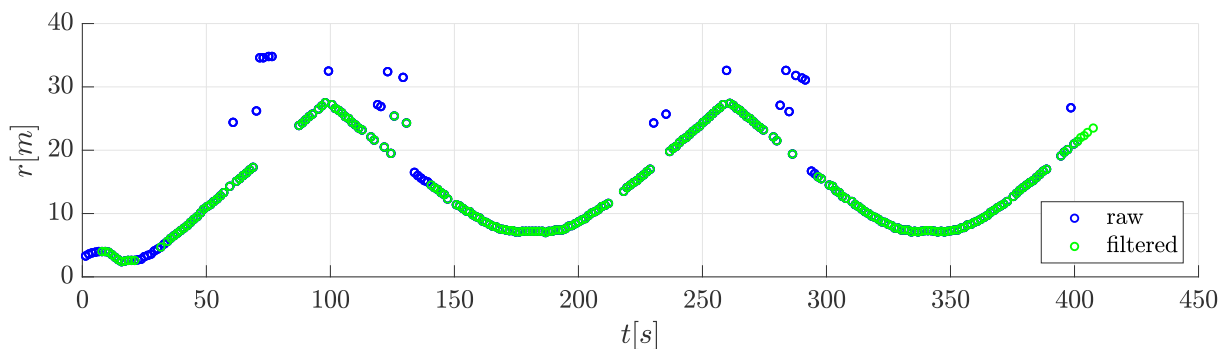


**Figure 2.5:** Outlier rejection test with range data acquired by SeaTrac USBL unit.

### 2.2.2   High–level control

In order to control the vehicle position and orientation, set of high–level controllers was deployed. Their inputs are position and orientation references and state estimates, while outputs are speed references in $\{\mathbf{B}\}$. Proportional-Integral (PI) controllers were used

in high–level controllers since such type of controller compensates all environmental disturbances. In addition to that, the integral action will compensate all the unmodelled dynamics and ensure convergence of the desired position or orientation. In general, PI controllers are defined with:

$$u(t) = K_P e(t) + K_I \int_0^t e(\tau) \mathrm{d}\tau. \tag{2.41}$$

where $e(t)$ is error value calculated as difference between desired setpoint and measured process value, while $K_P$ and $K_I$ are proportional and integral gain respectively. Each controller parameter is selected in such a way that the desired caracteristic equation and convergence of the closed loop is ensured. More about controller prameter tuning can be found in [24]. Going further, all the references for the low–level and high–level controllers are marked with superscript "$*$".

**Heading control**

The controller generates the desired yaw rate $r^*$ and can be written in the form

$$r^* = K_{P\psi} \left( \psi^* - \psi \right) + K_{I\psi} \int \left( \psi^* - \psi \right) \mathrm{d}t. \tag{2.42}$$

**Depth control**

The controller generates the desired heave speed $w^*$ and can be written in the form

$$w^* = K_{Pw} \left( z^* - z \right) + K_{Iw} \int \left( z^* - z \right) \mathrm{d}t. \tag{2.43}$$

**Dynamic positioning (DP) controller**

Fully actuated vehicles can move in a horizontal plane while keeping a desired heading. Here it is assumed that the dynamic positioning controller is in charge only of position keeping, while the heading controller described in the previous subsection is in charge of heading control. In order to perform the dynamic positioning algorithm, difference between the desired position and the current position in the horizontal plane is defined with:

$$\mathbf{e} = \begin{bmatrix} x^* - x \\ y^* - y \end{bmatrix}. \tag{2.44}$$

The kinematic positioning model can be obtained by differentiation, resulting in (2.45), under the assumption that the desired positions are constant values.

$$\dot{\mathbf{e}} = -\mathbf{R}\left(\psi\right) \begin{bmatrix} u \\ v \end{bmatrix} \tag{2.45}$$

Based on the DP model given with (2.45), the high–level dynamic positioning controller can be written in the form

$$\begin{bmatrix} u^* \\ v^* \end{bmatrix} = \mathbf{R}^{\mathrm{T}}\left(\psi\right)\left(\mathbf{K_{P,DP}}\mathbf{e} + \mathbf{K_{I,DP}} \int \mathbf{e}dt\right) \tag{2.46}$$

where $\mathbf{e}$ is given with (2.44). Algorithm, as presented herein, can be deployed strictly on fully actuated vehicles.

**Underactuated line following control**

Underactuated USVs (usually rudder actuated) can perform line following behaviour by changing the attack angle towards the desired line using the rudder. In [50] it was shown that this nonlinear system converges to the desired line even under the presence of external disturbances. This behaviour, where heading is changed to approach the line, can sometimes also be useful in overactuated vehicles, regardless of the superior performance capabilities. For example, if PLADYPOS is used to tug an object between its legs along a line, such as in [51], it is much more convenient to use the underactuated behaviour to prevent losing the tugged object due to lateral motion.



(a) Underactuated

(b) Fully actuated
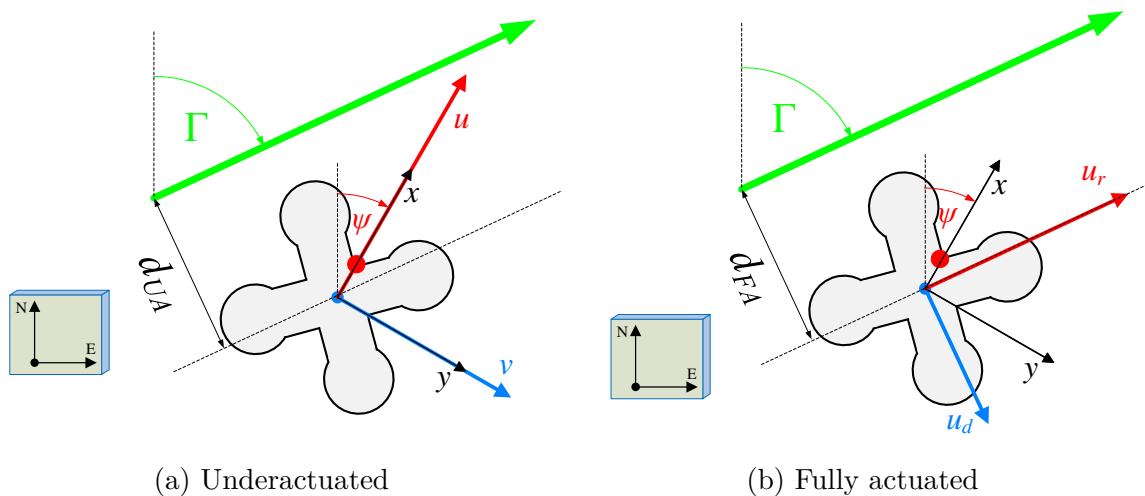
**Figure 2.6:** While in b the USV changes the attack angle ($\beta = \psi - \Gamma$) to converge to the line, in a the USV is capable of vectored control, generating the speed perpendicular to the desired line.

The underactuated line following approach is shown in Figure 2.6a. As described in [50], the aim is to steer the USV moving at surge speed $u$ in such a way that its path converges to the desired line. If $\Gamma$ is orientation of the line that should be followed, a new parameter $\beta = \psi - \Gamma$ (vehicle's orientation relative to the line) is defined. The kinematic line following equation for underactuated vehicles is then described with (2.47) and (2.48), where $\xi$ is drift due to projection of external disturbances along the direction perpendicular to the commanded line.

$$\dot{\beta} = r \tag{2.47}$$

$$\dot{d}_{UA} = u \sin \beta + \xi \tag{2.48}$$

The nonlinear equation (2.48) can be linearized if angle $\beta$ is assumed to be small, resulting in $\dot{d}_{UA} = u\beta + \xi$. The line–following model is in fact a special case of underactuated uncoupled kinematics providing linearised distance from the line. Based on the model given with (2.47) and (2.48) the line following controller for underactuated vehicles (or fully actuated vehicles that are required to perform the manoeuver specific to the underactuated vehicles) is given with:

$$r^* = -K_{P,d_{UA}} d_{UA} - K_{D,d_{UA}} \dot{d}_{UA}. \tag{2.49}$$

It should be mentioned that controller parameters depend on the forward speed $u$ of the vehicle, what follows from (2.48).

**Fully actuated line following control**

In the case of fully actuated line following, the vehicle can converge to the desired line while holding an arbitrary heading. According to the notation in Fig. 2.6b, the kinematic model is given with (2.50) while $u_r$ and $u_d$ can be calculated using (2.51). The assumption in this model is that heading $\psi$ is constant during the manoeuvre.

$$\dot{d}_{FA} = u_d + \xi \tag{2.50}$$

$$\begin{bmatrix} u_r \\ u_d \end{bmatrix} = \begin{bmatrix} \cos(\Gamma - \psi) & \sin(\Gamma - \psi) \\ \sin(\Gamma - \psi) & \cos(\Gamma - \psi) \end{bmatrix} \begin{bmatrix} u \\ v \end{bmatrix} \tag{2.51}$$

Based on the model given with (2.50) the line following controller for fully actuated vehicles is given with:

$$u_d^* = -K_{P,d_{FA}} d_{FA} - K_{I,d_{FA}} \int d_{FA} \mathrm{d}t. \tag{2.52}$$

The desired $u^*$ and $v^*$ can then be calculated using (2.51).

## 2.2.3   Low–level (speed) control

For the low–level speed controller we choose a PI controller given with (2.53) where $\boldsymbol{\nu}^* = \begin{bmatrix} u^* & v^* & w^* & r^* \end{bmatrix}^{\mathrm{T}}$ are the desired linear and angular speeds of the vehicle, $\mathbf{K_{P\nu}} = diag\left(K_{Pu}, \ K_{Pv}, \ K_{Pw}, \ K_{Pr}\right)$ and $\mathbf{K_{I\nu}} = diag\left(K_{Iu}, \ K_{Iv}, \ K_{Iw}, \ K_{Ir}\right)$ are diagonal matrices with proportional and integral gains for individual degrees of freedom, respectively.

$$\boldsymbol{\tau} = \mathbf{K_{P\nu}}\left(\boldsymbol{\nu}^* - \tilde{\boldsymbol{\nu}}\right) + \mathbf{K_{I\nu}} \int \left(\boldsymbol{\nu}^* - \tilde{\boldsymbol{\nu}}\right) \mathrm{d}\mathbf{t} + \boldsymbol{\tau_F} \tag{2.53}$$

The tilde sign marks the estimated values – the vehicle's speeds are often estimated since they are either difficult to measure or are unreliable. The $\boldsymbol{\tau_F}$ term represents additional action introduced in the controller to improve the closed loop behaviour, [50]. This action can be in the form $\boldsymbol{\tau_F} = \mathbf{D}\left(\boldsymbol{\nu}\right)\boldsymbol{\nu}$ which results in the feedback linearisation procedure where measured or estimated speeds are used to compensate for the nonlinearity in the process. It is more usual and convenient to use feedforward term $\boldsymbol{\tau_F} = \mathbf{D}\left(\boldsymbol{\nu}^*\right)\boldsymbol{\nu}^*$. Controller parameters $\mathbf{K_{P\nu}}$ and $\mathbf{K_{I\nu}}$ can be calculated based on the desired closed loop characteristic equation as it is shown in [50]. These parameters will naturally depend on the parameters of the dynamic model which have to be identified. The dynamic model parameters of the platform that is addressed in this article have been identified using the identification method based on self–oscillations reported in [52].

# Chapter 3

# Navigation and Control of Marine Vehicles Using Single Range Measurements

Autonomous surface marine vessels navigate using available measurements from sensors such as Global Positioning System (GPS) for position, sensors based on the Doppler effect as the Doppler velocity logger (DVL) to measure speed, and inertial sensors that measure acceleration of the vessel. However, underwater localization and tracking of underwater targets presents a great challenge in marine robotics due to absence of global positioning signals that are usually available in areas reachable by satellites. Due to that, AUVs rely on dead–reckoning, using measurements obtained from speed and inertial sensors. Because of measurement noise and model inaccuracies, localization error is unbounded over time, so many autonomous underwater vehicles occasionally surface in order to get GPS measurements and thereby determine their own position. In order to tackle this problem, acoustic based localization techniques such as LBL, SBL, USBL, briefly described in Section 1.1, are used for underwater localization and navigation. While LBLs require inconvenient deployment of multiple underwater beacons around the operational area, USBLs that enable relative underwater localization using acoustic propagation and are most often used for tracking underwater objects are quite expensive. In order to overcome these problems in some situations, a navigation method of using range measurements from a single beacon can be applied. The general assumption is that an underwater agent, e.g. AUV or diver, is trying to navigate underwater (determine its position in the global frame) by using proprioceptive sensors (DVL and/or inertial measurements) and range measurements from the beacon that is stationary or mobile and knows its absolute position.

In order to use single range navigation, range measurements must be acquired. There-

fore, in Section 3.1 short overview of the techniques used for acquisition of acoustic range measurements is given before single range navigation is presented in Section 3.2. In there, mathematical models of two beacon scenarios are presented. First scenario, in which the beacon is stationary, is practical for applications like homing. However, in order to estimate its position, the vehicle has to travel sufficiently informative trajectories and that disables the vehicle from doing other useful activities, e.g. bathymetry, which require trajectories that are not informative enough. In order to avoid that, a scenario with two vehicles, where one of them is a beacon, can be used. In that case a mobile beacon, which knows its position accurately, is responsible for travelling trajectories which will provide informative range measurements. Nonlinear systems can be poorly– or non–observable along specific state and output trajectories and ensuring the observability of range-only navigation systems is an important issue discussed in Section 3.2.3.

In order to reach some object of interest it is necessary to localize that object, and then use some control algorithm to steer the vehicle to that location. However, in the literature there are also the so–called extremum seeking approaches, where location of some object is not explicitly known but gradient that shows the direction toward the object can be determined. Example of such applications is vehicle homing/docking or black box localization. In Section 3.3 brief overview of the extremum seeking control technique is given, while in Section 3.3.2 extremum seeking is presented as a means of navigating towards the underwater objects by using single range measurements.

## 3.1 Acoustic acquisition of range measurements

In Section 1.1, difficulties encountered in the underwater communication and localization were presented. In this section, the topic of underwater range acquisition using acoustic modems is covered. The acoustic range measurements are acquired using one–way travel time or two–way travel time ranging techniques, as shown in Figure 3.1. One–way time travel (OWTT) range is estimated from the Time–of–Flight (TOF) of acoustic data packets propagating between an underwater acoustic modems on the beacon and the vehicle side (See Figure 3.1a), and such ranging requires precision clocks to synchronize the modems. The one–way TOF is calculated from the difference between the Time–of–Launch (TOL) encoded in the acoustic packet, measured by a precision clock aboard the beacon, and the Time–of–Arrival (TOA), measured by a precision clock aboard the underwater vehicle. The mathematical expression for OWTT range calculation is

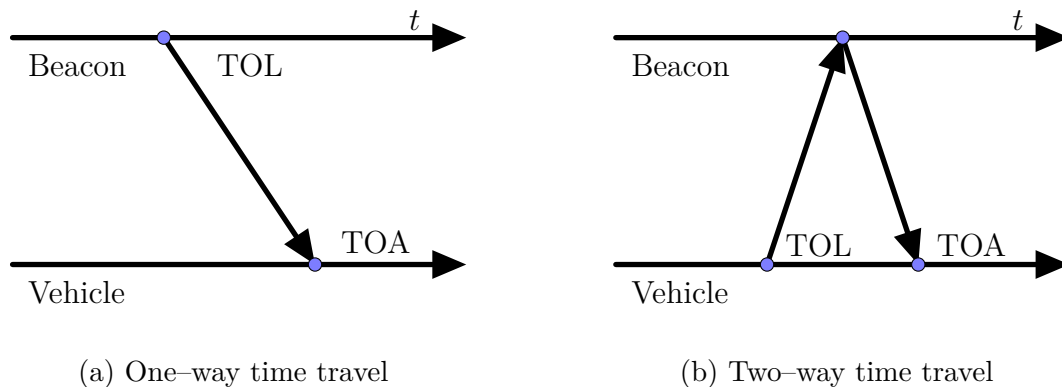$$r_{OWTT} = (TOA - TOL)\, c, \qquad (3.1)$$

(a) One–way time travel        (b) Two–way time travel

**Figure 3.1:** One–way time travel and two–way time travel interrogation scheme.

where $c$ denotes speed of sound in the water, which is typically $c \approx 1500 \frac{m}{s}$. In practice, measured time of arrival difference also includes the signal processing time, which has to be taken into account during calculation. The accuracy of TOF measurements is limited by the accuracy of the precision clocks residing on the beacon and the underwater vehicle. To ensure valid TOF measurements, it is crucial that the clocks on the sender and the receiver remain synchronized throughout the dive to within an acceptable tolerance, [53].

Two–way time travel (TWTT) is the most commonly used ranging technique. It requires the interaction between the beacon and the vehicle in such way that the vehicle side acoustic modem sends a request, marking TOL, to the beacon vehicle modem which responds to the request. A vehicle modem receiving reply from the beacon marks TOA and the range is then estimated from the calculated time difference (See Figure 3.1b). The mathematical expression for TWTT range calculation is

$$r_{TWTT} = (TOA - TOL) \frac{c}{2}. \tag{3.2}$$

Since TOL and TOA are measured on the vehicle side, TWTT does not require a clock synchronization between two vehicles. The advantage of OWTT is that multiple vehicles can determine the range from the beacon at the same time, unlike TWTT where one vehicle can determine the range at once. On the other hand, clock synchronization over longer periods, required in OWTT, is difficult to achieve in practice.

Using range measurements, acquired by an acoustic ranging technique, for position estimation poses a great challenge because these measurements are not available at every time instant and outliers are a common phenomena. Also, underwater range measurements are affected by a different error inducing factors such as speed of sound profile dependent on the water physical characteristics, the reflections from physical obstacles, and a degrading signal–to–noise ratio as the distance from two objects rises, [54]. The range error model in which covariance depends on the distance between the two objects

whose distance we want to measure is given with, [55]:

$$\zeta_r = (1 + \mu r^\gamma) \zeta_0 \tag{3.3}$$

where $\zeta_r$ is the measurement noise, $\zeta_0$ is a zero mean Gaussian process $\mathcal{N}\left(0, \sigma_0^2\right)$, $r$ is range, and $\mu$ and $\gamma$ are the modelling parameters for the distance-dependent noise component. It must be noted that in practice, the assumption of range measurement noise as a zero mean Gaussian distribution, i.e. parameter $\eta = 0$, is often used.

## 3.2   Navigation using single range measurements
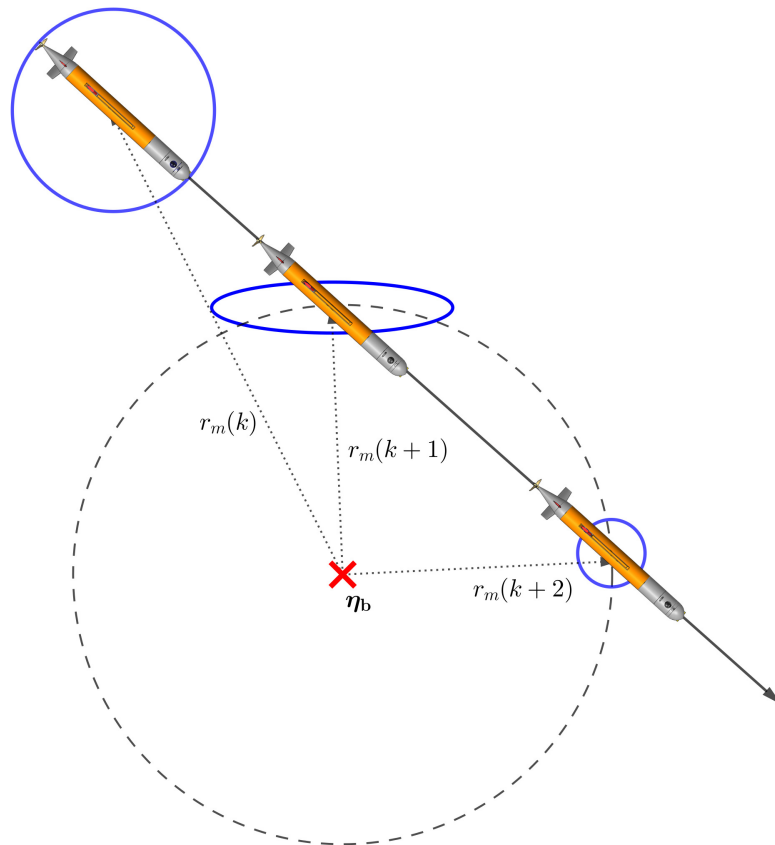


**Figure 3.2:** Single range navigation. Blue lines denote vehicle position error ellipses, red cross marks beacon position.

Single range navigation is a navigation technique which is used when no other means of acquiring a relative or an absolute position of the system is available and range measurements can be provided by the available sensors. The range measurements are acquired with a frequency that is usually very–low and in between the two measurements, systems usually rely on dead–reckoning in which the position error grows unbounded over time.

However, this localization error can be bounded by using the range measurements. In Figure 3.2, the main concept of the single range navigation is depicted. In there, AUV is shown travelling along the straight line in the horizontal plane at three different time instants denoted with variable $k$. The range measurement is defined as a norm of the vector between the vehicle and the beacon:

$$r_m = \|\boldsymbol{r}\| = \|\boldsymbol{\eta} - \boldsymbol{\eta_b}\| \tag{3.4}$$

where vehicle position is denoted with $\boldsymbol{\eta}$, and beacon position is denoted with $\boldsymbol{\eta}_b$. In practice, the acoustic range measurements are taken at discrete time instants and symbol $k$ denotes the time instant at which a measurement is acquired. The error ellipses, drawn in blue color, represent an iso–contour of the Gaussian distribution, and allow visualization of a two dimensional (2D) confidence interval of the estimated AUV position, [56]. At the time instant $k$, the position uncertainty denoted with a blue error ellipse is the largest. At the time instant $(k + 1)$ new range measurement arrives and error is reduced in the direction of the measurement. The next measurement is taken at the $(k+2)$ time instant, and the position uncertainty is further reduced in the direction of that measurement. From this it can be seen that the relative position between the beacon and the AUV at the moment when the measurement is taken is very important. In [57], it is shown that localization uncertainty is the lowest in the direction of the measurement, while in all other directions it grows. Therefore, the vehicle has to move in order to acquire measurement in all directions and thus reduce uncertainty in the vehicle's position estimated by the single range navigation filter.

When using single range measurements for the vehicle localization, the relative position with respect to the beacon is estimated using a sequence of available range measurements which are fused into the state estimation model together with other available measurements. In Section 3.2.1 and Section 3.2.2 state estimation models used in the single range navigation are shown. In Section 3.2.3, vehicle motion required in order to make navigation system observable is discussed.

### 3.2.1  Static beacon state estimation model

In this chapter's introduction, possibility of using both static and mobile beacons was mentioned. First, we consider a scenario where the vehicle is navigating while the range is measured with respect to a stationary beacon. The vehicle's navigation filter which uses single range measurements is derived from the model given with equations (3.30) and, together with the available measurements, it is used to estimate all the states. The

navigation filter state vector, in this case, is defined with

$$\mathbf{x} = \begin{bmatrix} \boldsymbol{\nu}_1^T & \boldsymbol{\eta}_1^T & \boldsymbol{\xi}_c^T \end{bmatrix}^T \tag{3.5}$$

where the state $\boldsymbol{\nu}_1$ denotes vehicle's translational velocities, $\boldsymbol{\eta}$ denotes vehicle's position, and $\boldsymbol{\xi_c}$ denotes the influence of the sea currents. For such state definition, the estimation model is given with

$$\begin{bmatrix} \dot{\boldsymbol{\nu}}_1 \\ \dot{\boldsymbol{\eta}}_1 \\ \dot{\boldsymbol{\xi}}_c \end{bmatrix} = \begin{bmatrix} \boldsymbol{A}(\boldsymbol{\nu}) & \mathbf{0} & \mathbf{0} \\ \mathbf{R}_b^n & \mathbf{0} & \boldsymbol{I} \\ \mathbf{0} & \mathbf{0} & \mathbf{0} \end{bmatrix} \begin{bmatrix} \boldsymbol{\nu}_1 \\ \boldsymbol{\eta}_1 \\ \boldsymbol{\xi}_c \end{bmatrix} + \begin{bmatrix} \boldsymbol{B}(\boldsymbol{\nu}) \\ \mathbf{0} \\ \mathbf{0} \end{bmatrix} \begin{bmatrix} \boldsymbol{\tau} \end{bmatrix} + \boldsymbol{\zeta}, \tag{3.6}$$

where $\mathbf{A}(\boldsymbol{\nu}) = \text{diag}\left(-\frac{\beta(u)}{\alpha_u}, \ -\frac{\beta(v)}{\alpha_v}, \ -\frac{\beta(w)}{\alpha_w}\right), \mathbf{B}(\boldsymbol{\nu}) = \text{diag}\left(\frac{1}{\alpha_u}, \ \frac{1}{\alpha_v}, \ \frac{1}{\alpha_w}\right)$, terms $\alpha_i$ represent vehicle's dynamics in respective directions, and $\beta_i$ represents the linear hydrodynamic damping terms, as shown in Section 2.1.2. The navigation filter measurement model, in the case of a stationary beacon, is

$$\mathbf{y} = \begin{bmatrix} \boldsymbol{\nu}_{\mathbf{1m}}^T & r_m \end{bmatrix}^T, \tag{3.7}$$

with range measurement $r_m$ modelled as

$$r_m = \|\boldsymbol{\eta} - \boldsymbol{\eta_b}\| + \zeta_r, \tag{3.8}$$

where $\zeta_r \sim \mathcal{N}(0, \sigma_r^2)$ is the Gaussian measurement noise. The measurement $\boldsymbol{\nu_m}$ represents a nonlinear measurement model of the vehicle's absolute velocity in $\{\mathbf{B}\}$ coordinate frame which can be provided by the sensors such as DVL. DVL sensor measures the velocity of the sensor relative to the water or bottom, based on the Doppler effect, [58]. DVL measurements are usually fused with an Attitude Heading Reference System (AHRS) to provide improved dead-reckoning navigation, [59]. For example, the DVL sensor measurement $\mathbf{y}_{DVL}$ can be modelled with

$$\mathbf{y}_{DVL} = \boldsymbol{\nu}_1 + \mathbf{R}_e^b \boldsymbol{\xi_c} + \boldsymbol{\zeta}_D, \tag{3.9}$$

where $\boldsymbol{\zeta}_D \sim \mathcal{N}(0, \sigma_D^2)$ is a Gaussian measurement noise, $\boldsymbol{\nu}_1$ are the vehicle's linear velocities, $\boldsymbol{\xi_c}$ are currents acting on the vehicle, and $\mathbf{R}_e^b$ is rotation from $\{\mathbf{E}\}$ to $\{\mathbf{B}\}$ frame. The measurement model (3.9) assumes that the so–called DVL bottom–lock is available, i.e. it measures vehicle speed over seabed. If no bottom–lock is available, DVL measures only vehicle speed with respect to the surrounding water, and the model is then $\mathbf{y}_{DVL} = \boldsymbol{\nu}_1 + \boldsymbol{\zeta}_D$.

The measurement model, presented herein, assumes that velocity measurement is avail-

able. However, depending on the available sensors, this measurement may not be available, while in some other cases additional measurements which can further improve filter convergence will be available. In the model, we neglected vehicle's orientation $\boldsymbol{\eta}_2$ and rotational speeds $\boldsymbol{\nu}_2$, since in most common cases vehicle orientation in $\{\mathbf{E}\}$ can be measured using AHRS, filtered if necessary, and then used as an input to single range navigation estimation filter. In practice, depth measurements are usually available, thereby three dimensional (3D) single range estimation problem can be reduced to a 2D localization problem.

As it was already mentioned, range measurements are not available at every time sample, so when the measurement is not available, vehicle is performing dead-reckoning and matrix $\mathbf{H}$ used to calculate measurement innovation in state estimation must be adjusted accordingly. Measurement matrix $\mathbf{H}$ used when the range measurement is available is defined as

$$
\begin{bmatrix}
1 & 0 & 0 & 0 & 0 & 0 & 0 & -v_x s\psi + v_y c\psi & c\psi & s\psi & 0 \\
0 & 1 & 0 & 0 & 0 & 0 & 0 & -v_x c\psi - v_y s\psi & -s\psi & c\psi & 0 \\
0 & 0 & 0 & 0 & 0 & 0 & 1 & 0 & 0 & 0 & 0 \\
0 & 0 & 0 & 0 & 0 & 0 & 0 & 1 & 0 & 0 & 0 \\
0 & 0 & 0 & 0 & \frac{x}{r} & \frac{y}{r} & \frac{z}{r} & 0 & 0 & 0 & 0
\end{bmatrix}, \tag{3.10}
$$

where the symbols $s(\cdot)$ and $c(\cdot)$ denote $\sin(\cdot)$ and $\cos(\cdot)$, respectively and $r = \sqrt{x^2 + y^2 + z^2}$. The matrix $\mathbf{H}$ used during the dead–reckoning phases of the estimation is

$$
\begin{bmatrix}
1 & 0 & 0 & 0 & 0 & 0 & 0 & -v_x s\psi + v_y c\psi & c\psi & s\psi & 0 \\
0 & 1 & 0 & 0 & 0 & 0 & 0 & -v_x c\psi - v_y s\psi & -s\psi & c\psi & 0 \\
0 & 0 & 0 & 0 & 0 & 0 & 1 & 0 & 0 & 0 & 0 \\
0 & 0 & 0 & 0 & 0 & 0 & 0 & 1 & 0 & 0 & 0 \\
0 & 0 & 0 & 0 & 0 & 0 & 0 & 0 & 0 & 0 & 0
\end{bmatrix}. \tag{3.11}
$$

Notice that the matrix $\boldsymbol{H}$ terms related to the range measurement are zero at the time instants when there are no range measurements and consequently there is no new information that can be fused to improve estimation.

When the static beacon is employed, its position is usually known in advance, or only relative localization with respect to the beacon is required. In those cases, the data transfer between the vehicle and the beacon is not needed. Notice that, for the static beacon scenario, without the loss of generality, we assume that the beacon is in the coordinate frame $\{\mathbf{E}\}$ origin. By taking derivative of $\mathbf{r}$, we get $\dot{\mathbf{r}} = \dot{\boldsymbol{\eta}} - \dot{\boldsymbol{\eta}}_b$. In the case of a static beacon $\dot{\boldsymbol{\eta}}_b = \mathbf{0}$ and it follows that $\dot{\mathbf{r}} = \dot{\boldsymbol{\eta}}$, thus confirming earlier proposition.

## 3.2.2 Mobile beacon state estimation model

One of the main issues with single range navigation systems is the observability of the system. A range measurement, in conjunction with the depth of the vehicle measured from a pressure sensor, constrains the vehicle position to a circle of solutions. Between the two adjacent range measurements, the relative vehicle motion is estimated using the velocity and attitude measurements. It is known that the vehicle that is using the single range measurements for the localization must execute the trajectories that are persistently exciting in order to keep the system observable, otherwise acquired range measurements can result in false navigation. However, in real life situations, the underwater vehicle has a specific mission to perform and should not accommodate it to enhance the system's observability and therefore positioning quality. Using a mobile beacon as navigational aid removes the constraints imposed on the underwater vehicle trajectory because the mobile beacon executes trajectories that ensure the persistently exciting range measurements.

State vector of the centralized Kalman filter, containing both the vehicle and the beacon states, $\mathbf{x}_C$ is derived from the state vector (3.5), by augmentation with the mobile beacon states, resulting in

$$\mathbf{x}_C = \begin{bmatrix} \boldsymbol{x}^T & \boldsymbol{\nu}_b^T & \boldsymbol{\eta}_b^T \end{bmatrix}^T, \tag{3.12}$$

where subscript $\boldsymbol{b}$ denotes the mobile beacon states. The state estimation model is

$$\begin{bmatrix} \dot{\boldsymbol{x}} \\ \dot{\boldsymbol{\eta}}_b \\ \dot{\boldsymbol{\nu}}_b \end{bmatrix} = \begin{bmatrix} \mathbf{A_1} & \mathbf{0} & \mathbf{0} \\ \mathbf{0} & \mathbf{0} & \mathbf{R}_b^n \\ \mathbf{0} & \mathbf{0} & \mathbf{0} \end{bmatrix} \begin{bmatrix} \boldsymbol{x} \\ \boldsymbol{\eta}_b \\ \boldsymbol{\nu}_b \end{bmatrix} + \begin{bmatrix} \mathbf{B_1} \\ \mathbf{0} \\ \mathbf{0} \end{bmatrix} \begin{bmatrix} \boldsymbol{\tau} \end{bmatrix} + \boldsymbol{\zeta}, \tag{3.13}$$

where matrices $\mathbf{A_1}$ and $\mathbf{B_1}$ are state and input matrices from (3.6). The estimation model as presented herein, estimates both the underwater vehicle and mobile beacon states, thus the term centralized. In the most simple cases, beacon measurements can be used as an input to the model, therefore reducing the number of states in the filter. The accompanying measurement vector $\mathbf{y}_C$ is defined as

$$\mathbf{y}_C = \begin{bmatrix} \mathbf{y}^T & \boldsymbol{\nu}_{bm}^T & \boldsymbol{\eta}_{bm}^T \end{bmatrix}^T. \tag{3.14}$$

The measurement vector (3.14) is augmented with the beacon measurements, $\boldsymbol{\nu}_{bm}$ and $\boldsymbol{\eta}_{bm}$ which are received over the acoustic link. It is assumed that $\boldsymbol{\nu}_{bm}$ measurement already contains sea current contribution. It is important to notice that all these measurements, sent by the acoustic link, are delayed measurements. This delay can be ignored, during the measurement fusion, if the beacon is travelling at slower speed. In order to account for these delays, and improve the position estimate, the method of backward recalculation

presented in Section 2.2.1 can be applied. Also, due to the delay and the small measurement update rate, if the mobile beacon suddenly changes direction, that information is unknown to the vehicle until the data in the next communication cycle is exchanged. As already emphasized, the acoustic communication bandwidth is severely limited compared to the conventional wireless communication. Depending whether the mobile beacon kinematics are modelled as underactuated or fully actuated, data sets $\{u_b, r_b, x_b, y_b\}$ or $\{u_b, v_b, r_b, x_b, y_b\}$ sent over the acoustic link. In order to reduce the communication overhead, if necessary, only mobile beacon position can be sent to the vehicle, at the cost of deteriorated filter performance.

### 3.2.3 Observability in single range navigation

The notion of observability, of a linear or nonlinear dynamic system, concerns the possibility of recovering the state $x(t)$ from knowledge of the measured output $y(t)$, the input $u(t)$, and, possibly, a finite number of their time derivatives $y^{(k)}(t)$ and $u^{(l)}(t)$, where $k \geq 0$, and $l \geq 0$. The observability for the linear time-invariant systems is well understood and there exist several equivalent ways to define the observability, [60]. Observability of such systems is dependent exclusively on system parameters. On the other hand, nonlinear systems are more complicated since they can be poorly or non-observable along the specific state and output trajectories or in the certain regions of the state space, and observable in the others, [61]. Operating the system along such trajectories or in such regions can lead to poor state estimates being provided by an observer. Hence, it is desirable to avoid regions of weak observability in order to provide a satisfying estimation of the system states, e.g. in [62], approach to avoid weakly observable trajectories in the frame of nonlinear predictive control is presented. By using cost function that penalizes weakly observable trajectories, thus leading to avoidance of weakly or unobservable regions of operation, trade–off between following the predefined trajectory and good degree of observability is achieved.

Observability of the nonlinear system defined with $\dot{\mathbf{x}} = \mathbf{f}\left(\mathbf{x}, \mathbf{u}\right); \mathbf{y} = \mathbf{h}\left(\mathbf{x}\right)$ is usually inspected by performing the local observability analysis. Such system can be linearised about the nominal trajectory, resulting in a linear time–varying system defined with

$$
\begin{aligned}
\dot{\tilde{\mathbf{x}}}(t) &= \mathbf{A}(t)\tilde{\mathbf{x}}(t) \\
\tilde{\mathbf{y}}(t) &= \mathbf{C}(t)\tilde{\mathbf{x}}(t)
\end{aligned}
\tag{3.15}
$$

where $\tilde{x}(t) = x(t) - x^0(t)$, $x^0(t)$ and $u^0(t)$ denote the nominal trajectory, and the control

inputs around which system was linearised, and

$$\mathbf{A} = \left.\frac{\partial f}{\partial x}\right|_{x^0, u^0}, \quad \mathbf{C} = \left.\frac{\partial h}{\partial x}\right|_{x^0, u^0}. \tag{3.16}$$

The observability Gramian $\boldsymbol{W}$ for linear time–variant (LTV) systems is defined as, [63],

$$\boldsymbol{W}(t) = \int_0^t \boldsymbol{\Phi}(\tau)^T \mathbf{C}(\tau)^T \mathbf{C}(\tau) \boldsymbol{\Phi}(\tau) \, d\tau. \tag{3.17}$$

where $\boldsymbol{\Phi}(\tau) = e^{\mathbf{A}\tau}$ is the state transition matrix. The local observability properties of the original nonlinear system can be inferred using Gramian based tools for LTV systems applied to the linearised system (3.15). The most common observability test is a rank condition test. If the observability gramian $\boldsymbol{W}$ has full rank, meaning that matrix is nonsingular, then the system is locally observable.

In the case of nonlinear systems, particularly interesting is the notion of local weak observability given in [61]. Therein, definition of the indistinguishable states and local weak observability is given:

**Definition 1** *Two states* $\mathbf{x}_0$, $\mathbf{x}_1 \in \mathcal{M}$ *are said to be* indistinguishable, *if for every admissible input* $u(t)$, $t_0 \leq t \leq t_1$ *identical outputs result:* $y(t; \mathbf{x}_0) \equiv y(t; \mathbf{x}_1)$ *for* $t_0 \leq t \leq t_1$. *Notation* $I(\mathbf{x}_0)$ *denotes set of all points that are indistinguishable from* $\mathbf{x}_0$.

**Definition 2** *System* $\Sigma$ *is* locally weakly observable at $\mathbf{x}_0$ *if there is some neighbourhood* $\mathcal{V}$ *of* $\mathbf{x}_0$, *where* $I_{\mathcal{N}}(\mathbf{x}_0) \cap \mathcal{V} = \mathbf{x}_0$, *for all solutions* $\mathbf{x}(t)$ *completely in any neighbourhood* $\mathcal{N}$ *of* $\mathbf{x}_0$. *System* $\Sigma$ *is* locally weakly observable *if this property holds for all* $\mathbf{x} \in \mathcal{M}$.

Local weak observability of system, defined as $\dot{\mathbf{x}} = \mathbf{f}(\mathbf{x}, \mathbf{u})$, and $y = h(\mathbf{x})$, can be determined from the observability rank condition given in [61]. If observability matrix $\mathbf{O}$ calculated at $\mathbf{x_1}$, defined with:

$$\mathbf{O} = \begin{bmatrix} \nabla \mathcal{L}_f^0 h_j & \nabla \mathcal{L}_f^1 h_j & \dots & \nabla \mathcal{L}_f^k h_j \end{bmatrix}^T \tag{3.18}$$

has full rank for some input $\mathbf{u}$ than the system is locally weakly observable at $\mathbf{x}_1$. This criterion gives a sufficient condition for local weak observability. The Lie derivatives of the output, used in (3.18), are defined as: $\mathcal{L}_f^0 h_j = h_j, \mathcal{L}_f^1 h_j = \nabla h_j \cdot \mathbf{f} = \sum_{i=1}^n \frac{\partial h_j}{\partial x_i} \cdot f_i, \mathcal{L}_f^2 h_j = \nabla \left[\mathcal{L}_f^1 h_j\right] \cdot \mathbf{f}, \dots, \mathcal{L}_f^n h_j = \nabla \left[\mathcal{L}_f^{n-1} h_j\right] \cdot \mathbf{f}$, where $\nabla$ denotes gradient operator, and $\mathcal{L}_f^\alpha h_j$ represents set of the $\alpha$–order Lie derivative of the output $h_j$.

The rank condition, usually used in determining the observability of a system, does not give the information about the degree of observability, only whether the system is observable or not. In [64], the local unobservability index and the local estimation condition number were introduced to measure the degree of observability of a system. Local

unobservability index is reciprocal of the smallest local eigenvalue and it gives information on how difficult it is to estimate initial condition from the output. Local estimation condition number $\kappa$, given with (3.19), is the ratio between the largest and the smallest local eigenvalue $\lambda$ of the observability Gramian $\boldsymbol{W}$.

$$\kappa\left(\mathbf{W}\right) = \frac{\lambda_{max}\left(\mathbf{W}\right)}{\lambda_{min}\left(\mathbf{W}\right)} \tag{3.19}$$

Estimation problem is ill–conditioned when the condition number is much larger than 1 because that indicates that some outputs are more sensitive to small changes of the initial condition in one direction. In order to inspect the degree of observability for the notion of local weak observability, local estimation condition number can be calculated for the observability matrix $\mathbf{O}$ in the same fashion as for Gramian $\boldsymbol{W}$ in (3.19), i.e. by calculating $\kappa\left(\mathbf{O}\right)$.

Finally, the notion of Fisher Information Matrix (FIM) must be mentioned. FIM captures the amount of information that measured data provides about an unknown parameter to be estimated. Under known assumptions, the FIM is the inverse of the Cramer-Rao bound matrix ($CRB = FIM^{-1}$), which lower bounds the covariance of the estimation error that can possibly be obtained with any unbiased estimator, [65]. The FIM associated with a classical estimation problem is defined as the expected value of the logarithm of the derivative of the maximum likelihood function and in a case of a 3D single range measurement problem given in [54] as

$$FIM = \frac{1}{\sigma^2} \sum_{i=1}^{n} \begin{bmatrix} a_{ix}^2 & a_{iy}a_{ix} & a_{iz}a_{ix} \\ a_{ix}a_{iy} & a_{iy}^2 & a_{iz}a_{iy} \\ a_{ix}a_{iz} & a_{iy}a_{iz} & a_{iz}^2 \end{bmatrix} \tag{3.20}$$

where $\sigma^2$ is a measurement variance, and $a_{ij} = \frac{\partial \|q_i - p_i\|}{\partial q_{i,j}}$, for $i \in \{1, \ldots, n\}$, and $j \in \{x, y, z\}$. A point $q_i$ denotes vehicle position, while point $p_i$ denotes mobile beacon position. In [66], the link between the invertibility of the FIM and the observability status has been established, for a large class of probability laws in nonlinear regression problems and therefore FIM can be used in the study of observability.

## Observability analysis of a system using single range measurements

In the situations when absolute or relative position measurements are available, observability of the navigation system is practically guaranteed. However, using single range measurements for localization presents a big challenge, namely because certain trajectories can be poorly observable or even unobservable. Ensuring the observability of range-only navigation systems is an important issue and there is a great number of papers dealing

with that specific topic, [67, 68, 69, 70]. In single range estimation nonlinearity, and observability issues stem from the range measurement model (3.8). In both 2D and 3D environment, vehicle position cannot be determined from a single range measurement because such measurement yields multiple solutions bounded to a circle or a sphere with a certain radius. Also, the so–called kidnapping problem can appear. For a certain input, two initial states, symmetric with respect to the coordinate axis of the radial domain, despite being locally observable, give the same output and thus this initial states are indistinguishable, [69]. That means that, even if the system may be locally weakly observable along an assigned trajectory, if the initial state estimate of the EKF is not sufficiently close to the true initial state, there is no guarantee of the filter convergence, [70].

In [67], necessary and sufficient conditions for the observability of the nonlinear system are acquired by augmenting the states to obtain a linear time variant system. An important issue in determining the observability of the system is whether the currents influencing the vehicle are known. In [68] theoretical observability analysis using indistinguishable states is applied to cases with known and unknown constant currents, when the vehicles is executing constant course and constant course rate trajectories. It was shown that in the case of no ocean current, or known currents, observability is achieved for constant course trajectories, however in the case of unknown currents, constant course rate trajectories i.e. circular motion is needed to achieve observability. In [70] global observability analysis through state augmentation approach and local weak observability was analysed for 2D and 3D model. It was shown that the vehicle velocity with respect to the fluid and the ocean current cannot be distinguished one from the other if only range measurements are used for vehicle navigation.

In [69], by analysing simple 2D model, an observability metric for underwater vehicle localization using range measurements was given based on the condition number of the observability matrix. Such metric was used to characterize informative trajectories. Kinematic model of a system with known currents is defined with

$$\dot{\boldsymbol{\eta}} = \boldsymbol{v}; \quad h = \frac{1}{2}\boldsymbol{\eta}^T\boldsymbol{\eta} \tag{3.21}$$

where $\boldsymbol{\eta} = [x \ y]^T$ and $\boldsymbol{v} = [v_x \ v_y]$. Range measurements are represented as $\frac{1}{2}\boldsymbol{\eta}^T\boldsymbol{\eta}$ for easier calculation. Observability matrix for system (3.21) is

$$\mathbf{O} = \begin{bmatrix} \nabla\mathcal{L}_f^0 h \\ \nabla\mathcal{L}_f^1 h \end{bmatrix} = \begin{bmatrix} x & y \\ v_x & v_y \end{bmatrix} \tag{3.22}$$

From matrix (3.22) it is clearly visible that matrix has full rank and therefore observability rank condition is satisfied if $\boldsymbol{v} \neq \boldsymbol{0}$. To better inspect local estimation condition number

we can write vehicle position and relative speed vectors given in (3.22) in polar–like form as $\boldsymbol{\eta} = r \left[\cos\theta \sin\theta\right]^T$, and $\mathbf{v} = u \left[\cos\phi \sin\phi\right]^T$. Using these expressions observability matrix (3.22) can be written as

$$\mathbf{O} = u \begin{bmatrix} \gamma\cos\theta & \gamma\sin\theta \\ \cos\phi & \sin\phi \end{bmatrix}, \tag{3.23}$$

where $\gamma = \frac{r}{u}$, $r = \|\boldsymbol{\eta}\|$ and $u = \|\boldsymbol{v}\|$. Using (3.19) and substitution $\tilde{\alpha} = \phi - \theta$, yields local estimation condition number

$$\kappa\left(\mathbf{O}\right) = \frac{\gamma^2 + 1 + \sqrt{\gamma^4 + 2\gamma^2 \cos\left(2\tilde{\alpha}\right) + 1}}{2\gamma \left|\sin\left(\tilde{\alpha}\right)\right|}. \tag{3.24}$$

Inverse of local estimation condition number is shown in Figure 3.3. It shows that the degree of observability is the highest when relative position and velocity vectors are orthogonal and have same magnitude.
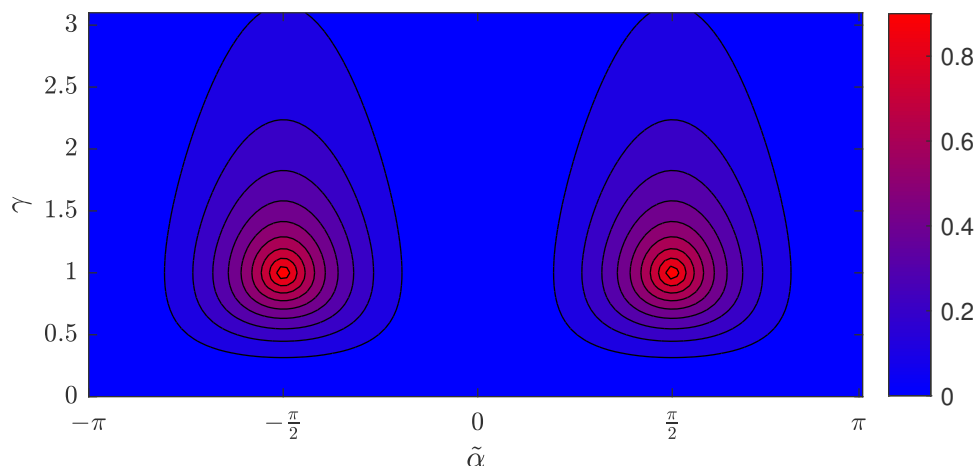


**Figure 3.3:** Local estimation condition number inverse $\kappa\left(\mathbf{O}\right)^{-1}$

The general conclusion from all of these papers is that in order to achieve certain degree of observability of the navigation filter, the vehicle must execute informative trajectories, i.e. trajectories with some curvature in the presence of unknown currents. The action of executing an informative trajectory clearly distracts the AUV from performing its original mission. In order to completely avoid that trade–off, it is left to the beacon to ensure informative measurements, thus resulting in the scenario of *mobile beacons*, which is already considered in Section 3.2.2. There is a number of ways of determining the path of a mobile beacon which ensures observablity of the underwater vehicle navigating using single range measurements, [57, 71]. Short overview of such techniques is given in Section 4.1.

## 3.2.4 Performance quality indices for single range localization algorithms

Fisher Information Matrix is used in the single range navigation literature, [72, 73], to measure how much the localization uncertainty can be reduced for a particular sequence of range measurements, e.g. in [72], FIM determinant, normalized by number of samples $|FIM|_n \in [0, 1]$, is used as a performance index, which for the 2D case is

$$|FIM|_n = \frac{|FIM|}{|FIM|^*} = \frac{4\sigma^4}{m^2} |FIM| \tag{3.25}$$

where term $|FIM|^*$ represents theoretical optimum that can be achived (See [55].), $m$ is the number of range measurements, $\sigma^2$ is measurement variance, and FIM determinant for the 2D single range navigation problem is calculated as, [73]:

$$|FIM| = \frac{1}{\sigma^4} \left[ \sum_{k=0}^{m-1} \left(\frac{x_k}{r_k}\right)^2 \sum_{k=0}^{m-1} \left(\frac{y_k}{r_k}\right)^2 - \left(\sum_{k=0}^{m-1} \frac{x_k}{r_k}\frac{y_k}{r_k}\right)^2 \right], \tag{3.26}$$

where $\boldsymbol{\eta}_k = \begin{bmatrix} x_k & y_k \end{bmatrix}^T$ denotes the vehicle position and $r_k$ range with respect to the beacon at time instant $k$. Larger value of the FIM determinant indicates that the sequence of measurements realized by the particular trajectory is more informative than the trajectory which produces the smaller value of the FIM determinant.

Validation of the vehicle trajectories used in single range navigation can be done for two distinct scenarios, with FIM based indices used as a main performance differentiator. The first scenario assumes that beacon is not cooperative and vehicle has to perform informative trajectories by itself. This does not necessarily assume that beacon is static, only that it does not take into account vehicle's trajectory while planning its own. In order to improve its localization, the vehicle needs to deviate from the nominal trajectory and therefore the quantities we are interested are trajectory tracking error and achieved localization accuracy. In general objectives of increasing localization accuracy and following trajectory required by the mission are conflicting objectives and trade–off has to be made for which the concept of Pareto optimality can be used, [74]. Pareto optimality is a formally defined concept used to determine when an allocation is optimal. An allocation is not Pareto optimal if there is an alternative allocation where improvements can be made to at least one objective without deteriorating any other objective, and it is commonly used in engineering problems to to examine the trade–off between different objectives.

Maximizing of the FIM determinant, as in [73], can be used to calculate the optimal vehicle trajectories. It is assumed that vehicle has a nominal trajectory that it needs to traverse, but limited deviation from nominal trajectory is allowed. If a second objective,

(a) Pareto front.
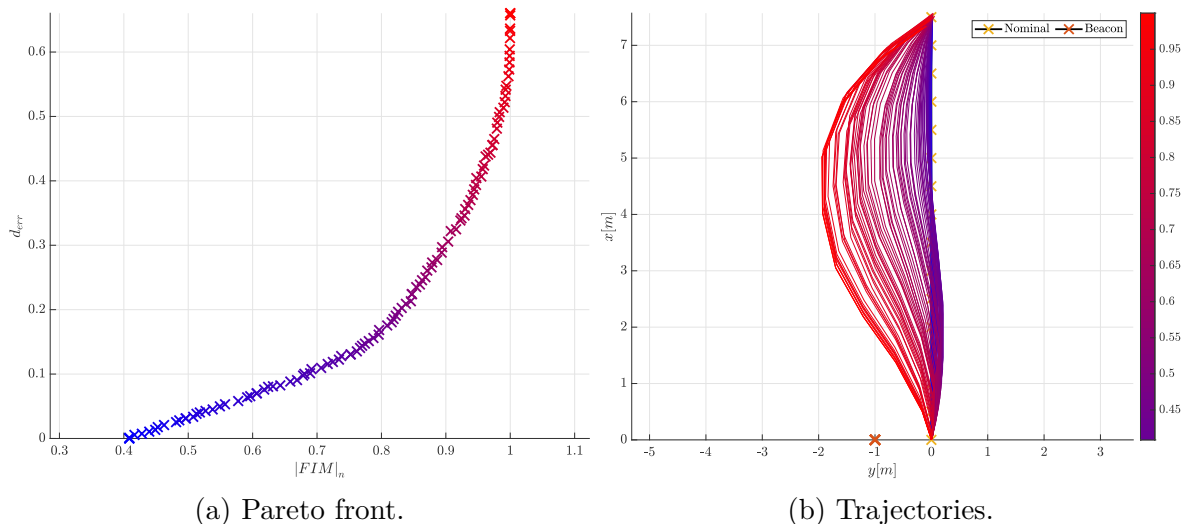
(b) Trajectories.

**Figure 3.4:** Pareto front and Pareto optimal trajectories.

i.e. deviation from the nominal path, is added then Pareto frontier can be found for such multi–objective optimization problem, as shown in Figure 3.4. The bigger the deviation from the nominal trajectory, the better localization can be achieved and therefore, depending on the mission requirements, trade–off must be done when planning trajectories.

The second scenario assumes that the vehicle executes nominal trajectory and mobile beacon executes trajectories which provide informative range measurements. In this case priority is localization accuracy of the single range navigation system. Depending on the requirements, the beacon's energy consumption can be variable of interest, traversed path length, and even distance from the target. It is worth noting that the problem where the vehicle executes the informative trajectory with respect to the uncooperative beacon, without any constraint regarding nominal trajectory, can be observed as an inverse problem of this scenario, in which vehicle is considered as a beacon and beacon as a target executing some trajectory. In the scope of this thesis, second scenario is more important and therefore performance indices for second scenario are given.

**Performance indices used in validation of the beacon executing informative trajectory**

As mentioned, this scenario assumes that the vehicle is executing the trajectory that is completely defined by its mission, and mobile beacon is responsible for assuming the trajectory which will provide informative range measurements. If FIM determinant, normalized by number of samples, (3.25), is used to account for every measurement acquired during the mission, for large number of samples possible sections of the trajectory which are far from optimal, are somewhat filtered. Acceptable trajectory will provide the informative measurements during the entire mission time. Thus, in order to validate the

beacon trajectory on a particular mission segment, a validation horizon $N_h$ is introduced and FIM determinant normalized by number of samples for the particular segment $i$ of the size $N_h$ is calculated as

$$|FIM|_{seg}(i) = \left| \sum_{k=iN_h}^{iN_h+N_h} FIM(k) \right|_n . \tag{3.27}$$

Using validation horizon, defined with parameter $N_h$, which is user assigned, and calculating $|FIM|_n$ over smaller number of samples, gives a more realistic picture about beacon trajectory. Finally, performance index, which summarizes how informative is the beacon trajectory during the whole mission, is calculated as an average of $|FIM|_{seg}$ cumulatively summed for total trajectory as

$$|FIM|_{avg} = \frac{1}{N_{seg}} \sum_{k=0}^{N_{seg}-1} |FIM|_{seg}(k), \tag{3.28}$$

where $|FIM|_n$ is given in (3.25), $N_{seg} = \text{floor}(\frac{N}{N_h})$, and $N$ is the total number of samples during the mission.

The second performance index $\Sigma_s$, that can be used for validation, is given with total path traversed by the beacon

$$\Sigma_s = \sum_{k=0}^{N-1} \left\| \boldsymbol{\eta}_{b|k+1} - \boldsymbol{\eta}_{b|k} \right\| . \tag{3.29}$$

In equation (3.29), total path is calculated by doing cumulative sum of line segments between the two measurement points because in between these measurements there is no information that can improve localization and linear approximation of vehicle trajectory is justified. In practice, the total path and how vehicle reaches the next measurement point depends on the vehicle dynamics and deployed control algorithms.

### 3.2.5 Simulation results

During the course of this thesis, single range navigation algorithms were tested in simulations, prior to any other work, since they were preprequisite for the algorithm presented in Chapter 4. The simulation experiments for both static and mobile beacon scenario were conducted in MATLAB simulation environment, where full vehicle dynamics together with velocity and position controllers were simulated and used to perform various vehicle trajectories. In order to estimate vehicle's position using single range measurements, EKF shown in Section 2.2.1, was deployed. Vehicle's navigation filter state model was implemented by discretizing vehicle kinematic equations (2.11) and vehicle dynamics equations

(2.7)–(2.10) by using Euler discretization method, [75], which yielded set of discrete equations (3.30).

$$u_{k+1} = u_k - \frac{\beta_{uu}}{\alpha_u} |u_k| u_k T + \frac{1}{\alpha_u} XT + \zeta_u T$$

$$v_{k+1} = v_k - \frac{\beta_{vv}}{\alpha_v} |v_k| v_k T + \frac{1}{\alpha_v} YT + \zeta_v T$$

$$w_{k+1} = w_k - \frac{\beta_{ww}}{\alpha_w} |w_k| w_k T + \frac{1}{\alpha_w} ZT + \frac{1}{\alpha_w} v_{zk} T + \zeta_w T$$

$$r_{k+1} = r_k - \frac{\beta_{rr}}{\alpha_r} |r_k| r_k T + \frac{1}{\alpha_r} NT + \zeta_r T$$

$$x_{k+1} = x_k + \cos\psi_k u_k T - \sin\psi_k v_k T + \xi_{xk} T \qquad (3.30)$$

$$y_{k+1} = y_k + \sin\psi_k u_k T + \cos\psi_k v_k T + \xi_{yk} T$$

$$z_{k+1} = z_k + w_k T$$

$$\psi_{k+1} = \psi_k + r_k T$$

$$\xi_{xk+1} = \xi_{xk} + \zeta_{vx} T$$

$$\xi_{yk+1} = \xi_{yk} + \zeta_{vy} T$$

$$\xi_{zk+1} = \xi_{zk} + \zeta_{vz} T$$

In (3.30), $\zeta_i$ represents process noise, $\alpha_i$ and $\beta_{ii}$ dynamic model parameters, $T$ denotes filter sampling time with value of 0.1s, while states $\xi_i$ denote constant disturbances acting on vehicle. Notice that $\xi_z$ denotes influence of restoring forces in vertical direction that affect the vehicle. Dynamic model parameters that were used had been identified with the PLADYPOS vehicle in real–life experiments using identification by self–oscilations method presented in [52]. Associated measurement model is given with (3.31)–(3.35).

$$u_{mk} = u_k + \cos\psi_k \xi_{xk} + \sin\psi_k \xi_{yk} + \zeta_{um} \qquad (3.31)$$

$$v_{mk} = v_k - \sin\psi_k \xi_{xk} + \cos\psi_k \xi_{yk} + \zeta_{vm} \qquad (3.32)$$

$$\psi_{mk} = \psi_k + \zeta_{\psi m} \qquad (3.33)$$

$$z_{mk} = z_k + \zeta_{zm} \qquad (3.34)$$

$$r_{mk} = \sqrt{x_k{}^2 + y_k{}^2 + z_k{}^2} + \zeta_{rm} \qquad (3.35)$$

Equations (3.31) and (3.32) represent nonlinear measurement model of the vehicle's absolute velocity in fixed coordinate frame provided from a sensor such as DVL. The vehicle heading and depth measurements, which are directly measured onboard the vehicle, are defined with (3.33) and (3.34). Range measurement represented by Euclidian norm between the vehicle and the beacon position is shown in (3.35). All measurements were affected by the simulated measurement noise $\zeta_i$, modelled as Gaussian white noise. Range

measurement model that accounts for the mobile beacon is defined as

$$r_{mk} = \sqrt{(x_k - x_k^B)^2 + (y_k - y_k^B)^2 + (z_k - z_k^B)^2} + \zeta_{rm}. \tag{3.36}$$

**Single range navigation with respect to the static beacon**

Using presented estimation model, the single range navigation with respect to the static beacon was simulated. In the static beacon scenario, two cases of vehicle movement were analysed: *i*) vehicle trajectories with constant curvature and *ii*) vehicle trajectories with variable curvature. In the constant curvature scenario the AUV is executing three circular



(a) Vehicle trajectories (dashed line), trajectory estimates (solid line), and beacon position (red cross).

(b) Position coordinates $x$, $y$ (solid line) and coordinate $x$, $y$ estimates (dashed line), estimate error $\|\hat{\boldsymbol{\eta}} - \boldsymbol{\eta}\|$ (solid line), and $|FIM|_{seg}$ index (dotted line).
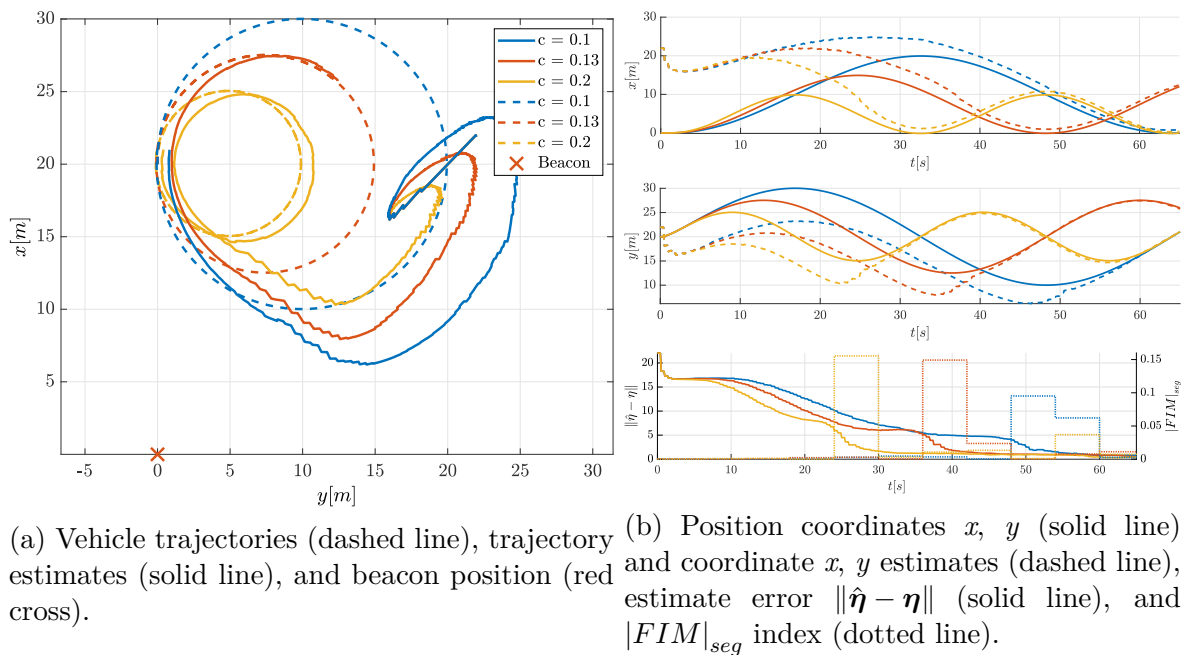
**Figure 3.5:** Trajectories with constant curvature.

trajectories with radii $r_c = 5$, $r_c = 7.5$ and $r_c = 10$ meters, while the beacon is stationary. The circles have property that their curvature is constant and it is defined as $c = \frac{1}{r_c}$. From Figure 3.5b, it can be seen that position estimate converges to the true position values sooner for circle trajectory with smaller radius. Since circles with smaller radii have larger curvature it could be concluded that convergence rate of navigation filter depends on the curvature of assumed trajectory. However that is not true in general, for the circles with very small radius influence of noise affecting range measurements may become dominant factor and in that case measurements are not informative enough. Also, depending on the vehicle speed and update of range measurements, aliasing is possible for circle trajectory because vehicle may pass whole circle trajectory between two adjacent range measurements which are in that case equal and not informative enough. As already discussed, in order to successfully navigate using single range measurements, these measurements should be taken at different bearing angles of the vehicle using single

range measurements. Looking at the Figure 3.5b, estimate error for each trajectory is reduced the most, during the mission segment with the highest value of index $|FIM|_{seg}$, thus indicating that such index is a good candidate for determining how suitable trajectory segments are for achieving observability in single range navigation.



(a) Vehicle trajectories (dashed line), trajectory estimates (solid line), and beacon position (red cross).

(b) Position coordinates $x$, $y$ (solid line) and coordinate $x$, $y$ estimates (dashed line), estimate error $\|\hat{\boldsymbol{\eta}} - \boldsymbol{\eta}\|$ (solid line), and $|FIM|_{seg}$ index (dotted line).
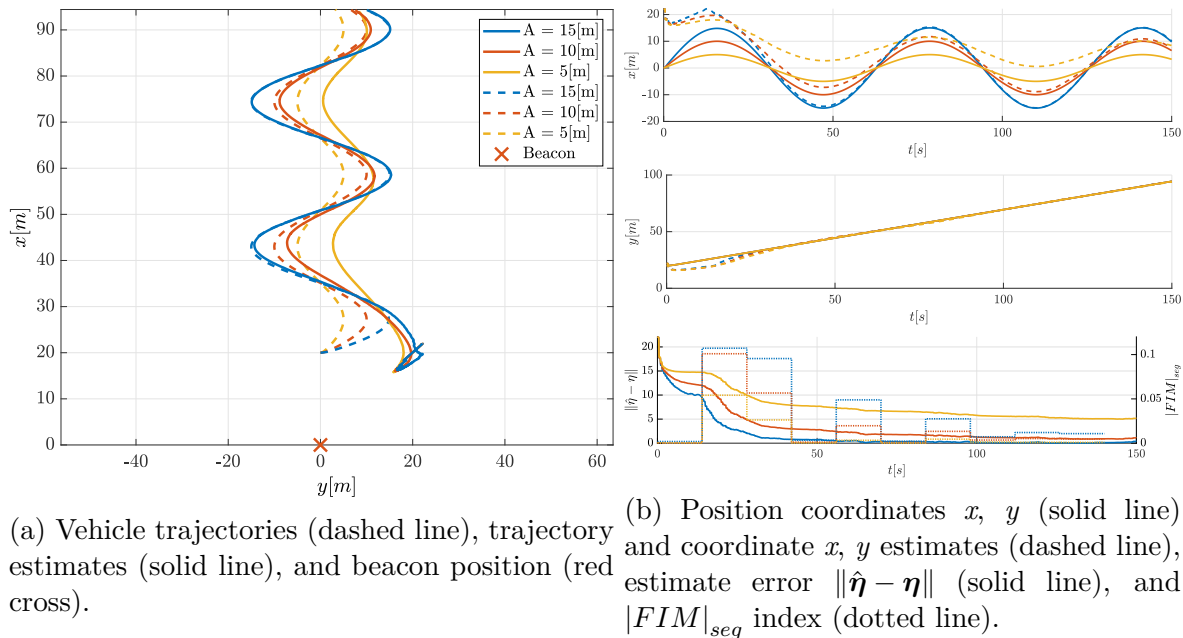
**Figure 3.6:** Trajectories with variable curvature.

The circular trajectory is very informative when it comes to determining the vehicle's position. However, the disadvantage is that AUVs rarely execute circular trajectories during the standard operation. Due to that, case when the vehicle travels to a desired point, while the beacon is stationary, is considered. Earlier in the thesis, it was emphasized that the vehicle position is poorly observable or even unobservable when performing the straight line trajectories, and that the vehicle must deviate from the straight line trajectory to achieve satisfying degree of observability of the navigation filter. Figures 3.6b and 3.6a show the vehicle's position coordintes, and trajectory for the simulated scenario, in which the vehicle is travelling to a desired point, but it is doing excursions in sine pattern along straight line connecting two points. Dashed line represents true vehicle's trajectory, and solid line, which represents estimate, should converge towards it. It is visible that the navigation filter of the vehicle executing the trajectory with bigger deviation from the straight line trajectory is converging faster which is expected. However, larger amplitude implies larger deviation from the straight path connecting the two waypoints, and consequently larger energy consumption, which is also shown numerically in [73]. Notice that, as the distance from the beacon increases, vehicle trajectory is less and less informative, as clearly seen by $|FIM|_{seg}$ values in Figure 3.6b.

**Single range navigation with respect to the mobile beacon**
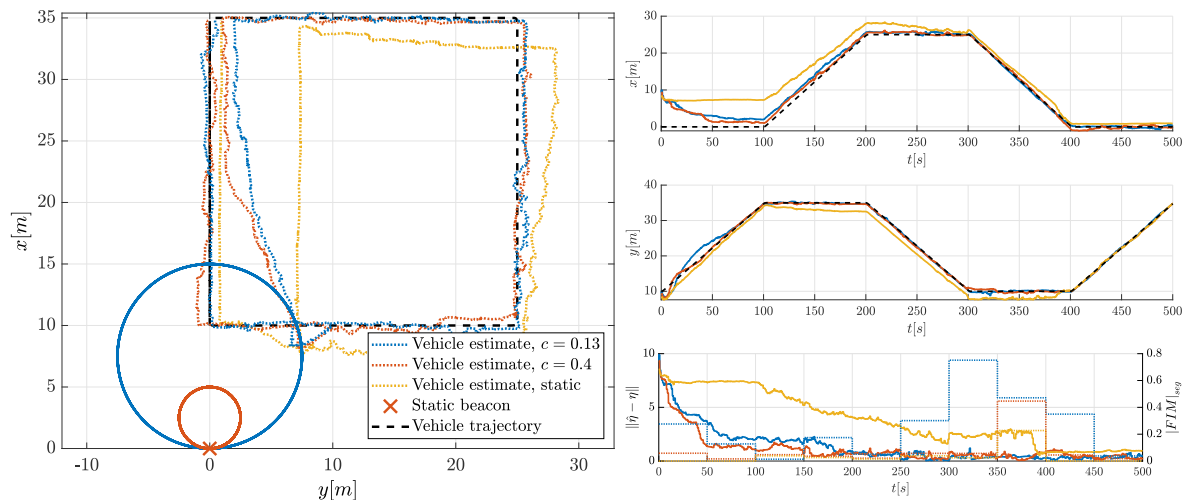


(a) Vehicle trajectory (black dashed line), trajectory estimates (dotted line), beacon trajectories (solid line), and static beacon position (red cross).

(b) Position coordinates $x$, $y$ (black dashed line) and coordinate $x$, $y$ estimates (solid line), estimate error $\|\hat{\boldsymbol{\eta}} - \boldsymbol{\eta}\|$ (solid line), and $|FIM|_{seg}$ index (dotted line).

**Figure 3.7:** Single range navigation using mobile beacon.

For a single range navigation with respect to a mobile beacon, scenario, where the vehicle is travelling along a square trajectory and the mobile beacon is doing a circular trajectory, was simulated, as shown in Figure 3.7a. Using the mobile beacon, while underwater vehicle executes trajectory with straight line segments, enables much better observability and faster convergence of navigation filter compared to fixed beacon, as seen in Figure 3.7b. In the case of a static beacon, notice that on the 350–400 seconds interval, when the value of the $|FIM|_{seg}$ index is significantly higher compared to other segments, the estimate error suddenly decreases.

Using the mobile beacon removes constraints imposed on the underwater vehicle trajectory, however this approach requires additional vehicle which raises the costs of the whole system. Additionally, when planning the trajectories that a vehicle has to execute in order to successfully navigate, duration of the mission and energy consumption must be taken into consideration.

## 3.3  Extremum Seeking Control Using Single Range Measurements

The problem of reaching a source signal, formally known as the source seeking problem, is quite commonly addressed in scientific literature, [76, 77, 78, 79, 80]. In there presented objective is usually determining the minimum or maximum of an unknown signal field.

The majority of interest in the area stems from the need to achieve full vehicle autonomy in an unstructured environment where the position of specific objects of interest must be reached, but, due to a variety reasons, no position measurements are available. Such conditions can be found in different applications, e.g. the pollutant source detection [81] or autonomous vehicle homing [76]. Usually the problem being considered is that of seeking the source of a scalar signal which decays away from the source, e.g. [79], [77]. Such a signal can be electromagnetic, acoustic, thermal, or a concentration of a chemical or biological agent. Although, source seeking with movement towards the object of interest in the underwater environment can be achieved using an EKF deployed to determine source location using single range measurements, and the vehicle's conventional control algorithms to reach the desired position, e.g. in [82], in this thesis focus is on the Extremum seeking (ES) control technique.

The emergence of extremum control dates as far back as the 1922 paper of Leblanc [83], whose scheme may very well have been the first "adaptive" controller reported in the literature. The method of sinusoidal perturbation used in this work has been the most popular of extremum-seeking schemes. In fact, it is the only method that permits fast adaptation, going beyond numerically based methods that need the plant dynamics to settle down before optimization. Extremum seeking was popular tool in control applications in the 1940s-1960s. However, the emergence of computers steered the effort on real-time optimization toward general-purpose optimization algorithms. On the other side, a distinction between stabilization and optimization objectives for adaptive control crystallized, and model reference adaptive control methods appeared, which are analytically tractable by simpler, Lyapunov tools. As a result, extremum seeking as a research topic goes dormant for some 30 years. Extremum seeking has seen a return as an exciting research topic and industrial real-time optimization tool in the 1990's. Since the 2000, and publication of the Krstic's seminal paper, [84], it has seen great resurgence in academic community.

Extremum seeking is a method of adaptive control but it does not fit into the classical paradigm or model reference and related schemes, which deal with the problem of stabilization of a known reference trajectory or set point. A second distinction between classical adaptive control and extremum seeking is that the latter is not model based. As such, it provides a rigorous, high performance alternative to control methods involving neural networks. Its non-model based character explains the resurgence in popularity of extremum seeking in the last half a decade: the recent applications in fluid flow, combustion, and biomedical systems are all characterized by complex, unreliable models. Extremum seeking is applicable in situations where there is a nonlinearity in the control problem, and the nonlinearity has a local minimum or a maximum. The nonlinearity may be in the

plant, as a physical nonlinearity, possibly manifesting itself through an equilibrium map, or it may be in the control objective, added to the system through a cost functional of an optimization problem. Hence, one can use extremum seeking both for tuning a set point to achieve an optimal value of the output, or for tuning parameters of a feedback law [85]. An extremum seeking scheme is usually deployed when the system model is not known very well or even remains completely unknown.

In the following sections first the overview of the extremum seeking based vehicle control is given, before approach used in [86] where the extremum seeking-based control approach is presented as a means to converge towards the underwater source using single range measurements. Simulation and experimental results of the extremum seeking control algorithms using single range measurements with respect to the acoustic beacon are shown in Section 5.5 and Section 3.3.5, respectively.

## 3.3.1 Overview of Extremum Seeking Control

Before continuing with the overview of the Extremum seeking (ES) control, Laplace domain notation is given. Transfer function, the ratio of the output of a system to the input of a system, in the Laplace domain considering its initial conditions and equilibrium point to be zero, is denoted with $G(s)$ where variable $s$ is a complex frequency in Laplace domain, [87]. A time response $y(t)$ of a system, with a transfer function $G(s)$, to input signal $u(t)$ is denoted with $y(t) = G(s)[u(t)]$.

The basic idea of extremum seeking control is to find control input $u^*$ which generates output $y^*$, where $y^*$ is minimum steady-state system output of unknown map $y = F(u)$. Optimal control input $u^*$ is found by performing online gradient estimation. Classical extremum seeking scheme, as presented in [84], achieves that by using a combination of high–pass and low–pass filters, as shown in Fig. 3.8. First control input is superimposed by a sinusoidal perturbation signal $u_{pert} = a \sin \omega t$, which is then passed through plant that we wish to control. Parameter $a$ denotes perturbation signal amplitude, while parameter $\omega$ denotes perturbation signal radial frequency. Output of static map is then passed through high–pass filter $G_{HP}(s)$ to remove signal mean value. This zero-mean signal is then demodulated by multiplying that signal with sinusoidal perturbation. Low pass component of resulting signal is proportional to local gradient of static-map, so that signal can be passed through low–pass filter $G_{LP}(s)$. In order to acquire control input, output of low–pass filter is integrated and multiplied with gain $k$. This scheme can also be deployed on dynamic systems, not only static maps, because if the perturbation frequency is sufficiently slow then dynamic system behaves as a static map with respect to extremum seeking controller.

Greatest contribution of Krstic's paper, [84], was local stability proof of extremum
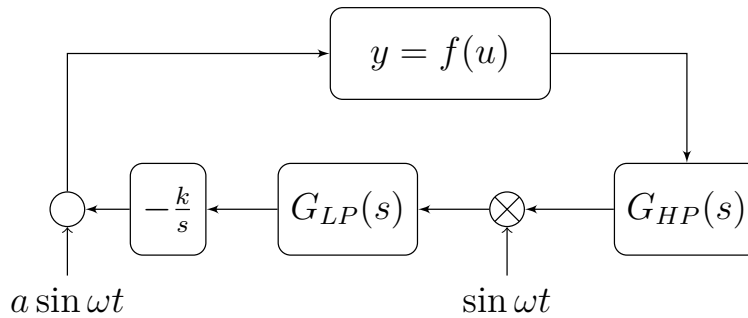
**Figure 3.8:** Classical extremum seeking scheme for single input static map.

seeking scheme given using averaging and singular perturbation theory. However in the last decade, global stability has been proven using Lie bracket averaging theory, [88].

Besides gradient based approach, there are many more extremum seeking approches shown in the literature. In [89] Newton–based extremum seeking algorithm, which in comparison with the standard gradient-based multivariable extremum seeking, removes the dependence of the convergence rate on the unknown Hessian matrix and makes the convergence rate, of both the parameter estimates and of the estimates of the Hessian inverse, user–assignable. Authors in [80] have presented ES algorithm in which the unknown function being minimized enters the system's dynamics as the argument of a cosine or sine term and therefore guaranteeing known bounds on update rates and control efforts.

### 3.3.2 Extremum seeking vehicle control using single range measurements

A classical extremum seeking scheme for navigating stable and moderately unstable force actuated point mass in 2D plane is presented in [78]. In [77] extremum seeking scheme for systems with slow or drifting sensors is proposed. Authors in [80] introduced form of extremum seeking which guarantees known bounds on update rates and control efforts. Algorithm is presented for a case of 2D vehicle with bounded velocity. In [90] 3D environmental extremum seeking navigation of a nonholonomic mobile robot using field value and time derivative of field value in a new kinematic control paradigm which does not employ gradient estimation is presented. Extremum seeking scheme is usually deployed when system model is not known very well or even completely unknown. A significant advantage of the ES control algorithms is the fact that the extremum seeking control loop compensates constant disturbances acting on the vehicle, i.e. gravity, buoyancy, or currents.

In the following subsections, results from [86] are presented. These results extend the advanced gradient estimation algorithm based on EKF for multiple input systems, that was investigated in [91]. The main contribution in [86] is derivation of EKF based

gradient estimation scheme enhanced with static map data which enables faster gradient estimation in presence of intermittent range measurements from acoustic modems and consequently easier tracking of underwater targets. The envisioned scenario, which was a part of FP7 CADDY project and which motivated the work on the subject, was that USV is trying to locate or track position of an underwater object, e.g. AUV or diver, by using range only measurements acquired by acoustic modems.

**Classic Extremum seeking vehicle control**

An uncoupled model of a 2-DoF unmanned surface vehicle that is steered by ES algorithms is given with

$$
\begin{bmatrix} \dot{\boldsymbol{\eta}} \\ \dot{\boldsymbol{\nu}} \end{bmatrix} = \begin{bmatrix} \mathbf{0} & \mathbf{R}_b^n \\ \mathbf{0} & \mathbf{A} \end{bmatrix} \begin{bmatrix} \boldsymbol{\eta} \\ \boldsymbol{\nu} \end{bmatrix} + \begin{bmatrix} \mathbf{0} \\ \mathbf{BR}_b^{n\mathrm{T}} \end{bmatrix} \begin{bmatrix} \mathbf{F} \end{bmatrix},
\tag{3.37}
$$

where states are position $\boldsymbol{\eta} = \begin{bmatrix} x & y \end{bmatrix}^{\mathrm{T}}$ in $\{\mathbf{E}\}$, velocities $\boldsymbol{\nu} = \begin{bmatrix} u & v \end{bmatrix}^{\mathrm{T}}$ in $\{\mathbf{B}\}$, while matrices are $\mathbf{A} = \mathrm{diag}\left(-\frac{\beta_u}{\alpha_u}, -\frac{\beta_v}{\alpha_v}\right)$ and $\mathbf{B} = \mathrm{diag}\left(\frac{1}{\alpha_x}, \frac{1}{\alpha_y}\right)$ where terms $\alpha_i$ represent vehicle's dynamics in respective directions and $\beta_i$ linear hydrodynamic damping terms. Input vector is given with $\mathbf{F} = \begin{bmatrix} F_x & F_y \end{bmatrix}^{\mathrm{T}}$ where $F_x$ and $F_y$ are vehicle's actuating forces in x– and y–axis in the $\{\mathbf{E}\}$, respectively. Input forces are given in $\{\mathbf{E}\}$ since ES controller calculates scalar field gradient in the same coordinate frame. Modelled vehicle can move arbitrarily in any direction in horizontal plane. Vehicle's orientation is not relevant for ES algorithms presented herein, since it can be directly measured, and used for calculating rotation matrix $\mathbf{R}_b^n$. In [78], classical perturbation based ES algorithm is employed for 2D control of force actuated point mass. In that scheme vehicle is modelled as double integrator. In case of vehicle model given with (3.37), vehicle's one degree of freedom is modelled as first–order lag element with integrator at its output, so we are dealing with marginally stable system.

Extremum seeking scheme employed for target tracking is shown in Figure 3.9 where $J(x, y)$ denotes static map to be minimized. Since the goal is to track target position, the static map is represented by the relative distance between the vehicle and the target which is acquired through acoustic ranging. The integrator that is required in the extremum seeking scheme (Fig. 3.8) is inherently a part of the vehicle dynamics, hence it can be omitted. Controller output $(F)$ is

$$
\mathbf{F} = \begin{bmatrix} F_x \\ F_y \end{bmatrix} = \begin{bmatrix} -kG_{PL}(s)[\cos(\omega t)G_{HP}(s)[J()]] - a\sin(\omega t) \\ -kG_{PL}(s)[\sin(\omega t)G_{HP}(s)[J()]] + a\cos(\omega t) \end{bmatrix}.
\tag{3.38}
$$

In controller output (3.38), high–pass filter $G_{HP}(s)$ transfer function is given with

$$
G_{HP}(s) = \frac{s}{s + p_{HP}},
\tag{3.39}
$$
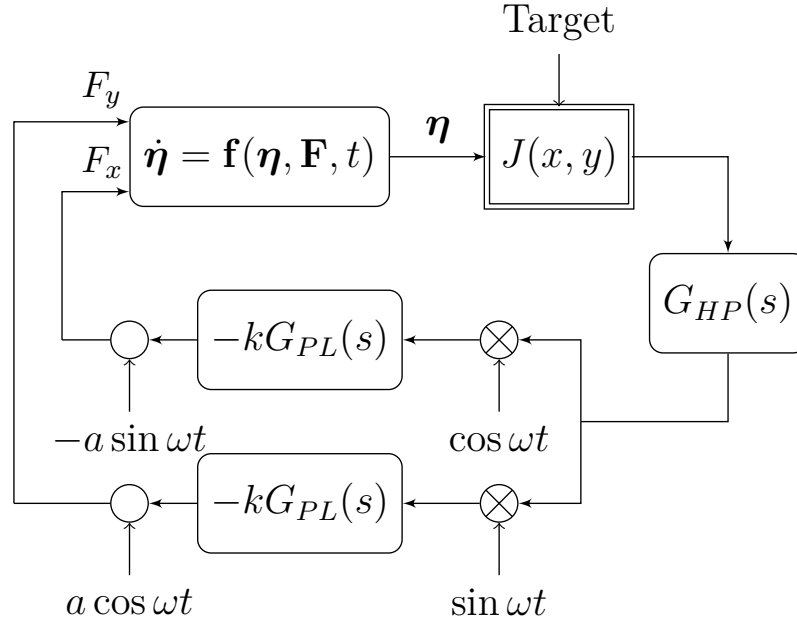
**Figure 3.9:** Classical extremum seeking scheme for dynamic vehicle control in 2D plane.

where $p_{HP}$ denotes high–pass filter pole, while filter $G_{PL}(s)$ transfer function is given with

$$G_{PL}(s) = \frac{s - z_{PL}}{s - p_{PL}}. \tag{3.40}$$

$G_{PL}(s)$ represents phase lead compensator, with pole $p_{PL}$ and zero $z_{PL}$, which raises phase margin lost due to vehicle dynamics. Since phase separation of perturbation signals can be used in 2D case, in order to estimate two gradients from one output, both inputs can be perturbed with same frequency signals.

**Extremum seeking with EKF gradient estimation**

In [91] advanced gradient estimation algorithm based on extended Kalman filter for seeking extremum of static function is presented. Advantage of EKF gradient estimation approach is that gradients in respective directions are estimated at once using a coupled model, unlike classic extremum seeking scheme where gradient estimation for different degrees of freedom is separated by selection of orthogonal perturbation signals.

In Fig. 3.10, classic extremum seeking gradient estimation scheme is replaced by extended Kalman filter, presented in Section 2.2.1, which estimates static map gradients $g_1$ and $g_2$ in respective directions in order to find unknown extremum of the static input–output map. Using these estimates, controller output ($F$) of the EKF based ES is calculated as

$$\mathbf{F} = \begin{bmatrix} F_x \\ F_y \end{bmatrix} = \begin{bmatrix} -kg_1 - a\sin(\omega t) \\ -kg_2 + a\cos(\omega t) \end{bmatrix}. \tag{3.41}$$
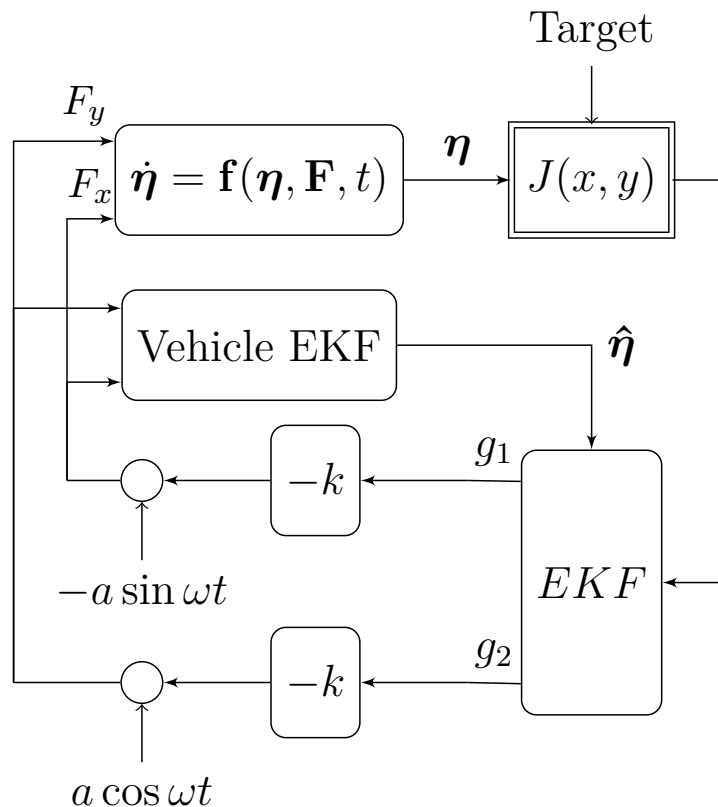
**Figure 3.10:** EKF based extremum seeking scheme for dynamic vehicle control in 2D plane.

In target tracking scenario all uncertainty stems from unknown relative position between autonomous vehicle and target. The position of the vehicle is estimated in the vehicle state estimation EKF filter block using known dynamic model (3.37) and these estimates can be used as inputs in the gradient estimation filter, instead of the real position measurements that are, in practice, noisy and often intermittent. In that way we are searching a minimum of static function $J(x, y)$, i.e. minimum distance between controlled vehicle and target. Like in classic case, integrator is omitted from extremum seeking scheme since integral action is already present in vehicle dynamics.

Gradient estimation EKF is used to fit a tangential plane to the map $J(x, y)$ at the current inputs $(x, y)$. Static map measurement equation can be estimated with

$$J(x, y) = \underbrace{J_0}_{g_0} + \underbrace{\frac{\partial J(x, y)}{\partial x}}_{g_1} x + \underbrace{\frac{\partial J(x, y)}{\partial y}}_{g_2} y \qquad (3.42)$$

where unknown parameters $g_0$, $g_1$ and $g_2$ from (3.42) represent states of the gradient estimation filter. It is assumed that these states are constant in deterministic sense. Parameter $g_0$ is intersection of fitted plane with $J$ axis at $(x, y) = (0, 0)$, and $g_1$ and $g_2$ are slopes of that plane in respective directions. The discrete state equations used for

gradient estimation are

$$\begin{bmatrix} g_{0_{k+1}} \\ g_{1_{k+1}} \\ g_{2_{k+1}} \end{bmatrix} = \underbrace{\begin{bmatrix} 1 & 0 & 0 \\ 0 & 1 & 0 \\ 0 & 0 & 1 \end{bmatrix}}_{\Phi} \begin{bmatrix} g_{0_k} \\ g_{1_k} \\ g_{2_k} \end{bmatrix} + \mathbf{w}_k, \tag{3.43}$$

where $\mathbf{w}_k$ is vector of process noise. In order to make system, defined with (3.43), observable three measurements are necessary. Therefore, the discrete measurement equations are

$$\begin{bmatrix} J_k \\ J_{k-n_1} \\ J_{k-n_2} \end{bmatrix} = \underbrace{\begin{bmatrix} 1 & x_k & y_k \\ 1 & x_{k-n_1} & y_{k-n_1} \\ 1 & x_{k-n_2} & y_{k-n_2} \end{bmatrix}}_{C_k} \begin{bmatrix} g_{0_k} \\ g_{1_k} \\ g_{2_k} \end{bmatrix} + \mathbf{v}_k, \tag{3.44}$$

where $J_{k-n_1}$ and $J_{k-n_2}$ represent delayed output measurements, $x_k$ and $y_k$ represent static map inputs which are in this case vehicle position coordinates and $\mathbf{v}_k$ is measurement noise vector. Time delay $n$ must be chosen in such way that observability gramian defined with (3.45) is not ill–conditioned, [91].

$$rank \begin{bmatrix} C_k \\ C_{k+1}\Phi \\ C_{k+2}\Phi^2 \end{bmatrix} = rank \, C_k = rank \begin{bmatrix} 1 & x_k & y_k \\ 1 & x_{k-n_1} & y_{k-n_1} \\ 1 & x_{k-n_2} & y_{k-n_2} \end{bmatrix} \tag{3.45}$$

In order to have observable system, appropriate $n_1$ and $n_2$ must be chosen so that measurement matrix has full rank and that the matrix is well conditioned. That is achieved by choosing time delay in relation to perturbation frequency. Since acoustic modems have low sampling rates, selection of the parameter $\omega$ and $n$ is limited by range measurement update frequency. Due to that, time delay is chosen as $n_1 = \frac{1}{f_{rm}}$ where $f_{rm} = \frac{1}{T_{rm}}$ is range measurement update frequency and perturbation frequency is selected as $\omega = \frac{2\pi}{4} f_{rm}$.

**Extremum seeking with EKF gradient estimation enhanced with model data**

Advantage of classical algorithm and gradient estimation is that they do not strictly rely on system model. However, since position estimates are already used as inputs to gradient estimation filter, gradient estimation filter state equations can be extended with model information, as in [86]. Assumption is that form of the static map and gradient change rate are known. In order to do that we have to select appropriate static function

$$J(x, y) = d^2, \tag{3.46}$$

where $d = \sqrt{\Delta x^2 + \Delta y^2}$ represents range, while $\Delta x = x - x_t$ and $\Delta y = y - y_t$ relative distance between the vehicle and the target in respective directions. We can ignore gradient changes produced by depth of the target we are tracking since underwater vehicles

(a) $J(x,y) = \sqrt{x^2 + y^2}$      (b) $J(x,y) = x^2 + y^2$
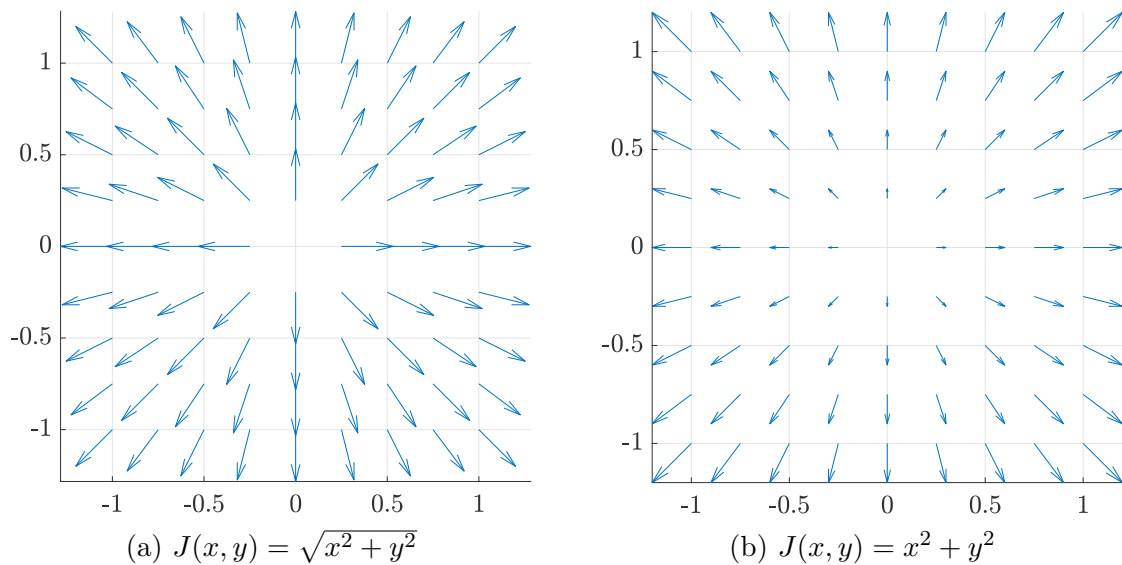
**Figure 3.11:** Gradient comparison of static maps $J(x,y)$.

usually operate at constant depth or the depth is changing much slower than position in horizontal plane so it can be regarded as constant. Contribution of target depth to range measurement is contained in term $g_0$ in (3.44). Gradients of static map (3.46) in x and y direction are defined by (3.47) and (3.48), respectively.

$$g_1 = \frac{\partial J}{\partial \Delta x} = 2\Delta x \tag{3.47}$$

$$g_2 = \frac{\partial J}{\partial \Delta y} = 2\Delta y \tag{3.48}$$

State equations which include model based information about gradient changes are $\dot{g}_1 = 2\Delta \dot{x}$, and $\dot{g}_2 = 2\Delta \dot{y}$. Since we assume that target is static, i.e. $\dot{x}_b = 0$ and $\dot{y}_b = 0$, then $\Delta \dot{x} = \dot{x}$ and $\Delta \dot{y} = \dot{y}$, where $\dot{x}$ and $\dot{y}$ are known quantities and can be included in gradient estimation. This shows the reason for selecting static function (3.46). Although only range can be used as static map output, its gradient time derivative is function of $\Delta x$ and $\Delta y$ which are unknown quantities, unlike the selected static map. Another benefit is that static map defined with (3.46) has smooth gradient around extremum as it can be seen in Figure 3.11. That enables much smoother control actions in the vicinity of the target. Full discrete state equations of EKF based gradient estimation filter enhanced with model information are given with (3.49) where $\Delta t$ is filter sampling time. Measurement equations are as in (3.44).

$$\begin{bmatrix} g_{0_{k+1}} \\ g_{1_{k+1}} \\ g_{2_{k+1}} \end{bmatrix} = \begin{bmatrix} 1 & 0 & 0 \\ 0 & 1 & 0 \\ 0 & 0 & 1 \end{bmatrix} \begin{bmatrix} g_{0_k} \\ g_{1_k} \\ g_{2_k} \end{bmatrix} + \begin{bmatrix} 0 & 0 \\ 2\Delta t & 0 \\ 0 & 2\Delta t \end{bmatrix} \begin{bmatrix} \dot{x}_k \\ \dot{y}_k \end{bmatrix} + \mathbf{w}_k \tag{3.49}$$

New inputs $\dot{x}_k$ and $\dot{y}_k$ of gradient estimation scheme can be seen as some kind of feed–forward information that enables smoother tracking of gradient changes in the filter.

### 3.3.3 Performance quality indices for single range control algorithms
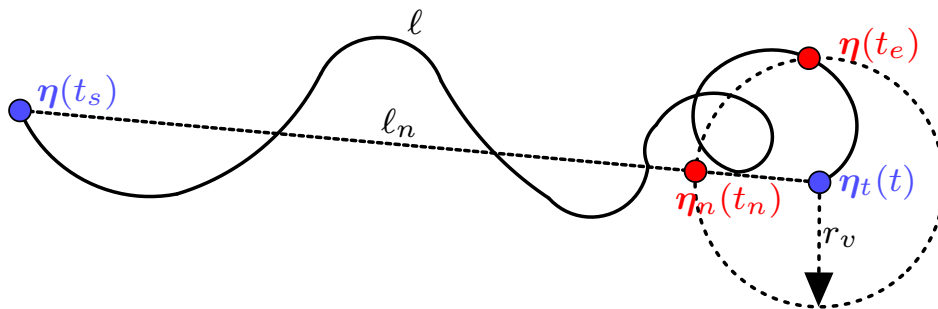


**Figure 3.12:** Definition of vehicle trajectory, nominal trajectory and victory radius used in source seeking performance validation.

In order to quantify performance of the extremum seeking control algorithms used for source seeking using single range measurements, several performance quality indices are used. In order to define indices, notion of nominal trajectory $\boldsymbol{\ell}_n$ is introduced. In Figure 3.12, nominal trajectory is defined as the shortest path between the vehicle initial position $\boldsymbol{\eta}(t_s)$ at initial time $t_s$ and final point $\boldsymbol{\eta}(t_n)$ at nominal trajectory end time $t_n$ traversed with nominal speed $\|\boldsymbol{\nu}\|_n$. In order to localize the target using single range measurements, informative trajectories must be assumed, e.g. the perturbations in the ES control algorithms are constantly exciting the vehicle. Due to that, it is difficult to settle the vehicle at the target location. More so, in real life disturbances acting on the vehicle and noise in the acquired measurement also prevent settling of the vehicle. Therefore, the so–called victory radius is introduced in order to define which conditions are required to consider the goal of reaching the target completed. It is assumed that target has been reached when the vehicle's trajectory enters the set defined with

$$B_v(\boldsymbol{\eta}_t, r_v) = \left\{ \boldsymbol{\eta} \in \mathbb{R} \,|\, \|\boldsymbol{\eta} - \boldsymbol{\eta}_t\| \leq r_v \right\}, \tag{3.50}$$

where $r_v$ is victory radius and does not leave that set for any $t > t_e$ where $t_e$ marks the time when the vehicle entered the set $B_v$ for the last time.

First index introduced is the ratio between the length of the nominal trajectory and

the length of true vehicle trajectory:

$$\Pi_s = \frac{L(\ell_n(t))}{L(\ell(t))} = \frac{\|\boldsymbol{\eta}_n(t_n) - \boldsymbol{\eta}(t_s)\|}{\int\limits_{t_s}^{t_e} \left\|\dot{\ell}(t)\right\| dt} \tag{3.51}$$

where operator $L(\ell)$ measures length of the vehicle trajectory defined with $\ell(t) = \{\boldsymbol{\eta}(t) \in \mathbb{R}^n \,|\, t \in [t_s, t_e]\}$. Second index used is ratio between the nominal time $\Delta t_n$ i.e. time necessary for traversing nominal trajectory at nominal speed and real time in which algorithm reached the target $\Delta t$:

$$\Pi_t = \frac{\Delta t_n}{\Delta t} = \frac{\frac{\|\boldsymbol{\eta}(t_n) - \boldsymbol{\eta}(t_s)\|}{\|\boldsymbol{\nu}\|_n}}{t_e - t_s} \tag{3.52}$$

where $\|\boldsymbol{\nu}\|_n$ denotes the absolute nominal vehicle speed. Introduced performance indices $\Pi_s$ and $\Pi_t$ can be used in order to validate performance of the different algorithms compared to the nominal trajectory using steps as follows:

1. Define nominal vehicle trajectory $\boldsymbol{\ell}_n$ and desired victory radius $v_r$.
2. Define performance requirements: $\Pi_s > \Pi_{smin}$ and $\Pi_t > \Pi_{tmin}$.
3. Execute the algorithm that needs to be validated and measure final trajectory length $L(\boldsymbol{\ell})$ and time in which vehicle reaches the target $\Delta t$.
4. Calculate indices $\Pi_s$ and $\Pi_t$ using (3.51) and (3.52).
5. Plot the results in $\Pi_t - \Pi_s$ plane as in Figure 3.13. If they are inside bounds defined in step 2 than the performance requirements are satisfied.

Step 1 requires definition of the nominal trajectory $\boldsymbol{\ell}(t)$. Nominal trajectory is a reference trajectory and it is the most efficient trajectory. Algorithm cannot reach the target in shorter path than nominal trajectory, i.e. $\Pi_s$ is always lower than 1, while $\Pi_t$ can be larger than 1 but that can be achieved only by going with average speed faster than nominal speed which requires more energy. Nominal velocity is selected depending on the requirements. If pure time performance is needed then nominal velocity can set as $\|\boldsymbol{\nu}\|_{max}$, i.e. maximal vehicle speed. In that case all the data points are located above the nominal speed $v_n$ contour and the algorithm with largest value of $\Pi_t$ is the best candidate. Sometimes, if an energy efficient approach is required, nominal velocity can be set to a lower value. In that case it is possible to get values of $\Pi_t$ larger than 1. But in that case, the average speed is larger than the nominal speed. Selection of victory radius $r_v$ largely depends if it is only important to come into vicinity of the target when slightly larger victory radius can be selected compared to the case when it is also important that vehicle settles in stable trajectory around the target.

Step 5 requires that calculated indices are plotted. Example of the $\Pi_t - \Pi_s$ plane used

(a) Linear scale.

(b) Logarithmic scale.
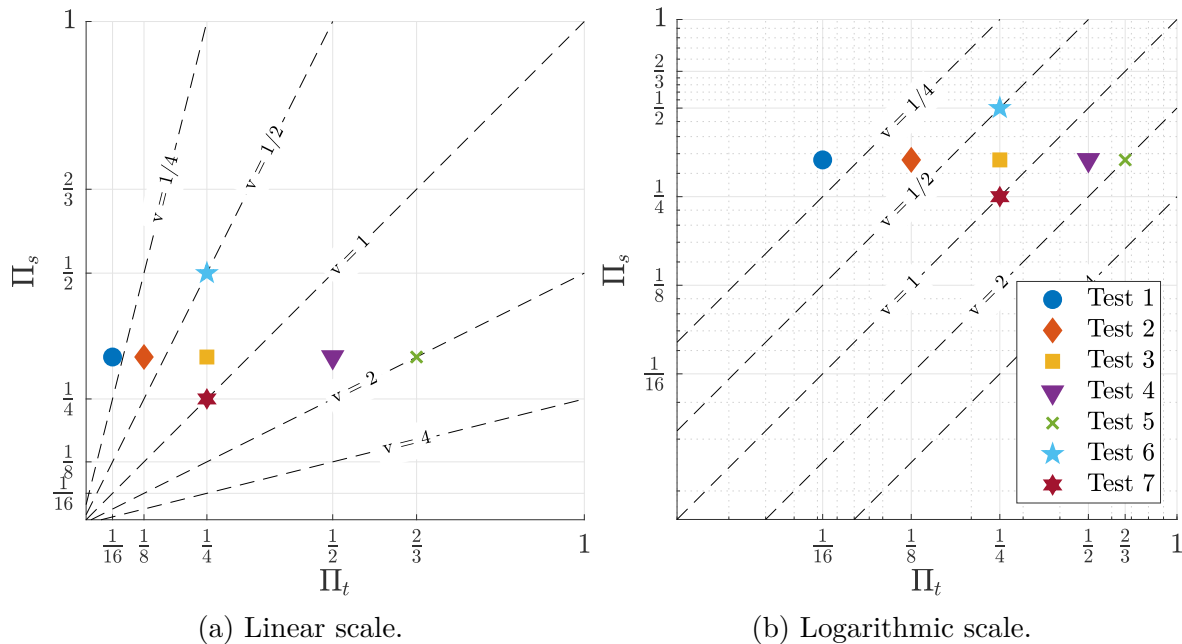
**Figure 3.13:** Parameter $\Pi_t$ – $\Pi_s$ plane used for comparison of ES algorithms using performance quality indices.

for comparing the performance of the algorithms is shown in Figure 3.13a and Figure 3.13b with linear and logarithmic axes, respectively. Dashed lines in Figure 3.13, denoted with $v$, represent contours where constant value of percentage of nominal speed is attained. Looking at Figure 3.13a, Test 1 took two times longer to execute with respect to Test 2, while Test 2 took two times more than Test 3. And all three test had the same path length. Advantage of the logarithmic scale is that distance between points denoting these tests is equal, and it is easier to compare different algorithms. Test 5 had the shortest execution time, but that was achieved with average speed twice bigger than nominal speed. Test 6 traversed the shortest path, while Test 7 traversed the longest path, 4 times larger than nominal path.

When climbing along the line, the efficiency of the algorithm increases, e.g. for contour where nominal speed $v_n$ is attained, energy consumed for nominal point $(1, 1)$ is at least two times lower than for the point $(\frac{1}{4}, \frac{1}{4})$ where vehicle passes four times the distance in the four times larger time interval. If there are two candidates with the same value of index $\Pi_s$ it is expected that the more energy efficient will be algorithm which assumes the shortest path with the lowest average speed, i.e. lower index $\Pi_t$. It must be noted that shown measure does not indicate exact energy consumption since calculated mean values do not account information that power consumption increases with the cube of the speed, and temporary higher speeds during algorithm execution are not captured in the criteria. If there are multiple points inside the bounds, the best one is selected depending on the priority, because trade off between energy consumption and shorter execution time must

be done.

### 3.3.4 Simulation results

Three extremum seeking schemes, classical extremum seeking (ESC), Kalman filter based gradient estimation scheme (EKF) and Kalman filter based gradient estimation scheme with additional model information (EKF+model) are simulated for two scenarios: stationary target and slowly moving target. In practice range measurements are discrete, therefore, discrete version of ES controller is employed in simulations, [92]. Algorithm parameters are given in Table 3.1. The Kalman filter sampling time is selected as $\Delta t = T_{rm}$, and in the case of EKF+model, filter sampling time is $\Delta t = T_{rm}/20$ where $T_{rm} = 2\,s$ since it receives model data with higher frequency. In order to make results comparable, all the algorithms use the cost function (3.46).

| Parameter | ESC | EKF | EKF+model |
|---|---|---|---|
| $\omega\left[\frac{rad}{s}\right]$ | 0.7854 | 0.7854 | 0.7854 |
| $a$ | 0.25 | 0.25 | 0.25 |
| $k$ (low gain) | 0.0059 | 0.0059 | 0.0059 |
| $k$ (high gain) | 0.03 | 0.03 | 0.03 |
| $p_{LP}$ | 0.1473 | $\times$ | $\times$ |
| $p_{HP}$ | 1.1781 | $\times$ | $\times$ |
| $\mathbf{Q}_k$ | $\times$ | $2\,\mathrm{diag}\,(10,\quad 10,\quad 1)$ | $2\,\mathrm{diag}\,(1,\quad 1,\quad 1)$ |
| $\mathbf{R}_k$ | $\times$ | $\mathrm{diag}\,(1,\quad 1,\quad 1)$ | $\mathrm{diag}\,(1,\quad 1,\quad 1)$ |
| $\Delta t\,[\mathrm{s}]$ | 2 | 2 | 0.1 |

**Table 3.1:** Algorithm parameters used in extremum seeking simulations.

**Stationary target**

Vehicle trajectories and ranges for the three algorithms, seeking target at position $(0,0)$ with vehicle's initial position $(5,0)$, are shown in Figure 3.14. The algorithms were simulated for two values of gain $k$, as noted in Table 3.1. It is clearly visible that all ES algorithms successfully converge towards the target with both high and low gain parameter using single range measurements as input. Both EKF based schemes converge to the target faster, as it can be seen in Figure 3.14c and Figure 3.14d. That is because EKF based algorithms are better at estimating static–map gradient, as seen in Figure 3.16.
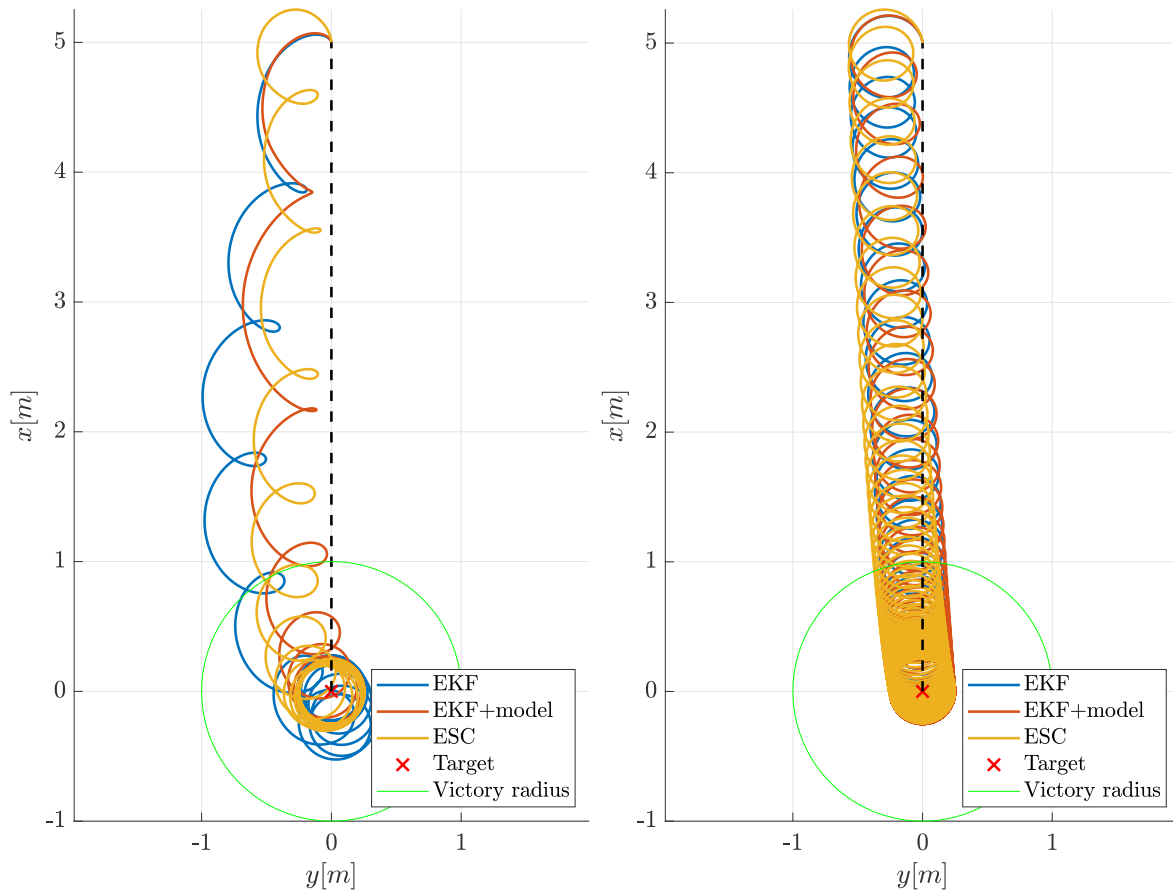
(a) Vehicle trajectory, high gain.

(b) Vehicle trajectory, low gain.
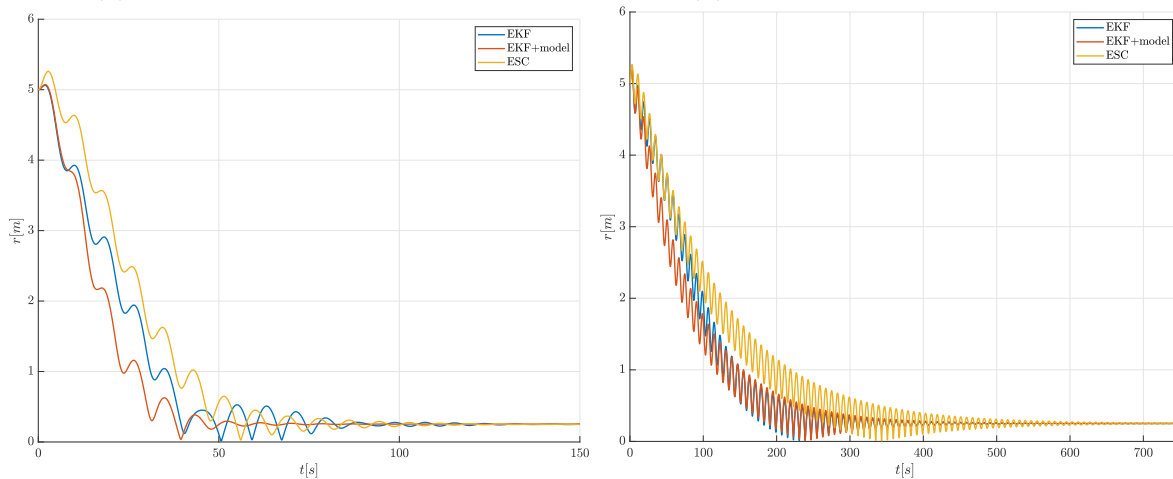
(c) Range to target, high gain

(d) Range to target, low gain.

**Figure 3.14:** ES control algorithm trajectories and ranges for two different values of gain $k$.

Namely, inputs and outputs of gradient estimation are also inputs and outputs of static–map, i.e. vehicle dynamics influence is reduced by using estimated position values, and gradient is estimated without additional low–pass and high–pass filters as in ESC algorithm. EKF based estimation enhanced with the model data converges faster to the real gradient since model information about gradient change is used in between two range measurements. Notice how, in the case of EKF algorithm, in Figure 3.14a slower gradient

63

(a) Absolute value of control force **F** and velocity $\boldsymbol{\nu}$.

(b) Control force **F** angle in $\{\mathbf{E}\}$.
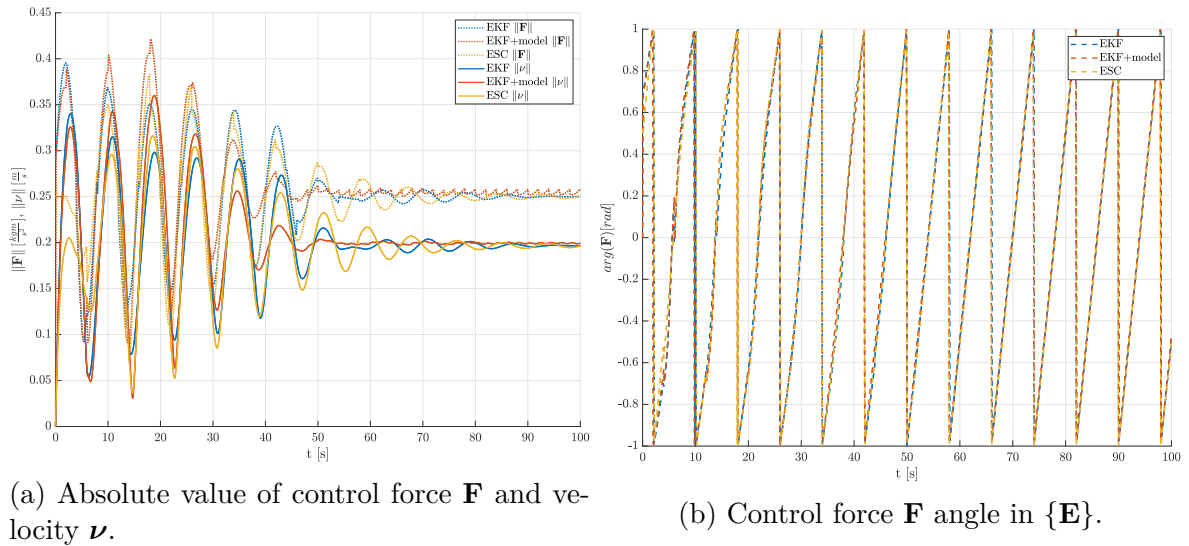
**Figure 3.15:** Controller output response and vehicle absolute velocity for gain $k_h$.



(a) Gradient $\frac{\partial J}{\partial x}$.

(b) Gradient $\frac{\partial J}{\partial x}$.

(c) Gradient $\frac{\partial J}{\partial y}$.
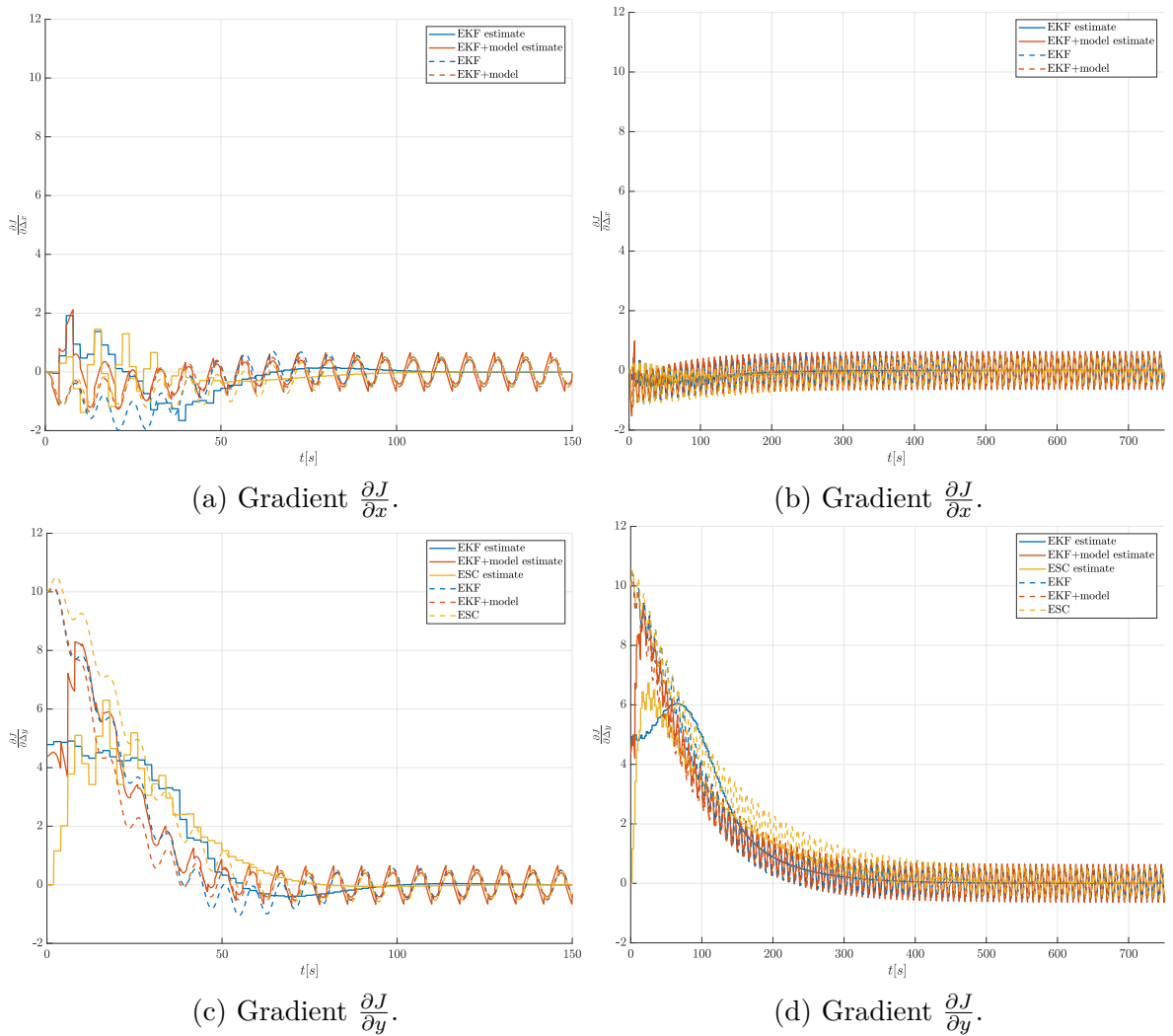
(d) Gradient $\frac{\partial J}{\partial y}$.

**Figure 3.16:** Static map gradient (dashed line) and gradient estimates (solid line) for two different values of gain $k$.

(a) Perturbation amplitude $a[N]$.

(b) Perturbation frequency $\omega \left[\frac{rad}{s}\right]$.
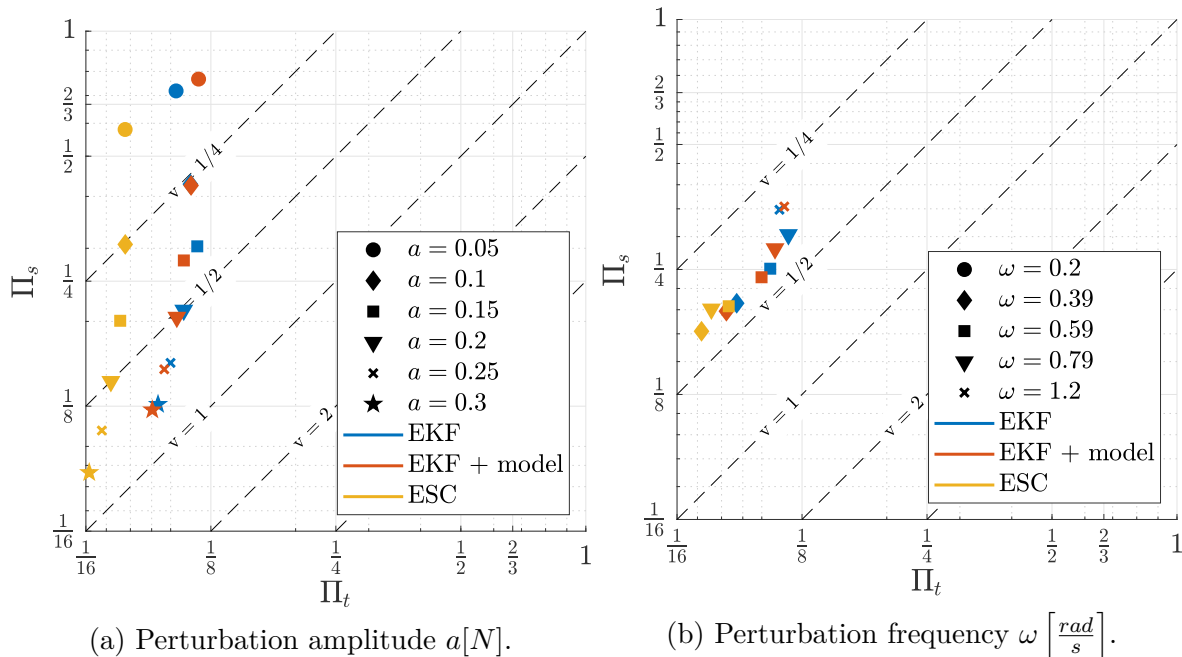
**Figure 3.17:** Evaluation of ES algorithms parameters using performance quality indices.

convergence causes the vehicle to slightly overshoot the target due to overestimation of the gradient.

Control effort produced by each algorithm is shown in Figure 3.15. When the vehicle enters stationary state around the extremum, EKF+model algorithm using model data follows fast gradient changes causing small jitter in the control value, unlike the EKF filter which assumes that all states are constant and has smooth control output.

The performance indices from Section 3.3.3 are used to compare the algorithm results for different sets of perturbation amplitude $a$ and perturbation frequency $\omega$ values with constant gain $k$. Cumulative results are given in Figure 3.17. By increasing the perturbation amplitude total path increases significantly. EKF based approach reaches the target along a shorter path and in less time compared to the ESC algorithm. Compared to the EKF approach, EKF+model approach performs slightly worse for bigger amplitudes, but slightly better for low amplitudes. Primarily because it is more difficult to estimate the gradient when the system is less excited by perturbations. Similar results are obtained for the change of perturbation frequency $\omega$ in Figure 3.17b. For the selected value of victory radius, the EKF+model algorithm performs better for higher frequencies. As seen from this example, the performance indices plot can be used to tune the algorithm parameters, since it allows the user to visualize how parameters improve criteria, and for which values further change of parameter does not introduce additional performance benefit.

(a) Vehicle trajectory.

(b) Range measurement.

(c) Gradient $\frac{\partial J}{\partial x}$.

(d) Gradient $\frac{\partial J}{\partial y}$.
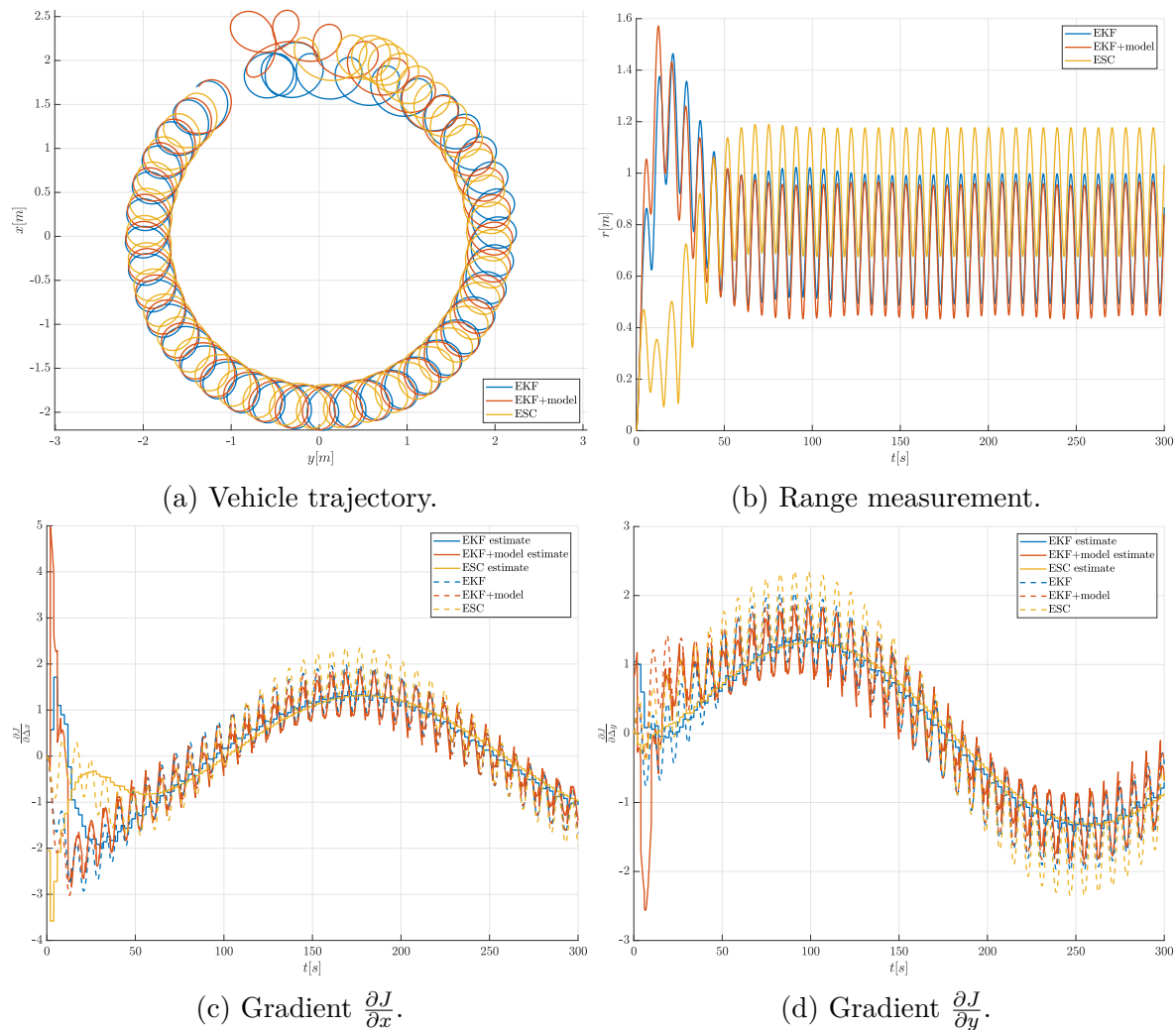
**Figure 3.18:** Single range navigation using mobile beacon.

## Slowly moving target

In Figure 3.18a trajectories of three different extremum seeking schemes are compared for a case of a slowly moving target which assumes circle trajectory with radius of 2 meters. It can be seen that ESC algorithm's trajectory follows the target trajectory with larger error compared to EKF based approaches because gradient estimation converges much slower with respect to algorithms using EKF for gradient estimation. Figure 3.18b shows that EKF based schemes can follow target closer than classic scheme. From tracking error it can be seen that ESC algorithm is influenced by phase delay from vehicle's dynamics because it reacts slower to target's direction change.

It must be noted that, in tracking operation, the EKF based estimation scheme enhanced with model will produce worse results if the target speed is comparable with vehicle speed because then the assumption of a static target used in deriving the model is no longer valid. That is the reason why there is a peak at the start of estimation in EKF+model estimated gradient response, shown in Figure 3.18c and 3.18d. However, it

can be seen that the target velocity is still low enough and enhanced EKF tracks the high frequency gradient changes. Using the assumption that target has some constant speed could enhance estimation in such cases but that speed should be estimated only with range measurements which is not an easy task due to mentioned observability problems present in such estimation.

Although the perturbation signal amplitude, used in the algorithms presented herein, could be set to a lower value to achieve even better performance in simulations, that is unrealistic because in real life range measurements are affected by a significant noise which could render the measurements useless.

### 3.3.5 Experimental Results
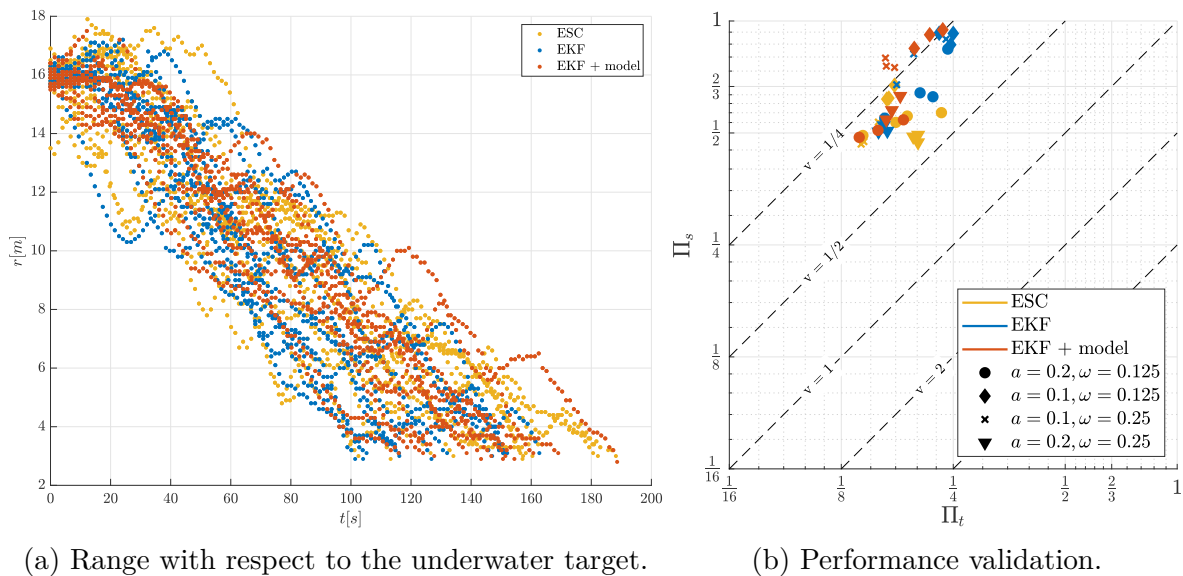


(a) Range with respect to the underwater target.

(b) Performance validation.

**Figure 3.19:** Source seeking of an underwater target using single range measurements.

The experiments, which tested the source seeking algorithms that use single range measurements provided by acoustic modems, were conducted in May 2015 in Biograd na Moru, Croatia. The experimental setup consisted of an autonomous surface platform PLADYPOS equipped with a SeaTrac USBL device, which provided range measurements to the target, i.e. SeaTrac modem positioned at the seabed.

Figure 3.19 represents the real life source–seeking results where the surface vehicle navigated towards the static underwater target positioned at approximately 2.5 m depth. In Figure 3.19a, range to the target measured during different ES experiments is shown. The influence of the perturbation introduced into system is clearly visible as oscillations in the range response. This persistently exciting motion is necessary in order to estimate gradient online.

The performance indices from Section 3.3.3 were used to compare the results of different algorithms for different set of perturbation amplitude $a$ and perturbation frequency $\omega$ parameters. Cumulative results are given in Figure 3.19b. The shortest path was achieved for parameters $a = 0.1$ and $\omega = 0.125$, which is expected since the perturbation amplitude is low and the perturbation period shorter, thus leading to the lower speeds and the lower position deviation during the gradient estimation. It can be seen that the performance of the ESC algorithm was not improved as much as in case of EKF based algorithms. Namely, because it is more difficult for the ESC algorithm to estimate the gradient with smaller perturbations. In general, it is clear that selecting the larger perturbation tends to make system more robust to measurement noise and causes the total path to be longer.

# Chapter 4

# Mobile Beacon Control in Single Range Navigation

As stated before, in order to estimate the position of the vehicle that is navigating using range measurements from a stationary beacon, vehicle needs to assume the trajectory along the which the system is observable. This can prevent the vehicle from doing other useful activities which require trajectories that are not informative enough. In order to completely avoid that trade–off, it is left to the mobile beacon to ensure informative measurements for the target vehicle's navigation system. The goal of the control algorithm presented in this chapter is to steer the mobile beacon in order to decrease the localization error of the single range navigation system by using an online algorithm with the very low computational and communication demands. The proposed method is particularly interesting for underwater applications due to limited bandwidth of the acoustic communication. In the proposed control loop, the only data that needs to be transmitted over the acoustic link between the vehicle and the beacon is the scalar value that holds information about current degree of navigation's filter observability, and the beacon current position data. Optionally, the beacon velocity can be sent in order to improve localization performance. Furthermore, the proposed algorithm does not require knowledge of the target vehicle's trajectory in advance. That can be particularly useful in real–life conditions when planned trajectories can be altered due to some unexpected situations. In summary, main assumptions are:

- underwater target model is unknown,
- underwater target trajectory is unknown,
- bandwidth of acoustic communication is limited,
- and beacon vehicle has only scalar information about target localization quality.

The main motivation for the presented work arrived from the FP7 "CADDY - Cog-

nitive Autonomous Diving Buddy" project which had the main objective to develop a multicomponent marine robotic system comprising of an autonomous underwater vehicle AUV and an autonomous surface marine platform that will enable cooperation between robots and human divers. In the context of the CADDY project one of the main prerequisites for executing envisioned control algorithms and ensuring the diver safety during the human-robot interaction was diver position estimation. The movement of the diver is usually slow and unpredictable, therefore all the techniques which use a priori knowledge of the target trajectory are not suitable for determining beacon's trajectory that makes system observable when using single range measurements.

This chapter is organized as follows. In Section 4.1 overview of the path planning algorithms for mobile beacons is presented. Section 4.2 describes the novel concept of a mobile beacon control, which is used to increase the underwater vehicle's quality of navigation by using function which captures current degree of observability. Section presents what features this function needs to posses, analyses convergence properties of the proposed control, and finally it gives control scheme implementation details. In Section Section 4.4 simulation results of the proposed algorithma are given, while experimental results acquired during several field trials are given in Section 4.5.

# 4.1 Brief Overview of Path planning methods for the mobile beacon

When deploying AUVs the desired trajectories are usually known in advance. Therefore, it is possible to determine, also in advance, the trajectory of a mobile beacon in order to acquire the most informative range measurements for an AUV and improve observability of it's navigation filter. By introducing certain modifications it is possible to use these algorithms in online operation where knowledge of the complete mission trajectory is potentially unknown. In literature, several ways of determining optimal trajectory of a mobile beacon are present. In [54, 72, 73], the optimal beacon trajectory is found by maximizing Fisher Information Matrix determinant, while in [57] Dynamic Programming (DP) formulation and Markov Decision Process (MDP) formulation of optimization problem are presented.

**Maximizing Fisher Information Matrix determinant approach**

In [54], measure based on Fisher Information Matrix (FIM) is proposed as a way to determine a persistently exciting trajectory of a mobile beacon. The goal is to maximize the FIM determinant to determine the optimal beacon trajectory that maximizes the

expected positioning accuracy. In described scenario, surface beacon vehicle that carries the acoustic ranging sensor must localize a single moving target. The acoustic signals are emitted at constant intervals of time $\Delta t$ and there exists a delay between the emission by the modem on board the beacon vehicle and the reply from the target. Therefore, the reception of the acoustic reply takes place at a different point from the emission point. Beacon vehicle moves with constant speed that is always larger than that of the target. It is considered that the measured ranges $r_k$ used to define the FIM correspond to the time for the acoustic signal to travel from the target back to the sensor. In the initial step beacon is located in point $p_k$ and objective is to determine the next measurement point which will maximize FIM determinant of the matrix defined with (3.20) and consequently system observability. If the next measurement point is defined as $p_{k+1} = p_k + \begin{bmatrix} \xi \cos \alpha_{k+1} & \xi \sin \alpha_{k+1} & 0 \end{bmatrix}^T$, where $\xi$ is distance which beacon travels between two adjacent measurements and, $\alpha$ is vehicle course during that time, then the FIM in the step $k+1$ is $FIM_{k+1} = FIM_k^* + FIM_{k+1}^{'}$. Consider that $FIM_k^*$ is the FIM computed with the current $m$ known range measurements except the oldest one, and $FIM_{k+1}^{'}$ is the updated FIM that has been computed with the new range measurement obtained from a point to be defined which is function of course angle $\alpha$. Then, optimization problem is given as $\alpha_{k+1}^* = \arg \max_{\alpha_{k+1}} |FIM_{k+1}|$. In order to improve performance, beacon trajectories can be calculated for extended horizon, i.e. larger sequence of expected future measurements as in [72, 73].

**Dynamic programming formulation approach**

Another path planning approach is presented in [57]. Therein, the path planning algorithm which uses the estimated error ellipse of multiple AUVs, which navigate themselves using range measurements, is used to plan the beacon vehicle motion. The vehicle position error can be minimized if the beacon vehicle can manoeuvre in such way that next range measurement occurs along the direction of major axis of error ellipse. It is assumed that vehicles use OWTT ranging which requires that the vehicle's clocks are synchronized. The error in range estimation is modelled as a zero mean Gaussian random variable $\left| \mathbf{x}_k^j - \mathbf{x}_k^B \right|$ with variance $\sigma$ as $R_k^j = \mathcal{N}\left( \left| \mathbf{x}_k^j - \mathbf{x}_k^B \right|, \sigma^2 \right)$, where $\mathbf{x}_k^j$ denotes $j$-th vehicle position, and $\mathbf{x}_k^B$ beacon position at time instant $k$. Vehicle position error is also defined as a zero mean Gaussian random variable described with three parameters: the direction of minimum error $\theta_{k+1}^j$, error along the the direction of minimum error $\epsilon_{k+1}^j$ and error in tangential

direction $\vec{\epsilon}_{k+1}^j$

$$\theta_{k+1}^j = \angle \left( \mathbf{x}_{k+1}^j - \mathbf{x}_{k+1}^B \right), \tag{4.1}$$

$$\epsilon_{k+1}^j = \sigma, \tag{4.2}$$

$$\left( \vec{\epsilon}_{k+1}^j \right)^2 = \frac{\left( \vec{\epsilon}_k^j \epsilon_k^j \right)^2}{\left( \epsilon_k^j \cos \gamma_k^j \right)^2 + \left( \vec{\epsilon}_k^j \sin \gamma_k^j \right)^2} + \alpha \tau, \tag{4.3}$$

where $\gamma_k^j = \theta_{k+1}^j - \theta_k^j$. The constant parameter $\alpha$ is tuned according to the quality of the each vehicle's speed estimate. The better the estimate, the error grows more slowly over time, therefore the parameter $\alpha$ has a lower value. The beacon vehicle kinematic model used in optimization problem is given with

$$\phi_{k+1}^B = \phi_k^B + \delta_k^B \tag{4.4}$$

$$\mathbf{x}_{k+1}^B = \mathbf{x}_k^B + \tau s^B \left[ \cos \phi_{k+1}^B \quad \sin \phi_{k+1}^B \right]^T, \tag{4.5}$$

where $s^B$ represents mobile beacon speed and $\delta_k^B$ beacon vehicle heading change. Optimization problem in $k$-th step can be written as

$$\min_{a_k} \quad C \left( S_k, a_k \right) \tag{4.6}$$

$$\text{s.t.} \quad \left| \delta_k^B \right| \leq \dot{\Phi}_{max}^B \tau \tag{4.7}$$

$$D_{min} \leq \left| \mathbf{x}_{k+1}^j - \mathbf{x}_{k+1}^B \right| \leq D_{max} \quad \forall j \tag{4.8}$$

where $S_k = \left\{ \mathbf{x}_k^B, \phi_k^B, \left( \epsilon_k^j, \vec{\epsilon}_k^j, \theta_k^j \right) \forall j \right\}$ is system state, $C \left( S_k, a_k \right)$ decision incurred cost and $a_k$ control decision. Nonlinear constraints present in optimization problem are given with (4.7) and (4.8). First constraint limits maximal course change in single time step $\tau$, while other ensures that beacon and the vehicle do not collide while staying within communication range. Complete beacon vehicle path can be determined by computing sequence of decisions (4.9).

$$\left\{ \delta_k^B \right\} = \arg \ \min \sum_{j,k} \left[ \left( \epsilon_{k+1}^j \right)^2 + \left( \vec{\epsilon}_{k+1}^j \right)^2 \right] \tag{4.9}$$

The optimization problem is solved using the recursive formulation of dynamic programming (DP) based on Bellman's principle of optimality which states that optimal policy has the property that whatever the initial state and initial decision are, the remaining decisions must constitute an optimal policy with regard to the state resulting from the first decision. Optimal control decision in any step is given with: $a_k =$

arg $\min\limits_{a \in \mathcal{A}(S_k)} [C(S_k, a) + V_{k+1}(S_{k+1})]$, where $V_k(S_k)$ represents cost of applying an optimal policy from the state $S_k$ until the end of mission. Since state space and decision space are continuous, decision space $\mathcal{A}(S_k)$ is discretized in order to have finite set of decisions in every time step. Also, since state space has large dimensionality and some states are unbounded, e.g. position state, value function approximation is preformed. It is possible to deploy trivial approximation $\tilde{V}_k(S_k) = 0$, called *greedy* strategy. Better approximation of the value function can be achieved by using *look-ahead* strategy which takes into consideration the cost incurred by current and the next $L$ actions but at the expense of a greater computational complexity and communication requirements.

**Markov Decision Process formulation approach**

Another interesting approach, also presented in [57], is using Markov decision process (MDP) framework for solving vehicle's path planing problem. The goal is to minimize cost over the entire mission, i.e we want to determine sequence of decisions given with (4.9). MDP policy is the state–action mapping that determines probability distribution of action $a_k$ when the process is in state $S_k$. The policy matrix $\mathbf{P}_{sa} = (p_{sa})$ gives probability $p_{sa}$ that we choose action $a_k$ when we are in state $S_k$ for discretized action and state space. Looking at particular navigation problem that means we have a matrix which gives us probability of choosing turning angle from the beacon's vehicle current bearing given the current system state as well as relative distance between vehicles. Path planning policy can be derived using cross-entropy method. More information on cross-entropy method and policy learning algorithms can be found in [57]. When the policy learning is completed, which can be done offline, beacon vehicle needs to preform policy matrix lookup in order to decide next control action.

All of the presented approaches successfully accomplish their task but also they have some disadvantages. Although FIM and DP approach can be deployed online in real–life situations, at least part of the vehicle trajectory needs to be known in advance, which is not always the case. If the vehicle trajectory is changed during the mission, willingly or due to some external disturbances, this updated trajectory must be sent to the beacon vehicle which puts great stress on the communication channel. FIM and DP approach require online computations while MDP approach calculates possible actions offline, thus the online computations are very low. However, the process of decision making in the MDP method is heuristic and generated path is suboptimal.

## 4.2 Problem description and control algorithm

Let the vehicle and the mobile beacon dynamics and kinematics be described with a set of a nonlinear differential equations

$$\dot{\boldsymbol{\eta}}_v = f_v(\boldsymbol{\eta}_v, \boldsymbol{\nu}_v, t)$$
$$\dot{\boldsymbol{\eta}}_b = f_b(\boldsymbol{\eta}_b, \boldsymbol{\nu}_b, t),$$

(4.10)

where subscripts $b$ and $v$ denote the beacon and the vehicle related states and functions, respectively. In order to execute the proposed algorithm, the beacon vehicle does not need to know the target vehicle's dynamic and kinematic properties and there are no special requirements on the vehicle or beacon dynamics necessary to execute the algorithm except

**Beacon (surface vehicle)**



**Target (underwater vehicle)**
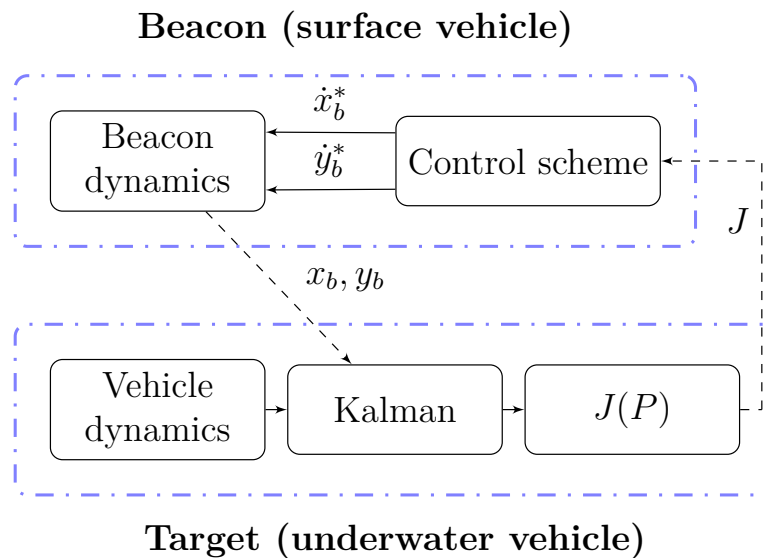
(a) The concept of observable trajectory tracking using extremum seeking based control scheme. Dashed signals represent acoustic communication.



(b) Vehicle–beacon acoustic interogation scheme.
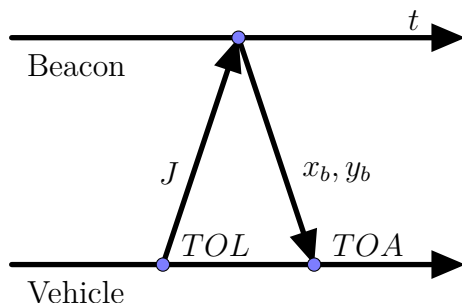
| Sender modem | Exchanged data |
|---|---|
| Target | cost value $J$ |
| Beacon | $x_b, y_b$ |

(c) Acoustically exchanged data.

**Figure 4.1:** The concept of mobile beacon control in single range navigation.

that the beacon's maximum absolute velocity $\|\boldsymbol{\nu}_b\|$ must be much higher than the target's absolute velocity $\|\boldsymbol{\nu}_t\|$. This requirement results from the fact that the beacon has to traverse much longer path while following the vehicle in order to provide informative range measurements.

Figure 4.1a depicts the main idea behind the control algorithm that steers the mobile beacon in order to decrease the localization error of the single range navigation system running on the underwater vehicle. The mobile beacon sends its position $(x_b, y_b)$ to the vehicle's Kalman filter used for navigation. Optionally, the beacon's velocity $(\dot{x}_b, \dot{y}_b)$ can be sent in order to improve localization performance. Information generated in the target vehicle's navigation filter is then used to calculate observability function value $J(\mathbf{P})$ which gives a measure of observability. This scalar value is then sent to the mobile beacon which tries to reduce it online by using an extremum seeking scheme which steers the mobile beacon towards the observable trajectory. The beacon again sends its position to the vehicle, thus closing the control loop. The range measurement used for determining the vehicle's position is acquired during the acoustic communication cycle using TWTT ranging technique presented in Section 3.1 (See Figure 4.1b.). Also, notice that unlike the algorithms presented in Section 4.1, which are path planning based, proposed method is strictly control based.
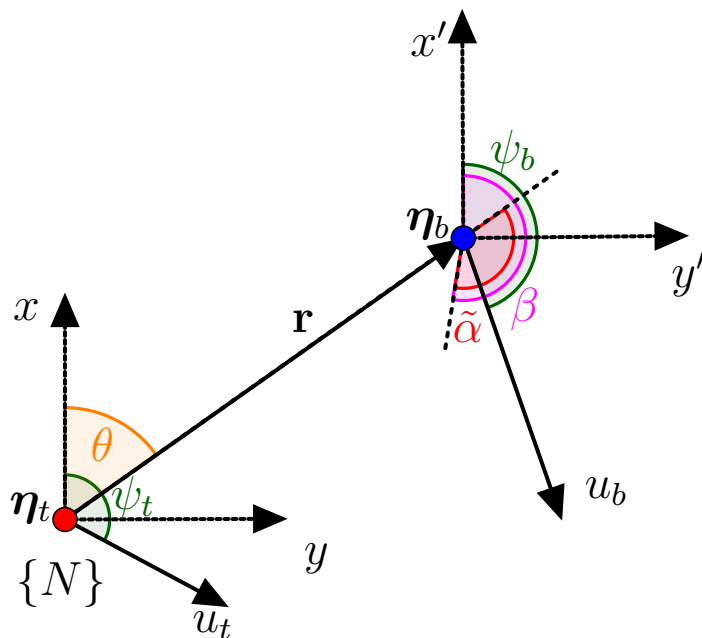


**Figure 4.2:** Beacon–vehicle system in horizontal plane.

In order to introduce the control algorithm which accomplishes the presented idea, system kinematic model is first introduced. The beacon–vehicle relative position system

in the horizontal plane is shown in Figure 4.2, where $\boldsymbol{\eta_t}$ and $\boldsymbol{\eta_b}$ denote the target and the beacon vehicle position, respectively. Assuming underactuated kinematic model, the vehicle's speeds in $\{\mathbf{E}\}$ are

$$\begin{bmatrix} \dot{x}_b \\ \dot{y}_b \end{bmatrix} = u_b \begin{bmatrix} \cos(\psi_b) \\ \sin(\psi_b) \end{bmatrix}, \begin{bmatrix} \dot{x}_t \\ \dot{y}_t \end{bmatrix} = u_t \begin{bmatrix} \cos(\psi_t) \\ \sin(\psi_t) \end{bmatrix}, \tag{4.11}$$

where $\psi_t$ and $\psi_b$ denote respective vehicle orientations, while $u_t$ and $u_b$ denote vehicle surge speeds. In Section 3.2.3 it was shown that in order to achieve maximum conditioning of the observability Gramian, the relative position and velocity vectors between the beacon and the target need to be orthogonal, i.e. circular beacon trajectory around the target will be the one resulting in the highest degree of observability. If we define angle of bearing vector between beacon and the target as $\theta = atan2(\Delta y, \Delta x)$ and the angle of the relative velocity vector as $\beta = atan2(\Delta \dot{y}, \Delta \dot{x})$, then the angle between these two vectors is defined as $\tilde{\alpha} = \beta - \theta$. The degree of observability of the relative beacon–vehicle system will be the highest when $|\tilde{\alpha}| = \frac{\pi}{2}$ rad. For this application, the most convenient way to model beacon position with respect to the target vehicle is using polar coordinates

$$r = \sqrt{(x_b - x_t)^2 + (y_b - y_t)^2}, \tag{4.12}$$

$$\theta = atan2(y_b - y_t, x_b - x_t), \tag{4.13}$$

where $r$ denotes range and $\theta$ denotes bearing between the vehicle and the beacon in the horizontal plane. The beacon position in polar coordinates is

$$\begin{bmatrix} x_b \\ y_b \end{bmatrix} = r \begin{bmatrix} \cos(\theta) \\ \sin(\theta) \end{bmatrix} + \begin{bmatrix} 1 & 0 & 0 \\ 0 & 1 & 0 \end{bmatrix} \boldsymbol{\eta_t}. \tag{4.14}$$

Going further it is assumed that the origin of the relative coordinate frame is located in target's location i.e. $\boldsymbol{\eta_t} = \begin{bmatrix} 0 & 0 \end{bmatrix}^T$. The kinematic model in the polar coordinates is given with

$$\dot{r} = u_b \cos(\psi_b - \theta) - u_t \cos(\psi_t - \theta) \tag{4.15}$$

$$\dot{\theta} = \frac{1}{r} \left[ u_b \sin(\psi_b - \theta) - u_t \sin(\psi_t - \theta) \right] \tag{4.16}$$

Next, the substitution $\alpha = \psi_b - \theta - \frac{\pi}{2}$ is introduced, which under the assumption that $u_t \ll u_b$, defines the angle orthogonal to the previously introduced $\tilde{\alpha}$, i.e. the angle between the relative position and velocity vectors of the beacon–target system. This assumption is justified since beacon speed must be larger than the target speed in order to track it while executing circular trajectories. Going further, in order to determine the

control laws which steer the beacon towards the circular trajectory around the target, it is assumed that the target vehicle is static or slowly drifting, i.e. $u_t \approx 0$. Taking all this into account, yields

$$\dot{r} = u_b \sin(\alpha), \tag{4.17}$$

$$\dot{\alpha} = \dot{\psi}_b + \frac{1}{r} u_b \cos(\alpha). \tag{4.18}$$

In the envisioned control algorithm, constant yaw rate and surge speed control, which is a function of an observability state $j$, are defined as

$$\dot{\psi}_b = \omega, \quad u_b = kj, \tag{4.19}$$

where $\omega$ is perturbation frequency, $k$ controller gain and additional state $j$ is given with

$$\dot{j} = -\frac{j}{k_j}(a - sin(\alpha)) + \frac{q}{k_j}, \tag{4.20}$$

where $a > 1$ and $k_j > 0$ are tuning parameters. As it can be seen from the state equations, and the selected control law, system equilibrium is achieved for $\alpha = 2n\pi$ where $n \in \mathbb{Z}$, i.e only potentially stable trajectory is the circular trajectory around the target and its stability needs to be inferred. Therefore, for the system (4.17)–(4.20), whose state vector is defined as $\mathbf{x} = \begin{bmatrix} r & \alpha & j \end{bmatrix}^T$, and assuming that $a \to 1$, equilibrium point is $\mathbf{x}_e = \begin{bmatrix} -\frac{kq}{\omega} & 2n\pi & q \end{bmatrix}$. The system shifted into the equilibrium states, yields:

$$\dot{r} = k(j + q)\sin(\alpha), \tag{4.21}$$

$$\dot{\alpha} = \omega + \frac{1}{r - \frac{kq}{w}}k(j + q)\cos(\alpha), \tag{4.22}$$

$$\dot{j} = -\frac{1}{k_j}(j + q)(1 - sin(\alpha)) + \frac{q}{k_j}. \tag{4.23}$$

For a very small $k_j$, the state $j$ dynamics are much faster then the dynamics of the rest of the system, and using the singular perturbation theory, [93], order of the system can be reduced by substituting the root of the (4.23) calculated as

$$j = \frac{q\sin(\alpha)}{1 - sin(\alpha)}, \tag{4.24}$$

into (4.17) and (4.18), which yields the reduced system

$$\dot{r} = k\frac{q}{1 - sin(\alpha)} \sin{(\alpha)}, \tag{4.25}$$

$$\dot{\alpha} = \omega + \frac{1}{r - \frac{kq}{w}} k\frac{q}{1 - sin(\alpha)} \cos{(\alpha)}. \tag{4.26}$$

The local stability of the reduced system's equilibrium point $\mathbf{x}_e$ is checked using the first Lyapunov method, [93], i.e. by linearising the system (4.25) – (4.26) as:

$$\mathbf{A} = \left.\frac{\partial \mathbf{f}(\mathbf{x})}{\partial \mathbf{x}}\right|_{\mathbf{x}=\mathbf{x}_e} = \begin{bmatrix} 0 & kq \\ -\frac{\omega^2}{kq} & -\omega \end{bmatrix} \tag{4.27}$$

and analysing its eigenvalues $\lambda$, which are found by solving the equation $\det(\lambda \mathbf{I}_{2 \times 2} - \mathbf{A}) = 0$, yielding:

$$\lambda_{1,2} = -\frac{1}{2}\omega \pm i\frac{\sqrt{3}}{2}\omega. \tag{4.28}$$

Since both eigenvalues are negative for $\omega > 0$, it is concluded that the equilibrium point is asymptotically stable. the phase portrait of the reduced system can be seen in Figure 4.3. Although the equilibrium point is stable for a small change of initial conditions, and $\alpha$
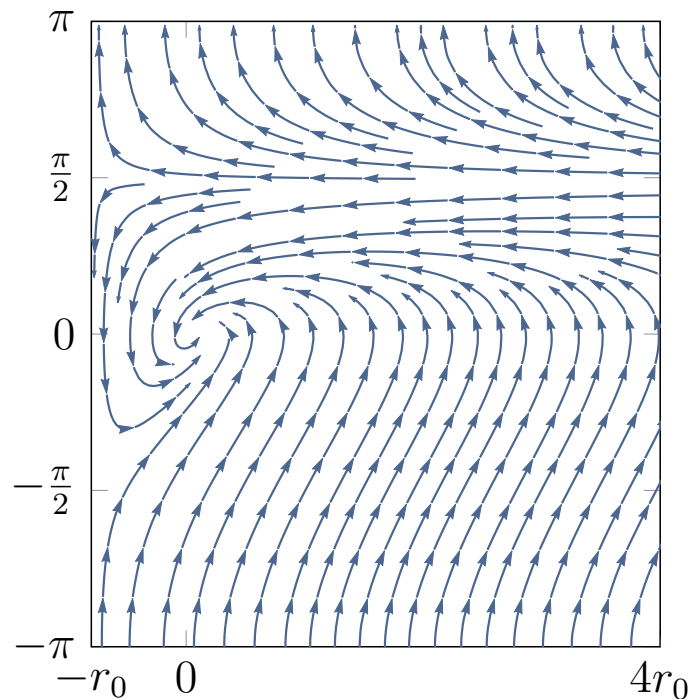


**Figure 4.3:** Reduced system vector field.

cannot remain identically at any angle besides $\alpha = 2n\pi$, it remains to be seen how the range converges when the beacon is far away from the target, i.e. $r$ is large. In that case,

the second term in (4.18) tends to zero and state reduces to $\dot{\alpha} = \omega$ yielding $\alpha(t) = \omega t + \alpha_0$, which results in the following system

$$\dot{r} = kj \sin\left(\omega t + \alpha_0\right) \tag{4.29}$$

$$\dot{j} = -\frac{j}{k_j}(a - sin(\omega t + \alpha_0)) + \frac{q}{k_j} \tag{4.30}$$

As already mentioned, for a very small $k_j$, the state $j$ dynamics are much faster and order of the system can be reduced by finding the solution of the equation $0 = -j(a - sin(\omega t + \alpha_0)) + q$, which yields single isolated root

$$j = \frac{q}{a - sin(\omega t + \alpha_0)}. \tag{4.31}$$

By substituting the expression (4.31) into (4.29), the reduced system is obtained

$$\dot{r} = kq\frac{\sin\left(\omega t + \alpha_0\right)}{a - sin(\omega t + \alpha_0)}. \tag{4.32}$$

Before going further, Table 4.1 is used to intuitively show how the selected cost state enables the beacon to converge to the target vehicle. Relation between the relative angle $\alpha$ and the absolute surge speed $\|u_b\|$ is calculated using (4.31), to show that the beacon speed is reduced when the beacon is pointing away from the target ($\alpha = -\frac{\pi}{2}$), while it is increased when the beacon is pointing towards the target ($\alpha = \frac{\pi}{2}$). It is expected that

| Relative angle $\alpha\,[rad]$ | Absolute surge speed $\|u_b\|\,\left[\frac{m}{s}\right]$ |
|---|---|
| $\alpha = 0$ | $\|u_b\|_e$ |
| $\alpha = \frac{\pi}{2}$ | $\|u_b\|_{max}$ |
| $\alpha = \pi$ | $\|u_b\|_e$ |
| $\alpha = -\frac{\pi}{2}$ | $\frac{1}{2}\|u_b\|_e$ |

**Table 4.1:** Relation between relative angle $\alpha$ and absolute surge speed $\|u_b\|$ for $a \approx 1$. Symbol $\|u_b\|_e$ denotes equilibrium speed, while $\|u_b\|_{max}$ denotes maximum beacon speed.

due to the such behaviour and persistent excitation introduced by the parameter $q$, the beacon range with respect to the target should reduce on average. In order to check that, the reduced system (4.32) is averaged, resulting in

$$\dot{r}_{avg} = kq\frac{1}{2\pi}\int\limits_{-\pi}^{\pi}\frac{\sin\left(\tau + \alpha_0\right)}{a - sin(\tau + \alpha_0)}\,d\tau = kqI(a) \tag{4.33}$$

where $I(a) > 0$ for $a \in (1, a_1)$. Taking derivative of a Lyapunov function defined as $V = r_{avg}^2$ yields $\dot{V} = kqr_{avg}I(a)$. Due to the problem formulation, $r_{avg} \geq 0$ for $\forall t$ and for $k < 0$ the derivative is negative definite, which implies that the system, defined with (4.32), on average converges towards the set $B_l(r_l) = \{r \geq 0 \,|\, r < r_l\}$, where $r_l$ is the smallest value for which the large range assumption is still valid.

## 4.3 Algorithm implementation

As mentioned in the concept description, the main idea of the proposed algorithm is to steer the mobile beacon towards a trajectory where underwater vehicle's navigation system is observable at all times by using some scalar measure in the control scheme that is calculated from the information generated in the vehicle's navigation filter. In this section, scalar measure calculated from navigation filter covariance matrix is presented, before full control scheme implementation is given.

### 4.3.1 Estimator state model

In order to calculate the signal $J(\mathbf{P})$ on the target vehicle, its position variance must be estimated. The state space estimation model of a vehicle – beacon system relative position in the horizontal plane, used in the Kalman filter estimator shown in "Kalman" block in Figure 4.1a, is described with

$$\dot{\boldsymbol{\eta}} = \mathbf{A}\boldsymbol{\eta} + \boldsymbol{v} + \boldsymbol{\zeta}, \tag{4.34}$$

$$r_m = \|\boldsymbol{\eta}\| + \zeta_r, \tag{4.35}$$

where $\boldsymbol{A} = \mathbf{0} \in \mathbb{R}^{2 \times 1}$, the state vector is given with $\boldsymbol{\eta} = \begin{bmatrix} \Delta x & \Delta y \end{bmatrix}^{\mathrm{T}}$ where $\Delta x = x_t - x_b$ and $\Delta y = y_t - y_b$ are relative positions in $\{\mathbf{E}\}$ coordinate frame. The input $\boldsymbol{v} = \begin{bmatrix} \Delta v_x & \Delta v_y \end{bmatrix}^{T}$ contains measured relative speeds between the vehicle and the beacon in Earth–fixed $\{\mathbf{E}\}$ coordinate frame produced by the actuators, sea currents or some other disturbances that act on the vehicle and the beacon, while $\boldsymbol{\zeta} \in \mathrm{R}^{2 \times 1}$ represent the process noise. Depending on the vehicle's sensor configuration, some of the quantities acting on the vehicle cannot be measured, so they can be considered as a process noise. The system measurement model (4.35) is represented by the Euclidean norm between the vehicle and the beacon position where $\zeta_r \sim \mathcal{N}(0, \sigma)$ is measurement noise modelled as Gaussian white noise with variance $\sigma$.

The equation (4.35) represents the range measurement in the horizontal plane, however, the acoustic range measurements are acquired by acoustic modems in a three dimensional space. Since depth sensors are affordable, range measurements in horizontal

plane are easily calculated as $r_m = \sqrt{R^2 - z^2}$ where $R$ is measured range and $z$ is target vehicle depth. Achieving observability of the system (4.34)–(4.35) ensures that relative distance between the vehicle and the mobile beacon in the respective directions can be successfully estimated. The beacon position is known and sent to the target vehicle via acoustic link, therefore determining target vehicle absolute position in $\{\mathbf{E}\}$ coordinate frame is straightforward.

## 4.3.2  Observability function $J(\mathbf{P})$

In [94] the link between the system's observability Gramian $\mathbf{W}$ and estimation covariance matrix $\mathbf{P}$ for the system given with (4.34) and (4.35) is established (See Appendix 6.). It is shown that the problem of maximizing the minimal eigenvalue of the observability Gramian $\mathbf{W}$ corresponds to minimizing the maximal eigenvalue of the estimation covariance $\mathbf{P}$. As mentioned in Section 3.2.3, the rank condition, usually used in determining the observability of a system, does not give information on the quality of observability, only whether the system is observable or not. Therefore, the local estimation condition number $\kappa$ introduced in Section 3.2.3 is used to measure the degree of observability of a system. Calculating local estimation condition number of the covariance matrix $\mathbf{P}$ yields

$$\kappa = \frac{Tr\left(\mathbf{P}\right) + \sqrt{[tr\left(\mathbf{P}\right)]^2 - 4\,det\mathbf{P}}}{tr\left(\mathbf{P}\right) - \sqrt{[tr\left(\mathbf{P}\right)]^2 - 4\,det\mathbf{P}}}, \tag{4.36}$$

where operators $tr(\cdot)$ and $det(\cdot)$ stand for matrix trace and determinant, respectively. Finally, function that gives observability measure of the navigation system, and is used in "$J(\mathbf{P})$" block in Figure 4.1a, is given with

$$J\left(\mathbf{P}\right) = \sqrt{[tr\left(\mathbf{P}\right)]^2 - 4\,det\mathbf{P}}. \tag{4.37}$$

The minimum of the function $J\left(\mathbf{P}\right)$, as it is defined, is achieved when the eigenvalues of the matrix $\mathbf{P}$ are equal, meaning that localization error in respective directions is the same. The single range measurement can be taken from only one direction at the time, therefore that minimum value cannot be obtained and the goal of the proposed control algorithm is only to reduce value of this function. What is more important, function (4.37) exhibits practically the same behaviour as state $j$ given with (4.20). Namely, presence of the process noise matrix $\mathbf{Q}$ is an integral part of the Kalman filter design. It accounts for the possible state model errors and in the presented case it enables variation of the state variables which are assumed to be constant. The process noise increases covariance with time, which directly influences the proposed observability function in a way that, when the vehicle trajectories have bad degree of observability, the function value grows

unbounded and therefore introduces the persistent excitation in system.

The function (4.37) is very convenient for use since a navigation filter is necessary for vehicle's localization when using single range measurements and the covariance matrix $\mathbf{P}$ is already available aboard the vehicle. Thus, additional computational complexity is low. The state model (4.34) used herein is rudimentary but it was used in order to show the concept, in practice, it is possible to use more complex state models like those in Sections 2.1.2 and 2.1.3, and use covariance from that filter to determine function $J(\mathbf{P})$.

### 4.3.3 Control scheme

The control algorithm, defined with (4.19), that utilizes observability measure $J(\mathbf{P})$ is shown in Figure 4.4. Such implementation, where control reference inputs are the beacon's heading $\psi_b^*$ and surge speed $u_b^*$, is suitable for underactuated vehicles. In real–life implementation vehicle constraints are an important consideration. In order to avoid saturation of control input, in the cases when the cost is high, additional filtering is used, thus the pre–filter block in Figure 4.1a. A high pass filter implementation, defined with

$$\gamma = \left(1 - \frac{\omega}{s + \omega}\right) J(\mathbf{P}) + c, \tag{4.38}$$

eliminates the low frequency changes in signal $J(\mathbf{P})$. In that way the signal $\gamma$ value is always bounded and by selecting the appropriate gain $k$ value, control reference input does not go into saturation. However, an additional constant offset $c$ is needed in order to shift $\gamma$ value into positive domain. This value is proportional with surge speed which should be always positive. Additionally, the value of offset $c$ determines the beacon's surge speed when the stationary state around the target is achieved.
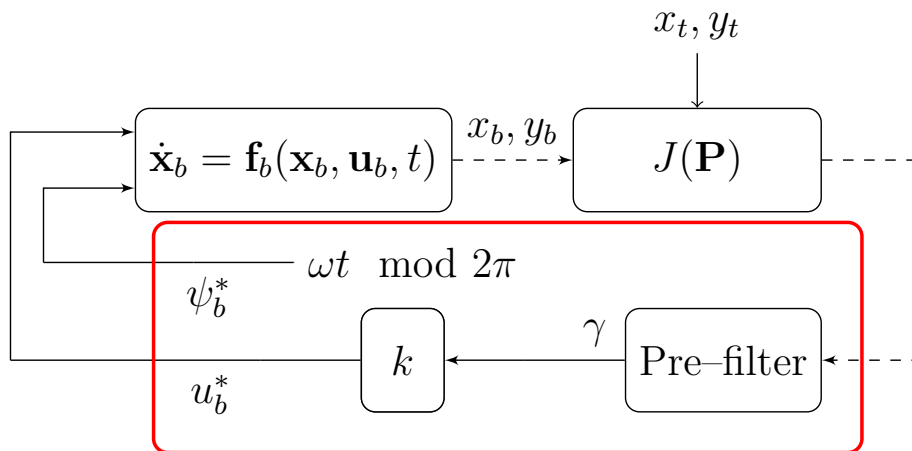


**Figure 4.4:** Control scheme employed for steering underactuated mobile beacon in 2D plane. Red box marks "Control scheme" block from Fig. 4.1a.
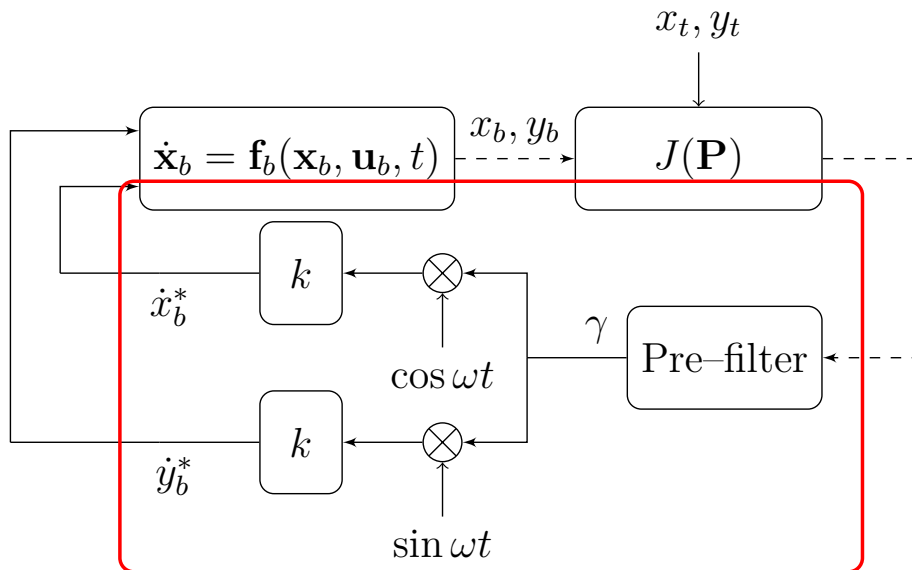
**Figure 4.5:** Control scheme employed for steering mobile beacon in 2D plane. Red box marks "Control scheme" block from Fig. 4.1a.

Figure 4.5 represents an equivalent scheme to the one in Figure 4.4 where the control reference inputs $\dot{x}_b^*$ and $\dot{y}_b^*$ are low–level velocity controller references:

$$\dot{x}_b^* = k\gamma \cos \omega t \tag{4.39}$$

$$\dot{y}_b^* = k\gamma \sin \omega t \tag{4.40}$$

Looking at the scheme, and ignoring pre–filter block, first the cost signal $J$ is demodulated by multiplication with two orthogonal sinusoidal perturbations with angular frequency $\omega$. Demodulated signals are then multiplied by a constant gain $k$ in order to get velocity reference for the beacon vehicle in respective directions. Consequently, the beacon movement influences change of the cost function, thus closing the control loop. There is a similarity of the presented scheme to the extremum seeking scheme in Section 3.3. However, unlike extremum seeking control, in the presented implementation there is no control input perturbation signal and no gradient estimation of the static map. Instead, persistent excitation exhibited by process covariance in the $J(\mathbf{P})$ function is exploited by the control scheme. Circular motion is achieved with constant yaw rate control law, while center of the circular motion is converging towards the target on the principle already mentioned in Section 4.2. Beacon starts executing circular motion with surge speed defined by current observability function value and constant yaw rate, which causes angle $\alpha$ to change (See Figure 4.6a.). When $|\alpha|$ is near $\frac{\pi}{2}$ i.e when the bearing vector between the beacon and the target and the relative velocity vector is nearly orthogonal system is observable and the observability function decreases. Notice that during one perturbation period the bearing and relative velocity vectors are orthogonal at the at least two points (See Figure 4.6b.).

These two points are the minimum and maximum range distance during the current de-modulation signal period. While the beacon is approaching the minimum range point, the value of the function $J(\mathbf{P})$ is high and the beacon approach speed is high. As beacon passes minimum range point, and starts to point away from the target, the beacon speed has already decreased significantly. The beacon continues to point away from the target, while still maintaining constant yaw rate. By going away from the target, beacon assumes a trajectory with the lower degree of observability which causes increase of the value of the function $J(\mathbf{P})$ and cycle starts again. Due to such behaviour, on average, the beacon vehicle approaches the target faster than it departs the target i.e. the beacon converges and remains close to the underwater target (See Figure 4.6c.).



(a) Beacon starts executing circular motion with surge speed defined by current cost value and constant yaw rate, which causes the angle $\tilde{\alpha}$ to change.
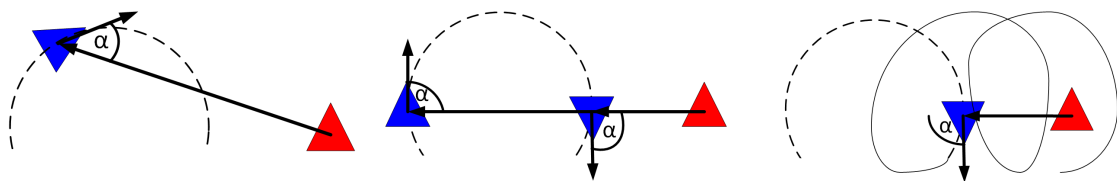
(b) During one perturbation period the bearing and relative velocity vectors are orthogonal at the at least two points.

(c) On average, the beacon vehicle approaches the target faster than it departs the target, which results in spiral motion.

**Figure 4.6:** Depiction of MBC algorithm operation. Blue and red triangles represent the beacon and the target vehicles, respectively.

## 4.4 Simulation results

The algorithm implementation proposed in Section 4.3 was simulated for two different scenarios, in MATLAB simulation environment: stationary vehicle and mobile vehicle assuming curved trajectory. For both scenarios, we compared the basic case where mobile beacon executes constant speed circle trajectory which ensures the system's observability, and the case where the mobile beacon is assuming the trajectory generated by the proposed Mobile beacon control (MBC) control algorithm. The simulations included the full vehicle dynamics introduced in Section 2.1.

Figure 4.7 represents results for a case of stationary vehicle. The vehicle is stationary in position $(5,5)$, while the mobile beacon start position is in point $(0,5)$. Both the vehicle's and the beacon's navigation filters were initialized with wrong initial position. Figure 5.2 shows the trajectories of the beacon moving in both circular (green) and extremum seeking (red) trajectory. Figure 4.7b and 4.7c show that extremum seeking approach steers the

(a) Vehicle an beacon trajectories.

(b) $x$-coordinate estimate error.

(c) $y$-coordinate estimate error.

(d) Observability function $J(\mathbf{P})$.

(e) Power consumption.

(f) Energy consumption.
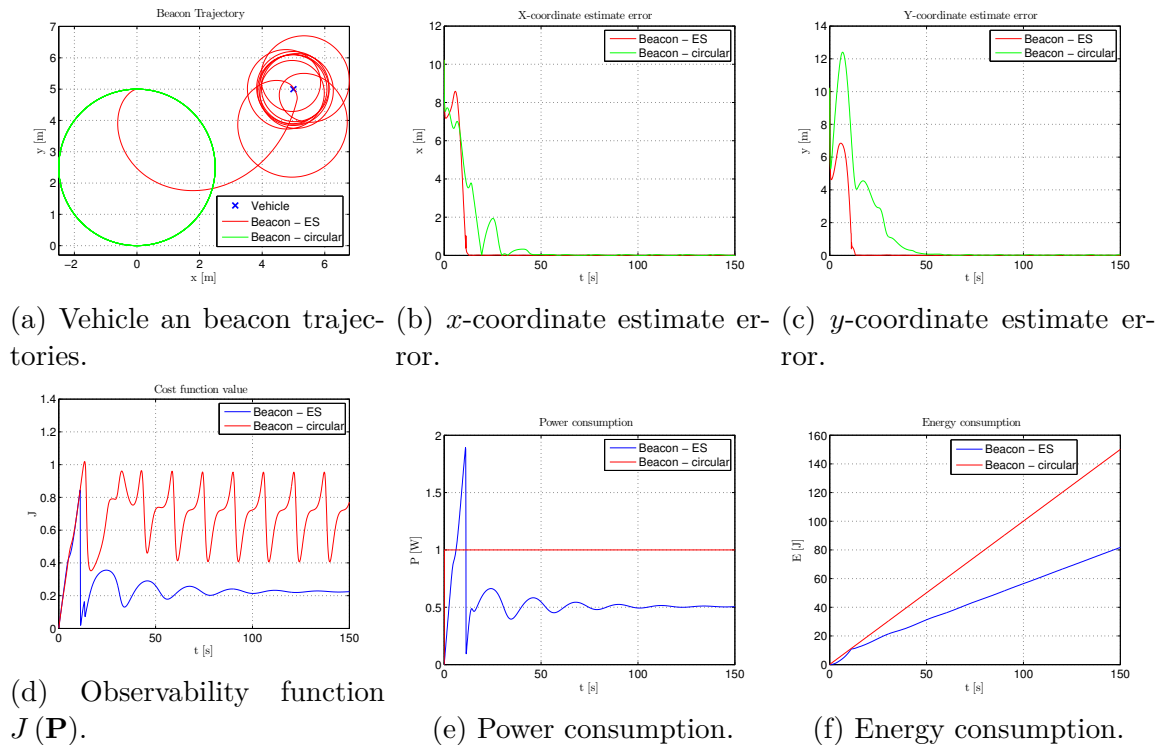
**Figure 4.7:** Scenario 1: Stationary vehicle.

mobile beacon along the path which enables faster convergence of the vehicle's navigation filter. Such convergence is achieved with higher peek power (See Figure 4.7e.), but overall lower energy consumed (See Figure 4.7f.) compared to the mobile beacon doing circular constant speed trajectory. This higher initial power demand is present because beacon converges towards the target vehicle.

In the second scenario, the target vehicle is executing circular trajectory with radius $r_c \approx 7.5\,m$, as shown in Figure 4.9. The target and a mobile beacon trajectories are shown in Figure 4.8a, where it is visible that mobile beacon using extremum seeking approach (red line) follows the target along it's path, confirming that despite target movement, which can be considered as an outside disturbance, alogrithm steers the beacon to a circular trajectory around the target. Looking at the Figure 4.9a, it is visible that the observability function increases with distance between vehicle and mobile beacon, while it is bounded when the MBC algorithm is deployed. That was expected, since, in [69] it was shown that observability of system using single range navigation decreases with the larger distance to the beacon. The coordinate estimate errors, shown in Figure 4.8c and 4.8d, show that error when using MBC approach is smaller, and similar at all times since the beacon is following vehicle, while consuming much less energy at the same time.

(a) Vehicle and beacon trajectories.

(b) Estimated vehicle trajectories.

(c) $x$-coordinate estimate error.

(d) $y$-coordinate estimate error.
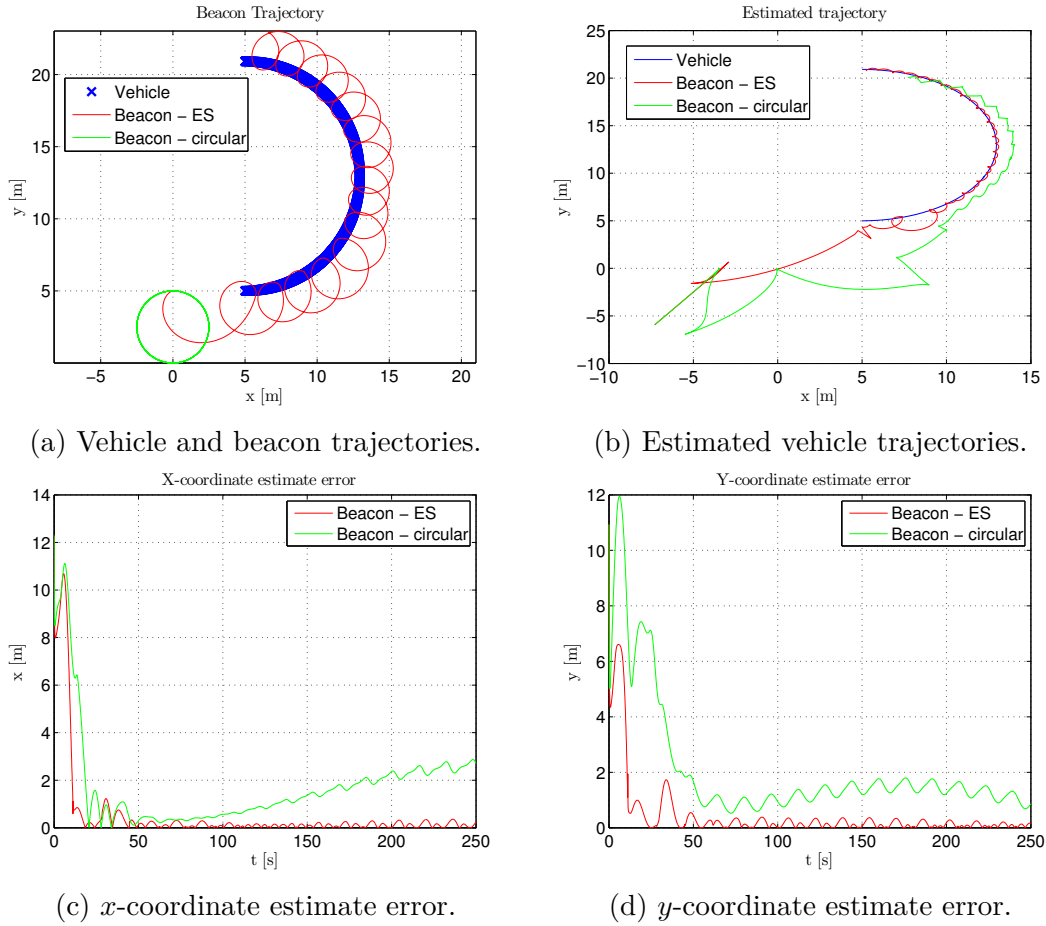
**Figure 4.8:** Scenario 2: Mobile vehicle executing circular trajectory.



(a) Observability function $J(\mathbf{P})$.

(b) Power consumption.

(c) Energy consumption.
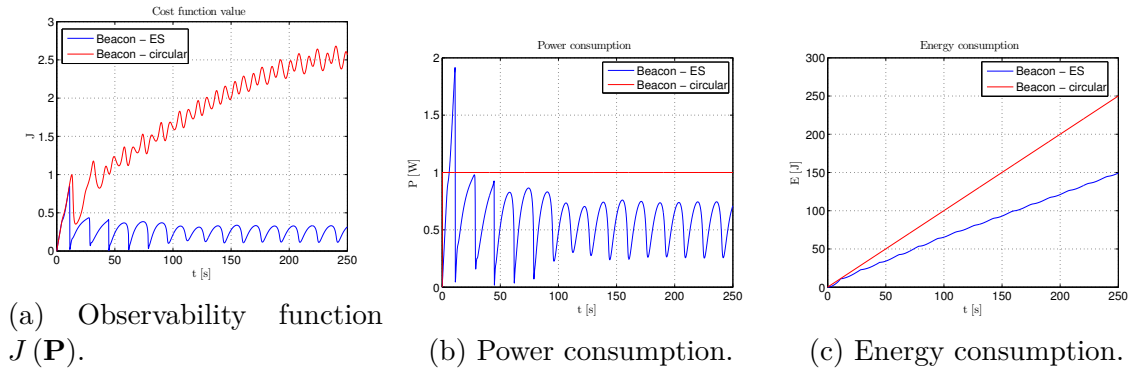
**Figure 4.9:** Scenario 2: Mobile vehicle executing circular trajectory.

## 4.5 Experimental results

Proposed MBC algorithm was tested in real–life conditions at sea trials on both fully–actuated and underactuated mobile beacon vehicles. In the following subsections, results from these trials are summarized.

### 4.5.1 Fully–actuated mobile beacon experiments

The experimental setup, in the case of a fully–actuated beacon vehicle, consisted of an autonomous underwater robot (BUDDY) and an autonomous surface platform (PLADYPOS), seen in Figure 4.10, all developed in the Laboratory for Underwater Systems and Technologies, [34, 95]. The experiments were conducted in October 2015 in Bigorad na Moru, Croatia. The experimental setup consisted of an AUV and an USV which had roles of the target and the beacon vehicle, respectively. USBL modems were installed on both vehicles, and were used for communication and to acquire the range measurements.



(a) Beacon vehicle, PlaDyPos.                    (b) Target vehicle, Buddy
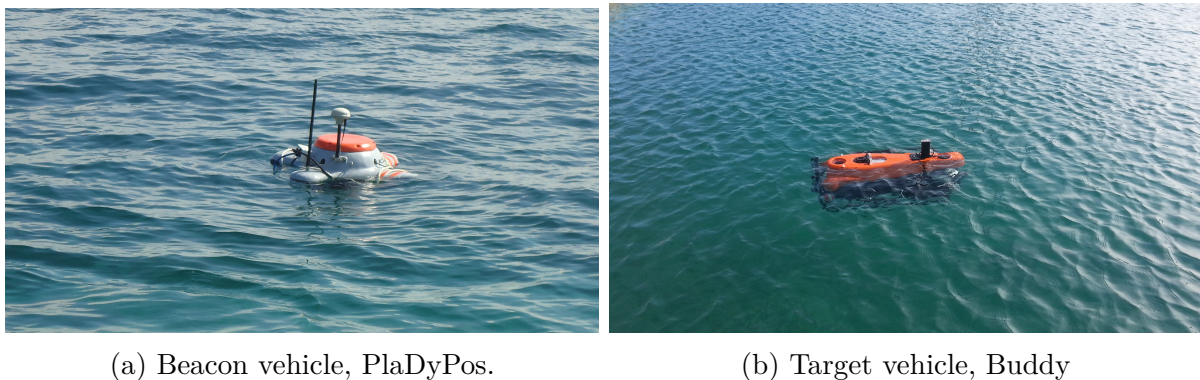
**Figure 4.10:** Vehicles used in the experiment.

In the initial experiment virtual underwater target was used instead of a real vehicle to test the implemented control law, meaning that the underwater target position was simulated onboard the beacon vehicle which executed the MBC algorithm. Figure 4.11 represents the results of such virtual target experiment, which confirmed that the proposed algorithm steers the observability function towards its minimum value and the beacon vehicle towards circular trajectory around the vehicle when deployed on the real vehicle with its dynamics. In the end of the test, around 1100 seconds mark, algorithm was stopped in order to show how function $J(\mathbf{P})$, i.e. position estimate covariance, grows unbounded when the algorithm is not active. Next, the experiments in which BUDDY vehicle was used as an underwater target were conducted. Figure 4.12a shows the underwater target and beacon trajectories for the scenario where the target is static. In the conducted experiments, USBL measurements were used as a ground truth, while underwater vehicle position was estimated using the simple relative distance navigation filter whose model is given with (4.34)–(4.35). The observability function response, calculated from covariance matrix $\mathbf{P}$, is shown in Figure 4.12b. It is visible that even in the case of the delayed and intermittent acoustic measurements, proposed algorithm steers the beacon vehicle towards circular trajectory around the vehicle, and reduces the value $J(\mathbf{P})$. Looking at vehicle trajectory, shown in Figure 4.12a, it is visible that curves are somewhat flattened due to saturated control input, since at the time of the execution,
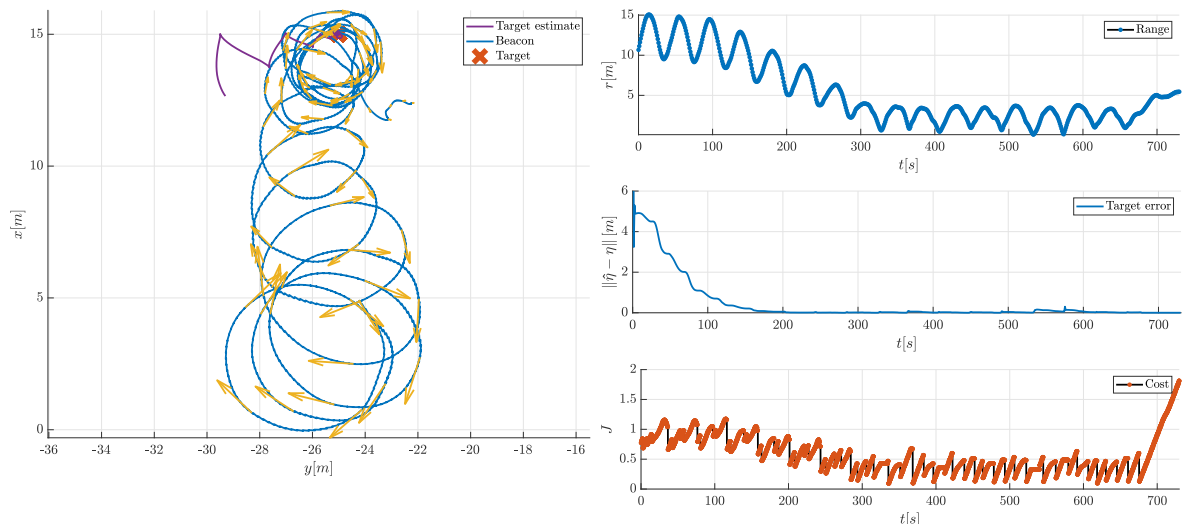
(a) Vehicle and beacon trajectories.

(b) Range, target estimate distance error and cost value responses.
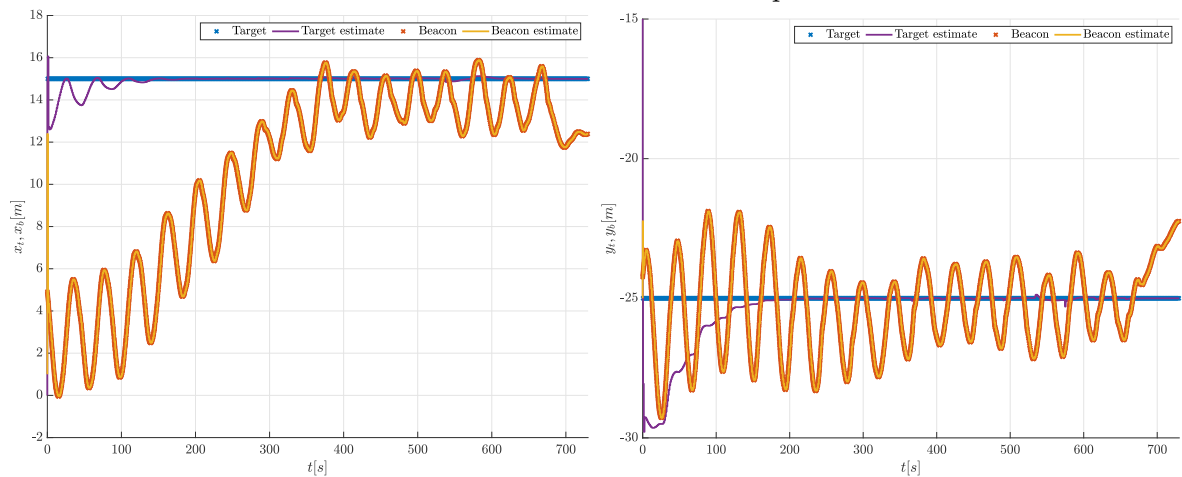
(c) $x$-coordinate estimates.

(d) $y$-coordinate estimates.

**Figure 4.11:** Fully actuated mobile beacon approaching static virtual target.

filter (4.38) was not yet implemented. Regardless, the algorithm successfully converged and decreased observability function which shows its robustness. Figure 4.13 shows the underwater vehicle and beacon trajectories for the scenario where the underwater target is assuming straight line trajectory. Even in the case of the moving underwater target, beacon follows it and reduces cost value, as explained in Section 4.3. In Figure 4.13b, correlation between range and observability function can be clearly seen. As the range between the target and the beacon increases, so is the function $J(\mathbf{P})$ value, and the error of the target distance estimate.

## 4.5.2 Underactuated mobile beacon experiments

The open sea experiments, during which the algorithm implementation presented in Section 4.3 was tested, were conducted in March 2016 in Spain during EXCELLABUST
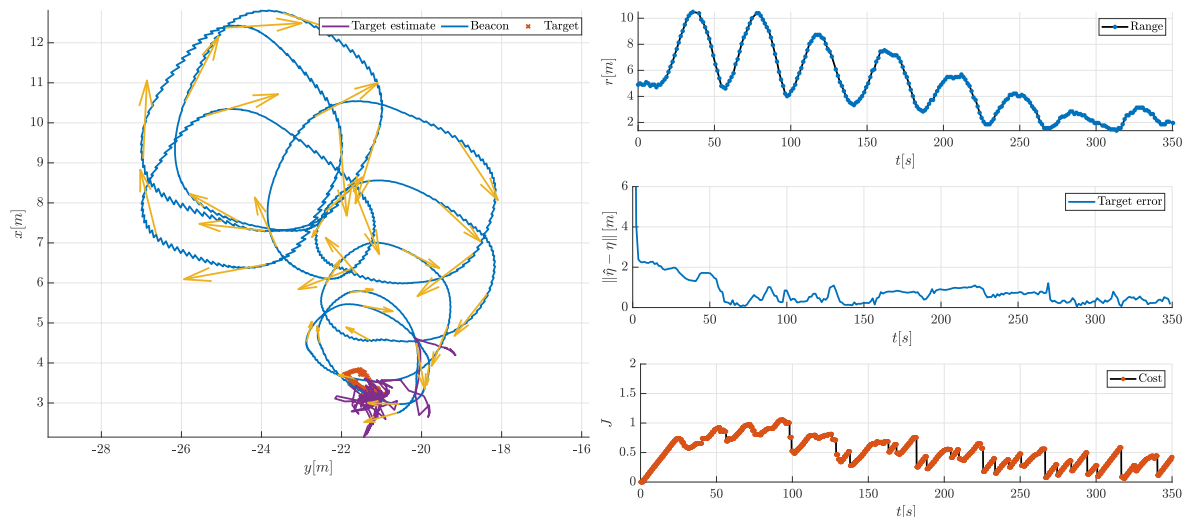
(a) Vehicle and beacon trajectories.

(b) Range, target estimate distance error and cost value responses.
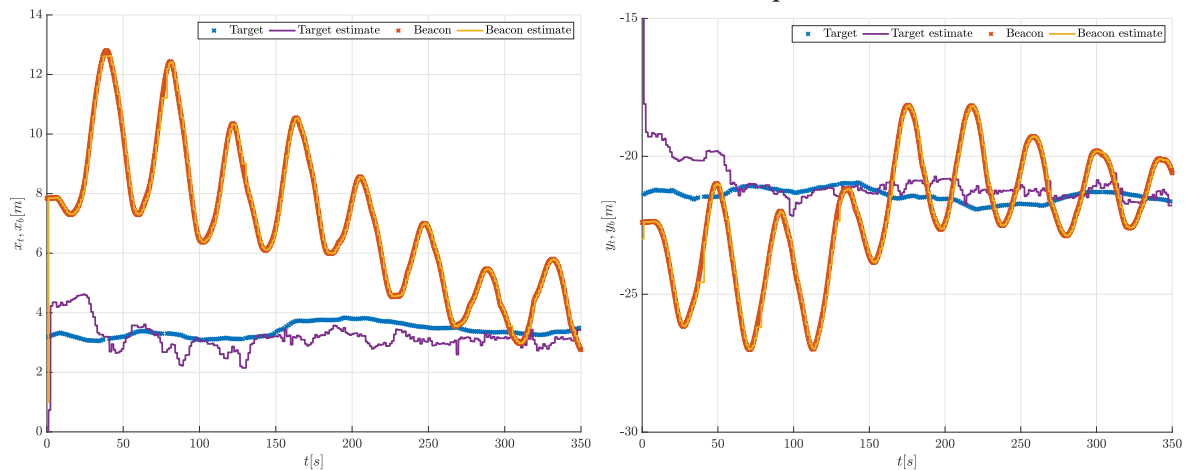
(c) $x$-coordinate estimates.

(d) $y$-coordinate estimates.

**Figure 4.12:** Fully actuated mobile beacon approaching static vehicle.

project staff exchange. The experimental setup consisted of two autonomous underwater vehicles, shown in Figure 4.14: GIRONA 500 and SPARUS II. Both vehicles were developed at the Underwater Robotics Laboratory of the University of Girona, Spain, [21, 96]. GIRONA 500 vehicle acted as the beacon vehicle, while SPARUS II was the target vehicle. The GIRONA 500 configuration used in the experiment was the five–thruster setup: two thrusters actuated surge and yaw, and two actuated the heave degree of freedom. An additional, lateral thruster, that is used in the presence of currents, or when the task at hand demands the capacity of executing lateral movements, was present. However, in order to execute beacon algorithms only two thrusters, those actuating surge and yaw, are necessary. Acoustic modems, used for communication and ranging, were installed aboard the both vehicles. The beacon's position and velocity vectors, and the the function $J(\mathbf{P})$ value were exchanged over the acoustic link. Also, USBL measurements from a stationary mounted USBL were used as a ground truth for the underwater vehicle position. All the
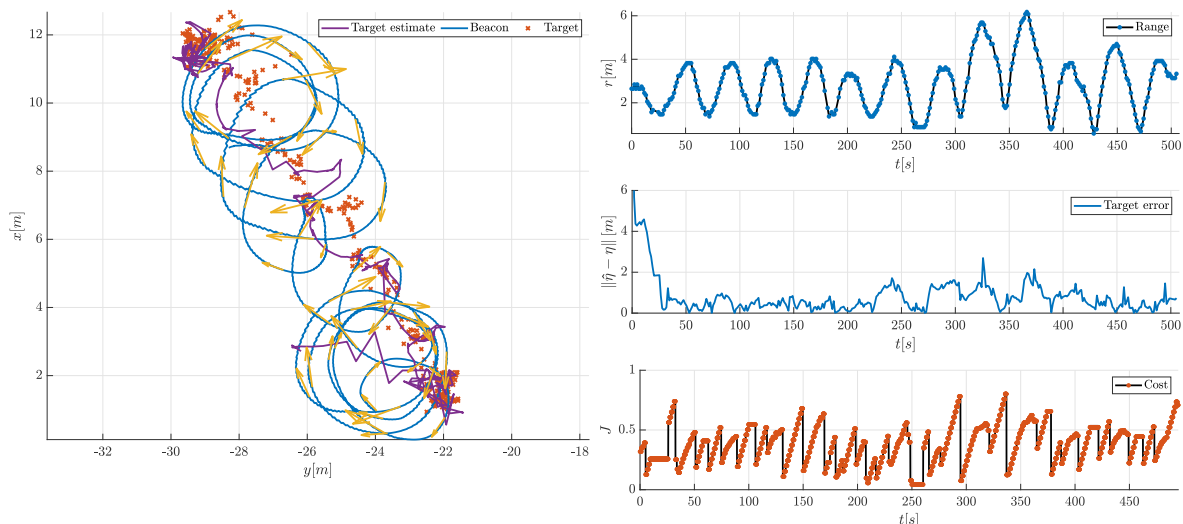
(a) Vehicle and beacon trajectories.

(b) Range, target estimate distance error and cost value responses.
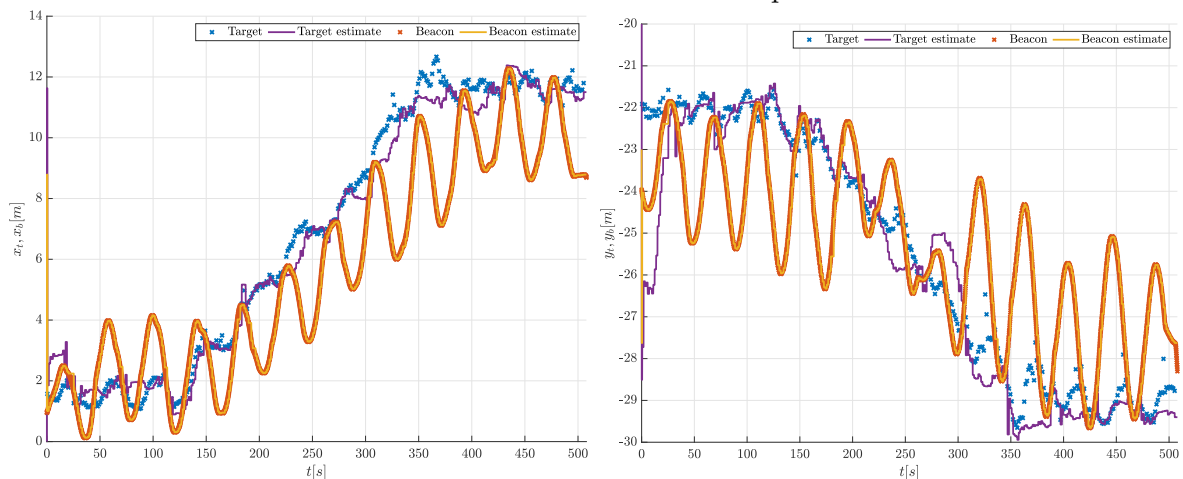
(c) $x$-coordinate estimates.

(d) $y$-coordinate estimates.

**Figure 4.13:** Fully actuated mobile beacon following vehicle assuming straight line trajectory.

computations were done online, aboard the vehicles.



(a) Beacon vehicle, Girona 500.
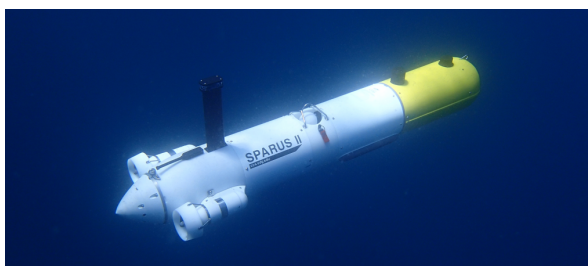
(b) Target vehicle, Sparus II

**Figure 4.14:** Vehicles used in the experiment.

Results of two experiments denoted with *"Experiment 1"* and *"Experiment 2"* are presented herein. During the each experiment, underwater target vehicle executed different trajectory, as shown in Figure 4.15, at the constant depth of 3 meters. During

the experiment the gain parameter was set to $k = 4$, the offset value to $c = 0.1$ and a perturbation frequency of $\omega = \frac{2\pi}{80} \frac{\text{rad}}{\text{s}}$ was selected. The parameters were manually tuned to achieve satisfying performance. In real–life experiments, the perturbation frequency selection depends on acoustic communication constraints. With a higher perturbation frequency faster reaction to target position changes can be achieved, however in that case it is necessary to have a high acoustic update rate in order to capture cost changes. During the experiment the mean communication period was $3.4\,\text{s}$.



(a) The experiment 1.      (b) The experiment 2.
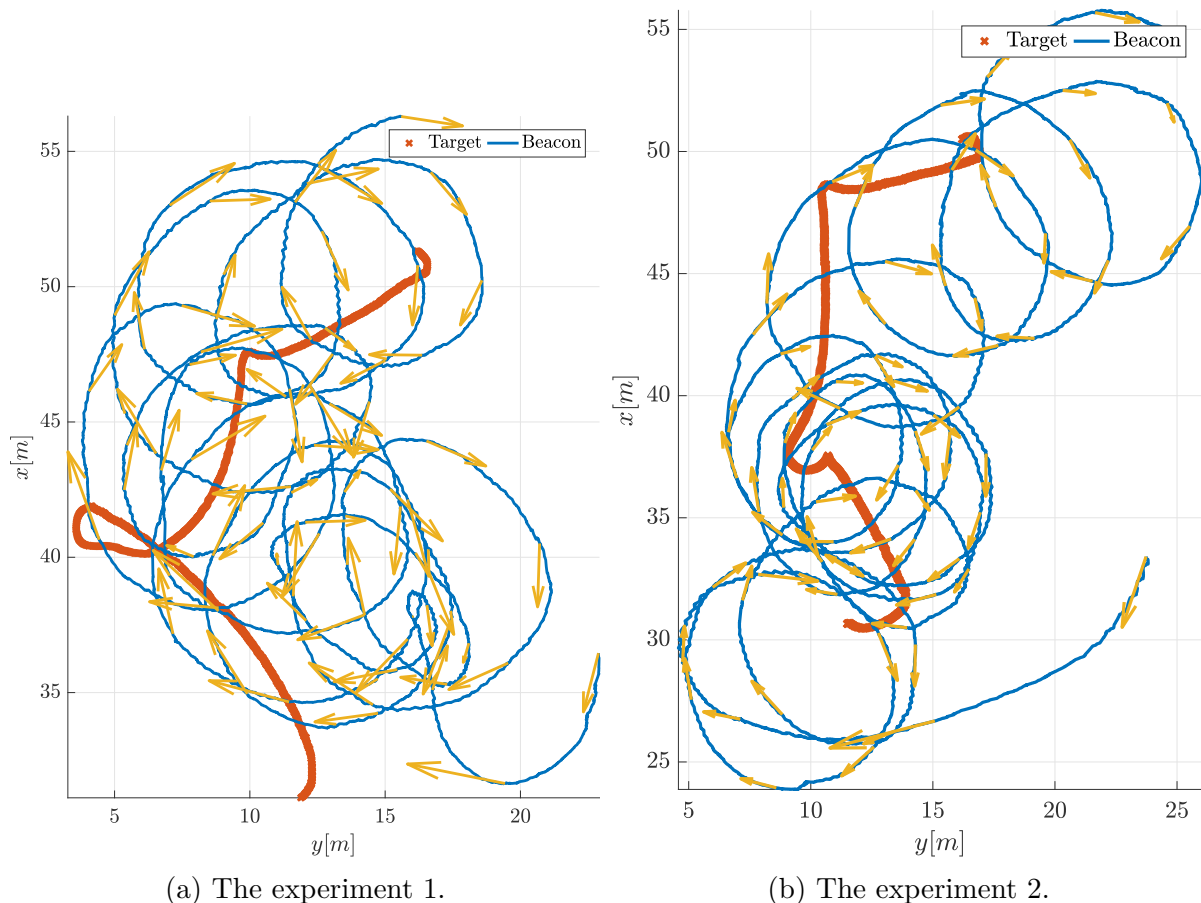
**Figure 4.15:** The target and the beacon trajectories recorded during the two conducted experiments. The yellow arrows denote velocity vectors at respective positions.

Figure 4.15 shows the executed target and beacon trajectories. Purple arrows over the beacon trajectory represent the beacon velocity vector at respective position. It is immediately visible that the beacon vehicle is executing a circular motion which is known to be observable while tracking the underwater target movement. The observability function $J(\mathbf{P})$ and the filtered value $\gamma$ calculated on the target vehicle are shown in Figure 4.16a and 4.17a. Initially the observability function value is high and by executing the algorithm it decreases and stays bounded during the whole experiment, regardless of the target movement. The filtered value does not contain low frequency changes and it is bounded at all times regardless of the cost value, thus solving the problem of control input satura-

tion. The range between the vehicles, during the *Experiment 1*, is shown in Figure 4.16b. Towards the end, it is possible to observe that the range is stabilizing meaning that the circular trajectory around the target is being established. Such trajectory yields highest degree of observability which is confirmed by achieved cost value. In Figure 4.18, the underwater target estimate calculated from available range measurements and the beacon data acquired through the acoustic channel is shown. The position is estimated, as in fully actuated experiments, by a relative distance navigation filter whose covariance matrix $\mathbf{P}$ is used as an argument for calculating the observability function $J(\mathbf{P})$. The beacon's position estimates, estimated on the target vehicle in order to determine target's absolute position, also shown in Figure 4.18, are estimated using the assumed beacon speed in the interval between two adjacent measurements. When measurements are not available for a long time period, spikes in the estimate are present and the longer the acoustic channel is unavailable, the estimate error is larger. Looking at individual position coordinates, it is visible that the beacon tracks the target vehicle position changes while circulating.
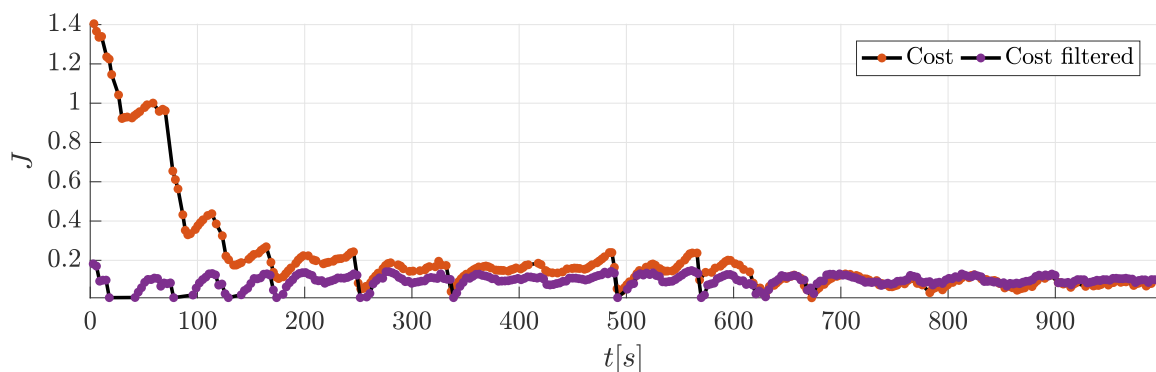


(a) Observability cost value and filtered cost value during experiment.
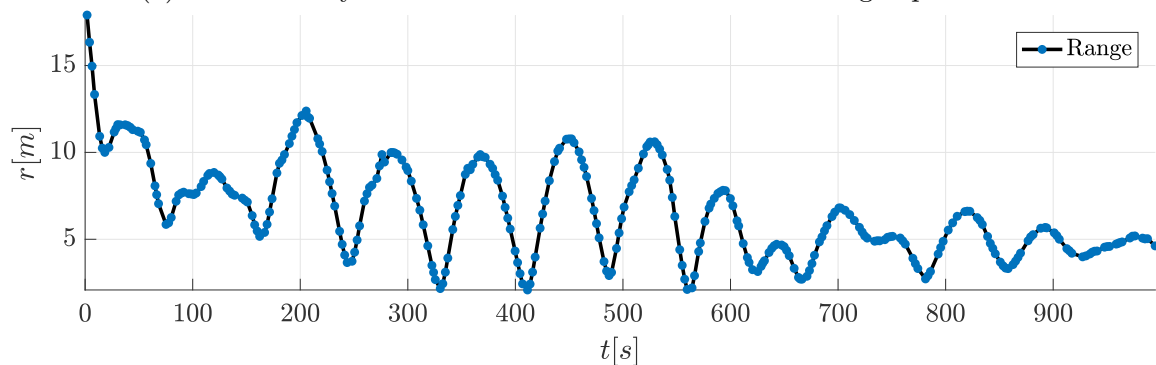


(b) Range measured on target vehicle.

**Figure 4.16:** Cost value and range response of experiment 1.

Figure 4.20c and 4.20d show how the angle between bearing vector and the relative velocity vector $\tilde{\alpha}$ is converging towards value $\tilde{\alpha} = -\frac{\pi}{2}$ rad while Figure 4.20a and 4.20b show at which angle $\tilde{\alpha}$ the individual range measurements are acquired during the experiment. Both results show that the most of the measurements are taken when the bearing
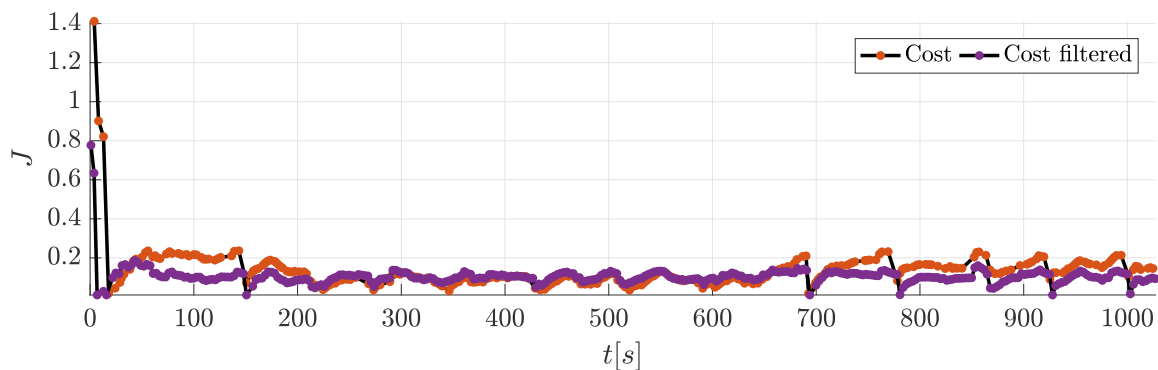
(a) Observability cost value and filtered cost value during experiment.
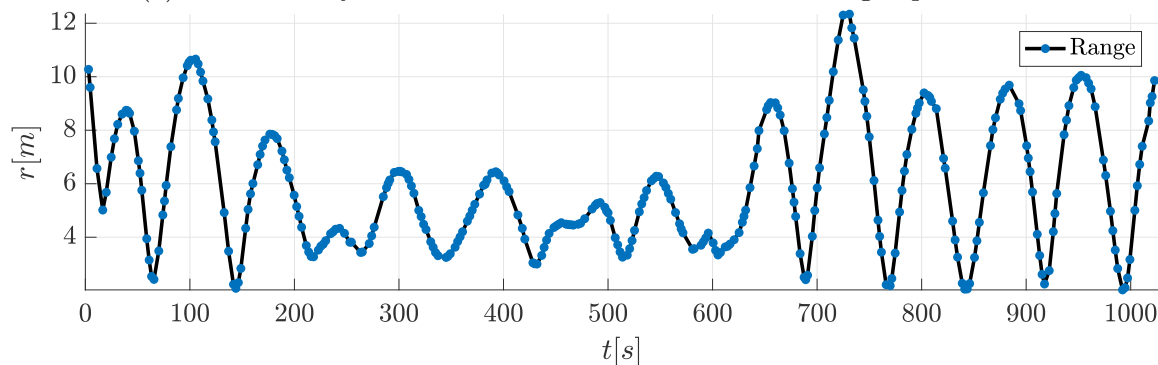


(b) Range measured on target vehicle.

**Figure 4.17:** Cost value and range response of experiment 2.
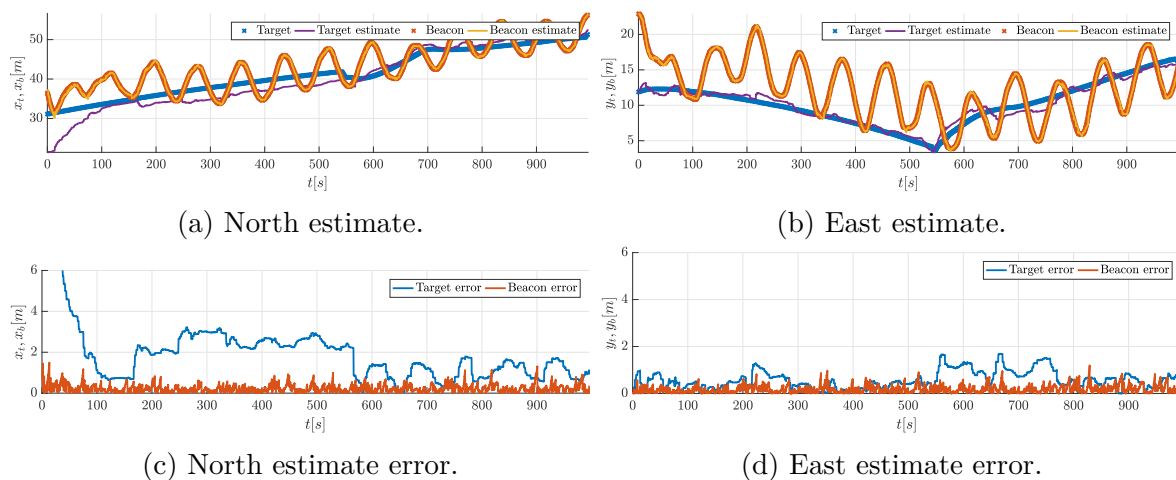


(a) North estimate.



(b) East estimate.



(c) North estimate error.



(d) East estimate error.

**Figure 4.18:** Target and beacon vehicle coordinate estimate and error during the experiment 1.

and velocity vectors are close to orthogonal, therefore confirming that the algorithm is accomplishing its task. Some range measurements are taken at a relative angle slightly larger than $\frac{\pi}{2}$ rad due to delayed cost but also because the target is always moving. In Figure 4.21, the boxplot comparison of the angle $\tilde{\alpha}$ and estimate distance error $\|\hat{\boldsymbol{\eta}} - \boldsymbol{\eta}\|$ of two experiments are shown, once again confirming that the majority of the measurements is distributed around the angle $|\alpha| = \frac{\pi}{2}$.

(a) North estimate.

(b) East estimate.

(c) North estimate error.

(d) East estimate error.
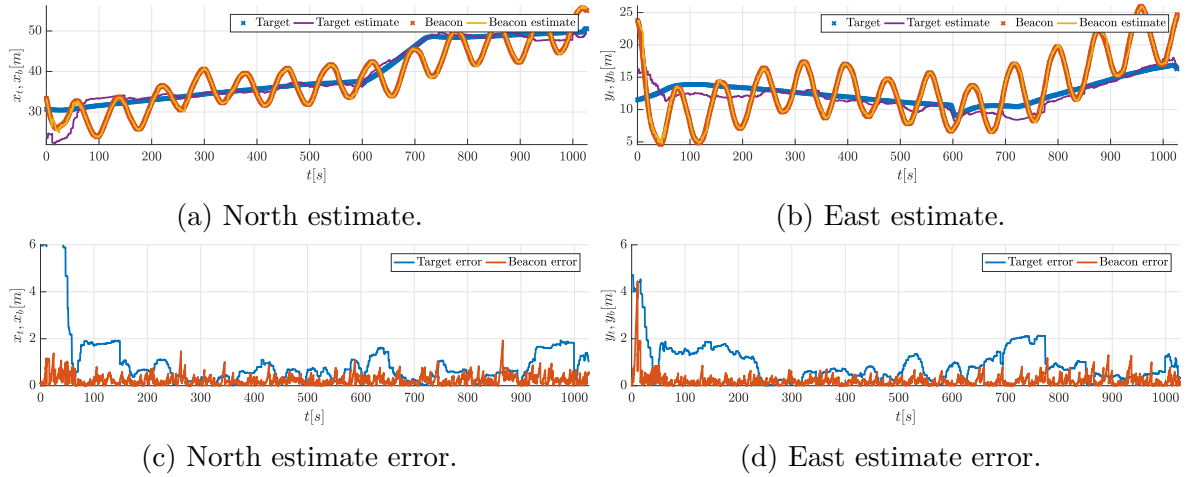
**Figure 4.19:** Target and beacon vehicle coordinate estimate and error during the experiment 2.



(a) Experiment 1.

(b) Experiment 2.

(c) Experiment 1.
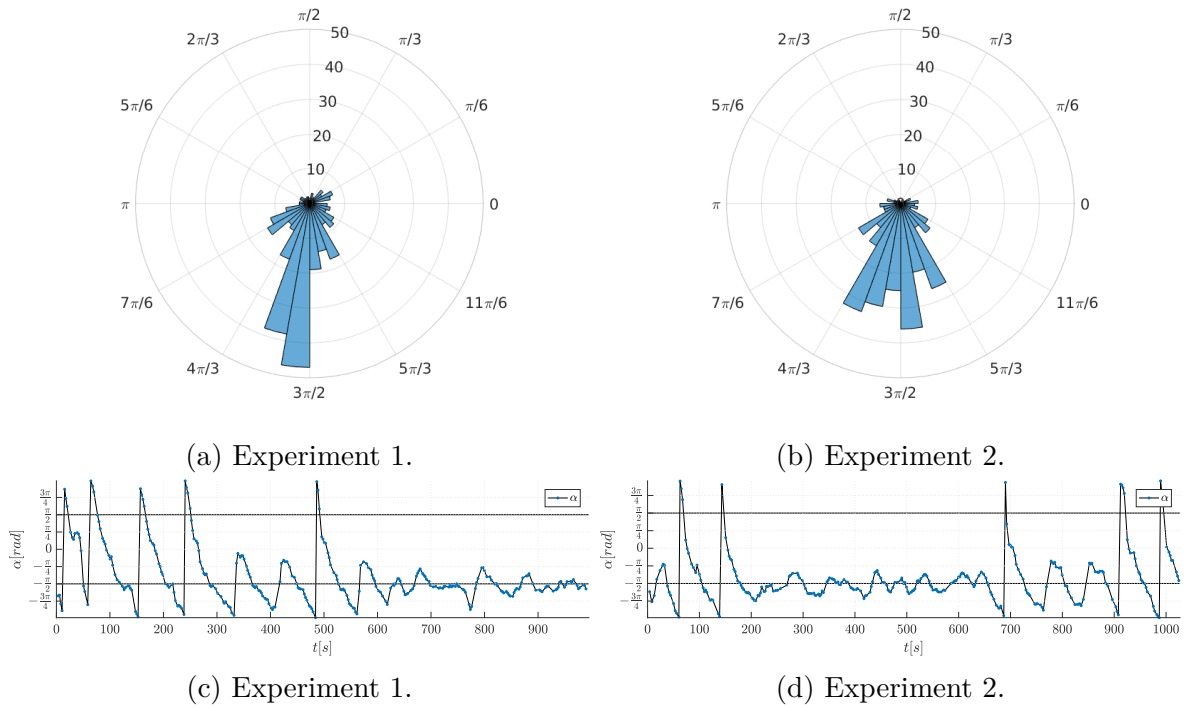
(d) Experiment 2.

**Figure 4.20:** Relative angle between bearing and relative velocity vectors $\alpha$ and angular distribution of acquired range measurements.

In Table 4.2, comparison of the beacon performance indices, presented in Section 3.2.4, for both experiments is given: total beacon path $\Sigma_s$, and average FIM performance index $FIM_{avg}$. In table, FIM denotes path planning approach presented in [54, 55, 72] (See Section 4.1.), which was used to compute trajectories and compare it to the MBC algorithm presented herein. This approach was selected because it can provide optimal trajectories which maximize the obervability of the system and therefore is a good reference. FIM approach trajectories and corresponding indices were calculated offline with known target trajectory for different number of measurements denoted with $m$. In [55],

(a) The angle $\alpha$.

(b) Estimate distance error.
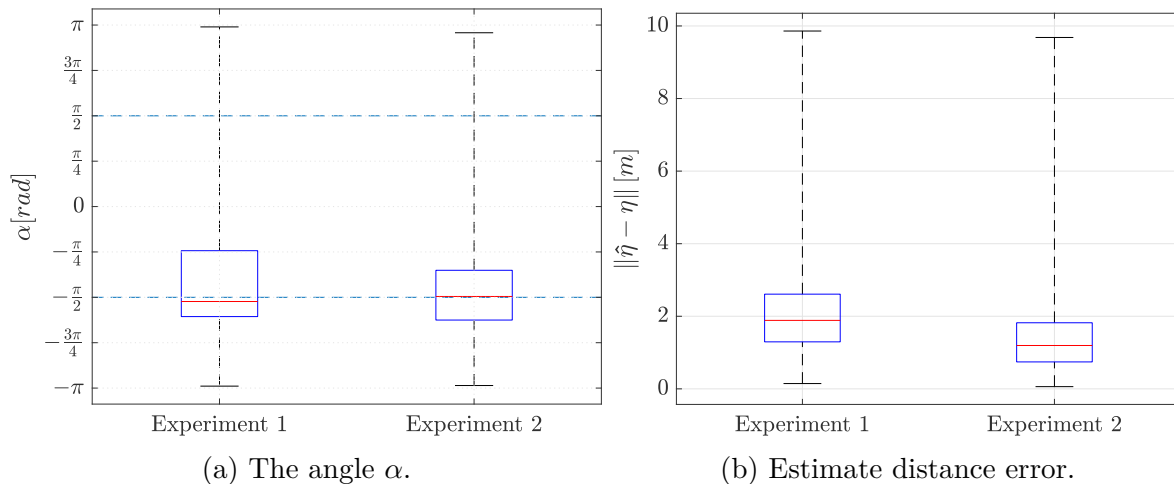
**Figure 4.21:** The boxplot comparison of the angle $\tilde{\alpha}$ and estimate distance error $\|\hat{\boldsymbol{\eta}} - \boldsymbol{\eta}\|$ of the two experiments.

simulation analysis has shown that if the beacon speed is not significantly higher than target speed, the final calculated trajectory is not as informative as it should be and it can even diverge. In such cases, planning the trajectory for the larger horizon, i.e. more measurements, provides a better result. The results shown in Table 4.2 agree with those observations.

There are couple of advantages of FIM approach. It is superior when larger number of future measurements is included and constraints can be easily included in the optimization problem. For the case where $m = 12$, largest average FIM value was achieved for a significantly shorter path. However, if the future target trajectory is not known, some assumption on the future trajectory must be introduced. In the initially envisioned scenario, where beacon does not have information about target position or target position is known for a very short horizon, proposed MBC algorithm performs reasonably good, comparable to the FIM approach with horizon $m = 3$. For the MBC algorithm, notice that the average FIM performance index is larger in *Experiment 2*, which is consistent with smaller estimate error achieved in same experiment.

## 4.6 Conclusion

With growing human interest in underwater environment, need for precise underwater localization and navigation is becoming more important. Single range navigation presents low–cost and easily deployable approach for achieving that. It requires that vehicle executes persistently exciting trajectories which is not always possible due to mission requirements. Using mobile beacon removes constraints imposed on the underwater vehicle trajectory, however this approach requires additional vehicle which raises the costs of the

|  | Experiment 1 | | Experiment 2 | |
|---|---|---|---|---|
|  | $\Sigma_s[m]$ | $|FIM|_{avg}$ | $\Sigma_s[m]$ | $|FIM|_{avg}$ |
| MBC | 330 | 0.59 | 361 | 0.71 |
| FIM $m = 1$ | 458 | 0.08 | 468 | 0.12 |
| FIM $m = 3$ | 348 | 0.85 | 337 | 0.72 |
| FIM $m = 12$ | 194 | 0.95 | 204 | 0.93 |

**Table 4.2:** Summary of performance quality validation for underactuated mobile beacon experiments.

whole system. In real life situations, when planning trajectories which ensure system observability, duration of mission and energy consumption must be taken into consideration. Therefore, optimum must be found between localization accuracy and energy required to achieve such accuracy. Also, there is additional challenge due to delayed and intermittent nature of acoustic communication and presence of distance dependent measurement noise.

The experiments have shown that, even in the presence of unknown vehicle dynamics, unknown disturbances and delayed acoustic measurements, the proposed mobile beacon control algorithm steers the beacon vehicle, both fully actuated and underactuated, towards a circular trajectory around the target vehicle and improves target localization. Proposed mobile beacon control algorithm is suited for underwater application because of the limited bandwidth of acoustic communication. In the proposed beacon control scheme, only observability function value and the beacon position data are sent via acoustic link. As noted, algorithm can be easily deployed on different types of vehicles. It could be particularly interesting in cases when the target model is difficult or impossible to obtain, and when vehicle's trajectory is not known in advance, i.e. in the case when the vehicle is replaced with a human diver. Although the main goal of the algorithm is to enhance underwater target localization, as a consequence it also decreases range between the target and the beacon in the horizontal plane i.e. the beacon is tracking target. All things considered MBC algorithm is reasonable choice for enhancing single range navigation of slowly–moving underwater targets.

# Chapter 5

# Time Difference of Arrival Source Seeking

## 5.1 Motivation

Determining the location of an unknown acoustic signal in an underwater environment is of great interest to the scientific community. Subaqueous sound was first used in navigation to determine the direction of an underwater sound source by means of two hydrophones (underwater sound receivers) installed on a ship, one on each side near the ship's bow. A patent was granted for this device in 1894, [9]. Today, acoustic pingers of various frequencies and signal strengths are commonly used for a variety of purposes, from marking the objects of interest such as black boxes (for search and rescue operations, [97]), to tagging the animals residing underwater (for marine biology purposes, [98]), or simply marking specific locations where an artifact or particular phenomena have been detected by the human divers (for marine archeology, [99]).

As already shown in Chapter 3, source seeking with movement towards the object of interest in the underwater environment can be achieved using range measurements, e.g. acoustic range measurements are used in [86], where the extremum seeking-based control approach from [84] is presented as a means to converge towards the underwater source, while in [82] an extended Kalman filter (EKF) is used to determine source location using range measurements, and the vehicle's conventional control algorithms are then used to reach the desired position. As mentioned in Chapter 3, one of the main issues with estimation–based single range localization systems is the observability of the system. There is a great number of papers dealing with observability of range–only navigation systems using different methodologies, [67], [69], [68]. Should the system not be observable, range measurements can result in false navigation. Therefore, to estimate the source position, the vehicle that is navigating using range measurements from a stationary

source needs to preform trajectories along which the system is observable, e.g. in [76], a method for homing an autonomous underwater vehicle using single range measurements to a subsea docking station is presented, where a Sum of Gaussian filter is used to estimate the docking location while the autonomous vehicle is guided along an observable trajectory.

In order to acoustically acquire range measurements cooperation with the underwater acoustic source (in the form of send-reply communication, or clock synchronization) needs to be established, making these systems inapplicable to solving the problem of determining the location of an unknown underwater acoustic source. One solution to this problem can be found in applying time difference of arrival techniques, which require having at least three receivers that allow the localization of an unknown acoustic source in the horizontal plane, [17]. In general, Time Difference of Arrival (TDOA) is a method that calculates location from the differences of arrival times measured on transmission paths between the source and fixed receivers, [14]. TDOA–based localization schemes usually consist of two steps: the measurement acquisition step and the multilateration step. In the measurement acquisition step, the differences of acoustic signal arrival times on several receiver nodes are measured. Based on the property of a hyperbola, the source will be located on a hyperbola whose difference between the ranges to respective receivers is a constant. The difference in ranges is easily calculated from the measured difference in time of arrival and the known speed of the acoustic signal. With more than two receivers, we can compute more hyperbolic functions which ideally intersect in one unique point, thus determining source location, [15]. Traditional 3D underwater localization techniques require four non-coplanar receivers to localize the underwater signal source successfully, [16]. However, that need can be eliminated via the use of depth information acquired by a pressure sensor, and a projection-based technique that translates receiver nodes to the plane of the signal source, [17]. This makes localization using only three anchors possible, assuming the projection of the three non–colinear anchors is non–degenerative.

The research presented in this chapter, and published in [100], is aimed at developing a control algorithm for an autonomous surface system capable of measuring time difference of arrival of a quasiperiodic underwater acoustic signal passively emitted on a predefined frequency by an acoustic pinger, then utilizing this value to steer the system towards the signal source in the horizontal plane. In the scenario presented herein, time difference of arrival is measured only for one pair of acoustic receivers. Initially, at the TOL, the acoustic signal is emitted from the acoustic source. The signal then travels through the acoustic medium, and is received by the two acoustic receivers at their respective TOA instants. The assumption is that the TOL is unknown, and quasiperiodicity in the envisioned scenario means that the acoustic source regularly emits the signal but

not necessarily with an identical period each time. To the authors' best knowledge, the approach presented herein differs from other source seeking approaches in that it does not use signal amplitude to determine source location. Instead, a single time difference of arrival measurement, acquired by adding second receiver, coupled with an appropriate receiver movement strategy, enables convergence to the signal source in the horizontal plane. One of the advantages of the proposed method over the methods that use signal amplitude to determine source location is that it can be unambiguously determined when the source has been reached since in that case for any change of the baseline orientation, that is formed by two receivers, measured time difference of arrival remains zero. When the signal amplitude is used that is not the case, even when the maximum amplitude of the signal is known, since depth to the source is unknown. Also, much less deviation from the shortest path between the source and the vehicle is needed during the convergence phase to the source compared to perturbation based source seeking systems using signal amplitude. Approaches using two moving receivers can also be found in [101] and [102]. These approaches are estimation–based, unlike the approach presented herein, where raw measurements are used as control algorithm input. Therefore, in the this chapter following subjects are presented:

1. development of a source seeking control algorithm that enables convergence towards an underwater acoustic signal source in the horizontal plane by using single time difference of arrival measurements,

2. stability analysis of the proposed algorithm,

3. experimental validation of the proposed algorithm.

The chapter is organized as follows. Section 5.2 presents the mathematical model of the problem and introduces the surge speed and yaw rate controllers deployed in the source seeking scheme. In the Section 5.3 stability analysis of the proposed control algorithm using Lie bracket approximation technique is given. Section 5.4 describes the practical implementation limitations, discusses how to mitigate them and presents the complete algorithm implementation scheme. The simulation results of the proposed control scheme are given in Section 5.5 where influence of the measurement noise on algorithm operation is the main focus. Section 5.6 presents the experimental results obtained in a real-life environment.

## 5.2   Problem description and control algorithm

In this section, the source seeking problem using time difference of arrival measurements is described and the system's kinematic model is given. Then, the control algorithm, consisting of surge speed and yaw rate controllers that steer the system towards the
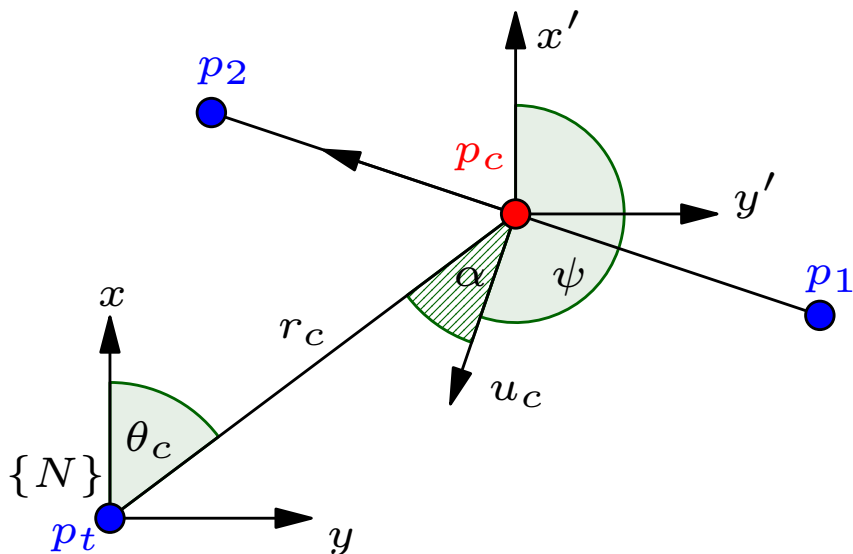
**Figure 5.1:** Sensor baseline $d$ formed by acoustic sensors located at $\mathbf{p_1}$ and $\mathbf{p_2}$, where $\mathbf{p_c}$ denotes baseline center and $\mathbf{p_t}$ underwater acoustic signal source position depicted in the horizontal plane.

source, is presented.

### 5.2.1 Problem description

The system holding two acoustic receivers is modelled as a nonholonomic unicycle, where the heading angle in the global coordinate frame $\{N\}$ is denoted with $\psi$, and the position of the vehicle center is denoted with $\mathbf{p_c} = \begin{bmatrix} x_c & y_c & 0 \end{bmatrix}^T$. Acoustic sensors are mounted orthogonally respective to the system heading $\psi$, thus forming a baseline with point $\mathbf{p_c}$ in
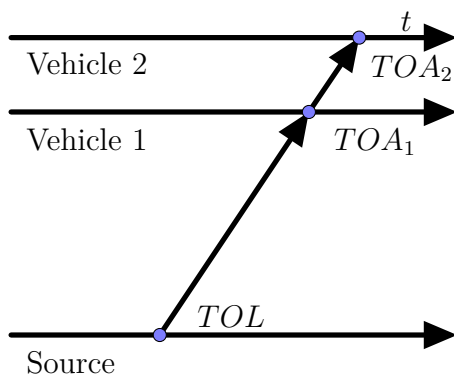


**Figure 5.2:** Time difference of arrival measurement acquisition.

the middle of the baseline. Acoustic source position is denoted as $\mathbf{p_t} = \begin{bmatrix} x_t & y_t & z_t \end{bmatrix}^T$, and the position of the acoustic receivers as $\mathbf{p_i} = \begin{bmatrix} x_i & y_i & 0 \end{bmatrix}^T$ where $i = \{1, 2\}$. Therefore, acoustic receiver positions are defined with $\mathbf{p_1} = \mathbf{p_c} + \mathbf{p_{off}}$ and $\mathbf{p_2} = \mathbf{p_c} - \mathbf{p_{off}}$ where vector $\mathbf{p_{off}} = \begin{bmatrix} \frac{d}{2}\sin\psi & -\frac{d}{2}\cos\psi \end{bmatrix}^T$ is the offset of the receivers from the baseline center $\mathbf{p_c}$ in their respective directions. Parameter $d$ denotes the length of the baseline formed by the acoustic receivers. Depending on the application, if sufficient baseline can be achieved, acoustic receivers can be mounted on a single vehicle, or on two separate vehicles keeping a formation that allows variable baseline length. If mounted on a single vehicle, independent control of the system yaw and surge degrees of freedom is required for algorithm operation, while in the scenario with two vehicles, it is required that the vehicles are fully actuated in order to keep formation. However, in the Section 5.4.2 it is discussed that even in the single vehicle scenario it is desirable that the vehicle is fully actuated in order to compensate for the disturbances affecting it. In the scenario where the vehicles are keeping a formation, it is further assumed that a formation–keeping algorithm is deployed on the controlled vehicles, so that, for the purpose of this analysis, we can mathematically observe both the formation and the vehicle as a single entity with virtual actuators that are used to impart the forward velocity $u_c$ and the angular velocity $\dot{\psi}$.

Only information about the source position can be inferred from the time difference of arrival measurement, therefore, using the notation introduced above, the signal time of arrival difference $\Delta_{TOA}$ is defined as

$$\Delta_{TOA} = TOA_1 - TOA_2 = \frac{\|\mathbf{p_1} - \mathbf{p_t}\| - \|\mathbf{p_2} - \mathbf{p_t}\|}{v} \tag{5.1}$$

where $TOA_1$ and $TOA_2$ present time–of–arrival measurements taken at the respective receivers and $v$ is the speed of sound in water. Going further, normalized non-dimensional measurement $\Delta \in [-1, 1]$, given in the form

$$\Delta = \Delta_{TOA}\frac{v}{d}, \tag{5.2}$$

is used in the control algorithm. The overall control algorithm goal - baseline center convergence towards the acoustic source in the horizontal plane - is achieved through two subgoals: *i)* to orient the baseline towards the signal source, and *ii)* to approach the signal source. These subgoals are achieved through yaw rate and surge speed control of the system, respectively.

## 5.2.2 Yaw rate control law

The first subgoal, positioning the acoustic receiver baseline orthogonally with respect to the bearing vector between the source and the baseline center, can be achieved by bringing $\Delta$ value to zero. In order to do that, in the yaw degree of freedom (5.5) a gradient based extremum seeking controller, as presented in [84], is employed. The Cartesian representation of the unicycle system with such control of the yaw degree of freedom is described with the following set of differential equations:

$$\dot{x}_c = u_c \cos \psi, \tag{5.3}$$

$$\dot{y}_c = u_c \sin \psi, \tag{5.4}$$

$$\dot{\psi} = k(f - x_e h)\sqrt{\omega} \sin \omega t + a\sqrt{\omega} \cos \omega t, \tag{5.5}$$

$$\dot{x}_e = -x_e h + f. \tag{5.6}$$

The states $x_c$ and $y_c$ in (5.3) and (5.4) are kinematic equations of a unicycle–like model, [33]. The equation (5.5) defines the extremum seeking control law in the yaw degree of freedom where a sinusoidal perturbation $a\sqrt{\omega} \cos \omega t$ with perturbation frequency $\omega$ and scaling factor $a$ is added to persistently excite the system while the corresponding demodulation term $\sqrt{\omega} \sin \omega t$ is used to estimate the gradient of the nonlinear map, i.e. the cost function $f$. The cost function that achieves the minimum for $\Delta = 0$ is defined as $f = \Delta^2$. The term $(f - x_e h)$ represents the high–pass filter that is a part of the extremum seeking scheme and it is used to remove possible constant offsets present in the cost function measurement. The state $x_e$ in (5.6) is the filter state and the parameter $h$ is a filter time constant.

## 5.2.3 Surge speed control law

Since the extremum seeking control law in (5.5) only ensures that the baseline is orthogonal with respect to the bearing vector, an additional surge speed control law needs to be introduced. It should steer the center of the baseline towards the source of the acoustic signal, thus achieving the second subgoal. In order to derive an appropriate surge speed control law and later show the stability of the proposed control scheme we resort to use of polar coordinates, defined as

$$r_c = \sqrt{(x_c - x_t)^2 + (y_c - y_t)^2} \tag{5.7}$$

$$\theta_c = \text{atan2}(y_c - y_t, x_c - x_t) \tag{5.8}$$

where $r_c$ denotes range and $\theta_c$ denotes bearing between the baseline center and the source of the acoustic signal in the horizontal plane. Using relations

$$\begin{bmatrix} x_c \\ y_c \end{bmatrix} = r_c \begin{bmatrix} \cos(\theta_c) \\ \sin(\theta_c) \end{bmatrix} + \begin{bmatrix} 1 & 0 & 0 \\ 0 & 1 & 0 \end{bmatrix} \mathbf{p_t}, \qquad \begin{bmatrix} \dot{x}_c \\ \dot{y}_c \end{bmatrix} = u_c \begin{bmatrix} \cos(\psi) \\ \sin(\psi) \end{bmatrix}, \tag{5.9}$$

and assuming that the source is located at the origin of the coordinate frame, i.e. $\mathbf{p_t} = \begin{bmatrix} 0 & 0 & z_t \end{bmatrix}^T$, differential equations in the polar coordinate system are derived as

$$\dot{r}_c = u_c \cos(\psi - \theta_c), \tag{5.10}$$

$$\dot{\theta}_c = \frac{1}{r_c} \left[ u_c \sin(\psi - \theta_c) \right]. \tag{5.11}$$

*Remark.* In the controlled system (5.3)–(5.6), the influence of the source depth $z_t$ is not explicitly present. However, its influence appears in the cost function $f$ amplitude. Since there is no movement in the vertical axis, we use polar coordinates instead of cylindrical coordinates. Influence of the source depth on the algorithm performance is discussed in Section 5.3 and Section 5.5.

Normalized time of arrival difference measurement $\Delta$ in polar coordinates is given with $\Delta = (r_1 - r_2)/d$, where ranges between the acoustic receivers and the signal source are expressed with:

$$r_1 = \sqrt{d^2/4 + r_c^2 + dr_c \sin(\psi - \theta_c) + z_t^2}, \tag{5.12}$$

$$r_2 = \sqrt{d^2/4 + r_c^2 - dr_c \sin(\psi - \theta_c) + z_t^2}. \tag{5.13}$$

Finally, the polar representation of the system (5.3)–(5.6) is

$$\dot{r}_c = -u_c \cos \alpha, \tag{5.14}$$

$$\dot{\theta}_c = -\frac{u_c}{r_c} \sin \alpha, \tag{5.15}$$

$$\dot{\alpha} = k(f - x_e h)\sqrt{\omega} \sin \omega t + a\sqrt{\omega} \cos \omega t + \frac{u_c}{r_c} \sin \alpha, \tag{5.16}$$

$$\dot{x}_e = -x_e h + f, \tag{5.17}$$

where the substitution $\alpha = \psi - \theta_c + \pi$ is introduced. State $\alpha$ represents the relative angle formed by the bearing vector between the source and the baseline center and baseline heading, as can be seen in Figure 5.1.

After the polar coordinate transformation has been done, a surge speed control law can be introduced. The surge speed control law needs to accomplish three tasks. The first one is determining surge speed sign, i.e., the direction of the signal source. From

the single $\Delta$ value, and only if $\Delta$ equals zero, we can infer in which plane the acoustic signal source is located, or, looking merely at the horizontal plane, on which line the source point is located. However, the direction in which the system should be steered in order to reach the desired point is not known. The main idea is to exploit perturbations introduced in the yaw degree of freedom in order to determine the desired direction in a fashion that somewhat resembles sound localization present in human beings - in everyday perception, human beings use head motion to determine sound direction and distance in an attempt to acquire sound sources visually. Therefore, an important source of information for localization is obtained from head motion cues. When we hear a sound we wish to localize, we move our head to minimize the interaural time differences, i.e., the arrival time of a sound between two ears, using our head as a sort of "pointer", [103].

The second task is to ensure that the system has surge speed greater than zero only when the cost function $f$ is low enough, meaning that system is oriented towards the source. In this way, the vehicle will not diverge from the source while its heading is still converging under the influence of the extremum seeking controller.

The third task is reducing surge speed to zero when the system has approached the target. When the system travelling at a constant surge speed passes over the target, the surge speed sign suddenly changes, and an oscillating behaviour appears, meaning that the system position cannot ultimately settle even if it has reached the source. In addition, it quickly overshoots the source and has to go backwards if it was travelling at full speed in the vicinity of the source.

Finally, the surge speed control law that accomplishes all stated tasks is introduced as:

$$u_c = u_\zeta \underbrace{\operatorname{sgn}\left(\Delta \sin(2\alpha)\right)}_{u_{dir}} \cdot \underbrace{u_0\left(1 - \tanh(mf)\right)}_{u_{amp}}. \tag{5.18}$$

The part of the control law denoted with $u_{amp}$ handles the requirement regarding surge speed amplitude, where parameter $u_0$ is the maximum surge speed the system can achieve and $m$ is a tunable parameter that determines how much the system heading can deviate from the signal source direction before surge speed is set to zero. Part $u_{dir}$ handles surge sign resolution. State $\alpha$ constantly changes due to perturbations and both $\alpha$ and $\Delta$ being positive signifies that the signal source is in front of the vehicle, whereas, if their signs are opposite, the signal source is behind the vehicle. A nonlinear damping term $u_\zeta$ is added to tune forward velocity in the vicinity of the target. The properties $u_\zeta$ has to satisfy are:

$$u_\zeta \in [0, 1), \ u_\zeta \approx 1 \text{ for } r_c \gg \varepsilon, \text{ and } \lim_{r_c \to 0} u_\zeta = 0. \tag{5.19}$$

This means that $u_\zeta \approx 1$ for a range sufficiently larger than some user defined value $\varepsilon$ and, as range reduces, the term approaches zero, e.g. the following class of damping function $u_\zeta$ satisfies given conditions:

$$u_\zeta = \frac{r_c^q}{(r_c + \varepsilon)^q}. \tag{5.20}$$

In Section 5.1, it was emphasized that in the envisioned scenario range measurements are not available, however in Section 5.4 a signal that satisfies the conditions given in (5.19) will be presented. Furthermore, in a real–life situation, relative angle $\alpha$ cannot be measured since the source position is not known. This problem is also considered in Section 5.4.

## 5.3   Stability analysis

Using Lie bracket approximation results from [88], we investigate the stability of the system defined with (5.14), (5.16) and (5.17). The procedure starts by writing the extremum seeking system in input-affine form, then calculating its corresponding Lie bracket system. From there, the asymptotic stability of the Lie bracket system, if proven, implies practical asymptotic stability for the initial extremum seeking system.

The following class of input–affine systems is considered:

$$\dot{\boldsymbol{x}} = \boldsymbol{b_0}(t, \boldsymbol{\eta}) + \sum_{i=1}^{m} \boldsymbol{b_i}(t, \boldsymbol{x})\sqrt{w}, g_i(t, wt) \tag{5.21}$$

with $\boldsymbol{x}(t_0) = \boldsymbol{\eta_0} \in \mathbb{R}^n$ and $\omega \in (0, \infty)$. The Lie bracket system corresponding to (5.21) is defined with

$$\dot{\boldsymbol{z}} = \boldsymbol{b_0}(t, \boldsymbol{z}) + \sum_{\substack{i=1 \\ j=i+1}}^{m} [\boldsymbol{b_i}, \boldsymbol{b_j}](t, \boldsymbol{z})\nu_{ji}(t), \tag{5.22}$$

where

$$\nu_{ji}(t) = \frac{1}{T}\int_0^T g_j(t, \theta)\int_0^\theta g_i(t, \tau)d\tau d\theta. \tag{5.23}$$

In order to perform Lie bracket averaging step several assumptions on $\boldsymbol{b_i}$ and $g_i$ are imposed. For the sake of completeness we restate several theorems and assumptions which can be found in [88]. The vector fields of (5.21) satisfy the following properties:

A1  $\boldsymbol{b_i} \in C^2 : \mathbb{R} \times \mathbb{R}^n \to \mathbb{R}^n, i = 0, ..., m$.

A2  For every compact set $\mathcal{C} \subseteq \mathbb{R}^n$ there exist $\boldsymbol{A_1}, ..., \boldsymbol{A_6} \in [0, \infty)$ such that $|\boldsymbol{b_i}(t, \boldsymbol{x})| \leq \boldsymbol{A_1}, \left|\frac{\partial \boldsymbol{b_i}(t,\boldsymbol{x})}{\partial t}\right| \leq \boldsymbol{A_2}, \left|\frac{\partial \boldsymbol{b_i}(t,\boldsymbol{x})}{\partial x}\right| \leq \boldsymbol{A_3}, \left|\frac{\partial^2 \boldsymbol{b_j}(t,\boldsymbol{x})}{\partial t\partial \boldsymbol{x}}\right| \leq \boldsymbol{A_4}, \left|\frac{\partial [\boldsymbol{b_j}, \boldsymbol{b_k}](t,\boldsymbol{x})}{\partial \boldsymbol{x}}\right| \leq \boldsymbol{A_5}, \left|\frac{\partial [\boldsymbol{b_j}, \boldsymbol{b_k}](t,\boldsymbol{x})}{\partial t}\right| \leq \boldsymbol{A_6}$ for all $x \in \mathcal{C}, t \in \mathrm{R}, i = 0, ..., m, j = 1, ..., m, k = j, ..., m$.

A3  $g_i : \mathbb{R} \times \mathbb{R} \to \mathbb{R}, i = 1, ..., N$ are measurable functions. Moreover, for all $i = 1, ..., N$
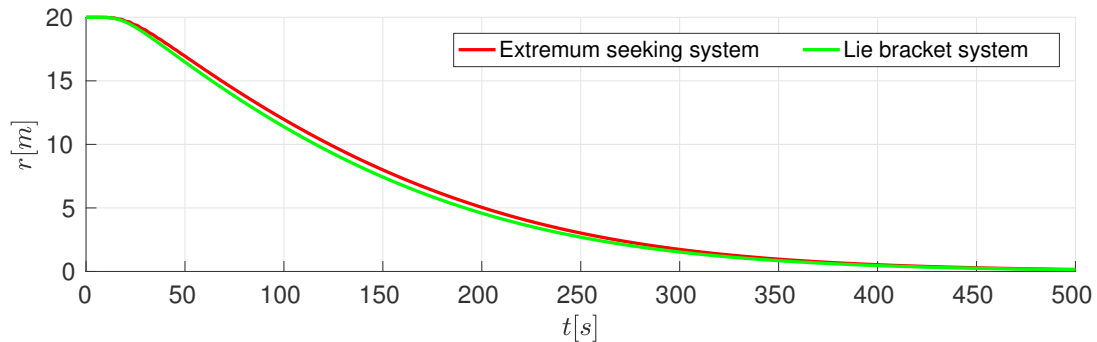
(a) Range state $r$.
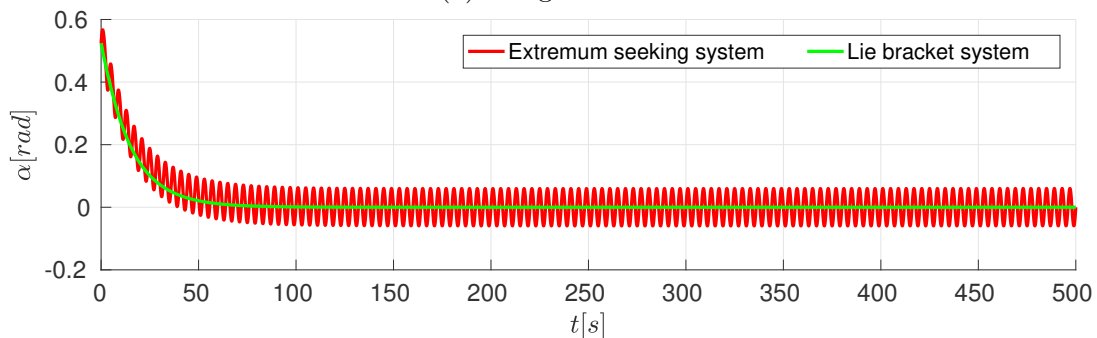
(b) Relative angle state $\alpha$.
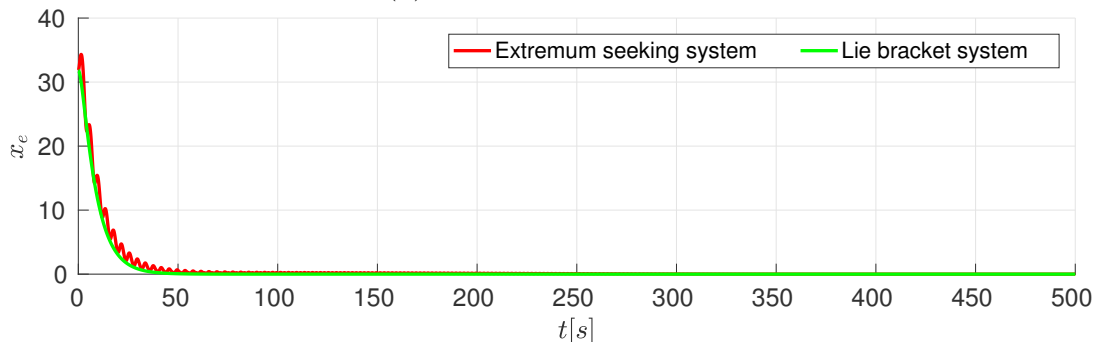
(c) Filter state $x_e$.

**Figure 5.3:** Extremum seeking system and its Lie bracket system approximation with parameters $a = 0.075$, $\omega = 1.57$, $k = -0.01$, $h = 0.75$, $u_0 = 0.25$, $d = 10$, $m = 0.25$, $\epsilon = 20$ and $q = 1$.

there exist constants $L_i, M_i \in (0, \infty)$ such that $|g_i(t_1, \theta) - g_i(t_2, \theta)| \leq L_i |t_1 - t_2|$ for all $t_1, t_2 \in \mathbb{R}$ and such that $\sup_{t, \theta \in \mathbb{R}} |g_i(t, \theta)| \leq M_i$.

A4 $u_i(t, \cdot)$ is $T$–periodic, i.e. $g_i(t, \theta + T) = g_i(t, \theta)$, and has zero average , i.e. $\int_0^T g_i(z, \tau) d\tau = 0$, with $T \in (0, \infty)$ for all $t, \theta \in \mathbb{R}$, $i = 1, ..., m$.

In summary, vector fields $\boldsymbol{b_i}$ are required to be $C^2$ smooth and expressions involving $\boldsymbol{b_i}$ and their derivatives must be bounded uniformly in $t$. The inputs $g_i$ must be measurable, Lipschitz continuous, and bounded. Furthermore, they have to be $T$–periodic, and have a zero average. In [88], the authors give and prove a theorem which states that the semi-global (local) practical uniform asymptotic stability of the input-affine system (5.21) follows from the global (local) uniform asymptotic stability of the corresponding

Lie bracket system (5.22) if stated assumptions are satisfied.

We start the stability proof by rewriting the system (5.14), (5.16), and (5.17) in a form suitable for the Lie bracket approximation step:

$$
\dot{\boldsymbol{x}} = \begin{bmatrix} \dot{r}_c \\ \dot{\alpha} \\ \dot{x}_e \end{bmatrix} = \underbrace{\begin{bmatrix} -u_c \cos \alpha \\ \frac{u_c}{r_c} \sin \alpha \\ -x_e h + f \end{bmatrix}}_{\boldsymbol{b_0}} + \underbrace{\begin{bmatrix} 0 \\ k(f - x_e h) \\ 0 \end{bmatrix}}_{\boldsymbol{b_1}} \sqrt{\omega} \underbrace{\sin(\omega t)}_{g_1} + \underbrace{\begin{bmatrix} 0 \\ a \\ 0 \end{bmatrix}}_{\boldsymbol{b_2}} \sqrt{\omega} \underbrace{\cos(\omega t)}_{g_2}. \tag{5.24}
$$

The sinusoidal inputs $g_1$ and $g_2$ used in the extremum seeking scheme satisfy assumptions stated earlier, as shown in [88], while the validity of the assumptions on the vector fields $\boldsymbol{b_0}$, $\boldsymbol{b_1}$ and $\boldsymbol{b_2}$ is shown in the Appendix 6. The Lie bracket system that captures the behavior of the trajectories of the original extremum seeking system, computed from (5.24), is

$$
\dot{\tilde{r}}_c = -u_c \cos \tilde{\alpha}, \tag{5.25}
$$

$$
\dot{\tilde{\alpha}} = \frac{u_c}{\tilde{r}_c} \sin \tilde{\alpha} + \frac{1}{2} ak \frac{\partial f(\tilde{r}_c, \tilde{\alpha})}{\partial \tilde{\alpha}}, \tag{5.26}
$$

$$
\dot{\tilde{x}}_e = -\tilde{x}_e h + f, \tag{5.27}
$$

where $\frac{\partial f}{\partial \tilde{\alpha}}(\tilde{r}_c, \tilde{\alpha})$ is

$$
\frac{\partial f(\tilde{r}_c, \tilde{\alpha})}{\partial \tilde{\alpha}} = \frac{\tilde{r}_c^2 \sin(2\tilde{\alpha})}{r_1 r_2}. \tag{5.28}
$$

Figures 5.3a, 5.3b and 5.3c compare state evolution of original perturbed system (5.21) and its Lie bracket system approximation (5.25)-(5.27). Next, we must show the asymptotic stability of the derived Lie bracket system. Going forward, the damping function (5.20) with $q = 3$ is used. Equilibrium states are $\boldsymbol{z_e} = \begin{bmatrix} 0 & n\pi & 0 \end{bmatrix}^T$ where $n \in \mathbb{Z}$. The relative angle $\alpha$ state has multiple equilibrium points. Geometrically, in the case of an even $n$, the source is in front of the baseline, while in the case of an odd $n$, the source is behind the baseline. For an odd $n$, if we shift the state $\alpha$, the signs of the trigonometric functions change, i.e. $\sin(\tilde{\alpha} + n\pi) = -\sin\tilde{\alpha}$ and $\cos(\tilde{\alpha} + n\pi) = -\cos\tilde{\alpha}$, but at the same time the $u_{dir}$ term changes its sign, so in equations (5.25) and (5.26) they cancel each other out. With that in mind, we proceed by analyzing only the equilibrium point $\boldsymbol{z_e} = \boldsymbol{0}^T$ without losing generality. We define a positive definite Lyapunov function:

$$
V = V_{r_c} + V_\alpha + V_{x_e} = \frac{1}{2} \tilde{r}^2 + \frac{1}{2} \tilde{\alpha}^2 + \frac{1}{2} \tilde{x}_e^2. \tag{5.29}
$$

By taking the derivative of the function $V$ we get

$$\dot{V}_{r_c} = -\tilde{r}_c u_c \cos \tilde{\alpha}, \tag{5.30}$$

$$\dot{V}_\alpha = \tilde{\alpha} \frac{u_c}{\tilde{r}_c} \sin \tilde{\alpha} + \frac{1}{2} \tilde{\alpha} a k \frac{\tilde{r}_c^2}{r_1 r_2} \sin 2\tilde{\alpha}, \tag{5.31}$$

$$\dot{V}_{x_e} = -\tilde{x}_e^2 h + \tilde{x}_e f(\tilde{r}_c, \tilde{\alpha}). \tag{5.32}$$

First, note that by selecting an appropriate value of the parameter $m$ in (5.18), the term $u_{amp}$ can be tuned in such way that for each $\tilde{\alpha} \notin (-\delta, \delta)$ where $|\delta| < \frac{\pi}{2}$ the surge speed value $u_c$ tends to zero. Also, note that the following is valid for each $\tilde{\alpha} \in (-\frac{\pi}{2}, \frac{\pi}{2})$:

$$\cos(\tilde{\alpha}) > 0, \quad \tilde{\alpha} \sin(\tilde{\alpha}) \geq 0, \quad \tilde{\alpha} \sin(2\tilde{\alpha}) \geq 0. \tag{5.33}$$

When the angle $\alpha \in (-\frac{\pi}{2}, -\delta) \cap (\delta, \frac{\pi}{2})$, i.e. it is far away from the equilibrium value, derivative (5.31) reduces to $\frac{1}{2} \tilde{\alpha} a k \frac{d^2 \tilde{r}_c^2}{r_1 r_2} \sin 2\tilde{\alpha}$ and from (5.33) it follows that $\dot{V}_\alpha \leq 0$ if parameter $k < 0$ for each $\alpha \in (-\frac{\pi}{2}, \frac{\pi}{2})$. Moreover, $\dot{V}_\alpha$ is negative definite since $\dot{V}_\alpha = 0$ only for $\tilde{\alpha} = 0$ when $\tilde{r}_c > 0$. Note, for $\tilde{r}_c = 0$, $\dot{V}_\alpha$ is also 0, which is acceptable since the baseline center is already at the desired position, and angle $\alpha$ is not defined. For angle $\tilde{\alpha} \in (-\delta, \delta)$, surge speed $u_c$ is present, which can be seen as a disturbance for the yaw rate controller. The derivative (5.31) can be written as:

$$\tilde{r}_c^2 \tilde{\alpha} \sin(\tilde{\alpha}) \left( \frac{u_{dir} u_{amp}}{(\tilde{r}_c + \varepsilon)^3} + \frac{ak}{r_1 r_2} \cos(\tilde{\alpha}) \right) \leq 0 \tag{5.34}$$

where the expression is negative definite if the sum inside the brackets is negative. For large range values, term $(r_c + \varepsilon)^3$ dominates and decreases the value of the positive term inside the bracket. Therefore, we observe the theoretical worst case scenario where $\tilde{r}_c \approx 0$ in which $\max \left( \frac{u_{amp}}{(\tilde{r}_c + \varepsilon)^3} \right) = \frac{u_0}{\varepsilon^3}$, $r_1 r_2 \approx d^2/4 + z_t^2$ and $\cos(\tilde{\alpha}) = \cos(\delta)$. A short calculation yields the condition

$$u_0 \left( d^2 + 4z_t^2 \right) + 4 a k \varepsilon^3 \cos(\delta) \leq 0. \tag{5.35}$$

Parameters $k$, $a$, $d$, $u_0$, and $\varepsilon$ are design parameters and, by appropriate tuning, the condition (5.35) can be satisfied. Looking at (5.31), we can observe how target depth influences yaw degree of freedom convergence. It is assumed that depth is constant. When the target depth $z_t$ is very high, so is the product $r_1 r_2$, meaning the value of the second term in (5.31), which forces the state to converge, decreases. Although $z_t$ is unknown, in most use cases the maximum depth of an area can be found out in advance and parameters can be tuned accordingly to achieve desired performance. Finally, checking the case when

the initial condition is $\tilde{\alpha}_0 = \pm\frac{\pi}{2}$ remains. From (5.26), and taking into account that surge speed $u_c = 0$ for $\tilde{\alpha} = \pm\frac{\pi}{2}$, it is clear that in the observed case the derivative is always zero and the state remains unchanged. In other words, the trajectory is between the two regions of attraction in the phase plane. This, however, is only the case in the approximated system, and the full system has a perturbation in the $\alpha$ degree of freedom, so it cannot stay identically at $\alpha = \pm\frac{\pi}{2}$. Taking all this into account, we conclude that the state $\tilde{\alpha}$ is locally asymptotically stable to a small neighborhood of the origin.

Next, the state $\tilde{r}_c$ is analyzed. Knowing that $\tilde{r}_c \geq 0$, from (5.33) it follows that $\dot{V}_{r_c} \leq 0$ for $\tilde{\alpha} \in (-\frac{\pi}{2}, \frac{\pi}{2})$. Since we have shown that state $\tilde{\alpha}$ converges to zero, yielding $u_c \neq 0$, $\tilde{r}_c$ cannot remain constantly at any $\tilde{r}_c > 0$ for $t \in (0, \infty)$.

Finally, we check the stability of the filter state $\tilde{x}_e$. The set for which the filter state should be attractive is defined with $\mathcal{E} := \left\{ \tilde{x}_e \in \mathbb{R} : \tilde{x}_e = \frac{f(\tilde{r}_c, \tilde{\alpha})}{h}, \tilde{r}_c > 0, \tilde{\alpha} \in (-\frac{\pi}{2}, \frac{\pi}{2}) \right\}$. We observe, as in [88], that state $\tilde{x}_e$ is linear and its origin is exponentially stable for $f(\tilde{r}_c, \tilde{\alpha}) = 0$. Therefore, if $f(\tilde{r}_c, \tilde{\alpha})$ is bounded then solution $\tilde{x}_e(t)$ exists and is bounded with gain $\frac{1}{h}$. Since we have shown that $\tilde{\alpha}$ tends to zero, consequently $f(\tilde{r}_c, \tilde{\alpha})$ also tends to zero.

Since the Lie bracket system (5.25)-(5.27) is locally uniformly asymptotically stable we conclude that the full system (5.24) is locally practically uniformly asymptotically stable to a small neighborhood of the origin.

## 5.4 Algorithm implementation

In Section 5.3 stability of the proposed control algorithm is shown, however in practice there are additional limitations that have to be considered. As already noted in Section 5.2.3, in practical algorithm implementation both range $r_c$ and relative angle $\alpha$ used in surge speed control law for determining the $u_{dir}$ and $u_\zeta$ terms are not available since the source position is unknown. In order to deploy the algorithm in real–life situations, it is necessary to approximate the required information from available measurements. Furthermore, the presence of a constant current acting on the system and modelling errors in the vehicle dynamics can cause the system to drift. This is a major issue, especially when the receivers are placed on the separate vehicles, which creates the need for additional position control loop. These implementation issues are covered in the following subsections, before the complete implementation of the time difference of arrival source seeking scheme is presented.
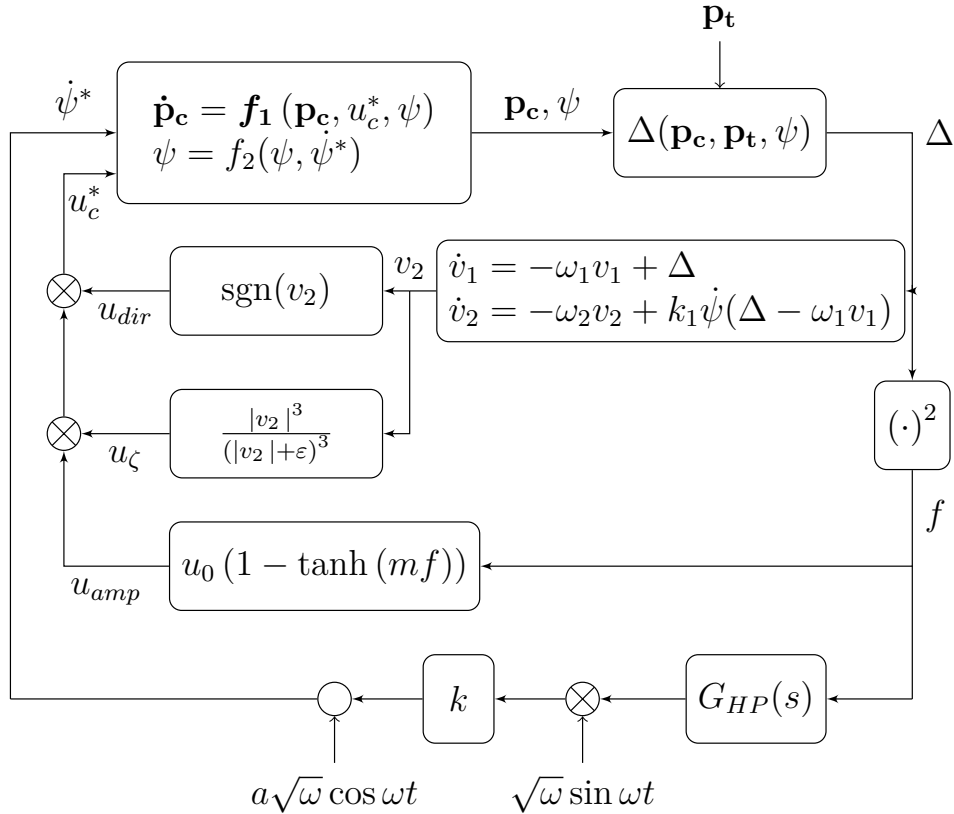
**Figure 5.4:** Time difference of arrival source seeking scheme.

## 5.4.1 Approximation of range $r_c$ and relative angle $\alpha$

In order to approximate information about the range $r_c$ and relative angle $\alpha$ from the available measurements – in this case yaw rate $\dot{\psi}$ and time difference of arrival $\Delta$ measurements, the following second order filter is proposed:

$$\dot{v}_1 = -\omega_1 v_1 + \Delta, \tag{5.36}$$

$$\dot{v}_2 = -\omega_2 v_2 + k_1 \dot{\psi}(\Delta - \omega_1 v_1), \tag{5.37}$$

where $\omega_1$, $\omega_2$ and $k_1$ are tunable filter parameters. In the proposed filter, state $v_1$ (5.36) is used to calculate the derivative of $\Delta$, while the additional low–pass filter (5.37) has a twofold purpose. It averages the signal in order to filter out perturbations, but also to remove brief changes in the signal sign caused by the small lag introduced by the derivative and the system dynamics that are present in a real–life scenario. The main idea behind the introduced filter is to extract the signal envelope value of the product $\dot{\psi}\dot{\Delta}$. Due to the introduced perturbation, the heading changes, and consequently $\Delta$ changes periodically during algorithm operation. As the vehicle approaches the source, for the same change in the yaw degree of freedom a smaller change of $\Delta$ is achieved, until the system is finally above the source where there is no change in $\Delta$ for any change in $\psi$. This behavior is

exploited to extract information that is correlated with range $r_c$. Furthermore, in order to determine surge speed sign, we observe the phase shift of the yaw rate and the time derivative of the $\Delta$ signal. When the source is in front of the baseline, both signals are in phase and their product is positive. When the source is behind, the signals are shifted by $\pi$ radians, and the resulting product is negative.

Using the calculated value $v_2$, the respective terms in (5.18) are replaced with

$$u_{dir} = \text{sgn}\,(v_2),\ \text{and}\ u_\zeta = \frac{|v_2|^3}{(|v_2|+\varepsilon)^3}. \tag{5.38}$$

### 5.4.2   Position reference control

The presence of a constant current acting on the system causes a constant position offset in the stationary state and position drift while converging towards the source. In order to remove static offset and improve convergence speed when dealing with the constant current or other unmodelled disturbances, a position control loop is added, where the system kinematic model described with $\dot{x}_c^* = u_c^* \cos\psi$ and $\dot{y}_c^* = u_c^* \sin\psi$, is used to calculate respective position references $x^*$ and $y^*$ from the velocity reference input $u_c^*$ and current baseline heading $\psi$. The vehicle's conventional control algorithms are then used to achieve the desired position. The addition of the position control loop introduces an additional delay inside the whole control loop, however that delay is negligible compared to the source seeking dynamics.

The complete time difference of arrival source seeking control scheme is given in Figure 5.4. In there, functions $\boldsymbol{f_1}\,(\mathbf{p_c}, u_c^*, \psi)$ and $f_2(\psi, \dot{\psi}^*)$ encapsulate the complete vehicle dynamics, including low–level velocity controllers and position controllers if they are utilized. Notice that all the references for the low-level velocity and position controllers are marked with superscript "$*$". The transfer function $G_{HP}(s)$ represents the high–pass filter in the extremum seeking scheme.

## 5.5   Simulation results

Numerical simulations with vehicle dynamics included were conducted to examine the behavior of the algorithm implementation depicted in Figure 5.4. For analysis purposes, the results of the yaw rate controller simulation with the surge speed controller turned off are first shown and discussed, before showing the results of the simulation of the full source seeking algorithm implementation.

(a) Relative angle $\alpha$.
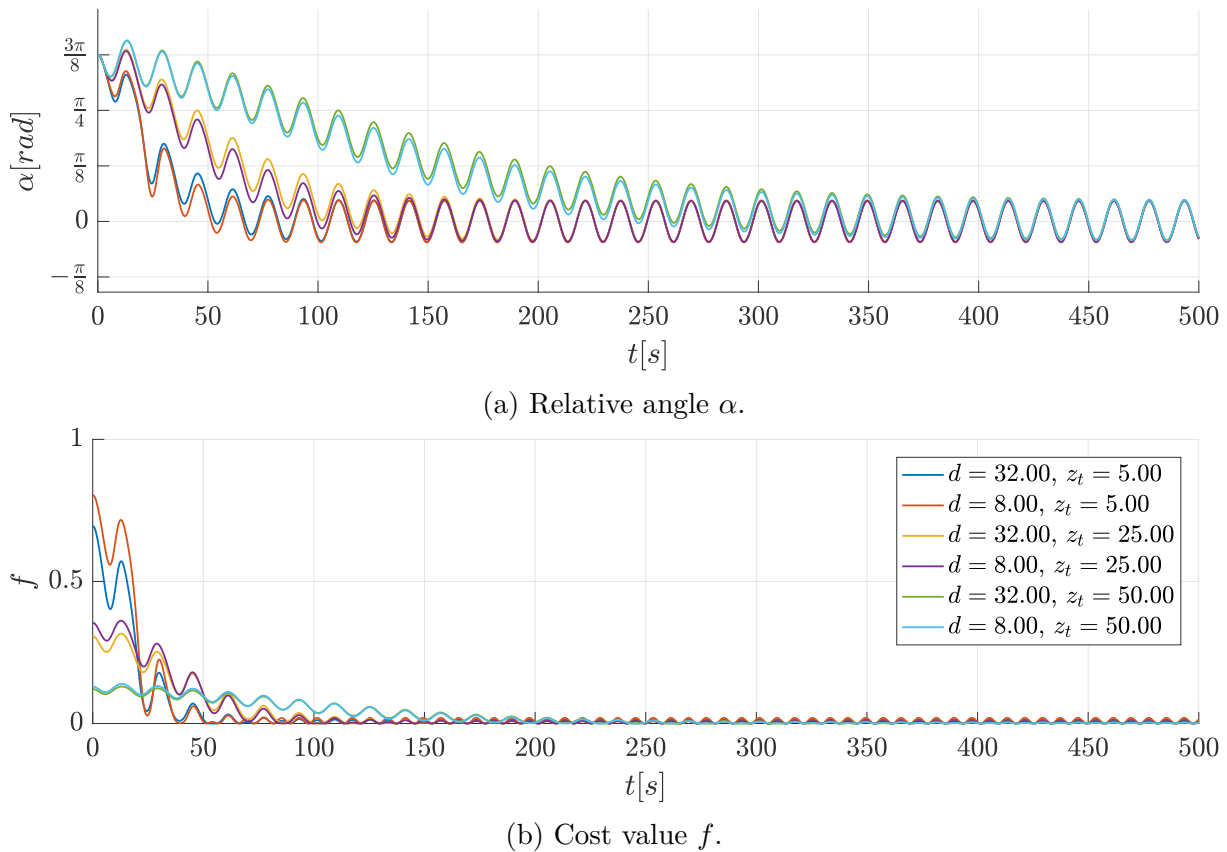


(b) Cost value $f$.

**Figure 5.5:** Angle $\alpha$ and cost $f$ response for different values of depth $z_t$ and baseline $d$ with disabled surge speed controller and with source located at $\mathbf{p_t} = [0\ 0\ z_t]^T$.

### 5.5.1 Yaw rate controller

Figure 5.5 shows the response of the angle $\alpha$ and the cost value $f$ for different source depths $z_t$ where only the yaw rate controller is active with parameters $a = 0.1\sqrt{\frac{\text{rad}}{\text{s}}}$, $\omega = 2\pi/16\,\frac{\text{rad}}{\text{s}}$, $k = -1.0\sqrt{\frac{\text{rad}}{\text{s}}}$, and $h = 0.19\,\frac{1}{\text{s}}$. As already discussed, for the same set of algorithm parameters, convergence is slower for the larger source depth. For the same perturbation amplitude, there is a smaller response in $\Delta$ and thus the extremum seeking controller takes more time to steer the system in the right direction. Due to the normalization of time difference of arrival measurement $\Delta_{TOA}$ with the value of the baseline $d$, increasing the baseline four times has practically no influence on the convergence rate. It is, however, a fraction slower for the larger baseline, as suggested in Section 5.3. This is true for the ideal case without measurement noise. Noise–influenced $\Delta$ measurement can be written as

$$\Delta = \frac{\Delta_{TOA}v + \zeta_\Delta}{d}, \tag{5.39}$$

where $\zeta_\Delta \sim \mathcal{N}(0, \sigma_\Delta^2)$ and standard deviation $\sigma_\Delta$ are given in meters. By increasing baseline $d$, noise influence in the measurement is diminished, which justifies the idea of an
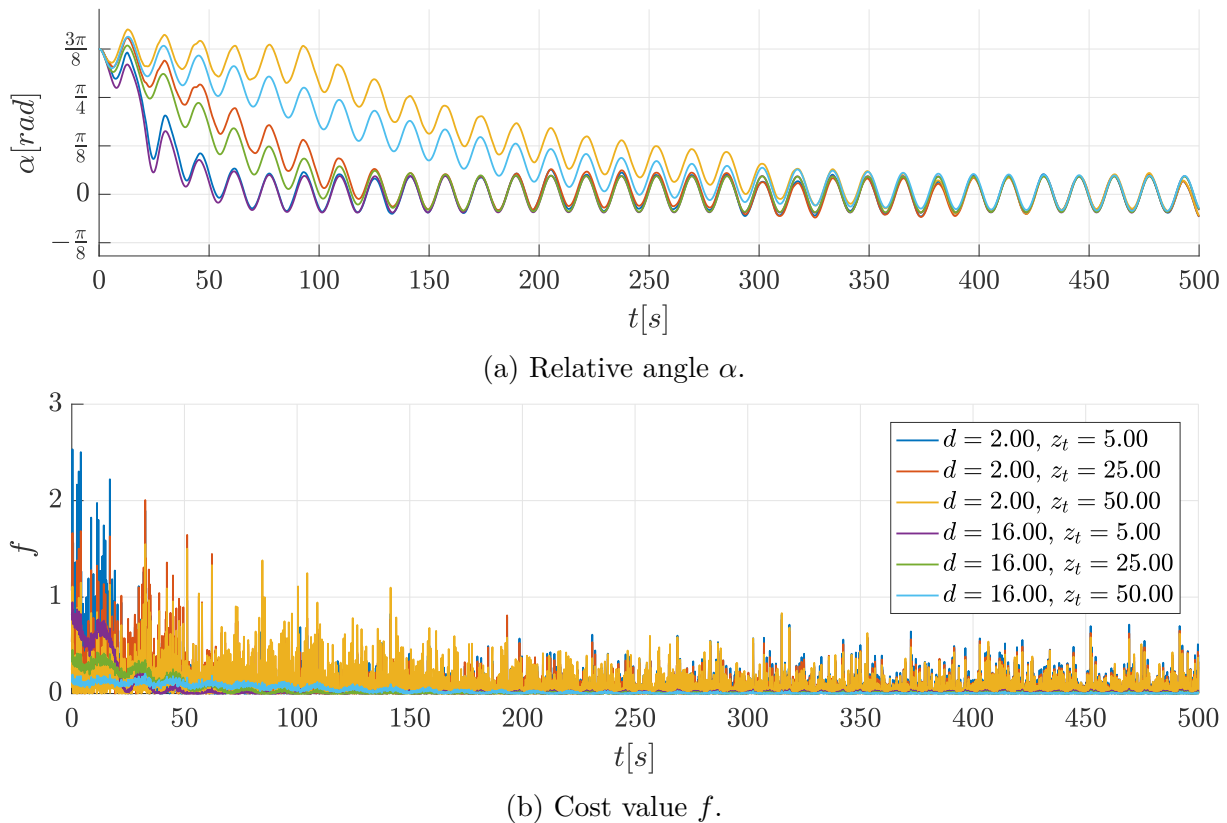
(a) Relative angle $\alpha$.



(b) Cost value $f$.

**Figure 5.6:** Angle $\alpha$ and cost $f$ response for different values of depth $z_t$ and baseline $d$ with measurement noise $\sigma_\Delta = 0.3\,\text{m}$ with disabled surge speed controller and with source located at $\mathbf{p_t} = [0\ 0\ z_t]^T$.

adjustable baseline. It is important to note that increasing the baseline can add additional noise, albeit small, to the measurement, due to the longer path that the acoustic signal needs to travel and which is not modelled in the presented case. In Figure 5.6, angle $\alpha$ and cost $f$ responses for different values of depth $z_t$ and baseline $d$ with measurement noise $\sigma_\Delta = 0.3\,\text{m}$ are shown. The remaining parameters are the same as in Figure 5.5. It is clearly visible that increasing the system baseline reduces the influence of measurement noise present in the $\Delta$ measurement. Angle $\alpha$ convergence is faster for the larger baseline, which is especially notable for the larger source depths.

### 5.5.2 Source seeking algorithm

In order to test the full algorithm behaviour with the scheme introduced in Section 5.4, a set of simulation experiments was done. Three cases are observed in detail: system behaviour with and without measurement noise present in the $\Delta$ measurement, and finally system behaviour with a constant current acting on the system.
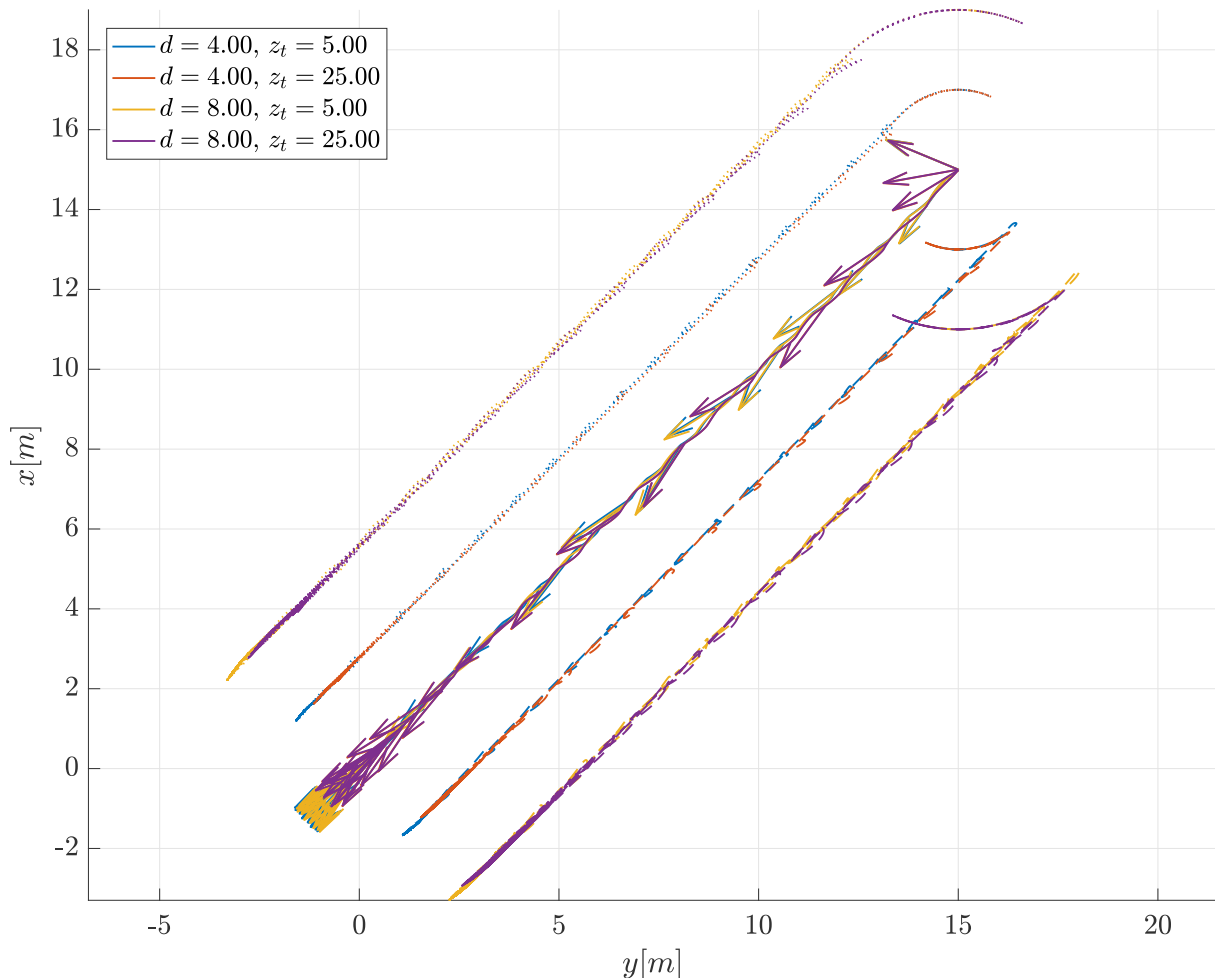
(a) Acoustic receiver $\mathbf{p_1}$ trajectory (dashed), acoustic receiver $\mathbf{p_2}$ trajectory (dotted) and baseline center $\mathbf{p_c}$ trajectory (solid).
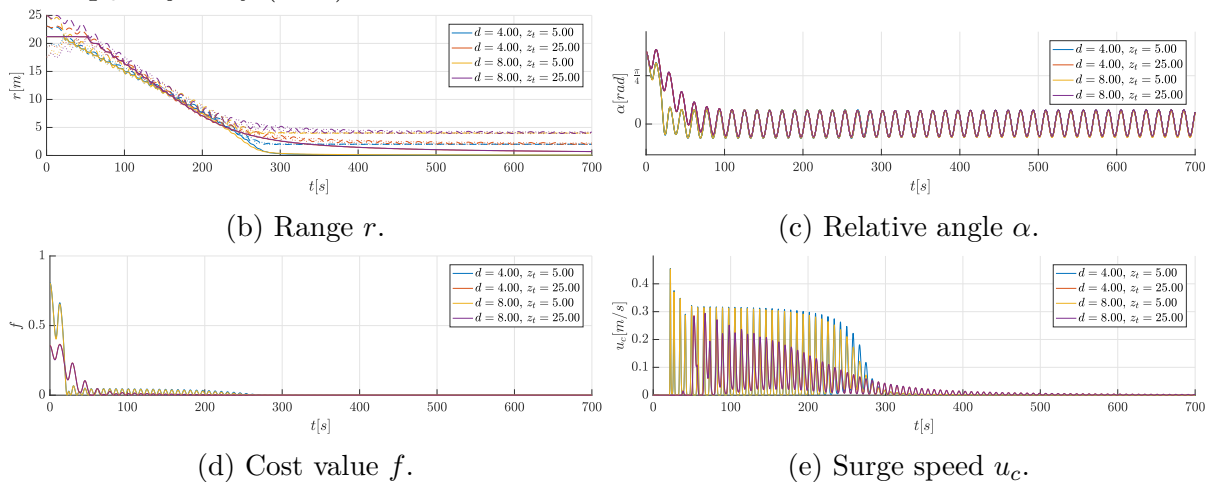

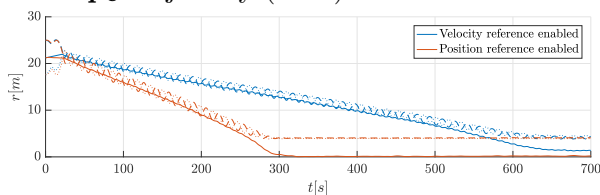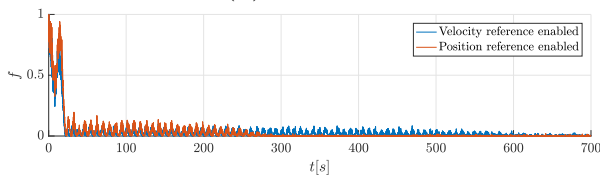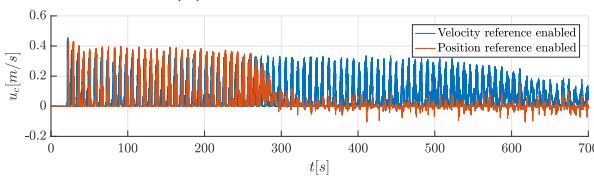
(b) Range $r$.

(c) Relative angle $\alpha$.

(d) Cost value $f$.

(e) Surge speed $u_c$.

**Figure 5.7:** Trajectories, ranges, relative angle $\alpha$, cost value $f$ and surge speed $u_c$ response for different values of target depth $z_t$ and baseline $d$ with target located at $\mathbf{p_t} = [0\ 0\ z_t]^T$.

## No measurement noise

In Figure 5.7, the responses of the system for different values of depth $z_t$ and baseline $d$ is shown with parameters $a = 0.15\sqrt{\frac{\text{rad}}{\text{s}}}$, $\omega = 2\pi/16\,\frac{\text{rad}}{\text{s}}$, $k = -1.0\sqrt{\frac{\text{rad}}{\text{s}}}$, $h = 0.19\,\frac{1}{\text{s}}$,

114

$u_0 = 0.5 \frac{m}{s}$, $m = 100$, $\varepsilon = 4\,\text{m}$, and $q = 3$, while the second order filter parameters are $\omega_1 = 0.8 \frac{1}{s}$, $\omega_2 = 0.15 \frac{1}{s}$, and $k_1 = 1000$. As already discussed in Section 5.3, increasing the baseline $d$ does not significantly influence the convergence speed of the system. From Figure 5.7b, we observe that initially the range $r_c$ is constant, while the baseline slowly turns towards the target. When the angle $\alpha$ is small enough, as defined by the parameter $m$, surge speed increases and the system starts approaching the source. Baseline surge speed $u_c$ is shown in Figure 5.7e. In Figure 5.7d it can be seen that while the angle $\alpha$, and consequently the cost $f$, is large, there is no surge speed $u_c$. It can also be noted that the surge speed keeps oscillating as the heading changes due to perturbations, but its average value decreases as the baseline approaches the signal source, i.e. it tends towards zero as the range to the source approaches zero, showing that the introduced second order filter successfully approximates distance information.

**With measurement noise**

In Figure 5.8 the responses of the system for different values of target depth $z_t$ and baseline $d$ are shown with measurement noise $\sigma_\Delta = 0.3\,\text{m}$ included, while all other parameters are the same as in the noiseless case. As expected, convergence is faster for the larger baseline. The benefit of the larger baseline is especially evident when looking at the surge speed direction in Figure 5.8e. Namely, there are many incorrect surge speed direction changes caused by the noisy $\Delta$ measurement in the case of the smaller baseline. In Figure 5.6a it is noticeable that when the system is very close to the source, angle $\alpha$ starts to change rapidly. This, however, is a numerical instability that happens due to the choice of the coordinate system since $\alpha$ is not defined for $r_c = 0$. Practically, this effect has no consequences on algorithm operation, but increasing the parameter $m$ can reduce it. For larger values of the parameter $m$ the baseline center deviates less from the line connecting the initial baseline position and the source position, but it also takes more time for the system to converge to the source's position due to a lower average speed.

**Constant current**

In Figure 5.9 the responses of the system with velocity reference control and the system with position reference control are compared for the baseline $d = 5\,\text{m}$, with constant current $v_c = \begin{bmatrix} 0.05 & 0 & 0 \end{bmatrix}^T \frac{m}{s}$ acting on the vehicles. It is visible that the system with position reference control has nearly the same performance as in the case without the currents, while the velocity reference controlled system cannot compensate for the disturbance. Even though the disturbance is small, the baseline slowly drifts and it takes twice as much time for the system to arrive near the signal source, with a constant offset present when it finally does reach it. This can be seen in the range response in Figure 5.9b. The
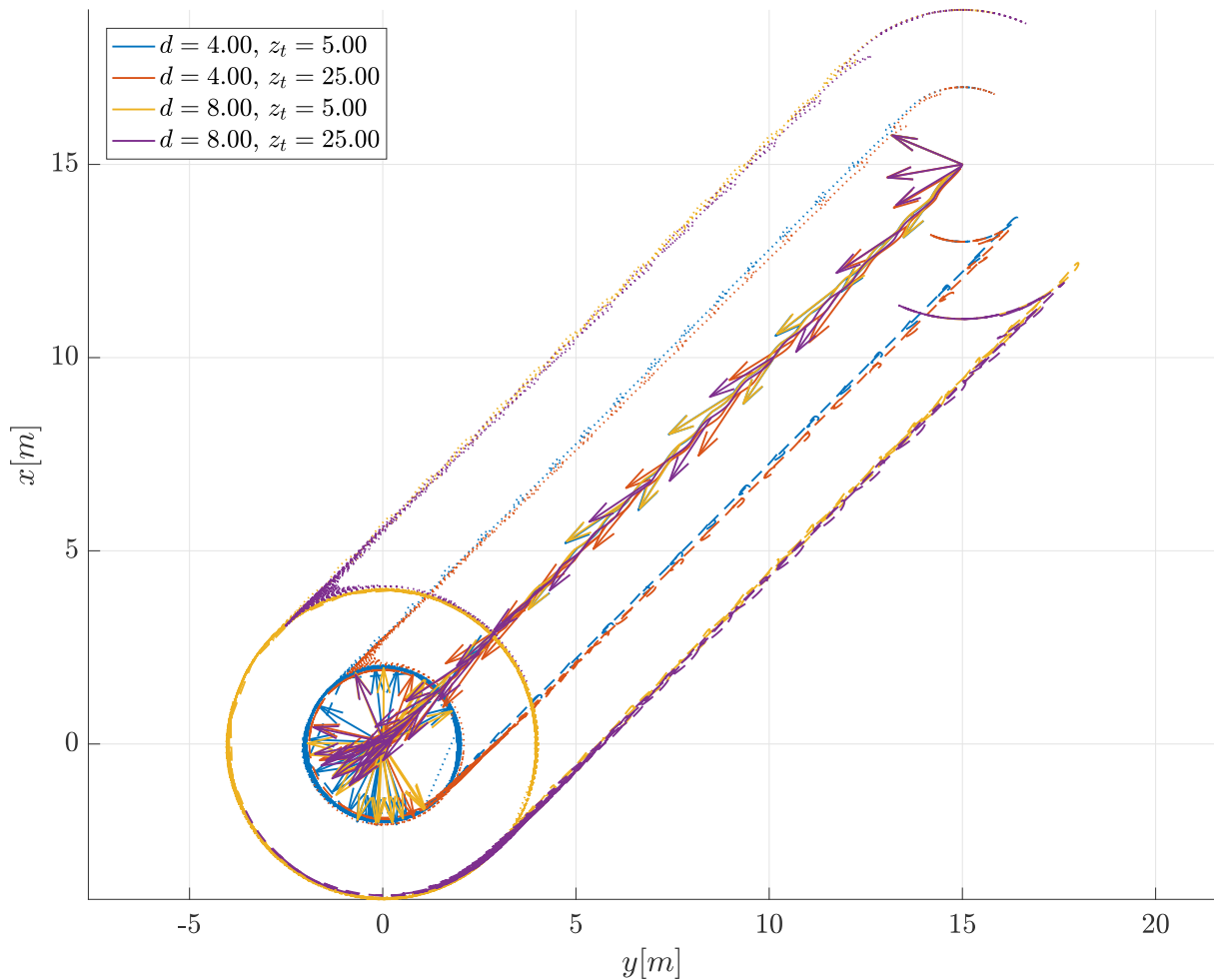
(a) Acoustic receiver $\mathbf{p_1}$ trajectory (dashed), acoustic receiver $\mathbf{p_2}$ trajectory (dotted) and baseline center $\mathbf{p_c}$ trajectory (solid).
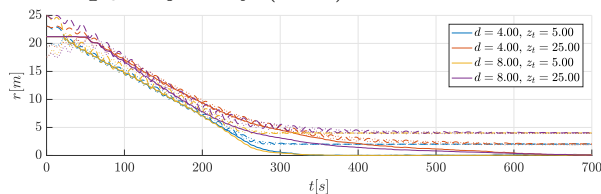


(b) Range $r$.
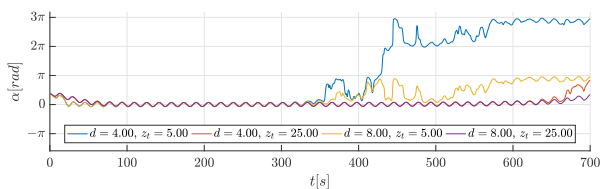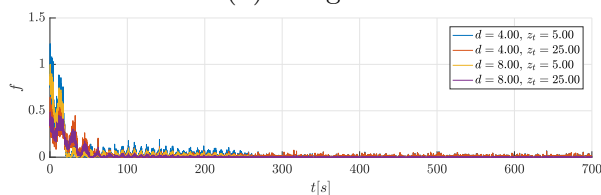


(c) Relative angle $\alpha$.
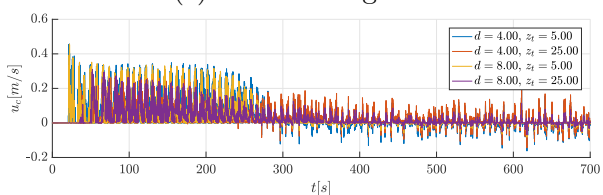


(d) Cost value $f$.



(e) Surge speed $u_c$.

**Figure 5.8:** Relative angle $\alpha$, cost value $f$ and surge speed $u_c$ response for different values of target depth $z_t$ and baseline $d$ with measurement noise $\zeta_\Delta = 0.3\,\mathrm{m}$ and with target located at $\mathbf{p_t} = [0\ 0\ z_t]^T$.

surge speed response in Fig. 5.9e, shows that the velocity reference controlled system, when close to the source, achieves the higher amplitudes of the surge speed necessary to counter the influence of the constant current.
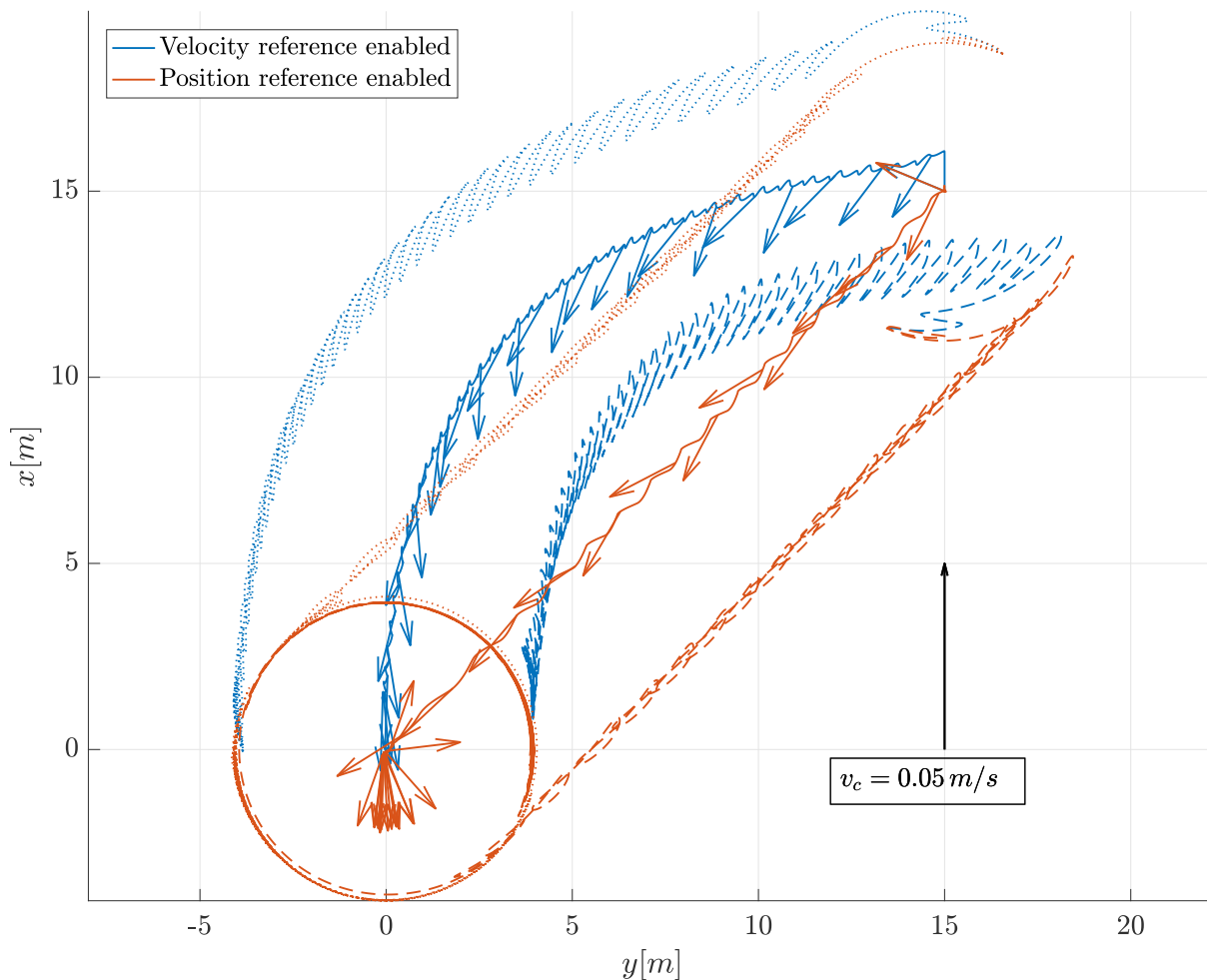
(a) Acoustic receiver $\mathbf{p_1}$ trajectory (dashed), acoustic receiver $\mathbf{p_2}$ trajectory (dotted) and baseline center $\mathbf{p_c}$ trajectory (solid).



(b) Range $r$.
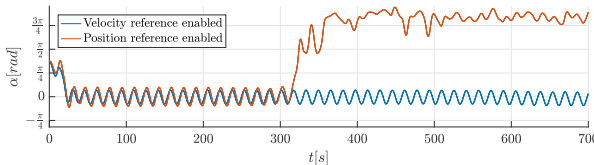


(c) Relative angle $\alpha$.



(d) Cost value $f$.



(e) Surge speed $u_c$.

**Figure 5.9:** Relative angle $\alpha$, cost value $f$ and surge speed $u_c$ response for different values of target depth $z_t$ and baseline $d$ with constant current $v_c = 0.05 \frac{\mathrm{m}}{\mathrm{s}}$ and with target located at $\mathbf{p_t} = [0\ 0\ 5]^T$.

## 5.6 Experimental results

### 5.6.1 Experimental setup
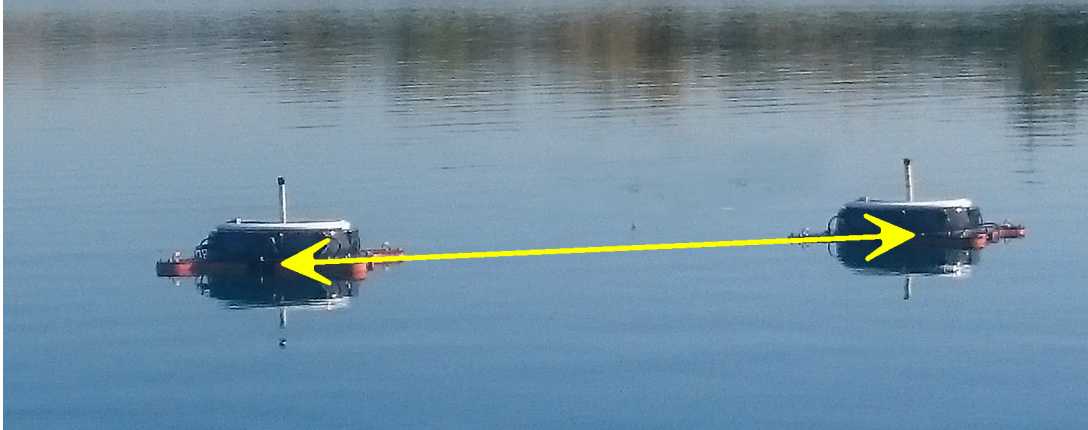


**Figure 5.10:** Two autonomous over–actuated marine surface platforms H2OMNI–X equipped with acoustic receivers performing the experiment. The receiver baseline is marked with yellow arrow.

A small set of proof-of-concept experiments was conducted in November 2017 at Jarun lake in Zagreb, Croatia. The experimental setup consisted of two autonomous over–actuated marine surface platforms APAD, shown in Figure 5.10 and developed in the Laboratory for Underwater Systems and Technologies, [34]. The APAD vehicle is a small scale over–actuated unmanned surface marine vehicle capable of omnidirectional motion. It is equipped with four thrusters in an "X" configuration which enables motion in the horizontal plane under any orientation. The vehicle is 0.385 m high, 0.756 m wide and long, and weighs approximately 25 kg. Both platforms were identically equipped with a Nanomodem, a low-cost acoustic modem developed at Newcastle University, [22]. An additional Nanomodem was used as the acoustic source emitter, and it was positioned on the lakebed at a depth of approximately 3 meters.
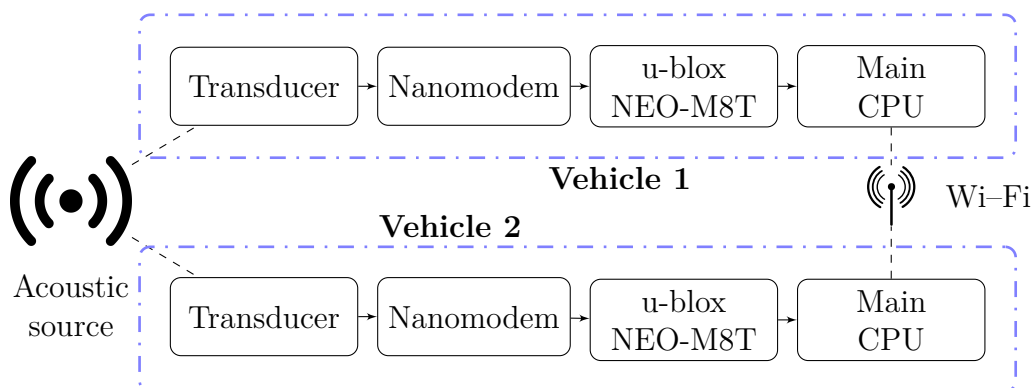


**Figure 5.11:** The time–of–arrival measurement acquisition setup scheme.

A precise measurement of the acoustic signal time of arrival was acquired in the following way: every two seconds, the Nanomodem positioned on the lakebed broadcast an acoustic package that was received by the receivers on the vehicles. When the header of the acoustic packet was decoded on the receiver side, a digital pin on the receiver, directly connected to the time mark input of the u-blox NEO-M8T chip, was triggered and a precise GPS timestamp was recorded on the same chip. This configuration made very low–latency measurements possible. The recorded timestamp was then exchanged between the two platforms using Wi-Fi communication and used in the time difference of arrival calculation. The time–of–arrival measurement acquisition setup scheme is shown in Figure 5.11. In order to successfully execute the algorithm using two vehicles equipped
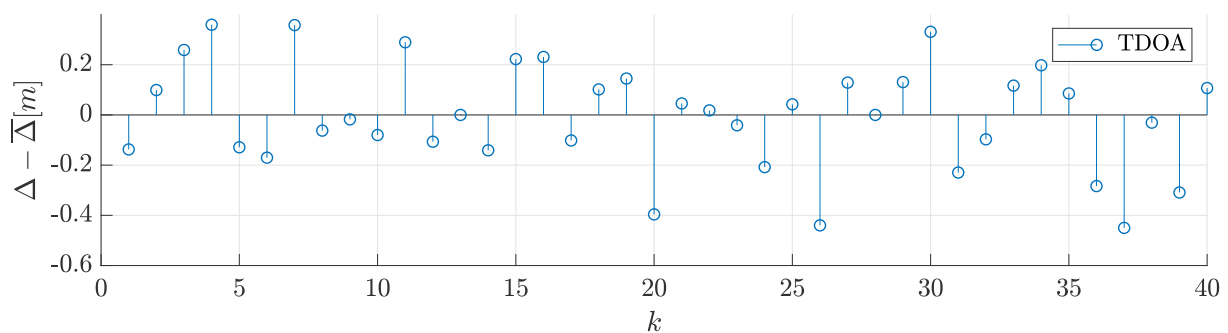


**Figure 5.12:** Time difference of arrival measurement error during static test.



(a) Acoustic receiver $\mathbf{p_1}$ trajectory (dashed), acoustic receiver $\mathbf{p_2}$ trajectory (dotted).

(b) Baseline $d$.

(c) Yaw rate reference $\dot{\psi}^*$.
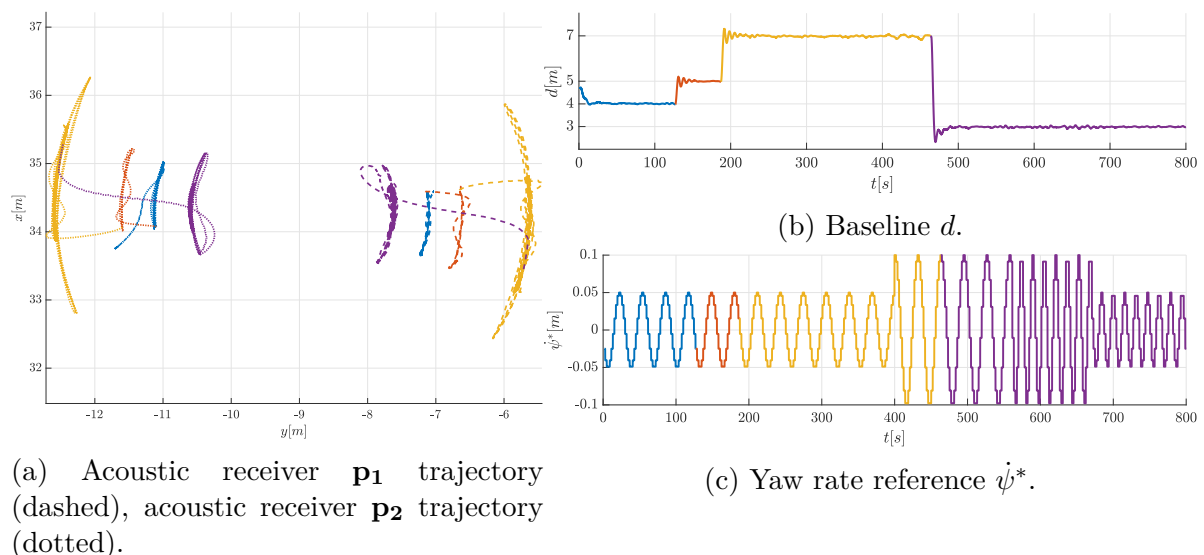
**Figure 5.13:** Trajectory, baseline and yaw rate reference responses of the real-life source seeking experiments with different colors denoting different baseline references.

with receivers baseline formation keeping algorithm was deployed. In Figure 5.13 results of the formation keeping test are shown. The baseline response is shown in Figure 5.13b where different colors denote different baseline reference values. Despite the step change

of the parameter $a$ and $\omega$ during the experiment, as seen in Figure 5.13c, baseline response remains steady which is prerequisite for successful deployment of the source seeking algorithm. Also, acquisition of time difference of arrival measurement was tested in static configuration. Time difference of arrival measurement error during static test with 40 samples is shown in Figure 5.12, where standard deviation of 0.21 meters was achieved.

## 5.6.2 Results
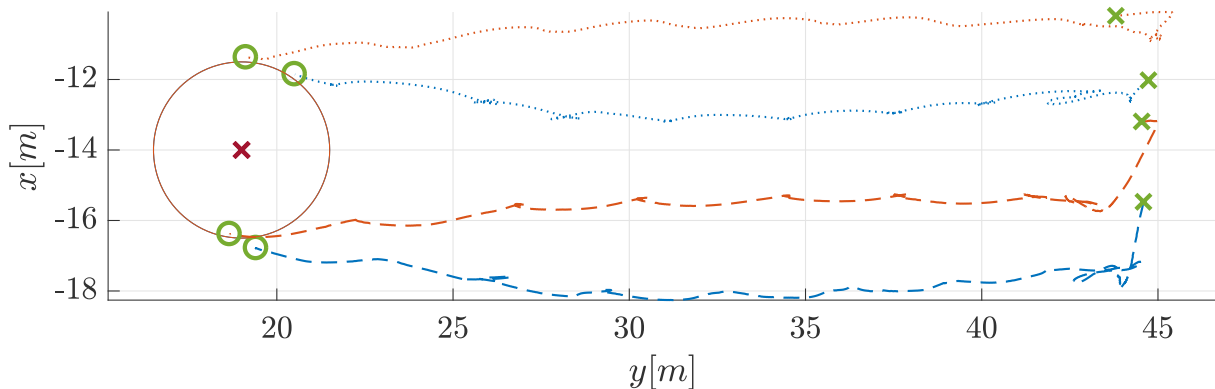


(a) Acoustic receiver $\mathbf{p_1}$ trajectory (dashed), acoustic receiver $\mathbf{p_2}$ trajectory (dotted). Green crosses denote the receivers' starting position, green circles denote ending position, while the red cross denotes source $\mathbf{p_t}$ surrounded with a 5 meter diameter circle.
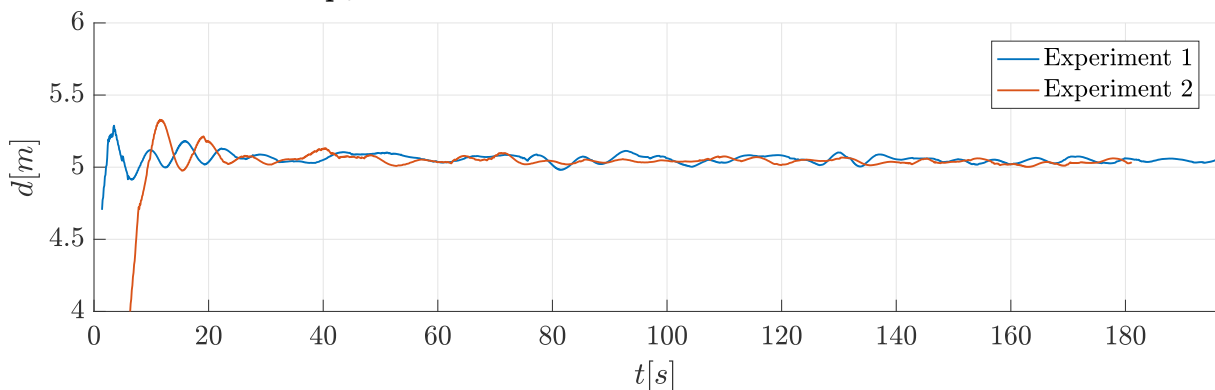


(b) Baseline $d$.

**Figure 5.14:** Trajectory and baseline responses of the real-life source seeking experiments with baseline reference $d = 5\,\mathrm{m}$ and source located at $\mathbf{p_t} \approx [-14\ 19\ 3]^T$.

The results of the two conducted experiments are shown in Figure 5.14 and Figure 5.15. During the experiments the following parameters were used: $a = 0.05\,\sqrt{\frac{\mathrm{rad}}{\mathrm{s}}}$, $\omega = 2\pi/30\,\frac{\mathrm{rad}}{\mathrm{s}}$, $k = -0.125\,\sqrt{\frac{\mathrm{rad}}{\mathrm{s}}}$, $h = 0.1\,\frac{1}{\mathrm{s}}$, $u_0 = 0.3\,\frac{\mathrm{m}}{\mathrm{s}}$, $d = 5\,\mathrm{m}, m = 20$, $\varepsilon = 0.5\,\mathrm{m}$, and $q = 3$, while the second order filter parameters were $\omega_1 = 0.8\,\frac{1}{\mathrm{s}}$, $\omega_2 = 0.15\,\frac{1}{\mathrm{s}}$, and $k_1 = 1000$. These experiments used position reference control in order to compensate for outside disturbances and model errors. In Figure 5.14b the formation baseline $d$ response is shown and it is clearly visible that after an initial transient, position controllers employed on the respective vehicles keep the two receivers at the desired distance of 5 meters.
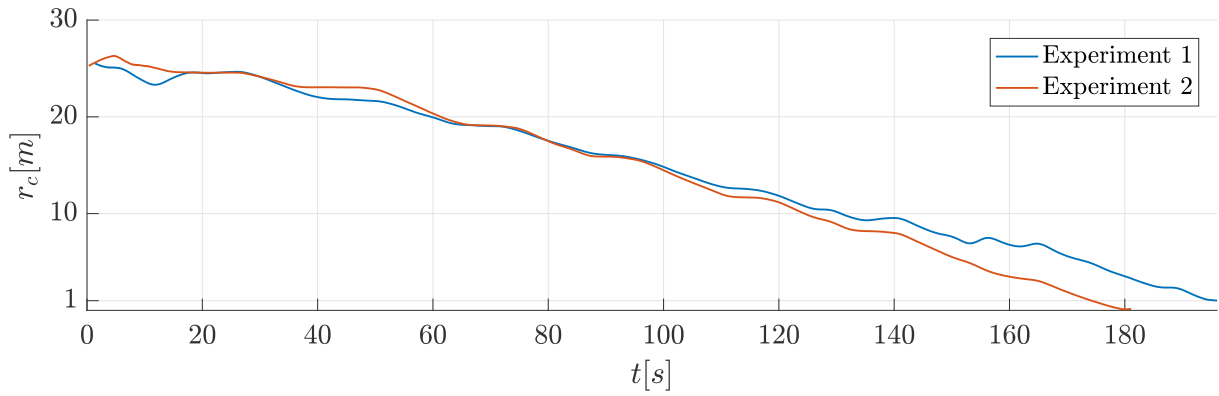
(a) Range $r_c$.
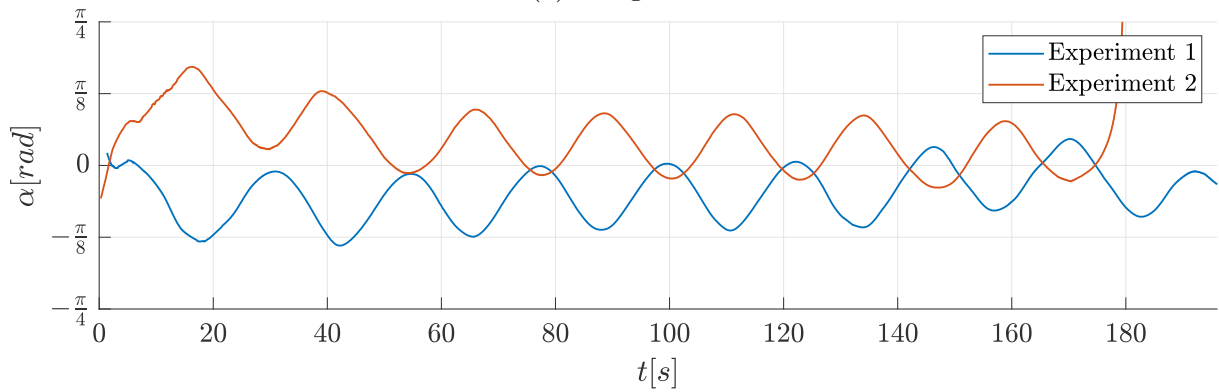


(b) Relative angle $\alpha$.
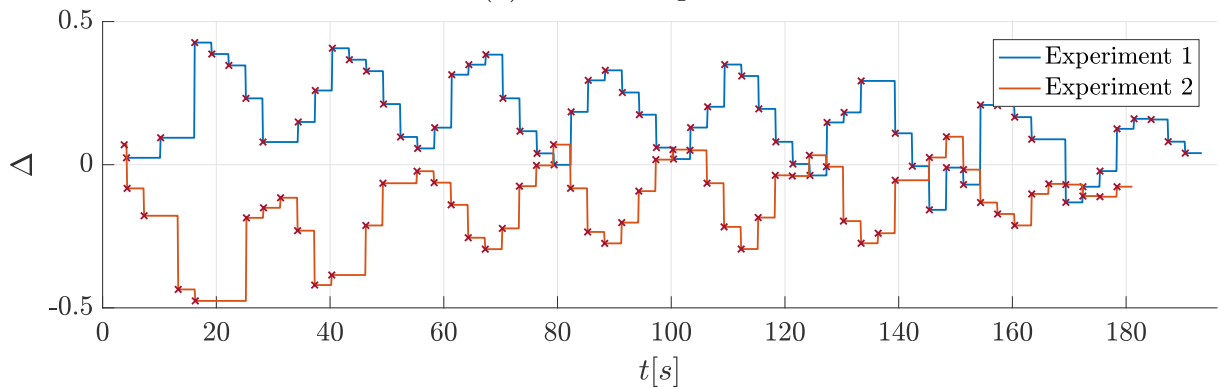


(c) Time difference of arrival $\Delta$.
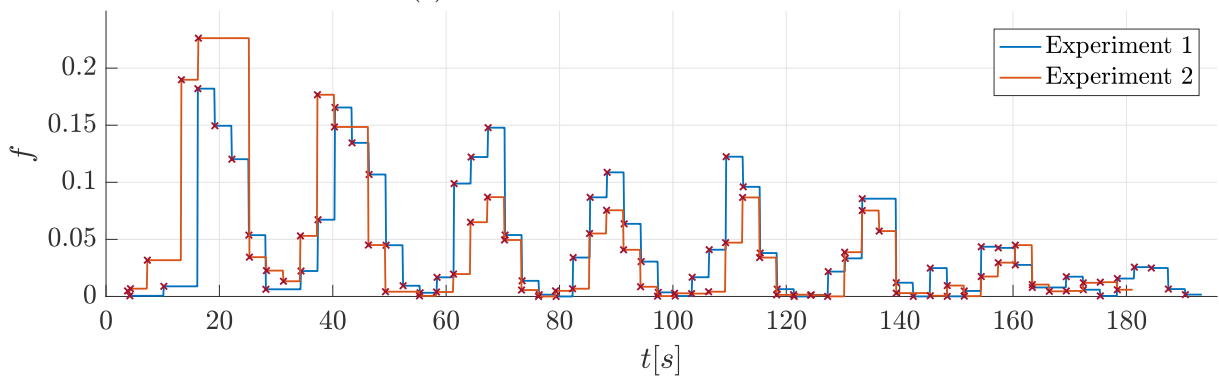


(d) Cost function value $f$.

**Figure 5.15:** Range $r_c$, relative angle $\alpha$, $\Delta$ measurement, and cost function responses of the real-life source seeking experiments with baseline reference $d = 5\,\text{m}$ and source located at $\mathbf{p_t} \approx [-14\ 19\ 3]^T$.

During the experiments, time difference of arrival measurements were rejected when the measurement was larger than the current baseline $d$ because then it could be safely assumed that a spurious measurement due to the signal reflection or some other interference had arrived. Looking at the normalized $\Delta$ measurement, shown in Figure 5.15c, it is clear that acquired measurements are intermittent. In spite of this, the formation successfully converged towards the acoustic source, as can be seen in Figure 5.15a. This was achieved by selecting a sufficiently large perturbation frequency for the extremum seeking controller.

## 5.7 Conclusion

The proposed algorithm can be used in cases where an underwater acoustic signal source needs to be approached and localized in the horizontal plane, and only two acoustic receivers are available, with no additional means of acquiring range measurements that could otherwise be used for localization. As shown herein, initial experimental results suggest that the proposed control scheme can be used in a real-life environment. The experiments have shown that the algorithm parameters are intuitive and easy to tune in order to achieve robust behaviour in the presence of the measurement noise. Also, despite the intermittent and delayed nature of the acoustic signals, by selecting a sufficiently large perturbation period, these effects can be successfully mitigated. Although convergence speed of the baseline orientation is currently satisfactory, considering the algorithm is intended for a marine environment, it could be further improved by using more advanced extremum seeking schemes in the yaw degree of freedom. Further work could include comprehensive experimental tests where the influence of different variables on algorithm performance will be inspected, such as setting different target depths, or using different baselines.

# Chapter 6

# Conclusion

The goal of this thesis was to develop online algorithms for the underwater localization and improving underwater localization of the objects of interest with affordable and easy to deploy sensors. To accomplish that, two novel control algorithms that can utilize measurements provided by such acoustic sensors were presented. Theoretical analysis of the control algorithms was given, but one of the important points was testing presented algorithms in real life conditions. The thesis stated several hypotheses and three major contributions in Section 1.2. These contributions are restated and reviewed in the context of the presented work. The first contribution stated:

- *Autonomous marine surface vessel control algorithm which improves the observability index of the underwater vehicle navigation system that uses single range measurements with respect to the beacon on the marine surface vessel.*

In Section 4, a control algorithm that steers the beacon vehicle, both fully actuated and underactuated, towards a circular trajectory around the target vehicle in order to improve the observability index of the underwater vehicle's navigation system that uses single range measurements with respect to the beacon vehicle was presented. Through both simulation and experimental results, stated hypotheses that such control can be achieved without knowing vehicle's trajectory in advance, and deployed on both fully-actuated and underactuated vehicles, were confirmed. The characteristic that knowledge of vehicle's trajectory is not known could be particularly useful in the case when the vehicle is replaced with a human diver. Also, through experimental results, proposed algorithm was shown to work in the presence of unknown currents.

The second contribution stated:

- *Cooperative control algorithm for two autonomous marine surface vessels that uses time of arrival difference of an acoustic signal for localization of an underwater source.*

In Section 5, a control algorithm for an autonomous surface system carrying a two-

sensor array consisting of two acoustic receivers, capable of measuring the time difference of arrival of a quasiperiodic underwater acoustic signal and utilizing this value in order to steer the system towards the acoustic source in the horizontal plane was presented. Stability properties of the proposed algorithm were analysed using the Lie bracket approximation technique. Furthermore, simulation results were presented, where particular attention was given to the relationship between the time difference of arrival measurement noise and the sensor baseline - the distance between the two acoustic receivers. Also, the influence of a constant disturbance caused by sea currents was considered. Finally, experimental results in which the algorithm was deployed on two autonomous surface vehicles, each equipped with a single acoustic receiver, were presented. The algorithm successfully steered the vehicle formation towards the acoustic source, despite the measurement noise and intermittent measurements, thus showing the feasibility of the proposed algorithm in real-life conditions, and confirming related hypothesis stated in Section 1.2.

The third contribution stated:

- *Validation method for underwater single range navigation and localization algorithm quality, and its application in the analysis of field experiment results.*

The performance indices used for validation of mobile beacon trajectories in single range navigation were given in Section 3.2.4. Validation was performed for experimental results of the underactuated mobile beacon experiments, where emphasis was on the quality of range measurements which trajectory of certain length can provide. In Section 3.3.3, performance indices for source seeking using single range measurements were presented. Their objective was to validate the distance, and elapsed time, that vehicle travelled while converging towards the acoustic source. Validation was performed for both simulation and experimental results of the extremum seeking algorithms presented in Section 3.3.2. Presented metric proved to be useful tool in analysing different algorithms and selecting appropriate values of their parameters.

# Bibliography

[1] Vukić, Z., Miskovic, N., "State and perspectives of underwater robotics - role of laboratory for underwater systems and technologies", Pomorski zbornik, Vol. vol.Special edition, No. 1, travanj 2016., pages 15 - 27.

[2] Beniwal, M., Singh, R. P., Sangwan, A., "A localization scheme for underwater sensor networks without time synchronization", Wirel. Pers. Commun., Vol. 88, No. 3, Jun. 2016, pages 537–552.

[3] subCULTron, "Official project website", 2015, (accessed November 1, 2018), available at: http://www.subcultron.eu

[4] Localization and Navigation. Berlin, Heidelberg: Springer Berlin Heidelberg, 2008, pages 241–269.

[5] Feezor, M. D., Sorrell, F. Y., Blankinship, P. R., Bellingham, J. G., "Autonomous underwater vehicle homing/docking via electromagnetic guidance", IEEE Journal of Oceanic Engineering, Vol. 26, No. 4, Oct 2001, pages 515-521.

[6] Gode, T., "Long baseline ranging acoustic positioning system", Master's thesis, 2015.

[7] Xiang-ping, G., yan, Y., Rong-lin, H., "Analyzing the performance of channel in underwater wireless sensor networks (uwsn)", Procedia Engineering, Vol. 15, 2011, pages 95 - 99, cEIS 2011.

[8] Stojanovic, J., M.; Preisig, "Underwater acoustic communication channels: Propagation models and statistical characterization", IEEE Communications Magazine, Vol. 47, 2009.

[9] ADAMS, K. T., "Radio acoustic ranging (r. a. r.)", Revista Geográfica, Vol. 4, No. 10/11/12, 1944, pages 1–24.

[10] Stojanovic, M., Beaujean, P., "Acoustic communication", 2013.

[11] Jakuba, M. V., Kinsey, J. C., Partan, J. W., Webster, S. E., "Feasibility of low-power one-way travel-time inverted ultra-short baseline navigation", in OCEANS 2015 - MTS/IEEE Washington, Oct 2015, pages 1-10.

[12] Tan, H.-P., Diamant, R., Seah, W. K., Waldmeyer, M., "A survey of techniques and challenges in underwater localization", Ocean Engineering, Vol. 38, No. 14, 2011, pages 1663 - 1676.

[13] Carroll, P., Zhou, S., Zhou, H., Xu, X., Cui, J.-H., Willett, P., "Underwater localization and tracking of physical systems", J. Electrical and Computer Engineering, Vol. 2012, 2012, pages 683 919:1-683 919:11.

[14] Bensky, A., Wireless Positioning Technologies and Applications. Norwood, MA, USA: Artech House, Inc., 2007.

[15] Gustafsson, F., Gunnarsson, F., "Positioning using time-difference of arrival measurements", in Acoustics, Speech, and Signal Processing, 2003. Proceedings. (ICASSP '03). 2003 IEEE International Conference on, Vol. 6, April 2003, pages

VI-553-6 vol.6.

[16] Smith, J., Abel, J., "The spherical interpolation method of source localization", IEEE Journal of Oceanic Engineering, Vol. 12, No. 1, Jan 1987, pages 246-252.

[17] Cheng, W., Thaeler, A., Cheng, X., Liu, F., Lu, X., Lu, Z., "Time-Synchronization Free Localization in Large Scale Underwater Acoustic Sensor Networks", IEEE International Conference on Distributed Computing Systems Workshops, No. i, 2009, pages 80–87.

[18] Mišković, N., Nađ, Đ., Vukić, Z., Marszalek, B., "Laboratory Platforms for Dynamic Positioning - Modeling and Identification", in 8th IFAC Conference on Control Applications in Marine Systems, 2010.

[19] Babić, A., Mandić, F., Vasiljević, G., Mišković, N., "Autonomous docking and energy sharing between two types of robotic agents", IFAC-PapersOnLine, Vol. 51, No. 29, 2018, pages 406 - 411, 11th IFAC Conference on Control Applications in Marine Systems, Robotics, and Vehicles CAMS 2018.

[20] Carreras, M., Hernández, J. D., Vidal, E., Palomeras, N., Ribas, D., Ridao, P., "Sparus ii auv – a hovering vehicle for seabed inspection", IEEE Journal of Oceanic Engineering, Vol. 43, No. 2, April 2018, pages 344-355.

[21] Ribas, D., Palomeras, N., Ridao, P., Carreras, M., Mallios, A., "Girona 500 AUV: From Survey to Intervention", IEEE/ASME Transactions on Mechatronics, Vol. 17, No. 1, Feb. 2012, pages 46–53.

[22] Neasham, J., "Towards large scale underwater communication networks – miniature, low cost, low power acoustic transceiver design", available at: https://udrc.eng.ed.ac.uk/sites/udrc.eng.ed.ac.uk/files/attachments\/Towards%20large%20scale%20underwater%20communication%2\0networks.pdf Accessed 2018-03-21.

[23] Suresh, B. N., Sivan, K., Navigation Guidance and Control System. New Delhi: Springer India, 2015, pages 581–661.

[24] Nad, D., "Guidance and control of autonomous underwater agents with acoustically aided navigation", PhD thesis, 2017.

[25] Đula Nađ, Mišković, N., Mandić, F., "Navigation, guidance and control of an over-actuated marine surface vehicle", Annual Reviews in Control, Vol. 40, 2015, pages 172 - 181.

[26] "Nomenclature for treating the motion of a submerged body through a fluid", The Society of Naval Architects and Marine Engineers, Technical and Reserach Bulletin No. 1-5, 1950.

[27] Fossen, T. I., Guidance and Control of Ocean Vehicles. John Wiley & Sons, 1994.

[28] Fossen, T., Handbook of Marine Craft Hydrodynamics and Motion Control. Wiley, 2011.

[29] Farrell, J., Aided Navigation: GPS with High Rate Sensors: GPS with High Rate Sensors, ser. McGraw-Hill professional engineering: Electronic engineering. McGraw-Hill Education, 2008.

[30] Mišković, N., "Use of self-oscillations in guidance and control of marine vessels", PhD thesis, 2010.

[31] Fossen, T. I., Johansen, T. A., "A survey of control allocation methods for ships and underwater vehicles", in 2006 14th Mediterranean Conference on Control and Automation, June 2006, pages 1-6.

[32] Fossen, T., Guidance and Control of Ocean Vehicles. New York, NY, USA: John

Wiley & Sons, 1994.

[33] Francis, B. A., Maggiore, M., Flocking and Rendezvous in Distributed Robotics. Cham: Springer International Publishing, 2016.

[34] Miskovic, N., Nad, D., Stilinovic, N., Vukic, Z., "Guidance and control of an overactuated autonomous surface platform for diver tracking", in Control & Automation (MED), 2013 21st Mediterranean Conference on. IEEE, 2013, pages 1280–1285.

[35] Simon, D., Optimal state estimation: Kalman, H infinity, and nonlinear approaches. John Wiley & Sons, 2006.

[36] Einicke, G. A., "Smoothing, filtering and prediction: Estimating the past, present and future", 2012.

[37] Simon, D., Optimal state estimation: Kalman, H-infinity and nonlinear approaches. Wiley-Interscience, 2006.

[38] Andersen, G., Christensen, A., Ravn, O., "Augmented models for improving vision control of a mobile robot", in Proceedings of the Third IEEE Conference on Control Applications, 1994, pages 53–58.

[39] Gopalakrishnan, A., Kaisare, N. S., Narasimhan, S., "Incorporating delayed and infrequent measurements in extended kalman filter based nonlinear state estimation", Journal of Process Control, Vol. 21, No. 1, 2011, pages 119 - 129.

[40] Larsen, T., Andersen, N., Ravn, O., Poulsen, N., "Incorporation of time delayed measurements in a discrete-time kalman filter", in Decision and Control, 1998. Proceedings of the 37th IEEE Conference on, Vol. 4, Dec 1998, pages 3972-3977 vol.4.

[41] Bar-Shalom, Y., "Update with out-of-sequence measurements in tracking: exact solution", IEEE Transactions on Aerospace and Electronic Systems, Vol. 38, No. 3, 2002, pages 769 - 777.

[42] Thomopoulos, S. C. A., "Decentralized filtering and control in the presence of delays: Discrete-time and continuous-time case", Information Sciences, Vol. 81, No. 1-2, 1994, pages 133 - 153.

[43] Alcocer, A., Oliveira, P., Pascoal, A., "Study and Implementation of an EKF GIB-Based Underwater Positioning System", in IFAC CAMS, 2004.

[44] Chang, G., "Robust kalman filtering based on mahalanobis distance as outlier judging criterion", Journal of Geodesy, Vol. 88, No. 4, Apr 2014, pages 391–401.

[45] Berman, Z., "Outliers rejection in kalman filtering — some new observations", in 2014 IEEE/ION Position, Location and Navigation Symposium - PLANS 2014, May 2014, pages 1008-1013.

[46] Mandić, F., Rendulić, I., Mišković, N., Đula Nađ, "Underwater object tracking using sonar and usbl measurements", Journal of Sensors, Vol. 2016, 2016, page 10.

[47] Soler, T., Chin, M., "On transformation of covariance matrices between local cartesian coordinate systems and commutative diagrams", in ASP-ACSM Convention, 1985, pages 393–406.

[48] Haug, A. J., Bayesian Estimation and Tracking: A Practical Guide. John Wiley & Sons, 2012.

[49] Ting, J., D'Souza, A., Schaal, S., "Automatic outlier detection: A bayesian approach", in Proceedings 2007 IEEE International Conference on Robotics and Automation, April 2007, pages 2489-2494.

[50] Caccia, M., Bibuli, M., Bono, R., Bruzzone, G., "Basic navigation, guidance and control of an Unmanned Surface Vehcile", Autonomous Robots, Vol. 25, No. 4, 2008, pages 349–365.

[51] Miskovic, N., Bogdan, S., Nad, D., Mandic, F., Orsag, M., Haus, T., "Unmanned marsupial sea-air system for object recovery", in 22nd Mediterranean Conference on Control and Automation, June 2014, pages 740-745.

[52] Miskovic, N., Vukic, Z., Bibuli, M., Bruzzone, G., Caccia, M., "Fast in-field identification of unmanned marine vehicles", Journal of Field Robotics, Vol. 28, No. 1, 2011, pages 101–120.

[53] Webster, S. E., Eustice, R. M., Singh, H., Whitcomb, L. L., "Advances in single-beacon one-way-travel-time acoustic navigation for underwater vehicles", The International Journal of Robotics Research, Vol. 31, No. 8, Jul. 2012, pages 935–950.

[54] Salinas, D., Pascoal, A., Aranda, J., "Optimal sensor trajectories for mobile underwater target positioning with noisy range measurements", in Proc. 19th IFAC World Congress 2014, Cape Town, South Africa, 24-29 August, 2014. IEEE, 2014, pages 24-29.

[55] Moreno Salinas, D., "Adaptive sensor networks for mobile target localization and tracking", PhD thesis, 2013.

[56] Davis, J. E., "Combining error ellipses version 0.3-3", 2011.

[57] Tan, Y. T., Gao, R., Chitre, M., "Cooperative path planning for range-only localization using a single moving beacon", Oceanic Engineering, IEEE Journal of, Vol. 39, No. 2, April 2014, pages 371-385.

[58] Young, J., Rowe, F., Brumley, B., Bradley, S., "Trends in acoustic velocity log technology at RD Instruments", in Proceedings Of The Workshop on Autonomous Underwater Vehicles, 1998, pages 89 -101.

[59] Larsen, M., "High performance Doppler-inertial navigation-experimental results", in MTS/IEEE OCEANS, Vol. 2, 2000, pages 1449 -1456.

[60] Antoulas, A. C., Sontag, E. D., Yamamoto, Y., Controllability and Observability. American Cancer Society, 1999.

[61] Hermann, R., Krener, A., "Nonlinear controllability and observability", Automatic Control, IEEE Transactions on, Vol. 22, No. 5, 1977, pages 728–740.

[62] Böhm, C., Findeisen, R., Allgöwer, F., "Avoidance of poorly observable trajectories: A predictive control perspective", {IFAC} Proceedings Volumes, Vol. 41, No. 2, 2008, pages 1952 - 1957, 17th {IFAC} World Congress.

[63] Chen, C.-T., Linear System Theory and Design, 3rd ed. New York, NY, USA: Oxford University Press, Inc., 1998.

[64] Krener, A. J., Ide, K., "Measures of unobservability", in Decision and Control, 2009 held jointly with the 2009 28th Chinese Control Conference. CDC/CCC 2009. Proceedings of the 48th IEEE Conference on, Dec 2009, pages 6401-6406.

[65] Moreno-Salinas, D., Pascoal, A., Aranda, J., "Optimal sensor placement for acoustic underwater target positioning with range-only measurements", IEEE Journal of Oceanic Engineering, Vol. 41, No. 3, July 2016, pages 620-643.

[66] Jauffret, C., "Observability and fisher information matrix in nonlinear regression", Aerospace and Electronic Systems, IEEE Transactions on, Vol. 43, 05 2007, pages 756 - 759.

[67] Batista, P., Silvestre, C., Oliveira, P., "Single range aided navigation and source localization: Observability and filter design", Systems & Control Letters, Vol. 60, No. 8, Aug. 2011, pages 665–673.

[68] Crasta, N., Bayat, M., Aguiar, A. P., Pascoal, A. M., "Observability analysis of 2d single beacon navigation in the presence of constant currents for two classes of

maneuvers", in Control Applications in Marine Systems, Vol. 9, 2013, pages 227–232.

[69] Arrichiello, F., Antonelli, G., Aguiar, A. P., Pascoal, A., "An observability metric for underwater vehicle localization using range measurements", Sensors, Vol. 13, No. 12, 2013, pages 16 191–16 215.

[70] Arrichiello, F., Palma, D. D., Indiveri, G., Parlangeli, G., "Observability analysis for single range localization", in OCEANS 2015 - Genova, May 2015, pages 1-10.

[71] Moreno-Salinas, D., Pascoal, A., Aranda, J., "Underwater target positioning with a single acoustic sensor", 9th IFAC Conference on Control Applications in Marine Systems, Osaka, Japan, 2013.

[72] Crasta, N., Moreno-Salinas, D., Bayat, M., Pascoal, A., Aranda, J., "Optimal motion planning for range-based marine vehicle positioning in the presence of unknown currents", IFAC-PapersOnLine, Vol. 49, No. 23, 2016, pages 41 - 47, 10th IFAC Conference on Control Applications in Marine Systems CAMS 2016.

[73] Pedro, M., Moreno-Salinas, D., Crasta, N., Pascoal, A., "Underwater single-beacon localization: Optimal trajectory planning and minimum-energy estimation", IFAC-PapersOnLine, Vol. 48, No. 2, 2015, pages 155 - 160, 4th IFAC Workshop onNavigation, Guidance and Controlof Underwater Vehicles NGCUV 2015.

[74] Luc, D. T., Pareto Optimality. New York, NY: Springer New York, 2008, pages 481–515.

[75] Stetter, H. J., Analysis of discretization methods for ordinary differential equations. Springer Berlin, New York, 1973.

[76] Vallicrosa, G., Bosch, J., Palomeras, N., Ridao, P., Carreras, M., Gracias, N., "Autonomous homing and docking for auvs using range-only localization and light beacons", IFAC-PapersOnLine, Vol. 49, No. 23, 2016, pages 54 - 60, 10th IFAC Conference on Control Applications in Marine Systems CAMS 2016.

[77] Ghods, N., Krstic, M., "Source seeking with very slow or drifting sensors", Journal of Dynamic Systems, Measurement, and Control, Vol. 133, No. 4, 2011, page 044504.

[78] Zhang, C., Siranosian, A., Krstic, M., "Extremum seeking for moderately unstable systems and for autonomous vehicle target tracking without position measurements", Automatica, Vol. 43, No. 10, Oct. 2007, pages 1832–1839.

[79] Zhang, C., Arnold, D., Ghods, N., Siranosian, A., Krstic, M., "Source seeking with non-holonomic unicycle without position measurement and with tuning of forward velocity", Systems & Control Letters, Vol. 56, No. 3, Mar. 2007, pages 245–252.

[80] Scheinker, A., Krstic, M., "Extremum seeking with bounded update rates", Systems & Control Letters, Vol. 63, Jan. 2014, pages 25–31.

[81] Bayat, B., Crasta, N., Li, H., Ijspeert, A., "Optimal search strategies for pollutant source localization", in 2016 IEEE/RSJ International Conference on Intelligent Robots and Systems (IROS), Oct 2016, pages 1801-1807.

[82] Ferreira, B., Matos, A., Cruz, N., "Single beacon navigation: Localization and control of the MARES AUV", in OCEANS 2010. IEEE, 2010, page 1–9.

[83] Leblanc, M., "Sur l'electrification des chemins de fer au moyen de courants alternatifs de frequence elevee", Revue Generale de l'Electricite, Vol. 12, No. 8, 1922, pages 275-277.

[84] Krstic, M., Wang, H.-H., "Stability of extremum seeking feedback for general nonlinear dynamic systems", Automatica, Vol. 36, No. 4, 2000, pages 595 - 601.

[85] Ariyur, K. B., Krstic, M., Real Time Optimization by Extremum Seeking Control.

New York, NY, USA: John Wiley & Sons, Inc., 2003.

[86] Mandić, F., Mišković, N., "Tracking underwater target using extremum seeking", IFAC-PapersOnLine, Vol. 48, No. 2, 2015, pages 149 - 154, 4th IFAC Workshop on Navigation, Guidance and Control of Underwater VehiclesNGCUV 2015.

[87] Weisstein, E. W., ""Laplace Transform." From MathWorld – A Wolfram Web Resource.", available at: http://mathworld.wolfram.com/LaplaceTransform.html

[88] Dürr, H.-B., Stankovic, M. S., Ebenbauer, C., Johansson, K. H., "Lie bracket approximation of extremum seeking systems", Automatica, Vol. 49, 2013, pages 1538-1552.

[89] Ghaffari, A., Krstić, M., Nešić, D., "Multivariable newton-based extremum seeking", Automatica, Vol. 48, No. 8, 2012, pages 1759 - 1767.

[90] Matveev, A. S., Hoy, M. C., Savkin, A. V., "3d environmental extremum seeking navigation of a nonholonomic mobile robot", Automatica, Vol. 50, No. 7, 2014, pages 1802 - 1815.

[91] Gelbert, G., Moeck, J. P., Paschereit, C. O., King, R., "Advanced algorithms for gradient estimation in one- and two-parameter extremum seeking controllers", Journal of Process Control, Vol. 22, No. 4, Apr. 2012, pages 700–709.

[92] Choi, J.-Y., Krstic, M., Ariyur, K. B., Lee, J. S., "Extremum seeking control for discrete-time systems", Automatic Control, IEEE Transactions on, Vol. 47, No. 2, 2002, pages 318–323.

[93] Khalil, H. K., Nonlinear systems; 3rd ed. Upper Saddle River, NJ: Prentice-Hall, 2002, the book can be consulted by contacting: PH-AID: Wallet, Lionel.

[94] Mandić, F., Mišković, N., Vukić, Z., "Range–only navigation – maximizing system observability by using extremum seeking", IFAC-PapersOnLine, Vol. 48, No. 16, 2015, pages 101 - 106, 10th IFAC Conference on Manoeuvring and Control of Marine Craft MCMC 2015, Copenhagen, 24–26 August 2015.

[95] Stilinovic, N., Nad, D., Miskovic, N., "Auv for diver assistance and safety - design and implementation", in OCEANS 2015 - Genova, May 2015, pages 1-4.

[96] Carreras, M., Candela, C., Ribas, D., Palomeras, N., Magí, L., Mallios, A., Vidal, E., Vidal, i., Ridao, P., "Testing Sparus II AUV, an open platform for industrial, scientific and academic applications", Instrumentation Viewpoint, No. 18, 2015, pages 54–55.

[97] Stone, L. D., Keller, C. M., Kratzke, T. M., Strumpfer, J. P., "Search analysis for the underwater wreckage of air france flight 447", in 14th International Conference on Information Fusion, July 2011, pages 1-8.

[98] Schmidt, V., Weber, T. C., Wiley, D. N., Johnson, M. P., "Underwater tracking of humpback whales (megaptera novaeangliae) with high-frequency pingers and acoustic recording tags", IEEE Journal of Oceanic Engineering, Vol. 35, No. 4, Oct 2010, pages 821-836.

[99] Society, N. A., Bowens, e., Amanda, Underwater archaeology : the NAS guide to principles and practice. Malden, MA ; Oxford : Blackwell Publishing ; Portsmouth, UK : Nautical Archaeology Society, 2009.

[100] Mandić, F., Mišković, N., Lončar, I., "Time difference of arrival source seeking", IEEE Journal of Oceanic Engineering, 2019, accepted for publication.

[101] Ferreira, B. M., Matos, A. C., Cruz, N. A., Almeida, R. M., "Towards cooperative localization of an acoustic pinger", in 2012 Oceans, Oct 2012, pages 1-5.

[102] Kouzoundjian, B., Beaubois, F., Reboul, S., Choquel, J. B., Noyer, J. C., "A tdoa

underwater localization approach for shallow water environment", in OCEANS 2017 - Aberdeen, June 2017, pages 1-4.

[103] Begault, D. R., 3DD Sound for Virtual Reality and Multimedia. San Diego, CA, USA: Academic Press Professional, Inc., 1994.

[104] Petersen, K. B., Pedersen, M. S., "The matrix cookbook", available at: http://www2.imm.dtu.dk/pubdb/p.php?3274 Version 20121115. nov 2012.

# Appendix

**Appendix A.** It is proceeded by establishing the connection between system observability Gramian $\mathbf{W}$ and estimate covariance matrix $\mathbf{P}$. Continuous time Kalman filter covariance equation is given with ([35]):

$$\dot{\mathbf{P}} = -\mathbf{P}\mathbf{C}^T\mathbf{R}^{-1}\mathbf{C}\mathbf{P} + \mathbf{A}\mathbf{P} + \mathbf{P}\mathbf{A}^T + \mathbf{Q}. \tag{1}$$

Using state matrix $\mathbf{A}$ from (4.34) and assuming that there is no process noise $\mathbf{Q}$ yields

$$\dot{\mathbf{P}} = -\mathbf{P}\mathbf{C}^T\mathbf{R}^{-1}\mathbf{C}\mathbf{P}. \tag{2}$$

Since there is single measurement available and we assumed that measurement noise in (5.7) is independent, with constant variance, we can substitute $\mathbf{R} = \sigma$ which yields

$$\dot{\mathbf{P}} = -\frac{1}{\sigma}\mathbf{P}\mathbf{C}^T\mathbf{C}\mathbf{P}. \tag{3}$$

In order to solve the equation, following algebraic manipulation, using identities from [104], is done:

$$\frac{d\mathbf{P}}{d\tau} = -\frac{1}{\sigma}\mathbf{P}\mathbf{C}^T\mathbf{C}\mathbf{P} \tag{4}$$

$$-\mathbf{P}^{-1}\frac{d\mathbf{P}}{d\tau}\mathbf{P}^{-1} = \frac{1}{\sigma}\mathbf{C}^T\mathbf{C} \tag{5}$$

$$\frac{d\mathbf{P}^{-1}}{d\tau} = \frac{1}{\sigma}\mathbf{C}^T\mathbf{C}d\tau \tag{6}$$

The solution to this differential equation is

$$\mathbf{P}^{-1} = \frac{1}{\sigma}\int \mathbf{C}^T\mathbf{C}d\tau. \tag{7}$$

Given that the state transition matrix of system (4.34) is $\boldsymbol{\Phi}(\tau) = e^{\mathbf{A}\tau} = \mathbf{I} \in \mathbb{R}^{2\times 2}$, the observability Gramian of the system is

$$\mathbf{W}(t) = \int_0^t \mathbf{C}(t)^T \mathbf{C}(t)\, d\tau. \tag{8}$$

By combining (8) and (6), the following result is obtained:

$$\mathbf{P} = \sigma\mathbf{W}^{-1} \tag{9}$$

As it can be seen from (9), the link between the system's observability Gramian and estimation covariance matrix is established.

**Appendix B.** In [88] a couple of assumptions on the vector fields $\boldsymbol{b_i}$ are given. The first one is that $\boldsymbol{b_i} \in C^2 : \mathbb{R} \times \mathbb{R}^n \to \mathbb{R}^n$ for $i = 0, ..., m$. In the case of the system (5.24) terms $\boldsymbol{b_0}$, $\boldsymbol{b_1}$ and $\boldsymbol{b_2}$ are sufficiently smooth vector fields if a simple modification is done. Namely, the signum function in (5.18) is discontinuous but for the mathematical analysis it can be easily approximated with a continuous function, i.e. $\text{sgn}(x) \approx \tanh(\mu x)$ if parameter $\mu \gg 1$.

The second assumption is that for every compact set $\mathcal{C} \subseteq \mathbb{R}^n$ there exist $\boldsymbol{A_1}, ..., \boldsymbol{A_6} \in [\boldsymbol{0}, \infty)$ such that $|\boldsymbol{b_i}(t, \boldsymbol{\eta})| \leq \boldsymbol{A_1}$, $\left|\frac{\partial \boldsymbol{b_i}(t,\boldsymbol{\eta})}{\partial t}\right| \leq \boldsymbol{A_2}$, $\left|\frac{\partial \boldsymbol{b_i}(t,\boldsymbol{\eta})}{\partial \boldsymbol{\eta}}\right| \leq \boldsymbol{A_3}$, $\left|\frac{\partial^2 \boldsymbol{b_j}(t,\boldsymbol{x})}{\partial t \partial \boldsymbol{x}}\right| \leq \boldsymbol{A_4}$, $\left|\frac{\partial [\boldsymbol{b_j}, \boldsymbol{b_k}](t,\boldsymbol{x})}{\partial \boldsymbol{x}}\right| \leq \boldsymbol{A_5}$, $\left|\frac{\partial [\boldsymbol{b_j}, \boldsymbol{b_k}](t,\boldsymbol{x})}{\partial t}\right| \leq \boldsymbol{A_6}$ for all $\boldsymbol{x} \in \mathcal{C}$, $t \in \mathbb{R}$, $i = 0, ..., m$, $j = 1, ..., m$, $k = j, ..., m$. For the system (5.21) state vector is defined with $\boldsymbol{x} = \begin{bmatrix} r_c & \alpha & x_e \end{bmatrix}^T$. Going further, without loss of generality, it is assumed that $q = 1$ and $d = 1$. Given inequalities are tested for vectors $\boldsymbol{b_0}$, $\boldsymbol{b_1}$ and $\boldsymbol{b_2}$, starting with:

$$|\boldsymbol{b_0}(t, \boldsymbol{x})| = \left|\left[-\frac{r_c u_{dir} u_{amp}}{r_c + \varepsilon} \cos \alpha \quad \frac{u_{dir} u_{amp}}{r_c + \varepsilon} \sin \alpha \quad -x_e h + f\right]^T\right| \leq \boldsymbol{A_1}. \tag{10}$$

The variables $u_{dir} \in [-1, 1]$ and $u_{amp} \in [0, u_0)$, and functions $|\sin \alpha| \leq 1$ and $|\cos \alpha| \leq 1$ are bounded for all $\boldsymbol{x} \in \mathcal{C}$, while the parameter $h$ is a constant. Since $\varepsilon > 0$ and $r_c \geq 0$, denominator $(r_c + \varepsilon)$ is larger than zero and it is clear that bound $\boldsymbol{A_1}$ exists. The solution for inequality $|b_2(t, \boldsymbol{x})| = \left|\begin{bmatrix} 0 & a & 0 \end{bmatrix}^T\right| \leq \boldsymbol{A_1}$ is trivial, while in the inequality $|\boldsymbol{b_1}(t, \boldsymbol{x})| = \left|\begin{bmatrix} 0 & k(f - x_e h) & 0 \end{bmatrix}^T\right| \leq \boldsymbol{A_1}$, variable $f \in [0, 1]$ and for the $x_e \in \mathcal{C}$ bound also exists. Next, boundedness of the $\left|\frac{\partial \boldsymbol{b_0}(t,\boldsymbol{x})}{\partial \boldsymbol{x}}\right| = \left|\left[\frac{\partial \boldsymbol{b_0}(t,\boldsymbol{x})}{\partial r_c} \quad \frac{\partial \boldsymbol{b_0}(t,\boldsymbol{x})}{\partial \alpha} \quad \frac{\partial \boldsymbol{b_0}(t,\boldsymbol{x})}{\partial x_e}\right]^T\right|$ is investigated. Calculating $\frac{\partial \boldsymbol{b_0}(t,\boldsymbol{x})}{\partial r_c}$ yields:

$$\left[\begin{matrix} -\frac{r_c \cos(\alpha) u_{dir} u_{amp}}{(r_c+\varepsilon)^2} + \frac{\cos(\alpha) u_{dir} u_{amp}}{r_c+\varepsilon} - \frac{r_c \sin(2\alpha) \cos(\alpha) u_{amp}\left(u_{dir}^2 - 1\right)\sigma_1}{r_c+\varepsilon} + \frac{2r_c \cos(\alpha) u_{dir}\left(\sigma_2^2 - 1\right)\sigma_1 \Delta}{r_c+\varepsilon} \\ \frac{\sin(\alpha) u_{dir} u_{amp}}{(r_c+\varepsilon)^2} - \frac{2 \sin(\alpha) u_{dir}\left(\sigma_2^2 - 1\right)\sigma_1 \Delta}{r_c+\varepsilon} + \frac{\sin(2\alpha) \sin(\alpha) u_{amp}\left(u_{dir}^2 - 1\right)\sigma_1}{r_c+\varepsilon} \\ 2\sigma_1 \Delta \end{matrix}\right] \tag{11}$$

where $\sigma_1 = \frac{2r_c + \sin(\alpha)}{2r_1} - \frac{2r_c - \sin(\alpha)}{2r_2}$ and $\sigma_2 = \tanh(\Delta^2)$. Partial derivative $\frac{\partial \boldsymbol{b_0}(t,\boldsymbol{x})}{\partial \alpha}$ is:

$$\left[\begin{matrix} -\frac{r_c \sin(\alpha) u_{dir} u_{amp}}{r_c+\varepsilon} - \frac{r_c \cos(\alpha)\sigma_1 u_{amp}\left(u_{dir}^2 - 1\right)}{r_c+\varepsilon} + \frac{2r_c \cos(\alpha) u_{dir}\left(\sigma_2^2 - 1\right)\sigma_3 \Delta}{r_c+\varepsilon} \\ -\frac{\cos(\alpha) u_{dir} u_{amp}}{r_c+\varepsilon} + \frac{\sin(\alpha)\sigma_1 u_{amp}\left(u_{dir}^2 - 1\right)}{r_c+\varepsilon} - \frac{2 \sin(\alpha) u_{dir}\left(\sigma_2^2 - 1\right)\sigma_3 \Delta}{r_c+\varepsilon} \\ \frac{r_c^2 \sin(2\alpha)}{r_1 r_2} \end{matrix}\right] \tag{12}$$

where $\sigma_1 = \sin(2\alpha)\sigma_3 + 2\cos(2\alpha)\Delta$, $\sigma_2 = \tanh(\Delta^2)$ and $\sigma_3 = \frac{r_c \cos(\alpha)}{2r_1} + \frac{r_c \cos(\alpha)}{2r_2}$ and

$$\frac{\partial \boldsymbol{b_0}(t, \boldsymbol{x})}{\partial x_e} = \begin{bmatrix} 0 & 0 & -h \end{bmatrix}^T. \tag{13}$$

In (11), (12), and (13) same bounds on terms $u_{amp}$, $u_{dir}$, $\varepsilon$, $h$ and $f$ apply as in (10). Additionally, variable $\Delta \in [-1, 1]$. Since $z_t > 0$, ranges $r_1$ and $r_2$ are greater than zero for every $\boldsymbol{x} \in \mathcal{C}$ and in the inequality $\left|\frac{\partial \boldsymbol{b_0}(t,\boldsymbol{x})}{\partial \boldsymbol{x}}\right| \leq \boldsymbol{A_3}$, bound $\boldsymbol{A_3}$ exists. Since $\boldsymbol{b_0}$, $\boldsymbol{b_1}$ and $\boldsymbol{b_2}$ do not explicitly depend on $t$, condition $\left|\frac{\partial \boldsymbol{b_i}(t,\boldsymbol{x})}{\partial t}\right| \leq \boldsymbol{A_2}$ and condition $\left|\frac{\partial^2 \boldsymbol{b_j}(t,\boldsymbol{x})}{\partial t \partial \boldsymbol{x}}\right| \leq \boldsymbol{A_4}$ are

satisfied trivially. The inequality $\left|\frac{\partial[\boldsymbol{b_1},\boldsymbol{b_2}](t,\boldsymbol{x})}{\partial \boldsymbol{x}}\right| \leq \boldsymbol{A_5}$, where $[\boldsymbol{b_1},\boldsymbol{b_2}] = \begin{bmatrix} 0 & ak\frac{r_c^2\sin(2\alpha)}{r_1 r_2} & 0 \end{bmatrix}^T$, is:

$$\left| \begin{bmatrix} 0 & \frac{8akr_c\left(16\sin(2\alpha)r_c^2 z_t^2 + 2\sin(4\alpha)r_c^2 + 16\sin(2\alpha)z_t^4 + 8\sin(2\alpha)z_t^2 + \sin(2\alpha)\right)}{r_1^3 r_2^3} & 0 \\ 0 & \frac{8akr_c^2\left(16r_c^4\cos(2\alpha) + 32r_c^2 z_t^2\cos(2\alpha) + 4r_c^2\cos(2\alpha)^2 + 4r_c^2 + 16z_t^4\cos(2\alpha) + 8z_t^2\cos(2\alpha) + \cos(2\alpha)\right)}{r_1^3 r_2^3} & 0 \\ 0 & 0 & 0 \end{bmatrix}^T \right| \leq \boldsymbol{A_5}$$

$$(14)$$

and the same argumentation is used as in (11), ranges $r_1$ and $r_2$ are greater than zero for every $\boldsymbol{x} \in \mathcal{C}$ and bound $\boldsymbol{A_5}$ exists. Finally, inequality $\left|\frac{\partial[\boldsymbol{b_1},\boldsymbol{b_2}](t,\boldsymbol{x})}{\partial t}\right| \leq \boldsymbol{A_6}$ is satisfied trivially since $[\boldsymbol{b_1},\boldsymbol{b_2}]$ does not explicitly depend on $t$.

# Acronyms

| | | |
|---|---|---|
| **LABUST** | the Laboratory for Underwater Systems and Technologies | 8, 9, 12 |
| **2D** | two dimensional | 35, 37, 41, 42, 44, 54, 55 |
| **3D** | three dimensional | 37, 41, 42 |
| **AHRS** | Attitude Heading Reference System | 36, 37 |
| **AUV** | Autonomous Underwater Vehicle | 1, 9–11, 13, 31, 35, 42, 48, 54, 70, 87 |
| **DoF** | degree of freedom | 9, 11, 13, 17–20, 54 |
| **DVL** | Doppler velocity logger | 10, 31, 36, 47 |
| **EKF** | Extended Kalman Filter | 21, 22, 24, 41, 46, 51, 53, 55, 56, 58, 62, 66 |
| **ES** | Extremum seeking | 51–55, 59, 61–63, 65, 67, 139, 140 |
| **FIM** | Fisher Information Matrix | 41, 43–45, 95 |
| **GIB** | GNSS Intelligent Buoy | 5 |
| **GNSS** | Global Navigation Satellite System | 2 |
| **GPS** | Global Positioning System | 31 |
| **IMU** | Inertial Measurement Unit | 9, 10 |
| **LBL** | Long Base-Line | 4, 5, 31 |
| **LTP** | Local Tangent Plane | 14, 138 |
| **LTV** | linear time–variant | 39, 40 |
| **MBC** | Mobile beacon control | 84–87, 94–96 |
| **NED** | North-East-Down | 14 |
| **NGC** | navigation, guidance and control | 8, 9, 13, 20 |
| **OWTT** | One–way time travel | 32, 33, 71 |
| **PI** | Proportional-Integral | 27 |
| **RAR** | Radio Acoustic Ranging | 3 |
| **ROS** | Robot Operating System | 26 |
| **SBL** | Short Base-Line | 4, 31 |
| **SNAME** | The Society of Naval Architects and Marine Engineers | 14, 142 |
| **TDOA** | Time Difference of Arrival | 5, 98 |
| **TOA** | Time–of–Arrival | 32, 33, 98 |

| | | |
|---|---|---|
| **TOF** | Time–of–Flight | 32 |
| **TOL** | Time–of–Launch | 32, 33, 98 |
| **TWTT** | Two–way time travel | 33, 75 |
| **USBL** | Ultra Short Base-Line | 3, 4, 12, 25, 31, 67 |
| **USV** | Unmanned Surface Vehicle | 8, 9, 13, 54, 87 |

# Nomenclature

| Term | Description |
|---|---|
| $K$ | rolling moment acting on the vehicle in $\{\mathbf{B}\}$ |
| $M$ | pitching moment acting on the vehicle in $\{\mathbf{B}\}$ |
| $N$ | yawing moment acting on the vehicle in $\{\mathbf{B}\}$ |
| $X$ | surge force acting on the vehicle in $\{\mathbf{B}\}$ |
| $Y$ | sway force acting on the vehicle in $\{\mathbf{B}\}$ |
| $Z$ | heave force acting on the vehicle in $\{\mathbf{B}\}$ |
| $\boldsymbol{W}$ | observability gramian |
| $\boldsymbol{\eta}_b$ | beacon vehicle position and orientation in $\{\mathbf{E}\}$ |
| $\boldsymbol{\eta}$ | vehicle position and orientation in $\{\mathbf{E}\}$ |
| $\boldsymbol{\nu}_b$ | beacon vehicle velocities in $\{\mathbf{B}\}$ |
| $\boldsymbol{\nu}$ | vehicle velocities in $\{\mathbf{B}\}$ |
| $\boldsymbol{\tau}$ | virtual forces and moments acting on the vehicle |
| $\boldsymbol{\xi}_c$ | disturbance velocities in $\{\mathbf{E}\}$ |
| $\boldsymbol{v}$ | vehicle velocities in $\{\mathbf{E}\}$ |
| $\{\mathbf{B}\}$ | vehicle body frame |
| $\{\mathbf{E}\}$ | the fixed North-East-Down frame defining the LTP |
| $\phi$ | roll angle in $\{\mathbf{E}\}$ |
| $\psi$ | yaw angle in $\{\mathbf{E}\}$ |
| $\theta$ | pitch angle in $\{\mathbf{E}\}$ |
| $p$ | roll rate in $\{\mathbf{B}\}$ |
| $q$ | pitch rate in $\{\mathbf{B}\}$ |
| $r$ | yaw rate in $\{\mathbf{B}\}$ |
| $u$ | surge speed in $\{\mathbf{B}\}$ |
| $v$ | sway speed in $\{\mathbf{B}\}$ |
| $w$ | heave speed in $\{\mathbf{B}\}$ |
| $x$ | north position in $\{\mathbf{E}\}$ |
| $y$ | east position $\{\mathbf{E}\}$ |
| $z$ | depth in $\{\mathbf{E}\}$ |

# List of Figures

# List of Tables

# Biography

**Filip Mandić** was born on 2nd of April, 1990 in Pula Croatia. In 2014 he graduated at the University of Zagreb, Faculty of electrical engineering and computing (FER) with his master thesis entitled "Range-only underwater navigation". From 2014, he is a PhD student and research and teaching assistant at the Department of control and computer engineering at FER. His work was funded by the Croatian Science Foundation through the Project for the young researcher career development. He was involved in several EU projects (FP7 CADDY, H2020 subCULTron, H2020 EXCELLABUST, etc.) and nationally funded HrZZ project CroMarX. His research interests include navigation and localization of underwater and surface marine vehicles, and extremum seeking control. Together with colleagues from LABUST he has co-authored 3 journal papers in scientific journals and above 10 papers in various national and international conferences.

## List of publications (Filip Mandić)

### Journal papers

[1] Mandić, F., Mišković, N., Lončar, I., "Time difference of arrival source seeking", IEEE Journal of Oceanic Engineering, 2019, accepted for publication.

[2] Vasilijević, A., Nad, D., Mandić, F., Mišković, N., Vukić, Z., "Coordinated navigation of surface and underwater marine robotic vehicles for ocean sampling and environmental monitoring", IEEE/ASME Transactions on Mechatronics, Vol. 22, No. 3, June 2017, pages 1174-1184.

[3] Mandić, F., Rendulić, I., Mišković, N., Nad, D., "Underwater object tracking using sonar and usbl measurements", Journal of Sensors, Vol. 2016, 2016, page 10.

[4] Nad, D., Mišković, N., Mandić, F., "Navigation, guidance and control of an overactuated marine surface vehicle", Annual Reviews in Control, Vol. 40, 2015, pages 172 - 181.

### Conference papers

[1] Babić, A., Mandić, F., Vasiljević, G., Mišković, N., "Autonomous docking and energy sharing between two types of robotic agents", IFAC-PapersOnLine, Vol. 51, No. 29, 2018, pages 406 - 411, 11th IFAC Conference on Control Applications in Marine Systems, Robotics, and Vehicles CAMS 2018.

[2] Djapic, V., Nad, D., Mandic, F., Miskovic, N., Kenny, A., "Navigational challenges in diver-auv interaction for underwater mapping and intervention missions", IFAC-PapersOnLine, Vol. 51, No. 29, 2018, pages 366 - 371, 11th IFAC Conference on Control Applications in Marine Systems, Robotics, and Vehicles CAMS 2018.

[3] Nad, D., Mandić, F., Mišković, N., "Diver tracking using path stabilization - the virtual diver experimental results", IFAC-PapersOnLine, Vol. 49, No. 23, 2016, pages 214 - 219, 10th IFAC Conference on Control Applications in Marine SystemsCAMS 2016.

[4] Mandić, F., Mišković, N., Palomeras, N., Carreras, M., Vallicrosa, G., "Mobile beacon control algorithm that ensures observability in single range navigation", IFAC-PapersOnLine, Vol. 49, No. 23, 2016, pages 48 - 53, 10th IFAC Conference on Control Applications in Marine SystemsCAMS 2016.

[5] Mandić, F., Mišković, N., Vukić, Z., "Range–only navigation – maximizing system observability by using extremum seeking", IFAC-PapersOnLine, Vol. 48, No. 16, 2015, pages 101 - 106, 10th IFAC Conference on Manoeuvring and Control of Marine Craft MCMC 2015, Copenhagen, 24–26 August 2015.

[6] Mandić, F., Mišković, N., "Tracking underwater target using extremum seeking", IFAC-PapersOnLine, Vol. 48, No. 2, 2015, pages 149 - 154, 4th IFAC Workshop on Navigation, Guidance and Control of Underwater VehiclesNGCUV 2015.

[7] Vasilijevic, A., Calado, P., Lopez-Castejon, F., Hayes, D., Stilinovic, N., Nad, D., Mandic, F., Dias, P., Gomes, J., Molina, J. C., Guerrero, A., Gilabert, J., Miskovic, N., Vukic, Z., Sousa, J., Georgiou, G., "Heterogeneous robotic system for underwater oil spill survey", in OCEANS 2015 - Genova, May 2015, pages 1-7.

[8] Vasilijevic, A., Stilinovic, N., Nad, D., Mandic, F., Miskovic, N., Vukic, Z., "Auv based mobile fluorometers: System for underwater oil-spill detection and quantification", in 2015 IEEE Sensors Applications Symposium (SAS), April 2015, pages 1-6.

[9] Mišković, N., Bogdan, S., Nad, D., Mandić, F., Orsag, M., Haus, T., "Unmanned marsupial sea-air system for object recovery", in 22nd Mediterranean Conference on Control and Automation, June 2014, pages 740-745.

# Životopis

**Filip Mandić** rođen je 2.4.1990. u Puli. Godine 2014. diplomirao je na Fakultetu elektrotehnike i računarstva, sa diplomskim radom naslovljenim "Podvodna navigacija korištenjem jednostrukog mjerenja udaljenosti". Od 2014. godine je doktorand, istraživač i asistent na Zavodu za automatiku i računalno inženjerstvo (ZARI), FER. Njegov rad je financiran kroz Hrvatsku zakladu za znanost (HrZZ) i projekt "Razvoj karijera mladih istraživača". Sudjelovao je u nekoliko EU projekata (FP7 CADDY, H2020 subCULTron, H2020 EXCELLABUST, itd.) i nacionalnom HrZZ projektu CroMarX. Znanstveni intersi su mu lokalizacija i navigacija plovila te upravljačka tehnika traženja ekstrema. Zajedno s kolegama iz Laboratorija za podvodne sustave i tehnologije, koautor je 3 rada u visoko rangiranim znanstvenim časopisima i više od 10 radova na nacionalnim i internacionalnim konferencijama.